THESIS TITLE:

INVESTIGATING A NOVEL GAMMA DELTA (γδ) T CELL-BASED CHIMERIC ANTIGEN RECEPTOR THERAPY FOR SOLID TUMOURS

CHARLES EROMOSELE AGBUDUWE

UCL

DOCTOR OF PHILOSOPHY IN HAEMATOLOGY

2023

I, Charles Agbuduwe, confirm that the work presented in this thesis is my own. Where information has been derived from other sources, I confirm that this has been indicated in the thesis.

ABSTRACT

Despite impressive outcomes for Chimeric Antigen Receptor (CAR) therapy in haematological cancers, little progress has so far been made for solid tumours. This is due to the hostile solid tumour microenvironment (TME) and the lack of ideal solid cancer targets. B7-H3, an immune checkpoint molecule which is overexpressed by a wide range of solid tumours with minimal expression in healthy tissues, was the cancer-associated antigen target selected for evaluation in this project.

The aims of this research were to develop an expansion protocol from peripheral blood for the potent Vδ1 subset of gamma delta (γδ) T cells which are naturally tissue-resident and thus more adapted towards tumour immune surveillance, the evaluation of a B7-H3 specific CAR and the development of a hypoxia-sensing CAR construct.

Expansion of Vδ1 γδ T cells was achieved by stimulation of healthy donor peripheral mononuclear blood cells (PBMCs) with a CD3 antibody (OKT3 clone) and Interleukin-15. The Vδ1-enriched γδ T cells demonstrated potent anti-cancer properties which were further enhanced by the B7-H3 targeting CAR based on a novel scFv binder. *In vitro* co-culture experiments with cancer cell lines demonstrated enhanced cytotoxicity, cytokine secretion and proliferation against cancer cell lines but not against allogeneic PBMCs.

Furthermore, proof-of-concept demonstration of a B7-H3 targeting hypoxiCAR encoding an oxygen degradation domain (ODD) and hypoxia responsive elements (HRE) showed dual oxygen sensing with reversible induction of CAR expression under hypoxic conditions and subsequent CAR degradation in normoxia.

To enhance persistence within the TME, transduction of a constitutively active *STAT5B* mutant construct conferred enhanced cytokine-independent survival and proliferation to γδ T cells.

In summary, this project has demonstrated successful expansion of the Vδ1 subset of γδ T cells using a technique that is permissive for retroviral transduction. A novel B7-H3 targeting CAR construct enhanced γδ T cell function and demonstrated proof-of-principle for hypoxia-induced finetuning of CAR expression.

IMPACT STATEMENT

As the world's population ages, the incidence of cancer is expected to rise hence new and more effective therapies are needed. Cell-based immune therapy, which involves the use of cells of the immune system to combat diseases including cancer, has recently seen a surge in interest following the development of a new technology called chimeric antigen receptor (CAR) therapy. This currently involves the collection of a patient's white blood cells followed by engineering of the cells in a laboratory to recognize and target a specific marker on cancer cells. The cells are then infused back to the patient to treat their cancer. This therapy has shown impressive results for blood cancers however, for solid cancers, very little progress has been made because of unique characteristics such as the lack of ideal cancer markers, low oxygen (hypoxia) within the tumour and the presence of cells which protect the cancer cells from the immune system.

The aim of this project was to develop strategies to improve the effectiveness of CAR therapy in solid tumours. First, a new method of growing rare immune cells called Vdelta1 (Vδ1) gamma/delta (γδ) T cells from the blood of healthy donors was developed. These cells are unique in that they can rapidly identify and eliminate tumour cells and act differently from the more abundant alpha/beta (αβ) T cells. Due to this difference in mode of action, γδ T cells can be collected from a healthy donor and potentially given to a patient without provoking a significant reaction.

Furthermore, the Vδ1 γδ T cells were engineered with a CAR targeting B7-H3, a marker present on a wide range of solid cancers and we demonstrated enhanced cancer-targeting functions for these γδ CAR T cells.

To ensure that the γδ CAR T cells function optimally within the low oxygen (hypoxic) environment present within tumours, a hypoxia-sensitive CAR was developed which is switched on under low oxygen conditions and switched off in the presence of normal levels of oxygen. This strategy ensures that the CAR T cells do not target healthy tissues. Finally, to make the γδ T cells survive for longer, we engineered them with a gene which provides signals to keep the cells alive, under the control of a safety switch which can be turned off when necessary.

In summary, this research presents novel strategies to enhance the function of immune cells against solid cancers. A simple, clinically relevant method for expanding potent immune cells from peripheral blood has been developed. We have, for the first time, successfully transduced Vδ1 T cells with a CAR targeting B7-H3 for use against many solid cancers. Furthermore, this research has produced a B7-H3-specific hypoxia-sensing CAR which has the potential for enhancing CAR function while minimizing unwanted effects.

The findings of this research constitute significant contributions to knowledge about γδ T cells and will significantly impact future academic and industry outputs. It is anticipated that further testing will ultimately lead to the development of an effective new cell therapy product for patients with cancer.

ACKNOWLEDGMENTS

This PhD research was part of a Clinical Research Training Fellowship which was funded by Cancer Research UK (CRUK). I am grateful for the generous funding and additional COVID-19-related funding extension which ensured that this thesis could be completed before my return to speciality training. My gratitude also goes to the CRUK City of London (CoL) centre for co-ordinating the multidisciplinary training aspects of the fellowship and to the ever-helpful CoL PhD co-ordinators; Annabelle Scott, subsequently replaced by Iris Lueke.

When I commenced this research fellowship in November of 2019, it was impossible to anticipate that our world would be completely transformed by a coronavirus by the end of it! The first COVID-19 lockdown in March 2020 meant that all laboratory experiments had to be suspended and the research put on hold while I went back to work for the NHS. The lifting of some restrictions in the summer of 2020 meant that the research could resume and our move to the brand new Zayed Centre for Research (ZCR) was finalized. After the initial resistance to change, I eventually got to love the ultra-modern building in which I spent many long days and nights performing experiments. I am grateful to the donors as well as management and staff of the ZCR for creating the conducive research environment. I greatly appreciate Ayad Eddaoudi, for flow cytometry training and support. I would also like to appreciate the ancillary staff who keep the building and its facilities well maintained and who were often my only companions during those long nights I spent performing experiments.

To all the past and current members of the Anderson, Fisher and Donovan Lab teams, your support certainly facilitated this project. I wish to specifically appreciate

the following members of the Anderson Lab team for their assistance in this project: Artemis Gavriil, thanks for being there to answer my questions at the start of the project and for introducing me to gene cloning. Marta Barisa, thanks for your assistance in optimising the gamma delta T cell expansion protocol. Gabby Ferry, thanks for your help with showing me around in the first few weeks of the project. To my fellow PhD colleagues; Dilu, Meshael, Farah and Rivani, thanks for being helpful with advice and for sharing reagents in those instances where I discovered that I had run out in the middle of my experiments!

I am also greatly indebted to my Thesis Committee members; Emma Morris, John Maher and Kerry Chester, for their immense scientific input in this project and for critically reviewing the PhD upgrade report. I am immensely grateful to Kerry Chester, my secondary supervisor for her support and for kindly providing the cervical cancer cell lines used in this project. I am also grateful to our collaborator, James Arnold at King's College London for providing the plasmid used for the hypoxiCAR project.

This project would not have been possible without the immense support and guidance provided by my primary supervisor, Professor John Anderson. I cannot thank you enough for the opportunity to undertake this fellowship in your lab. I found the advert for this clinical PhD studentship which was in a specific research area that I was interested in and submitted my application without any expectations as I had no previous contacts at UCL. I was subsequently shortlisted for interview and was pleasantly surprised when I received a call from you informing me that I had been successful. It is not very often that someone of my background gets such an opportunity! I will also never forget those amazing garden parties that you organised for the lab team where you showed how skilled and competitive you were at croquet!

Despite the challenges of COVID-19, I enjoyed my time at University College London and it has been very rewarding being part of the excellent multidisciplinary academic environment and the disruptive thinking that UCL is renowned for. I was also fortunate to discover a passion for Bachata and Salsa dancing through the UCL Salsa society even though I am still struggling to grasp the more complicated dance moves! I am grateful to the Salsa Society for providing the much-needed stress relief during the PhD and for the friendships established.

Finally, I am grateful for amazing friends and family who were very supportive during tumultuous times. For being willing to listen to my lamentations about failed experiments and other struggles, I am indebted to you all! To my sister, Eghonghon, and my nephews and niece, thank you.

This PhD is dedicated to my mum, Mrs Victoria Agbuduwe, whose personal sacrifices ensured that my education was never disrupted during tough times. It was only because of your unwavering commitment that it was possible for me to progress from being a child street vendor in Benin City, Nigeria, supporting you when you lost your job, to becoming an academic haematologist with a doctorate from one of the world's leading universities. *Obulu ma!*

TABLE OF CONTENTS

Index of Figures

Index of Tables

ABBREVIATIONS

2-OG 2-oxoglutarate

AICD activation-induced cell death

AML acute myeloid leukaemia

ANOVA Analysis of Variance

ARNT Aryl receptor nuclear translator

ATL adult T-cell leukaemia

B7-H3 B7 homolog 3 protein

BCG bacille Calmette-Guerin

BTN3A1 butyrophilin 3A1

CAR chimeric antigen receptor

CCR7 C-C chemokine receptor type 7

CD Cluster of differentiation

CDR3 Complementarity-determining region 3

CEA carcinoembryonic antigen

CLL Chronic Lymphocytic Leukaemia

CMV Cytomegalovirus

CNS central nervous system

CO_2 Carbon (IV) Oxide

CNS Central nervous system

CRS Cytokine Release Syndrome

CSF cerebrospinal fluid

DAMPs damage-associated molecular patterns

DFS disease-free survival

DIPG diffuse intrinsic pontine glioma

DMEM Dulbecco's Modified Eagle medium

DMSO Dimethyl Sulfoxide

DNA Deoxyribonucleic Acid

E.coli *Escherichia coli*

EBV Epstein-Barr virus

EDTA Ethylenediaminetetraacetic acid

EGFR Epidermal Growth Factor Receptor

EGFRvIII Epidermal growth factor receptor variant III

ELISA enzyme-linked immunosorbent assay

EPO Erythropoietin

ERBB2 erythroblastic oncogene B 2

FasL Fas ligand

FcR Fc Receptors

FDA Food and Drug Administration

FIH Factor inhibiting HIF

FOXO3 Forkhead box O3

GLUT-1 glucose transporter protein type 1

GM-CSF Granulocyte-macrophage colony-stimulating factor

GrB Granzyme B

GVHD Graft versus host disease

HER2 human epidermal growth factor receptor 2

HIF Hypoxia-inducible factor

HIV human immunodeficiency virus

HLA human leucocyte antigen

HMBPP (E)-4-hydroxy-3-methyl-but-2-enyl-pyrophosphate

HRE hypoxia responsive element

ICOS Inducible co-stimulatory molecule

IFNγ Interferon-gamma

Ig Immunoglobulin

IL interleukin

IL-15Rα Interleukin-15 receptor alpha

IMDM Iscove's Modified Dulbecco's Modified Eagle medium

iNKT invariant natural Killer T

IPP isopenthenyl pyrophosphate

ITAM immunoreceptor tyrosine-based activation motif

JAK Janus kinase

KanR Kanamycin resistance gene

LAG3 Lymphocyte activation gene 3

LAMP-1 lysosomal associated membrane protein 1

LGL Large Granular Lymphocytic leukaemia

mAb monoclonal antibody

MACS Magnetic-Activated Cell Sorting

MDSCs Myeloid Derived Suppressor Cells

MHC major histocompatibility complex

MICA/MICB MHC class I polypeptide–related sequence A/B

mRNA messenger ribonucleic acid

NCBI National Centre for Biotechnology Information

NK Natural Killer

NKG2D natural killer group 2D

NKR Natural Killer cell Receptors

ODD Oxygen degradation domain

OX40L OX40 Ligand

pAg phosphoantigen

PBMC Peripheral Blood mononuclear cell

PCR Polymerase Chain Reaction

PD-1 Programmed Cell Death Protein 1

PDGFR Platelet Derived Growth Factor Receptor

PD-L1 Programmed Cell Death ligand 1

PG PiggyBac

PHA Phytohemagglutinin

PIAS Protein Inhibitors of Activated STAT

PRR Pattern Recognition Receptors

pSTAT5 phosphorylated STAT5

PTP Protein Tyrosine Phosphatases

RPMI Roswell Park Memorial Institute (RPMI) medium

SB Sleeping Beauty

ScFv single chain fragment variable

sdAb single domain antibody

SDF1 Stromal derived factor 1

STAT5B Signal Transducers and Activators of Transcription 5B

TAA tumour associated antigen

TBE Tris/Borate/EDTA

T_{CM} Central memory T cell

TCR T cell receptor

T_{EM} Effector memory T cell

T_{EMRA} terminally differentiated effector memory

TIAN tumour inflammation-associated neuropathy

TIL tumour infiltrating lymphocyte

TIM3 T cell immunoglobulin domain and mucin domain 3

TLR Toll-like Receptors

TME tumour microenvironment

TNF-α Tumour necrosis factor alpha

TNP 2,4,6-trinitrophenyl

TRAIL TNF-related apoptosis-inducing ligand

TRD TCR delta locus

Treg regulatory T cell

TRG TCR gamma locus

TRUCK T cells redirected for universal cytokine-mediated killing

ULBP UL16-binding proteins

VEGF Vascular endothelial growth factor

VHL von Hippel-Lindau protein

αβ T cell alpha beta T cell

γδ T cell gamma delta T cell

γδT17 IL-17 producing gamma delta T cell

THESIS STRUCTURE

This thesis has evaluated a novel B7-H3 targeting chimeric antigen receptor (CAR) based on gamma delta (γδ) T cells and strategies for optimising cellular immunotherapy for solid tumours.

CHAPTER I reviews the literature on γδ T cells, CAR T cell therapy and strategies for optimising CAR efficacy in solid tumours.

CHAPTER II describes the general methods used in this project.

CHAPTER III reviews the literature on γδ T cell expansion methods and evaluates a novel method for expanding Vδ1 γδ T cells from the peripheral blood of healthy donors.

CHAPTER IV presents an evaluation of the efficacy of a B7-H3 targeting CAR based on γδ T cells against cancer cell lines.

CHAPTER V presents the result of a novel strategy to overcome the dependence of expanded γδ T cells on IL-15 by transducing a constitutively active STAT5 construct.

CHAPTER VI presents proof-of-concept for a hypoxia-sensing CAR which exploits the hypoxic tumour microenvironment to increase CAR expression.

CHAPTER VII discusses future research priorities and concluding remarks.

CHAPTER I: INTRODUCTION

1.1 Background

T lymphocytes are essential components of the adaptive immune system which protect against pathogens and play key roles in the elimination of malignantly transformed cells. The specificity of the adaptive immune system is mediated through the T-Cell Receptor (TCR) complex. The TCR of the majority of T lymphocytes, often referred to as alpha/beta (αβ) T cells, is a membrane-bound heterodimer composed of two glycoprotein alpha (α) and beta (β) chains associated with the CD3 molecule, forming the TCR complex.[1] In a minority of T cells, the TCR is composed of gamma (γ) and delta (δ) chains encoded by the TCR gamma locus (TRG) on chromosome 7 and the TCR delta locus (TRD) on chromosome 14 respectively.[2] These cells were first described in the 1980s following the serendipitous discovery of a distinct gene family expressed in a proportion of T cells.[3] Further work identified the delta chain as the other heterodimer of the gamma delta TCR complex.[4] The crucial roles of these cells in health and disease are becoming increasingly recognised.

1.2 Gamma Delta T cells

Gamma delta (γδ) T cells usually comprise up to 5% of peripheral blood lymphocytes [5] but this proportion rises significantly (up to 50%) in response to certain infections. Like the αβ TCR, the diversity of the gamma delta TCR repertoire is mediated by somatic recombination of the Variable (V), Diversity (D) and Joining (J) segments of the TCR gene loci. However, the γδ TCR differs from the αβ TCR in that there are fewer Vγ and Vδ segments for recombination[6] and is capable of activation by small molecules and whole proteins as opposed to the αβ TCR which recognises peptides presented in the context of self-MHC molecules.[7][8] In addition, the majority of γδ T

cells lack expression of CD4 and CD8 (although a small proportion are CD4+ CD8- or CD8+CD4-).[9] Interestingly, in this study, the authors found the CD4+ γδ T cells produced significant amounts of IL-2 and GM-CSF but lacked appreciable cytotoxicity compared with CD4-CD8- and CD8+ γδ T cells. The specific roles of these phenotypes have yet to be determined but appear to mirror the functions of the CD4+ and CD8+ αβ T lymphocytes.

Several subsets of γδ T cells have been recognised based on the type of Vδ chain expressed. The first two identified in humans were Vδ2 and Vδ1 which account for the vast majority of total γδ T cells.[10] Vδ2 chains almost exclusively pair with Vγ9 chains[11] and this Vγ9/δ2 subset predominates (~70%) in peripheral blood increasing from birth until puberty with levels generally declining after the third decade.[12] On the other hand, Vδ1-expressing γδ T lymphocytes are often associated with various Vγ chains.[13] While the Vδ2 subset declines with age, the Vδ1 fraction remains stable even in centenarians.[14] In a review of 104 healthy donors, Argentati et al found a higher proportion of TNF-α producing $\gamma\delta^+$ T cells in older donors but no difference in interferon-γ producing cells or cytotoxicity in this group of patients. Cells from older patients demonstrated a two-fold reduced expansion index for Vδ2 but not with Vδ1 subset in older compared with younger donors. The authors surmised that this alteration of γδ T cells could contribute to the age-related derangement of T cell-mediated, adoptive responses and may represent a new characteristic of immunosenescence.[14]

1.2.1 Variation in **Vδ2/ Vδ1 proportions in health and disease**

The median Vδ2/Vδ1 ratio in a Caucasian cohort of healthy adults was 2.7 (range 0.3-27.7)[15] however a predominance of the Vδ1 subset has been found among healthy donors in West Africa.[16] A study comparing γδ proportions between Caucasians and African Americans in Baltimore, reported significantly lower Vδ2 T cell proportions in African Americans but similar total lymphocyte counts in both groups.[17] Skewing of the Vδ2/Vδ1 ratio has also been reported in various pathologic conditions. A marked increase in Vδ1 subset has been reported in HIV[18], CMV[19][20], EBV[21] and Malaria[22]. While the precise mechanism for this observation is not clear, it is likely that Vδ1 T cells play a major role in the immune response to these infections and may, at least partially, account for regional differences in Vδ subset prevalence. Furthermore, adult females have been shown to have higher proportions of Vδ2 cells compared with men.[12]

1.2.2 Localisation of gamma delta T cell structural subsets

While Vγ9δ2 cells account for the majority (>70%) of peripheral blood γδ T cells in adults, Vδ1+ cells are enriched in epithelial tissues of the gut and skin as well as liver and spleen where they play important roles as the first line of defence against pathogens and in tumour immunosurveillance.[23] Vδ3+ cells account for the majority of Vδ2neg Vδ1neg γδ T cells and are found mainly in liver and peripheral blood.[11]

1.3 T cell Differentiation

The canonical description of the stepwise differentiation of αβ T lymphocytes from naïve cells through memory stage to terminal effectors is based on the expression of surface markers notably CD45RA, CCR7, CD27.[24][25][26][27] In brief, Naïve T lymphocytes (CD45RA+ CCR7+) migrate from the thymus to secondary lymphoid sites where they encounter antigens presented by dendritic cells. The adhesion and transmigration of Naïve lymphocytes through endothelial venules is mediated by CD62L and the chemokine receptor, CCR7.[28][29] Following antigen stimulation, T lymphocytes undergo differentiation and proliferate into effector cells secreting cytokines or cytolytic molecules depending on the functional type. T cells differentiate into one of two memory phenotypes; a CCR7- subtype which expresses receptors for migration to inflamed tissues and capable of immediate function or the lymph node homing CCR7+ subtype that lacks immediate effector function but capable of differentiation into CCR7- effectors on secondary antigen stimulation.[28] In general, expression of CCR7 in combination with CD45RA, has been shown to discriminate naïve (CD45RA+CCR7+) and Central Memory, T_{CM} (CD45RA−CCR7+) from Effector Memory, T_{EM} (CD45RA−CCR7−) and Terminal Effector, T_{EM}-RA+ (CD45RA+CCR7−, found mainly in CD8+ cells) subsets.[30][31] In healthy donors, the majority of T cells co-express both CCR7 and CD27 on the cell surface[27][32] and either marker has been used in various studies to define effector and memory subsets.[32][33] Further evidence for this stepwise differentiation model is the finding of progressive telomere shortening as well as increasing susceptibility to apoptosis progressively along this differentiation pathway.[27] While these differentiation stages have been well defined for CD8+ and CD4+ αβ T cells with similar $T_{naïve}$ and T_{EMRA} populations in Vδ1+ T cells recognised[34], the phenotypic characterisation of γδ differentiation stages using canonical homing

and cytokine receptors remains controversial. While Vγ9δ2 T cells are generally thought of as possessing innate-like properties given their semi-invariant TCR, conserved chain pairing, restricted CDR3 region diversity and generation in early gestation,[35] Vδ2 negative (predominantly Vδ1+) γδ T cells have been shown to demonstrate adaptive biological features similar to αβ T cells in terms of TCR repertoire focusing following clonal selection. Davey et al[35] obtained evidence for TCR repertoire focusing from comparative analyses of Vδ1 TCR repertoire of cord blood as well as CMV seronegative and seropositive healthy adults. In contrast to the cord blood samples which demonstrated extremely unfocused TCR repertoires, the Vδ1 TCR repertoires in adult blood samples were limited to a small number of individual clonotypes thereby providing evidence for potential antigen-mediated adaptive clonal selection. Furthermore, the persistence of CMV-reactive long-lived populations of murine effector γδ T cells following CMV infection[36,37] represents a memory subset, another adaptive function.

Further evidence for γδ T cell immunological memory was seen in marked expansion of antigen-specific Vδ2+ lymphocytes following reinfection of macaques with Bacille Calmette-Guerin (BCG).[38] Interestingly, in the same study, following intravenous inoculation of BCG, expansion of Vδ2+ lymphocytes was apparent in blood and tissue sites but minimal in lymph nodes, supporting the theory of anatomical localisation of memory γδ subsets. Furthermore, cytokine stimulation has been shown to skew the differentiation fate of γδ T cells. Vγ9/Vδ2 T cells grown in the presence of IL-15 differentiated into an effector memory population characterized by TNFα secretion and lacking expression of CD62L, CD81 and CCR7 while in contrast, IL-21 stimulated cells differentiated into central memory T cells expressing CD62L, CD81 and CCR7 and did not produce TNF-α, IFN-γ or IL-4.[39] Vδ2- T lymphocytes (which were predominantly

Vδ1+) in CMV+ donors were shown to be of TEMRA (CD45+ CD27-) differentiation, expressing high levels of cytolytic markers like perforin and Granzyme B in contrast to Vδ2- cells from CMV- donors which were mainly of the naïve phenotype (CD45RA+ CD27+).[40] This dichotomy was not present in the Vδ2+ compartment which was of central memory (CD45RA+ CD27-) phenotype in both CMV- and CMV+ donors. This observation provides supporting evidence for the role of Vδ1 cells in the immune response to CMV infection as well as the need for further research to elucidate the pathways of differentiation of the different γδ T cell subsets.

1.4 Gamma delta receptors and agonists in humans

Since the chance discovery of gamma delta T cells, efforts have been ongoing to understand the structure and function of these unconventional cells. Significant differences exist in the mechanism of antigen recognition by γδ T cells compared with αβ T cells. Crystal Structure analysis of the γδ TCR shows more similarities with immunoglobulins (Ig) rather than αβ TCR[41] which correlates with the ability of immunoglobulins to bind antigen without Major Histocompatibility Complex (MHC) presentation in contrast to MHC-restricted αβ TCR antigen recognition. Furthermore, thymic development of γδ T cells appears to proceed independent of MHC class I as β2-microglobulin-deficient mice produced functionally normal γδ T cells.[42] Therefore, even though conflicting evidence exists, it appears that MHC-mediated positive selection may not be essential for γδ T cell maturation in the thymus which is in contrast to αβ T cell development.[43]

Three main Vδ gene segments exist within the δ locus on chromosome 14 in humans; Vδ1, Vδ2 and Vδ3, are most frequently used in rearrangement of the δ chain and seven functional Vγ gene segments, Vγ2, Vγ3, Vγ4, Vγ5, Vγ8, Vγ9 and Vγ11, located

within the γ locus on chromosome 7 in humans, are used for rearrangement of the γ chain.[44] Despite this limited number of Vδ genes, the rearrangement of V, D and J region sequence elements during lymphocyte maturation creates an enormous degree of diversity in an area referred to as the complementarity determining region 3 (CDR3) loop.[45] As a result of variation in numbers of D and J elements used, D element reading frames, junctional diversity, and N region nucleotide addition, the estimated number of possible CDR3 sequences is greatest for γδ TCRs and least for immunoglobulins (irrespective of somatic mutation), with αβ TCRs being intermediate.[46]

The Vγ9δ2 TCR, via the butyrophilin proteins, recognises a restricted set of phosphorylated compounds (phosphoantigens), which are produced through the isoprenoid biosynthetic pathway and expressed by microbes such as *Mycobacterium tuberculosis* and stressed cells.[47][48][49][47][50] Vγ9δ2 also react strongly to isopentenyl pyrophosphate (IPP), an intermediate in the human mevalonate pathway and (E)-4-hydroxy-3-methyl-but-2-enyl-pyrophosphate (HMBPP), which is an isoprenoid intermediate found in microbes.[5] Some Vγ9δ2 T cells also recognise naturally occurring primary alkylamines, such as *iso*-butylamine that are secreted by bacteria and occur in some edible plants.[51] The presence of these antigenic alkylamines in the diet provide an opportunity for sensitisation of the immune system against pathogens.

Intracellular accumulation of phosphoantigens (pAgs) frequently occurs in tumour cells[52] and is sensed via the intracellular domain of the butyrophilin 3A1 (BTN3A1), a member of the BTN3A family of type-I membrane proteins with two Ig-like extracellular domains and structural homology to the B7 superfamily of proteins, triggering a conformational change in the molecule.[53][54,55] While the mechanism of BTN3A1 activation of Vγ9δ2 cells is not fully understood, it has been shown that specific

conformational changes in the molecule can differentiate antigenic small molecules which trigger Vγ9δ2 activation from other small molecules which merely bind.[56] BTN 2A1, another member of the butyrophilin family has been recently recognised as essential for γδ T cell recognition of pAgs.[57] BTN2A1 binds directly to the Vγ9δ2 TCR[58] and while it forms a complex with BTN3A1 to synergistically recognize pAg, loss of BTN2A1 cannot be compensated for by BTN3A1. BTN2A1 expression on cancer cells has also been shown to trigger Vγ9δ2 T cell cytotoxicity.[59]Taken together, these findings indicate crucial roles for BTN3A1 and BTN2A1 in the mechanism of pAg recognition by Vγ9δ2 T cells and raises the possibility of therapeutic targeting of these proteins in cancer.

In addition to sensing via the TCR, γδ T cells have the ability to detect pathogens and stress signals through Pattern Recognition Receptors (PRR) such as Toll-like Receptors (TLR) and natural cytotoxicity receptors, such as NKG2D which recognize stress-inducible MHC class I-related MICA/MICB molecules and UL16-binding proteins (ULBP).[60][61] An analysis of TLR expression suggested differential expression between Vδ1 and Vδ2 subsets with higher expression of TLR1 and TLR2 in Vδ1 compared with Vδ2 T cells[62] Vδ1 T cells also recognize several MHC superfamily members such as CD1d which presents lipid molecules.[44] In addition, Vδ1 cells recognise B7-H6, which is expressed on tumour cells, via the natural cytotoxicity receptor, NKp30.[11] These innate immune properties coupled with TCR specificity and the capability for immunological memory make γδ T cells ideal candidates for adoptive cell therapy.

1.5 Cancer targeting properties of human γδ T cells.

With unique abilities to detect cellular stress-induced changes, γδ T cells play key roles in tumour immunosurveillance. Evidence for this abounds both from clinical observations and *in vitro* experiments. Patients with increased (>10%) proportions of γδ T cells after an αβ T cell deplete allogeneic stem cell transplant for leukaemia had significantly improved disease-free survival compared with those with lower proportions of γδ T cells.[63] An extended study of T cell deplete allogeneic stem cell transplant recipients confirmed the overall and leukaemia-free survival advantage as patients who had high levels of γδ T cells on recovery had superior overall and leukaemia-free survival.[64] Interestingly, Vδ1 was the predominant γδ T cell subtype in >90% of survivors in the study. More recently, genome profiling across a wide range of tumours from about 18,000 patients identified tumour-infiltrating γδ T cells as the cell type with the strongest positive prediction of survival.[65]

Furthermore, intestinal epithelial Vδ1 T cells recognised and lysed MICA-expressing tumours *in vitro* in an MHC-independent manner.[66] MICA, an MHC Class I-related molecule of unknown function, is frequently upregulated by DNA damage[67] or other states of cell stress[68] hence this is a possible mechanism of tumour immune surveillance by intraepithelial Vδ1 T cells. It has long been recognised that Vδ1 T cell expansion occurs in Chronic Lymphocytic Leukaemia (CLL) with levels generally increasing with progression of disease[69] and Vδ1+ lymphocytes from CLL patients have been shown to lyse autologous CLL cells when MICA or ULBP were upregulated.[70] Moreover, a cytolytic innate-like Vδ1+ compartment in breast tissue has recently been described and was associated with improved survival in breast cancer patients.[71] Another study showed positive correlation between increased frequency of γδ tumour infiltrating lymphocytes (TILs) and improved disease-free

survival (DFS) in colon cancer.[72] Furthermore, recent data has shown that tumour infiltrating Vδ1 and Vδ3 T cells (but not Vδ2 T cells) can recognize and kill HLA Class I negative DNA mismatch repair deficient tumours.[73] Interestingly, these highly potent Vδ1 and Vδ3 T cells expressed PD-1 and the authors concluded that PD-1 expression may be a marker of antitumour reactivity rather than exhaustion in γδ T cells. However, individual outcomes appeared to depend on the phenotype of TILs. Gene expression profiling of the colorectal cancer-infiltrating TILs revealed a superior DFS in patients with a higher expression of *IFNG* (which codes for interferon-γ) as against those with high expression of *IL17A* which encodes IL-17A, an inflammatory cytokine. The presence in colorectal cancers of this IL-17 producing subset of γδ T cells, called γδT17, was also associated with recruitment of Myeloid Derived Suppressor Cells (MDSCs) and correlated with tumour size, invasion and lymph node metastasis.[74] This underlines the importance of characterisation of γδ phenotypes for cell therapy.

Most evidence for the cancer-targeting properties of Vδ1 T cells have been from co-culture experiments with primary tumour samples or cell lines. *Ex vivo* expanded Vδ1 T cells from healthy donors showed dose-dependent specific cytotoxicity against primary myeloma cells as well as cell lines.[75] Similar cytolytic effects of Vδ1 T cells have been observed against Chronic Lymphocytic Leukaemia (CLL)[76], cancers of epithelial origin; colorectal, pancreatic and renal.[77]

Cancer cell recognition by γδ T cells is mediated via various receptors including innate Natural Killer cell Receptors (NKR) such as NKG2D which sense a myriad of stress signals via ligands on the cell surface. Known ligands of NKG2D includes MHC Class I polypeptide-related sequence A (MICA) and UL16 Binding Protein 1 (ULBP1).[78,79] Pattern recognition receptors such as the Toll-like receptor (TLR) detect damage-associated molecular patterns (DAMPs)-endogenous molecules

released from damaged or distressed cells.[80] In contrast, while it has been recognized that stimulation via the γδ TCR plays a role in the cancer-targeting properties of these cells, the identity of the majority of γδ TCR ligands remains unknown. The best-known cancer-associated Vγ9δ2 ligands are pAgs such as isopenthenyl pyrophosphate (IPP), an intermediate of the mevalonate pathway which accumulates in malignantly transformed cells and this is sensed by the TCR via a conformational change in the ectodomain of butyrophillin 3.[81,82] Figure 1-1 summarises the mechanisms of the anti-cancer activity of γδ T cells. Given the myriad of receptors on γδ T cells, they represent an important link between the innate and adaptive immune system, allowing crosstalk between immune cells thereby maximizing anti-cancer responses.

Although a pro-inflammatory and potentially pro-tumour function for γδ T cells producing IL-17 (γδ17) has been postulated from observations in murine models,[83] there has been very little evidence for this in the clinical context. In an experimental model, naïve human Vγ9δ2 T cells were induced towards IL-17 production following culture with pAgs and IL-1-β, TGF-β, IL-6 and IL-23.[84] These cells expressed granzyme B, TRAIL, FasL and CD161 but not Interferon-γ. The pro-tumourigenic potential of IL-17 is thought to be due to its ability to promote angiogenesis, mobilize macrophages and directly promote tumour cell proliferation.[85] Furthermore, a population of CD39+ tumour-infiltrating γδ T cells, secreting IL-17A and GM-CSF, has been associated with an immunoregulatory phenotype and unfavourable outcomes in human colorectal cancer.[86] Since IL-17 γδ T cells have only rarely been identified in healthy humans,[87] It could be argued that these rare immunosuppressive γδ T cells are polarized towards the IL17A-producing phenotype within the specific tumour by mediators produced within the tumour

microenvironment (TME) since tumour infiltrating γδ T cells have otherwise been associated with favourable outcomes in most tumours.[88,89] Evidently, more research is needed to determine the factors which contribute to the induction of γδ17 T cells within the tumour microenvironment.

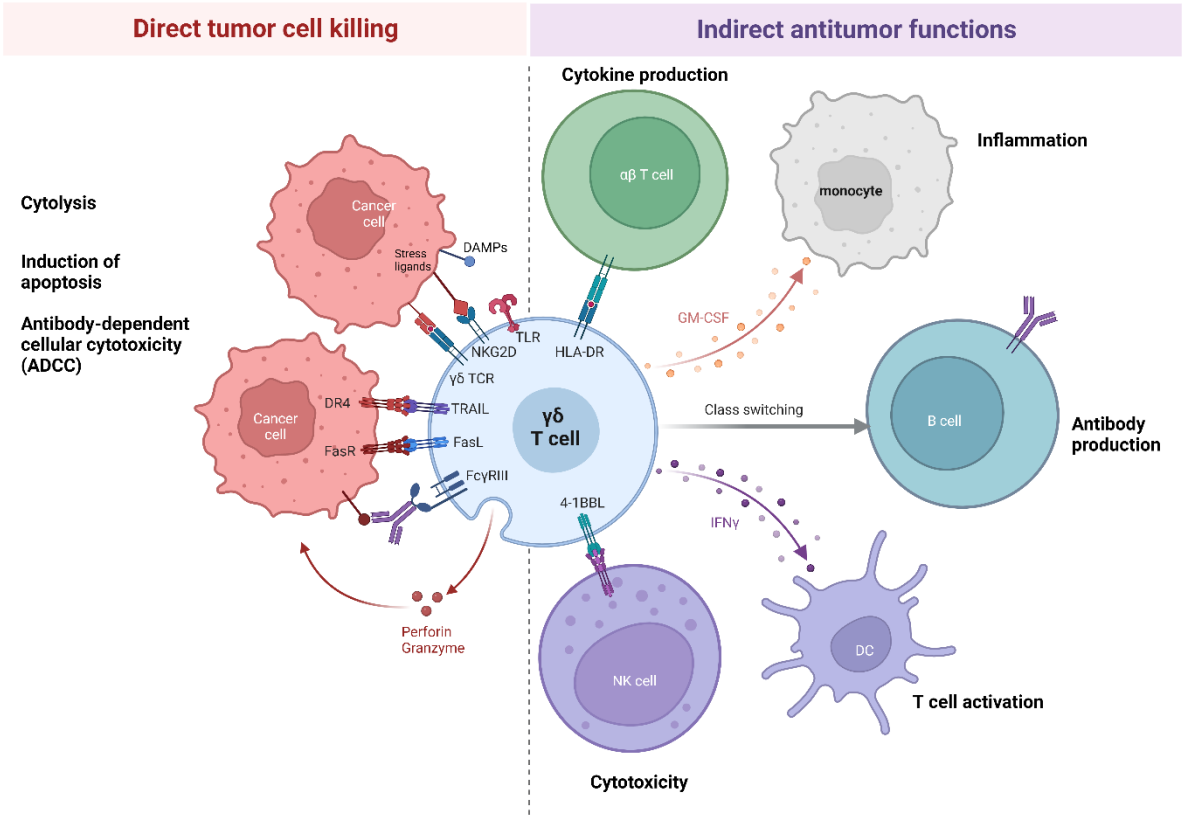

Figure 1-1. Schematic illustration of the anti-cancer properties of γδ T cells. Gamma Delta (γδ) T cells sense a wide range of cellular signals via innate receptors such as the Natural Killer Group 2D (NKG2D) receptor which is activated by a range of stress signals and Toll-like receptors which sense DAMPs, damage-associated molecular patterns.[71] Target cell engagement via the γδ TCR is also achieved via a range of ligands which are upregulated in malignant cells and other states of cellular stress. The anti-tumour activity of γδ T cells occurs via both direct mechanisms including the release of cytolytic enzymes such as perforin and granzyme, induction of apoptosis via the Fas Ligand (FasL) or Tumour Necrosis Factor-related apoptosis inducing Ligand (TRAIL) [106,107] as well as via antibody-dependent cellular cytotoxicity. Indirect anti-tumour mechanisms include activation of other immune cell mediators [108] such as macrophages and dendritic cells (DC) via secretion of chemokines such as Interferon-γ (IFNγ), Granulocyte-Macrophage Colony-Stimulating Factor (GM-CSF) [109,110]. Gamma delta T cells also act as professional antigen presenting cells to αβ T cells via the Class II Major Histocompatibility Complex molecule, HLA-DR. [111] Class switching of B cells to stimulate antibody production is induced by γδ T cells via secretion of IL-4 and IL-10.[112] Activation of NK cells also occurs via the 4-1BB:4-1BB ligand (4-1BBL) interaction. DR4, Death Receptor 4; FasR, Fas Receptor; FcγRIII, Fc gamma Receptor III. This figure was created with biorender.com.

1.6 Chimeric Antigen Receptor (CAR) T Cell Therapy

The most remarkable advancement in cellular immunotherapy over the last decade has been the development of therapeutic chimeric antigen receptor (CAR) T-cell products for use in the clinic. CAR T cell technology typically utilises the specificity of monoclonal antibodies in redirecting T-cell responses against antigens expressed on a target cell and has shown remarkable efficacy in some haematological cancers. The basic structure of the CAR comprises an extracellular antigen binding domain which is usually a single-chain variable fragment (ScFv) derived from a monoclonal antibody although other innovative binders have been developed (figure 1-2), a hinge and transmembrane domain and an intracellular signalling domain encoding an immunoreceptor tyrosine-based activation motif (ITAM) molecule, usually CD3ζ, as well as one or more co-stimulatory molecules e.g. CD28 (T cell-specific surface glycoprotein CD28) and/or 4-1BB (CD137, Tumour Necrosis Factor (TNF) receptor superfamily member 9).[90]

1.6.1 Chimeric antigen therapy: historical development

Following the initial report of the generation of a chimeric TCR by fusing the variable regions from an antibody to the constant regions of the TCR by Dr Yoshikazu Kurosawa,[91] a team led by Dr Zelig Eshhar in 1989 published the first demonstration of redirection of T cell responses towards a specific target in a non-MHC restricted manner.[92] The chimeric TCR was constructed by replacing the extracellular domains of the TCR with the heavy (V_H) and light (V_L) chain domains of an antibody against 2,4,6-trinitrophenyl (TNP). This was expressed onto a T cell hybridoma which conferred non-MHC-restricted response against TNP. Further work by Eshhar led to the development of the single chain (scFv) CAR in 1993.[93] Despite demonstration of

in vitro reactivity, the first-generation CARs which included CD3ζ chain as the sole intracellular signalling domain showed little or no efficacy *in vivo*.[94,95] This was due to the lack of the co-stimulation (signal 2) required for T cell activation thus the initial clinical trials with first generation CARs were disappointing with very poor CAR T cell persistence and efficacy.[96,97] Subsequent second- and third- generation CARs which include one[98] or two[99] co-stimulatory molecules respectively demonstrated superior T cell activation.

The big breakthrough for CAR T cell therapy came following the publication of results of the landmark Phase 1/2a study of Tisagenlecleucel (Kymriah) for relapsed or refractory B-acute lymphoblastic leukaemia.[100] The CD19-directed CAR therapy demonstrated remarkable efficacy with event-free and overall survival rates of 50% and 76% at 12 months respectively. The impressive clinical outcomes from this trial led to the approval of Tisagenlecleucel by the FDA in 2017.[101]

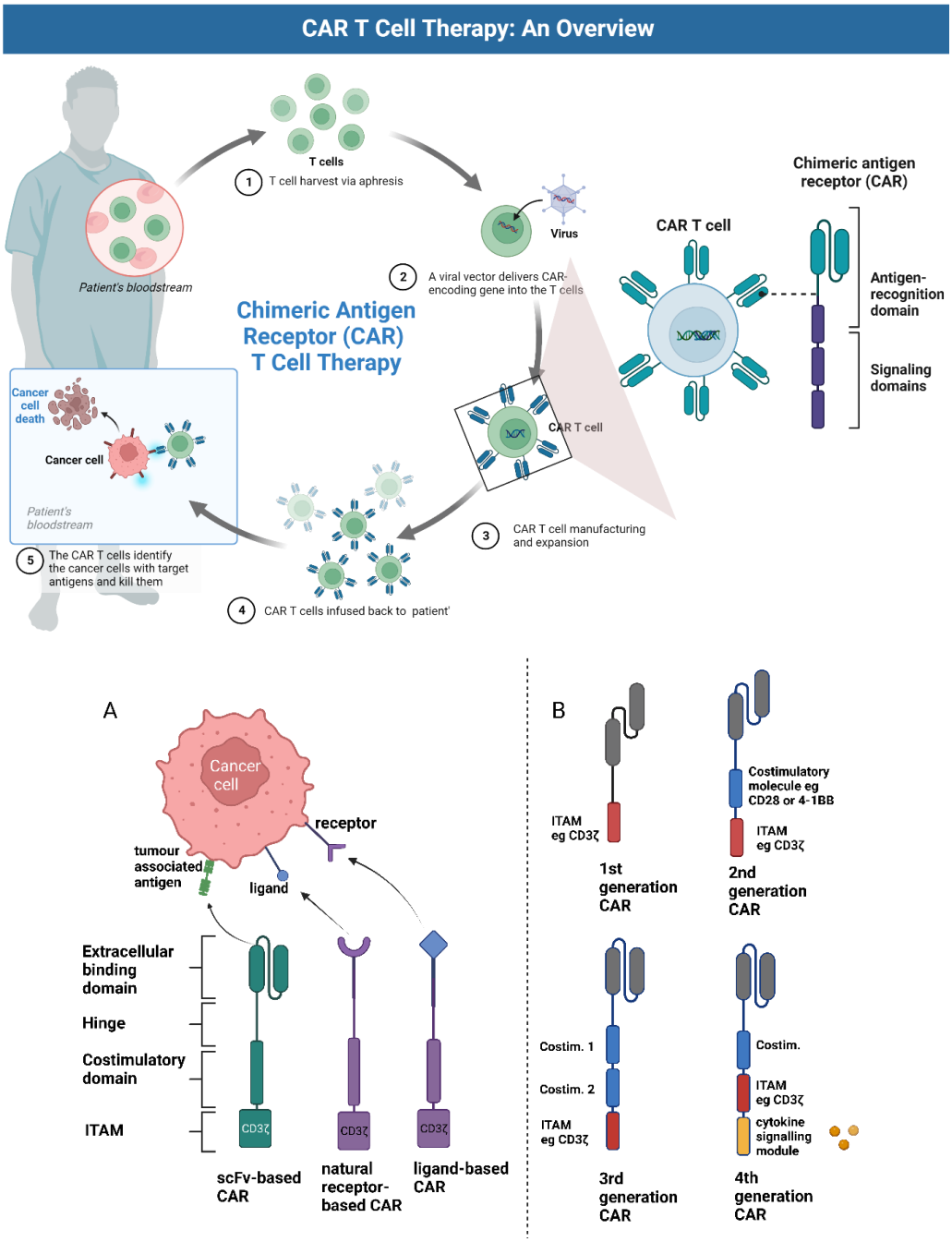

Figure 1-2: Overview of chimeric antigen receptor (CAR) therapy. Current clinical CAR T cell therapies are based on engineering of the patient's own cells with a synthetic receptor targeting a tumour associated antigen. Following successful CAR transduction, the cells are re-infused to the patient usually following lymphodepleting conditioning. **Below: Structure of the Chimeric Antigen Receptor (CAR).** (A) Schematic illustration of the binding strategies for target cell engagement by the chimeric antigen receptor. Conventional scFv CARs are based on antigen-antibody fragment interactions. Natural receptor-ligand interactions are alternative binding strategies for CARs. (B) Evolution of CAR generations. First generation CARs included one intracellular domain composed of an immunoreceptor tyrosine-based activation motif (ITAM) molecule, usually CD3ζ. Second and third generation CARs include one and two additional costimulatory intracellular domains respectively. Fourth generation CARs include a transgene eg cytokine-producing CARs.[307] This figure was created with biorender.com.

1.6.2 CAR binding domains

The single chain variable fragment (scFv) is the most common CAR binder in clinical CAR products. The scFv binder is usually derived from a murine heavy (V_H) and light chain (V_L) variable regions linked by a peptide sequence.[102] Alternative non-ScFv binders utilizing antibody fragments have been developed and these include single domain antibody fragments (sdAb) which are derived from camelid heavy chains (V_HH). SdAbs offer potential advantages over scFvs as they are smaller, more stable and can access cryptic epitopes.[103] A CAR T cell product utilizing two sdAb fragments, ciltacabtagene autoleucel (Cilta-cel), has recently been approved by the FDA for the treatment of relapsed and refractory multiple myeloma.[104] Results from the landmark CARTITUDE-1 trial reported deeper and longer duration of responses for Cilta-cel [105] compared with trial data for Idecabtagene vicleucel (Ide-cel)[106] even though they both target the same B-cell Maturation Antigen (BCMA). Furthermore, other non-antibody-based CAR binders utilize natural receptor-ligand interactions for T cell engagement and activation and these are summarised in figure 1-2A.[107–109] The advantages of these receptor and ligand-based binders approach include potential low cost of development and reduced immunogenicity of the natural receptor/ligand but unwanted effects e.g. increased proliferation from target cell activation via receptor-ligand interaction and lack of ligand specificity are potential drawbacks.

1.6.3 CAR Signalling domains

CD28 and 4-1BB are the commonly used co-stimulatory molecules in clinical CAR T cell products with 4 out of the 6 FDA-approved products being based on the latter. Several other co-stimulatory molecules belonging to the Immunoglobulin (Ig) and TNF receptor superfamilies including CD80, CD86, OX40L, Inducible co-stimulatory molecule (ICOS) have been used in experimental CAR constructs.[110] [111] While CD28 and 4-1BB co-stimulatory molecules have not been compared head-to-head in large Phase III clinical trials, preclinical studies and observations from patients suggest the latter may enhance CAR T cell persistence.[112][113] Furthermore, the choice of co-stimulation has been shown to determine the phenotypes of T cells with 4-1BB co-stimulation promoting CD8+ central memory T cells in contrast to CD28 which promotes effector memory T cell phenotype.[114] A small Phase I/IIa study directly comparing CD28 co-stimulation against 4-1BB in a CD19-specific CAR construct in patients with B cell Non-Hodgkin lymphoma, found similar clinical efficacy between the two constructs but the CD28 arm was discontinued due to a higher rate of severe cytokine release syndrome (CRS) although the hinge and transmembrane domains were different in either construct.[115] Recently, data has emerged suggesting distinct mechanisms for T cell dysfunction following chronic stimulation between CD28 and 4-1BB-based CARs. While CD28-based CARs activate classical exhaustion pathways characterised by expression of PD1, LAG3 and TIM3, 4-1BB-based CARs activate a novel pathway characterised by increased FOXO3 activity with low expression of the classical exhaustion markers.[116] Furthermore, some studies have suggested enhanced functionality with co-expression of CD28 and 4-1BB.[117,118] There is currently no consensus on an ideal co-stimulatory molecule and further studies are required to determine their impact on CAR functionality in specific contexts.

1.6.4 Obstacles to CAR T cell efficacy in solid tumours

The field of CAR T cell therapy has seen significant advancements with 6 products approved by the United States' Food and Drug Administration (FDA) as of February 2023 (Table 1-1). Notably, all the indications are for haematological malignancies and there are currently no licenced CAR T cell products for solid tumours. Published results of early phase clinical trials of CAR T cells in solid tumours have not shown much efficacy although several ongoing clinical trials have not been reported.[119][120] Several possible reasons have been postulated for the lack of progress in the solid tumour context. First, unlike B-cell malignancies in which targeting CD19, almost exclusively expressed on B cells means there is little risk of on-target, off-tumour toxicity, there is a lack of such ideal tumour targets in many solid cancers. In addition, the resulting B cell aplasia following anti-CD19 CAR therapy is tolerable as hypogammaglobulinemia can be managed with immunoglobulin infusions. A similar depletion of cells expressing a ubiquitous tumour-associated antigen (TAA) would result in unacceptable toxicity. Significant heterogeneity in expression of TAAs in solid tumours also limits the success of CAR targeting and potentially results in treatment failure due to selection of antigen-low or negative clones. Despite the absence of an ideal solid tumour target, a few antigens which are overexpressed in solid tumours have been targeted in experimental models and early phase clinical trials. These include Epidermal Growth Factor Receptor (EGFR), B7-H3, human epidermal growth factor receptor 2 (HER2) and carcinoembryonic antigen (CEA).[121]

Furthermore, the solid tumour microenvironment is now recognized to be hostile to immune cells as a result of a number of factors including the expression of inhibitory ligands such as PD-L1, infiltrating immune regulatory cells, intratumoural hypoxia and

physical barriers to immune cell infiltration e.g. the blood-brain barrier.[122,123] Current research efforts to overcome these obstacles include the use of unconventional T cells including gamma delta T cells and Natural Killer (NK) cells, expression of stimulatory cytokines and hypoxia-inducible expression of the CAR.[124,125]

1.6.5 Unconventional immune cells as vehicles for CAR therapy.

Current FDA-approved CAR products are based on unselected CD3+ lymphocytes with most of the cells bearing the αβ TCR. Due to the graft-host MHC mismatch and consequent risk of graft versus host disease, these products are currently limited to autologous use. The quest for cell products which can be used in the allogeneic setting has led to the investigation of non-MHC restricted immune cells for use as CAR effectors.

Gamma delta T cells, invariant natural Killer T (iNKT) cells and Natural killer (NK) cells are attractive candidates for immune therapy as their MHC-independent antigen recognition mechanisms make them ideal for allogeneic use. The most appealing feature of these cells is the potential for use as an “off the shelf” product. In this highly desired situation, the effector cells are harvested from the peripheral blood of a healthy donor, expanded in the lab and transduced with the CAR and either stored or made available for multiple patients. Several clinical trials using these unconventional immune cells as CAR effectors both in autologous and allogeneic settings are ongoing. Early phase clinical trial data has shown allogeneic anti-CD19 CAR-NK to be safe even in HLA-mismatched recipients with CD19 positive haematological cancers without evidence of cytokine release syndrome or graft-versus-host disease in the 11 study participants.[126]

Allogeneic CAR cell products would greatly cut the cost of production and eliminate the wait time for manufacturing of autologous products. An off-the-shelf cell therapy product could also be standardised to ensure consistent cell composition and quality.

1.6.6 Clinical trials for CAR products in solid tumours

Several clinical trials of CAR T cells in solid tumours have been reported and these have been almost exclusively early phase trials. A Phase 1/2 clinical trial of a 3rd generation GD2-targeting CAR in children (n=27) with relapsed or refractory neuroblastoma was recently published.[127] The toxicities reported were mainly cytokine release syndrome (CRS) and cytopenias. A complete response (CR) was observed in 33% of participants and this response was maintained over a median follow up duration of 1.7 years in 5 of the 9 patients achieving a CR. Another dose-escalation Phase 1 clinical trial of a GD2-specific CAR administered intravenously with a subsequent intracerebral(ventricle) infusion in patients with diffuse intrinsic pontine glioma (DIPG) demonstrated safety with no on target, off tumour toxicity reported.[128] However, a new syndrome of CAR T-mediated tumour inflammation-associated neuropathy (TIAN), manifesting as transient worsening of existing neurological deficits, was described. Another phase 1 clinical trial of B7-H3 targeting CAR T cells administered by repeated intracranial administration to children with DIPG demonstrated remarkable safety for this route of administration.[129] No dose limited toxicities were reported in 3 patients receiving a total of 40 intracranial infusions.

In a first-in-human clinical trial, CAR T cells targeting Epidermal growth factor receptor variant III (EGFRvIII) were administered intravenously to 10 patients with

recurrent glioblastoma and no clinical CRS events were reported.[130] Interestingly, in some patients subsequently treated surgically, EGFRvIII CAR T cells were detected in brain specimens up to 2 months following the infusion of CAR T cells indicating successful trafficking of CAR T cells into the CNS.

Unfortunately, severe on-target, off-tumour toxicity resulting in death was reported following administration of ERBB2-specific CAR T cells to a patient with metastatic colon cancer with widespread metastases to the lungs and liver.[131] The patient developed sudden respiratory distress shortly after the infusion of a single dose of 10^{10} CAR T cells, suffered multi-organ failure and succumbed within 5 days. The authors recommended a dose escalation approach, starting with the lowest possible dose, to avoid similar tragic outcomes in future first-in-man CAR T cell trials.

Furthermore, several clinical trials for CAR T cells for solid tumours are ongoing and have yet to be reported. These include Phase 1 trials of B7-H3 directed CAR T cells against ovarian cancer,[132] glioblastoma,[133] lung and triple negative breast cancer (together with EGFR-targeting),[134] advanced hepatocellular cancer[135] and pancreatic cancer.[136] Interestingly, there are a number of ongoing or planned trials of allogeneic CAR therapy using NK cells[137] and γδ T cells[138] against solid tumours.

In summary, results from published early phase clinical trials of CAR T cells in solid tumours indicate that this therapy could be safely administered to selected patients and while some early signals of efficacy are emerging, larger clinical trials are required.

Brand name	Company	Target	Co-stimulatory domain	Indication(s)
KYMRIAH (tisagenlecleucel)	Novartis	CD19	4-1BB (CD137)	Paediatric and Young Adult relapsed/refractory (r/r) B-cell ALL, Adult r/r Diffuse Large B Cell Lymphoma, adult r/r follicular lymphoma
YESCARTA (Axicabtagene ciloleucel)	Kite Pharma Inc	CD19	CD28	Adult r/r large B-cell lymphoma
TECARTUS (brexucabtagene autoleucel)	Kite Pharma Inc	CD19	CD28	Adult r/r mantle cell lymphoma (MCL). Adult r/r B-cell precursor acute lymphoblastic leukaemia (ALL)
ABECMA (idecabtagene vicleucel)	Celgene Corporation/ Bristol-Myers Squibb	B cell Maturation Antigen (BCMA)	4-1BB	Adult r/r multiple myeloma after four or more prior lines of therapy
BREYANZI (lisocabtagene maraleucel)	Juno Therapeutics, Inc., /Bristol-Myers Squibb	CD19	4-1BB	Adult r/r large B-cell lymphoma, primary mediastinal large B-cell lymphoma, and follicular lymphoma grade 3B.
CARVYKTI (ciltacabtagene autoleucel)	Janssen Biotech, Inc.	B cell Maturation Antigen (BCMA)	4-1BB	Adult r/r multiple myeloma previously treated with a proteosome inhibitor, an immunomodulatory agent and an anti-CD38 antibody.

Table 1-1: FDA-approved CAR T cell products as of 24 February 2023.[139]

1.7 B7-H3 as a targetable cancer antigen

B7 homolog 3 protein (B7-H3 or CD276), a type I transmembrane protein belonging to the immunoglobulin (Ig) superfamily which was first discovered in 2001, was initially thought to bind to a putative receptor (which has yet to be identified) on activated T cells to induce proliferation of CD4+ and CD8+ T cells.[140] Human B7-H3 has 2 isoforms; 2IgB7-H3 and 4IgB7-H3, the latter is the main isoform expressed in malignant cells.[141] While human B7-H3 mRNA can be detected in a wide range of tissues, the protein is only minimally expressed in normal tissues. Resting peripheral blood leucocytes do not express B7-H3 but its expression is inducible on dendritic cells and monocytes.[142] In the light of contrasting initial results, murine experiments subsequently showed that B7-H3 inhibited T cell proliferation, an effect which was overcome by CD28 co-stimulation.[143] Alongside other notable B7 family members which include B7-H1 (PD-L1), B7-1 (CD80) and B7-2(CD86), B7-H3 is now considered to be an inhibitory checkpoint molecule. The inhibitory role of B7-H3 was evidenced from the observation that B7-H3 knockout mice had a tendency to develop autoimmune disease.[144] B7-H3 inhibition in tumour-bearing mice suppressed tumour growth [145] and a synergistic effect was observed with co-administration of antibodies against B7-H3 and PD-1.[146] Furthermore, B7-H3 overexpression in various human cancers including glioblastoma, breast, pancreatic, colorectal, liver, lung cancers is often associated with a poor prognosis.[147][148][149] Overexpression of B7-H3 in glioma cell lines resulted in increased transwell migration and invasion while B7-H3 knockdown had the opposite effect.[147]

Given its overexpression across a broad range of cancers and its role as an immune regulator, considerable efforts are being channelled into developing immune therapies targeting B7H3. A humanised monoclonal antibody, enoblituzumab, is currently being

investigated for use across a broad range of B7-H3 expressing tumours and preliminary data suggests a favourable safety profile with no severe immune-related adverse events.[150] A Phase 2 single-arm clinical trial of enoblituzumab as a neoadjuvant therapy in men with operable prostate cancer[151] recently reported grade 3 adverse events (AEs) in 12% of the study population (n=32) these were infusion-related reactions, elevated lipase/amylase, hypotension and pericarditis. No Grade 4 AEs were reported and further large clinical trials are planned. Omburtamab, a murine IgG1 B7-H3 targeting monoclonal antibody conjugated to radioactive Iodine (^{124}I) has also been shown to be safe in Phase 1 clinical trials in patients with central nervous system (CNS) metastases.[152] The radioiodinated antibody was administered directly into the cerebrospinal fluid (CSF) via an intraventricular access device and the most common toxicity reported was Grade 3 or 4 thrombocytopenia.

Indeed, B7-H3 would be an ideal target for CAR T cell therapy as “on-target, off-tumour” side effects could be minimised due to minimal expression in healthy tissues. Furthermore, a combination of strategies including loco-regional administration of CAR T cells and conditional CAR expression within the tumour microenvironment would further minimize the risk of on-target, off tumour toxicity.

1.8 Strategies for optimising cellular immunotherapy in solid tumours.

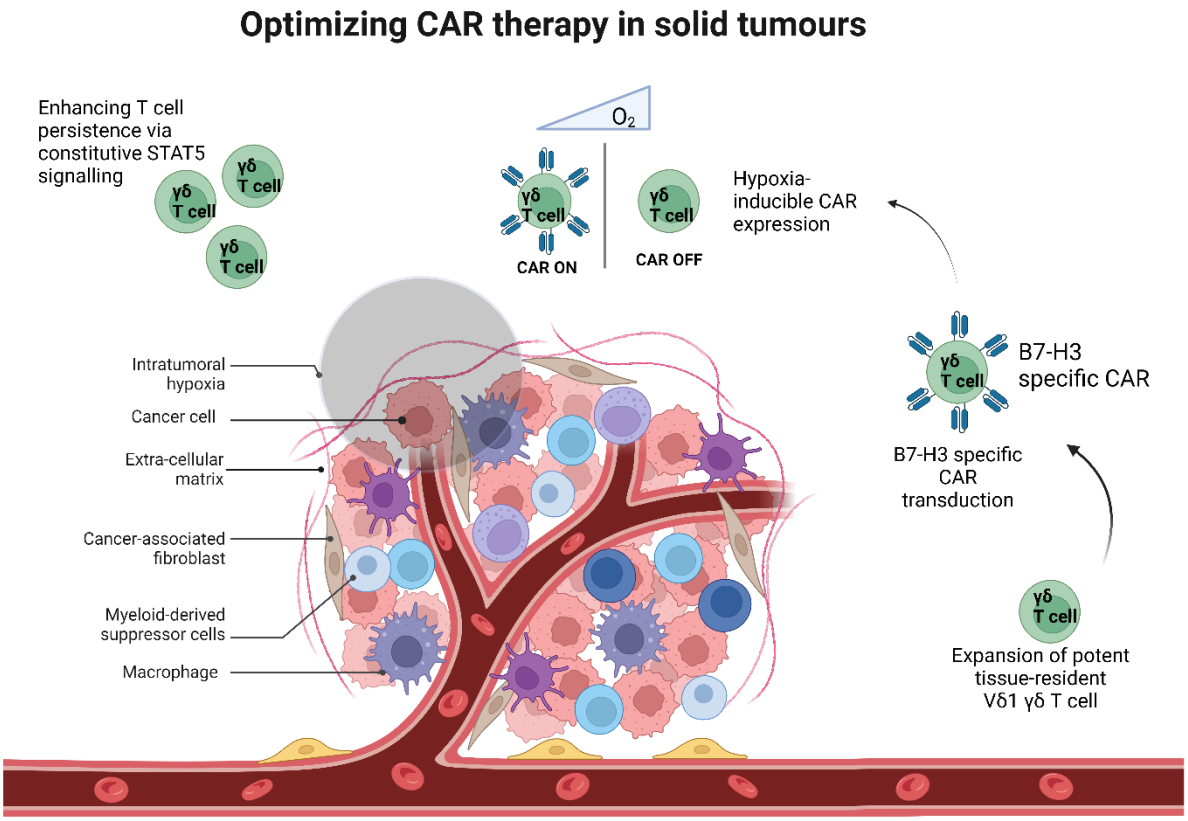

Figure 1-3. Strategies for optimising CAR therapy for solid tumours. The tumour microenvironment includes several physical and cellular components which support malignant cells. These include intratumoural hypoxia, cancer associated fibroblasts, regulatory immune cells such as myeloid-derived suppressor cells and macrophages. To overcome these challenges, the use of tissue-resident immune cells such as Vδ1 T cell transduced with a CAR targeting tumour associated antigens, hypoxia-inducible CAR expression and pro-survival signals such as constitutive activation of STAT5 will be explored in this project. CAR, chimeric antigen receptor. This figure was created with biorender.com.

In contrast to haematological cancers, several unique challenges exist which impede the efficacy of cellular immunotherapy in solid tumours (Figure 1-3). First, to exert their anti-tumour effects, immune cells need to access the site of the tumour and this can be impeded by physical barriers such as the blood-brain barrier. Since current clinical CAR T cell products are administered intravenously, immune cell trafficking and infiltration into immune-privileged sites such as the central nervous system, eye

and testes is limited. To overcome this barrier, loco-regional administration of cell products has been attempted. B7-H3 targeting CAR T cells were safely infused intracranially in a patient with glioblastoma and a transient tumour response was observed without toxicities of grade 3 or higher.[153] Similarly, multiple infusions of CAR T cells targeting IL13Rα2 were successfully administered intracranially in a patient with recurrent glioblastoma resulting in tumour regression, a response that was maintained for 7.5 months.[154] The loco-regional administration of CAR T cells may also minimize on-target off tumour toxicity in situations where the target antigen is expressed in healthy tissues.

Furthermore, some immune effectors such as Vδ1 γδ T cells naturally home to peripheral tissues where they are involved in tumour immunosurveillance via sensing of stress signals. Therefore, the use of these immune cells as cell therapy products, in theory, should offer significant advantages over conventional T cells. The tumour-targeting properties of these cells can be further enhanced by transduction of a CAR against tumour-associated antigens. As previously described, B7-H3 is an attractive target due to its high expression in a wide range of tumours, minimal expression in healthy tissues and its association with aggressive tumour phenotypes.

Intertumoral hypoxia offers another challenge to immune cell infiltration of the TME. Cancer cells often adapt their metabolic machinery to survive in the hypoxic TME by several mechanisms including stabilization of Hypoxia Inducible Factor (HIF). Hypoxia can also be exploited to achieve conditional CAR expression within the TME. A dual-oxygen sensing CAR construct, which is induced under hypoxic conditions and degraded by normoxia, was recently published.[125] This also offers a strategy to minimize unwanted toxicity in healthy tissues.

Finally, the lack of pro-survival signals in the TME could limit immune cell persistence and viability. Therefore, strategies supporting immune cells with transgenic cytokines or other pro-survival factors would potentially enhance CAR T cell fitness and efficacy. A constitutively-active STAT5B construct will be explored in this project.

1.9 Summary

Gamma delta T cells are highly potent immune cells with distinct but complementary roles to other immune effectors. A notable function of these cells is in immune surveillance against stressed or transformed cells. These cells are therefore ideal candidates for cell therapy against cancer. Chimeric antigen receptor therapy has emerged as a powerful tool in cancer immunotherapy and has shown remarkable efficacy in blood cancers however, several obstacles exist to its utilization in solid tumours. These obstacles include the lack of ideal tumour targets in solid tumours and the immunosuppressive tumour microenvironment. B7-H3 is an emerging rational target for solid tumours as it is overexpressed in a wide range of solid tumour but only minimally in healthy tissues. Therefore, achieving clinical efficacy for CAR therapy in the solid tumour context would require a combination of strategies including the use of highly potent immune effectors, novel targets and a host of innovative strategies to overcome the immunosuppressive microenvironment.

1.10 Project Objectives

The overarching objective of this research is to evaluate strategies to overcome on-target off tumour toxicity while enhancing the efficacy of CAR therapy in the solid tumour context. This will be addressed with these four specific objectives presented in the subsequent result chapters:

1) To optimise an expansion protocol for Vδ1 γδ T cells from peripheral blood.
2) To evaluate functional properties of Vδ1 γδ T cells transduced with a B7-H3 specific CAR.
3) To evaluate the impact of constitutively active STAT5B on IL-15 dependence in OKT3/IL-15 expanded γδ T cells.
4) To evaluate a dual hypoxia-sensing B7-H3 specific CAR construct.

CHAPTER II: MATERIALS AND METHODS

2.1 Cell culture

2.1.1 Cell culture media

2.1.1.1 Constitution of T cell culture medium

The complete serum-free, xeno-free T cell medium for expansion of PBMCs was constituted as follows; 50 millilitres (mls) of CTS™ Serum Replacement medium (Gibco, Life Technologies) was added to 1000 ml of CTS™ OpTmizer™ T-Cell Expansion SFM (Gibco, Life Technologies) and 26 ml of CTS™ OpTmizer™ T-Cell Expansion Supplement (Gibco, Life Technologies) as per manufacturer's recommendation. The resulting solution was supplemented with 10 ml of Penicillin/Streptomycin 100X (Gibco, Life Technologies) and 10 ml of Glutamax 100X (Gibco, Life Technologies). Storage was at 4^{o}C for up to 4 weeks.

2.1.1.2 Constitution of culture media for cell lines

Cell lines were maintained in the appropriate cell culture media as summarised in Appendix Table A1. The details of constitution of the cell culture media for cell lines are shown in Table 2-1.

Medium	Manufacturer	Supplements	Storage
RPMI 1640	Gibco	10% Foetal Calf Serum + 1:100 Glutamax (Gibco) +/- 1:100 Penicillin/Streptomycin (ThermoFisher)	Up to 21 days at 4ºC
Dulbecco's Modified Eagle Medium (DMEM)	Gibco	10% Foetal Calf Serum + 1:100 Glutamax (Gibco) +/- 1:100 Penicillin/Streptomycin (ThermoFisher)	Up to 21 days at 4ºC

Table 2-1: Details of the culture media for cell lines

2.1.2 Cell lines

Details of the cell lines, culture media and growth conditions are shown in Appendix Table A1. Apart from HEK293T, all cell lines were routinely grown in antibiotic-containing media and were regularly tested for bacterial contamination. All cell lines were grown in CellXpert C170i incubators (Eppendorf, Germany) set at 37ºC, 21% O_2 and 5% CO_2.

2.1.3 Cell counting

Cells were counted with either of two methods; manual counting was typically performed by resuspending 10 µl of cell suspension with 10 µl of Trypan Blue dye (ThermoFisher) (dilution factor of 2). The resulting suspension was loaded onto a

haemocytometer (Hausser Scientific) and cells were counted under the microscope. The final cell count was determined using the following formula:

Cell count/ml= number of cells in large haemocytometer square (1 mm^2) x Trypan Blue dilution factor x 10^4

An alternative counting method using a Countess 3 Automated Cell counter (Invitrogen) was used where large numbers of cells were to be enumerated. Cell counting was typically done in duplicate and mean values were recorded.

2.1.4 Propagation of adherent cell lines

Adherent cell lines were grown in appropriately sized flasks until about 80% confluence. They were subsequently passaged as follows; the spent culture media was gently aspirated without disturbing the cell layer and rinsed with Phosphate buffered saline (Sigma). This was followed by cellular dissociation with the addition of 3-5 mls of either Trypsin-EDTA or TrypLE^{TM} Express Enzyme (Thermofisher) incubated at 37^{o}C for 5 minutes. This was followed by the addition of excess fresh complete media and centrifugation at 400 x *g* for 5 minutes. The pellets were resuspended with fresh complete media and split 1:5 to 1:10. The cell lines were resuspended in complete media and incubated until the desired confluence was achieved.

2.1.5 Propagation of non-adherent cell lines

Non-adherent cell lines were maintained at densities of 0.2 - 1 x10^6/ml. To maintain this cell density, the cell lines were split as appropriate; the cell suspension was

aspirated from the culture flask and centrifuged at 400 x *g* for 5 minutes. The resulting cell pellet was resuspended in fresh complete media and split as appropriate. Cell passage was repeated every 2-4 days as required.

2.1.6 Cryopreservation and recovery of cell lines and PBMCs

Cell lines and PBMCs were centrifuged at 300 x *g* and the pellets were resuspended in freshly constituted freezing media composed of Foetal Calf Serum (FCS) (Gibco, Life Technologies) and 10% Dimethyl Sulfoxide (DMSO) (Sigma). Cryovials containing cells resuspended in freezing media were immediately transferred into Mr Frosty™ Freezing Containers (Thermo Scientific) and kept in a -80°C freezer or liquid nitrogen vapour phase for long term storage.

Cells recovery was performed by rapid thawing of each cryovial in a 37°C water bath followed by resuspension in 9 ml of the complete cell culture medium for each cell line and centrifugation at 300 x *g* for 5 minutes. The supernatant was discarded, and the cell pellet was subsequently resuspended in the appropriate cell culture medium in the required cell density.

2.2 Peripheral Blood mononuclear cell (PBMC) isolation and expansion

2.2.1 PBMC Isolation by Density Gradient Centrifugation

Peripheral blood cones obtained from healthy volunteer donors via the National Health Service Blood and Transplant (NHSBT) were collected in 50 ml tubes and diluted 1:1 with cold Phosphate Buffered Saline (PBS) (Sigma). The resulting solution was carefully layered onto Lymphopure™ reagent (Biolegend). The tubes were centrifuged

at 800 x *g* for 20 minutes at 20^{o}C without braking. Following clear separation of blood components, the intermediate mononuclear leucocyte layer was carefully aspirated using a 1ml pipette and transferred into a separate tube. The separated mononuclear cell layer was washed once with PBS by centrifuging at 300 x *g* for 5 minutes. The pellet was subsequently incubated for 5 minutes at room temperature with 5 ml of Ammonium-Chloride-Potassium (ACK) red cell lysis buffer (Lonza). Excess PBS was added to stop the reaction and subsequently centrifuged at 300 x *g* for 5 minutes. The cell pellet was resuspended in complete T cell media.

2.2.2 Alpha/Beta T cell and CD56 depletion by Magnetic-Activated Cell Sorting

Magnetic-Activated Cell Sorting (MACS) buffer was constituted by adding 0.5% Bovine Serum Albumin (Sigma-Aldrich) and 2 mM Ethylenediaminetetraacetic acid (EDTA) (Invitrogen) to 1000 ml of PBS. Following 12-18 hours of incubation in complete T cell media at 37^{o}C and 5% CO_2, PBMCs were counted and resuspended in 80 µl of freshly constituted MACS buffer per 10^7 PBMCs. A biotinylated antibody against human Alpha/Beta T cell Receptor (TCR) was added in manufacturer recommended volumes. The mixture was incubated for 20 minutes on ice. Following a wash step, anti-biotin magnetic microbeads (Miltenyi) and CD56 microbeads (Miltenyi) were added and incubated for 20 minutes on ice. Following incubation, PBMCs were washed with MACS buffer and resuspended in 500 µl per 10^7 PBMCs (appropriately scaled up for larger cell numbers). The mixture was run through MACS LD separation columns (Miltenyi) attached to a strong magnetic field according to manufacturer's recommendation. The LD column works on the principle of negative selection i.e., labelled cells bound to the biotin microbeads were retained within the column while the flowthrough containing the desired, unlabelled cells were collected in a falcon tube,

subsequently washed and plated in the appropriate culture medium. Depletion of alpha/beta T cells and CD56+ cells was confirmed by flow cytometry.

2.2.3 CliniMACS TCR α/β –Biotin antibody titration

To determine if the manufacturer recommended volume of antibody was optimal, an antibody titration was performed. Using the TCR α/β depletion method described above, increasing volumes of CliniMACS TCR α/β-Biotin were added to 10^7 PBMCs and the proportion of residual αβ T cells post depletion was determined by flow cytometry.

2.2.4 Expansion of Vδ1 gamma delta T cells with PHA

Alpha/Beta (αβ) TCR and CD56 depleted PBMCs were maintained at a density of $2x10^6$ cells/ml in 96-well U-bottom culture plates (Falcon). PBMCs were expanded in complete T cell medium supplemented with 1 µg/ml of Phytohaemagglutinin (Leucoagglutinin, PHA-L) (Merck) and either 20 ng/ml of IL-7 (Peprotech) or 200 U/ml of IL-2. The culture medium was refreshed every 2-3 days with complete media supplemented with 1 µg/ml of PHA-L plus either 20 ng/ml of IL-7 or 200 U/ml of IL-2. Aliquots of expanded cells were analysed by flow cytometry every 5-7 days.

2.2.5 Purification of Vδ1 T cells

For purification of expanded Vδ1 T lymphocytes, the cells were washed and resuspended in MACS buffer. This was followed by the addition of 2 µl of CliniMACS TCR αβ biotinylated antibody (Miltenyi) and 2 µl of anti-Vδ2 (Miltenyi) per 10^6 expanded cells in a 100 µl volume of MACS buffer. The cells were incubated for 20

minutes and washed with MACS buffer followed by incubation with anti-biotin immunomagnetic beads for 30 minutes. The cells were washed and resuspended in MACS buffer and run through MACS LD columns (Miltenyi). The desired flowthrough suspension depleted of residual αβ and Vδ2 T cells was collected and analysed by flow cytometry.

2.2.6 *Ex vivo* expansion of Vdelta1 gamma delta T cells with anti-CD3 and IL-15

Alpha/Beta (αβ) TCR and CD56 depleted PBMCs maintained at a density of $2x10^6$ cells/ml in 96-well U-bottom culture plates (Falcon) were expanded in complete T cell medium supplemented with 1 µg/ml of pure anti-CD3 (OKT3 clone) (Miltenyi) and 100ng/ml of Interleukin-15 (Peprotech). Cells were incubated at 37^{o}C and 5% CO_2. Following 2-3 days of incubation, spent media was carefully aspirated and replaced with fresh complete media supplemented with 100ng/ml of IL-15 only. Cell media was similarly changed every 2-3 days as required. Aliquots of expanded cells were collected every 5-7 days and analysed by flow cytometry for expansion of the Vδ1+ compartment. The Vδ1 expansion methods used are summarised in Figure 2-1.

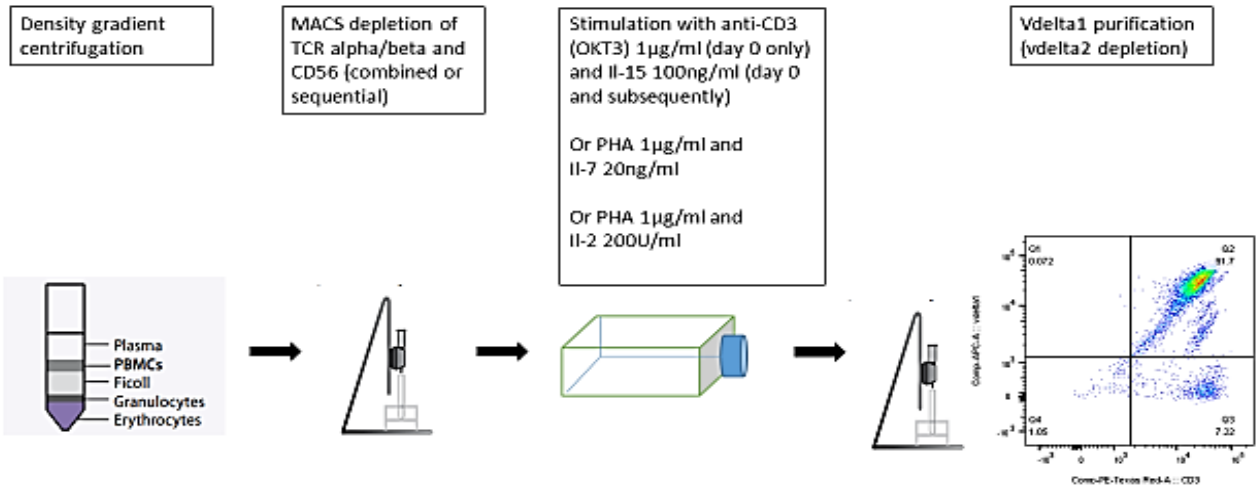

Figure 2-1. Summary of Vδ1 T cell expansion methods. Peripheral blood mononuclear cells (PBMCs) were isolated from peripheral blood of healthy donors. Following MACS depletion of immunomagnetically labelled αβ T cells and CD56+ cells, the cells were stimulated with 1µg/ml of anti-CD3 (OKT3) and 100ng/ml of IL-15. This OKT3/IL-15 method was compared with PHA-based methods using 1µg/ml of PHA-L plus either 20ng/ml of IL-7 or 200U/ml of IL-2. PHA, phytohemagglutinin. MACS, magnetic activated cell sorting. IL, Interleukin.

2.3 Flow cytometry

2.3.1 Flow cytometry for cell surface markers and gating strategy

Appropriate volumes of cells to be analysed were collected and resuspended in 100 µl of cold Cell Staining buffer (Biolegend) per 10^6 cells. Fc receptor blocking was done by adding 2 µl of Human FcR Blocking reagent (Miltenyi) per 10^6 cells and incubating at room temperature for 5 minutes. Appropriate mastermixes of fluorophore-conjugated antibodies (with an appropriate viability dye) were added in manufacturer recommended volumes. The mixture was subsequently incubated on ice for 20 minutes. Thereafter, the cells were washed once with PBS. A known volume of Precision Count Beads (Biolegend) was added where cell enumeration was desired. Where indicated, compensation controls using OneComp Beads (Invitrogen) stained with single antibodies were set up alongside test samples. Cells were acquired on LSR II Flow cytometer (BD Biosciences). The Subsequent analyses of flow cytometry data were done using FlowJo software version 10.7.1 (BD Life Sciences).

For basic T cell phenotyping, fluorophore-conjugated monoclonal antibodies against human CD3, TCR alpha/beta, Vδ2 and Vδ1 were used in addition to a viability dye. Precision count beads (Biolegend) were added for enumeration as required. Appendix Table A2 shows the list of antibodies used in this project. The gating strategy was as follows (Figure 2-2): A lymphocyte gate was first applied based on forward and side scatter properties followed by doublet exclusion on forward and side scatter. Live cells were then gated based on viability dye exclusion. Gamma delta (γδ) T cells were gated as $CD3^{pos}TCR\alpha/\beta^{neg}$ while Vdelta1+ gamma delta cells were positively identified as $CD3^{pos}$ Vdelta1 TCR^{pos}.

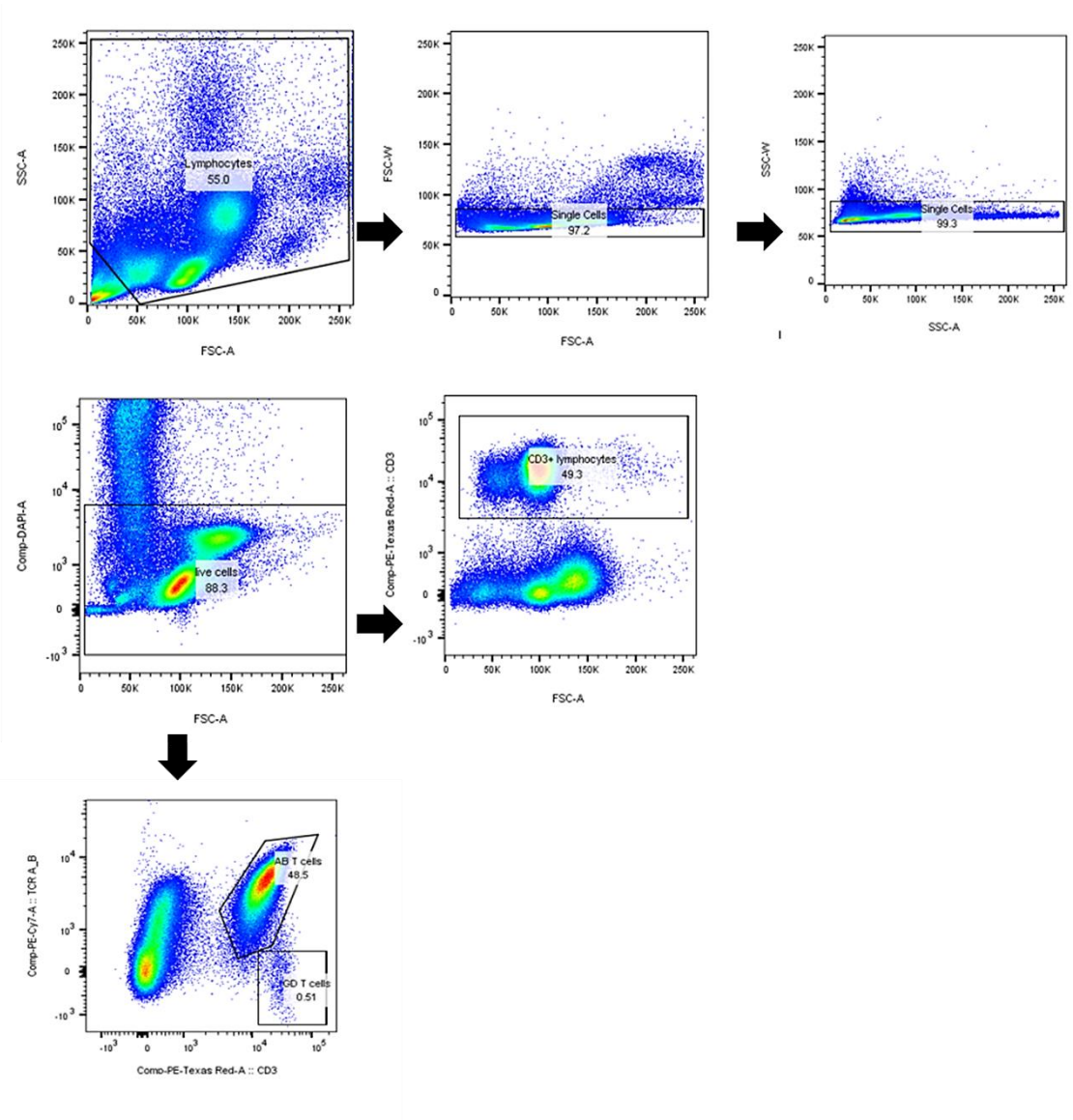

Figure 2-2. Flow cytometry gating strategy for PBMC characterisation. An initial gate on forward and side scatter was set to exclude cellular debris followed by doublet exclusion. Live cells were determined by viability dye exclusion. Various T cell populations were determined by surface staining for CD3 and αβ TCR, Vδ1 TCR or Vδ2 TCR. TCR, T cell receptor.

2.3.2 Intracellular flow cytometry

For staining of intracellular antigens, up to 10^6 cells per test were washed and resuspended in Cell staining buffer (Biolegend). In experiments where intracellular cytokines were to be determined in co-culture conditions, cells were treated with a 1x solution of Brefeldin A or Monensin (Biolegend) in the last 4 hours of incubation. Thereafter, staining for surface antigens was first performed with fluorophore-conjugated antibodies and a fixable viability dye as previously described. This was followed by the addition of excess buffer and centrifugation at 300 x *g* for 5 minutes. All subsequent wash steps were performed similarly. The cells were fixed by resuspending the pellet in 250 µl of 4% paraformaldehyde (Biolegend fixation buffer) per 10^6 cells at room temperature for 20 minutes. Following the fixation step, cells were washed twice with an excess of Intracellular staining permeabilization wash buffer (Biolegend) and resuspended in 50 µl of permeabilization buffer. Fluorophore-conjugated antibodies specific for intracellular antigens were added in volumes recommended by the manufacturer and incubated for 20 minutes at room temperature in the dark. This was followed by washing with excess permeabilization buffer. The cell pellet was then resuspended in cell staining buffer (Biolegend) and acquired on LSR II cytometer (BD Biosciences).

2.3.3 Phosphoflow cytometry

To assess STAT5 phosphorylation by flow cytometry, 0.5 - 1 million unstimulated (or IL-15 deprived for at least 48 hours) PBMCs were washed with PBS and resuspended in 100µl of PBS supplemented with or without IL-15 in various concentrations. Each cell culture condition was incubated for 60 minutes at 37^{o}C.

Subsequent sample preparation steps were on ice following the instructions of the Transcription Factor Phospho Buffer kit (BD Pharmigen). Briefly, following incubation, cells were washed twice with excess PBS by centrifuging at 1000 x *g* on a microcentrifuge (Eppendorf Centrifuge 5415R) for 1 minute each time. Antibodies against surface antigens and a fixable viability dye were added and incubated on ice for 20 minutes. Following a wash step, cells were resuspended with 1xFix/Perm buffer and incubated on ice for 50 minutes. The cells were subsequently washed with the 1xTranscription factor permeabilization (TFPerm) wash buffer and resuspended in Perm buffer III and incubated on ice for 20 minutes. This was followed by a wash step. The cell pellet was resuspended in 100 µl of 1xTFPerm wash buffer and 1µg/million cells of phosphoSTAT5 (pSTAT5) antibody (Biolegend) was added followed by incubation for 40 mins on ice. Cells were washed in 1xTFPerm wash buffer and resuspended in Cell staining buffer (Biolegend). Flow cytometry acquisition was on the LSRII cytometer (BD bioscience).

2.4 *In vitro* functional assays

2.4.1 Cytotoxicity assays

2.4.1.1 Chromium-51 Cytotoxicity assay

Tumour targets were incubated at 37^{o}C with 20 µl of Chromium-51 solution for 1 hour followed by five washes with excess complete media by centrifugation at 300 x *g* for 5 minutes. Serially diluted effectors were plated in 96-well U-bottom plate (Falcon). A pre-determined number of Chromium-51-labelled targets was added in the respective Effector-Target (E:T) ratios. Negative control (spontaneous release) wells containing target cells only and maximum release wells with 1% Triton X-100 (Sigma) were set

up alongside test wells. The resulting effector-target co-culture was incubated for 4 hours at 37ºC and subsequently centrifuged at 300 x *g* for 5 minutes to pellet cells. Fifty microliters of supernatant was carefully aspirated and transferred into fresh 96-well plates and 150 µl of scintillation cocktail (PerkinElmer, USA) was added. The plates were then kept at room temperature in the dark overnight. Radioactive wastes were disposed of following strict institutional protocols.

Scintillation values were recorded for each well using a 1450 MicroBeta Liquid Scintillation counter (PerkinElmer, Connecticut, USA). Specific lysis was calculated using the following formula:

$$\% \text{ Specific lysis} = \frac{(\text{Scintillation value in test well} - \text{scintillation value in spontaneous release})}{(\text{Scintillation value in maximum release} - \text{scintillation value in spontaneous release})} \times 100$$

2.4.1.2 CD107a (LAMP-1) Degranulation assay

To determine T cell degranulation in response to appropriate targets, co-culture conditions were set up with effectors and targets in 1:1 ratio in 96-well U-bottom plates. At the start of the co-culture, 1 µg of FITC-conjugated anti-CD107a (Biolegend) was added to each well and the plates were centrifuged at 300 x *g* for 5 minutes. The co-culture plates were incubated at 37ºC for 1 hour (for short term cultures) or overnight. The plates were retrieved from the incubator and Monensin or Brefeldin A (Biolegend) (supplied in 1000x stock concentrations) were added to the cell culture to a final concentration of 1:1000. The plates were returned to the incubator for 4 hours. Thereafter, the cells were retrieved and analysed by flow cytometry.

2.4.2 CellTrace Violet Proliferation assay

The cell lines and PBMCs to be labelled were counted and washed with PBS. A working solution of CellTrace™ Violet (Thermofisher) in DMSO was constituted following the manufacturer's instructions. The cells to be labelled were resuspended in PBS and CellTrace Violet solution was added to a final concentration of 5 µM. The cells were subsequently incubated at 37°C for 20 minutes. Excess complete media was added followed by incubation at 37°C for 5 minutes. The labelled cells were washed by addition of excess complete media and centrifugation at 300 x *g* for 5 minutes. Labelled cells were incubated at 37°C in complete T cell media with the appropriate stimulant(s) and assessed by flow cytometry after 5-7 days of culture.

2.4.3 Cytokine quantification by ELISA

Following co-culture with the appropriate stimulant for 24 hours, the culture plates were centrifuged at 300 x *g* for 5 minutes and the supernatants were gently aspirated and transferred to a new plate. Cytokine quantification was subsequently performed on diluted supernatants using the Deluxe ELISA kits (Biolegend) for IL-2 and Interferon-γ following manufacturer's instructions.

2.4.4 IL-15 Deprivation Experiment

Following 14 days of PBMC stimulation with anti-CD3 and IL-15, the culture medium was changed and replaced with complete medium without cytokines. A separate experimental condition with IL-2 replacing IL-15 was set up alongside a positive control condition with IL-15. Aliquots were taken and analysed at 48 and 96 hours for viability and Annexin V binding by flow cytometry.

2.4.5 Annexin V Binding assay

Cell suspensions were washed once with Annexin V Binding Buffer (Biolegend) and resuspended in 100 µl of Annexin V Binding Buffer per 10^6 cells or equivalent. Five microliters of Pacific Blue™ Annexin V (Biolegend) and 10 µL of Propidium Iodide Solution (Biolegend) or other viability dye were added to the suspension and incubated for 15 minutes at room temperature. Subsequently, 100 µL of Annexin V buffer was added prior to acquisition by flow cytometry.

2.5 Molecular Biology Methods

2.5.1 Bacterial transformation

A vial of 5-alpha competent *Escherichia coli* (New England Biolabs) was thawed on ice and up to 100 ng of plasmid DNA (see appendix Table A3 for details of the plasmids) was added to 50 µl of bacteria in a 200 µl microcentrifuge tube. The mixture was incubated on ice for 30 minutes followed by the heat shock process as follows; The mixture was transferred into a water bath set at 42^{o}C for 30 seconds immediately followed by incubation on ice for 2 minutes. The transformed bacteria suspension was added to 950 µl of SOC growth medium (supplied with the *E.coli* kit) and incubated at 37^{o}C for 40-60 minutes in an Innova S44i bacteria shaker (Eppendorf, Hamburg, Germany) at 250 revolutions per minute (rpm). The incubated bacteria suspension was subsequently retrieved and 50 µl of the mixture was plated onto agar plates containing the relevant selection antibiotic. The agar plate was incubated at 37^{o}C overnight (12-16 hours).

2.5.2 Polymerase Chain Reaction (PCR)

For PCR amplification of DNA fragments, the Phusion® High Fidelity PCR kit (Cat no: E0553S; New England Biolabs) was used. The typical PCR reaction was set up on ice as summarised in Table 2-2. The cycling conditions were as follows: 30 seconds of initial denaturation at 98ºC, followed by 30-35 cycles of denaturation at 98ºC (10 seconds), annealing at 72ºC (30 seconds) and extension at 72ºC (15-30 seconds/kb of amplicon) followed by a final extension step at 72ºC for 5-10 minutes. Cycling conditions were optimised for every PCR reaction as appropriate.

Component	**25 µl reaction**	**50 µl reaction**
Phusion DNA polymerase	0.25 µl	0.5 µl
5x Phusion high fidelity buffer	5 µl	10 µl
10uM forward primer	1.25 µl	2.5 µl
10uM reverse primer	1.25 µl	2.5 µl
10mM dNTPs	0.5 µl	1 µl
Template DNA	variable	Variable
Nuclease Free water	variable	variable
Total	**25 µl**	**50 µl**

Table 2-2: Composition of a typical PCR reaction

2.5.3 Miniprep Plasmid DNA purification

Individual bacterial colonies were selected from agar plates incubated overnight and transferred into 5 mls of LB Broth (Merck, Germany) containing the relevant antibiotic (see appendix A4). The mixture was incubated at 37^{o}C for 12-14 hours in an Innova S44i bacteria shaker (Eppendorf, Hamburg, Germany) at 250 rpm. The bacteria cultures were pelleted by centrifugation at 4500 x *g* for 5 minutes and the pellets were resuspended in the resuspension buffer in the Qiagen Spin Miniprep kit (Qiagen). The subsequent steps were as directed in the manufacturer's manual. Plasmid DNA concentration was assessed using a NanoDrop™ One Microvolume UV-Vis Spectrophotometer (Thermofisher).

2.5.4 Midiprep Plasmid DNA purification

For purification of larger amounts of plasmid DNA, the NucleoBond Xtra Midi kit (Macherey-Nagel) was used. In brief, up to 200 ml of overnight bacterial culture was centrifuged at 4500 x *g* at 4^{o}C for 30 minutes. The pellet was resuspended in the resuspension buffer supplied in the kit. The subsequent steps were as directed in the manufacturer's manual. Plasmid DNA concentration was assessed using a NanoDrop™ One Microvolume UV-Vis Spectrophotometer (Thermofisher).

2.5.5 Agarose gel electrophoresis

The electrophoresis gel was prepared by adding UltraPure^{TM} agarose (Invitrogen) to 1x Tris/Borate/EDTA (TBE) buffer (Geneflow) to a final concentration of 1%. The mixture was heated until dissolution of the agarose followed by addition of SYBR

Safe DNA gel stain (Invitrogen) in 1:10,000 volumes. The gel was transferred onto a tray with appropriate gel combs and cooled to solidification. For gel electrophoresis, DNA was mixed 1:5 with a DNA gel loading dye (Thermofisher) and added directly onto each lane on the gel. A DNA ladder (Thermofisher) was typically loaded onto the first well to guide estimation of DNA fragment size. The gel was typically run for 45-60 minutes at 125 volts.

2.5.6 Restriction digestion of plasmid DNA

For digestion of plasmid DNA, the reaction was set up as shown in Table 3. The mixture with the FastDigest enzymes (Thermofisher) was briefly spun down and incubated at 37^{o}C for 5 minutes. The digestion products were subsequently loaded directly onto an agarose gel for electrophoresis.

Component	Volume
Nuclease-free water	15 µl
10x FastDigest Green Buffer	2 µl
Plasmid DNA	2 µl (up to 1µg)
FastDigest enzyme	1 µl per enzyme
Total volume	**20 µl**

Table 2-3: Restriction digestion reaction composition

2.5.7 Gel purification

Following separation of digested DNA fragments by electrophoresis, the DNA fragment of interest was excised from the gel, weighed and transferred into a 1.5ml microcentrifuge tube. An equivalent volume of membrane binding solution supplied in the Wizard® SV Gel and PCR Clean-Up kit (Promega) was added and the mixture was incubated at 65^{o}C for 10 minutes or until the gel was completely dissolved. The dissolved gel was transferred into an SV mini-column assembly and centrifuged at 16,000 x *g* for 1 minute. The flow though liquid was discarded and the column was washed with 700 µl of Membrane Wash solution diluted with 95% ethanol. The column was transferred into a clean microcentrifuge tube and the purified DNA was

eluted with up to 50 µl of nuclease-free water. DNA concentration was assessed using a NanoDrop™ One Microvolume UV-Vis Spectrophotometer (Thermofisher).

2.5.8 DNA Ligation

Ligation of DNA fragments was performed using the Quick Ligase kit (New England Biolabs). The reaction mixture composed of 10 µl of the Quick Ligase reaction buffer, 1 µl of Quick Ligase enzyme and molar ratios of 1:3 vector to insert, was made up with nuclease-free water to a total reaction volume of 20 µl. The rection mixture was incubated at room temperature for 5 minutes. This was followed by bacterial transformation, as previously described, using 2 µl of the ligation product. The transformed bacteria were added onto Agar plates containing the relevant selection antibiotic and incubated at 37^{o}C overnight. Single bacteria colonies (clones) grown on the antibiotic-treated agar plates were selected and the plasmid DNA was purified by the miniprep method as previously described. The plasmid DNA from each clone was assessed for the presence of the correct ligation product by a screening restriction digest. Confirmation of the plasmid DNA sequence was by Sanger sequencing.

2.5.9 Sanger Sequencing

Approximately 100 ng of Plasmid DNA and relevant primers were sent to Source Bioscience (Cambridge, UK) for Sanger sequencing of the plasmid DNA. The obtained DNA sequence was compared with the expected DNA sequence using the National Centre for Biotechnology Information (NCBI) BLAST tool.[155]

2.6 Viral vector production and transduction

2.6.1 Retrovirus production

Plasmids encoding the expression vector, gag-pol and envelope were mixed in plain IMDM media (Sigma) and GeneJuice (Merck) as detailed in Table 4. The mixture was added onto the antibiotic-free cell culture medium of HEK293T cells which had been grown to a confluence of 50-60% in 10 cm round culture dishes (Corning). Transfected HEK293T cells were incubated at 37^{o}C and 5% CO_2. The cell culture media supernatant containing retroviral particles was subsequently harvested at 48 and 72 hours after transfection. The virus supernatant was either used immediately after harvest or snap-frozen and kept at -80^{o}C for future use.

Component	Quantity
Expression vector plasmid	4.6875 µg
Gag-pol	4.6875 µg
Envelope	3.1254 µg
GeneJuice	30 µl
IMDM plain medium	470 µl

Table 2-4: Gamma retrovirus transfection mixture composition per 10cm culture dish.

2.6.2 Retroviral transduction

Non-tissue-culture-treated 24-well plates (Falcon) were first coated with a 10 µg/ml solution of RetroNectin (Takara) and incubated at room temperature for 2 hours or overnight at 4°C. Thereafter, 5 x 10^5 cells to be transduced were plated in 500 µl volume per well and 1.5ml of virus supernatant was added to each well. The culture plates were centrifuged at 1000 x *g* for 40 minutes and subsequently incubated at 37°C and 5% CO_2 for 48 hours. Transduction efficiency was assessed by flow cytometry 48 hours after retroviral transduction.

2.7 Statistical analyses

All experiments (except in rare cases where, for technical reasons, this was not possible) were performed with a minimum of 3 technical and biological replicates. Statistical analyses of the data were performed with GraphPad Prism version 9.0. For comparison of differences of means for 2 groups, the T-test (for two groups) was used. For comparisons of 3 or more groups, the 2-way ANOVA statistical test was used. Differences in the distribution between categorical variables was determined by the chi-squared test. For correlation analysis, the Pearson Correlation Coefficient was computed. Statistical significance was set at 5%.

Error bars in figures represent standard error of means unless otherwise specified in the respective figure legends.

CHAPTER III: EVALUATION OF GAMMA DELTA (γδ) T CELL EXPANSION METHODS

3.1 Introduction

The immense potential for the clinical use of γδ T cells is increasingly being recognized hence significant efforts have gone into developing *ex vivo* expansion methods for these cells. This chapter reviews the literature for published expansion methods and evaluates a novel IL-15/anti-CD3 based Vδ1 γδ T cell expansion method.

3.2 Overview of Gamma Delta T cell expansion methods

3.2.1 Vδ2 expansion

The recognition of phosphoantigens (pAgs) by Vγ9δ2 cells has been successfully exploited in expanding these cells with bisphosphonates such as zoledronate (ZOL).[156] Nitrogen containing bisphosphonates (N-BPs) are currently used in inhibiting bone resorption in osteoporosis and metastatic bone disease through inhibition of farnesyl pyrophosphate synthase (FPPS) in osteoclasts which is required for protein prenylation.[157] FPPS inhibition leads to accumulation of its pAg substrates; isopentenyl diphosphate (IPP) and dimethylallyl diphosphate (DMAPP) in monocytes.[158] The mechanism described for the activation and expansion of Vγ9δ2 T cells in this scenario involves the sensing of pAgs by conformational changes in the butyrophylin proteins (reviewed in Chapter I).[159]

Furthermore, clinical trials of ZOL-expanded Vγ9δ2 in cancer patients have shown some interesting results. *In vivo* expansion of Vγ9δ2 cells was observed following

intravenous administration of ZOL (4mg every 21 days) and low-dose IL-2 (10^6 IU) in patients with advanced, chemotherapy-resistant breast cancer.[160] In the Phase I trial, administration of ZOL and IL-2 was well tolerated and three out of four patients surviving past 12 months demonstrated sustained levels of Vγ9δ2 cells. A clinical trial of ex vivo ZOL + IL-2 expanded autologous Vγ9δ2 in non-small cell lung cancer patients achieved successful expansions in 33 of 68 patients and was well tolerated with only one case of pneumonitis which resolved after steroid administration.[161] The expected progression-free survival was however not reached as patient accrual was significantly less than expected. Several other clinical trials of γδ T cell therapy for a range of malignancies are ongoing.[162,163]

Given the fact that γδ T cells do not typically require MHC molecules for activation, it has long been hoped that these cells would be suitable candidates for allogeneic use as the potentially devastating complication of Graft Versus Host Disease (GVHD) could be avoided. Indeed, a recently published small Phase I clinical trial of the use of allogeneic Vγ9δ2 cells in late-stage lung and liver cancer provides some evidence of safety as no GVHD events were reported.[164]

3.2.2 Vδ1 expansion methods

The development of efficient Vδ1 methods has been impeded by the limited understanding of natural agonists and the mechanism of expansion *in vivo*. Expansion of the Vδ1 subset from peripheral blood has been more challenging due to the fact that Vδ1 cells, being the minor γδ T cell subset in peripheral blood, require a highly efficient method to achieve sufficient numbers required for clinical use. As a result of lack of knowledge of the natural ligands of the Vδ1 TCR, most expansion methods have relied on T cell mitogens.

Knight et al expanded a pure population of Vδ1 T cells following 3 weeks of culture of fluorescence-activated cell sorting (FACS)-isolated Vδ1 cells with 1μg/ml of phytohaemagglutinin (PHA-L) and 200 IU/ml of recombinant IL-2.[75] The expanded Vδ1 cells were predominantly of Effector Memory (CD27-CD45RA-) and Central Memory (CD27+CD45RA-) phenotypes and demonstrated specific cytotoxicity against myeloma cells *in vitro.*

Siegers et al isolated polyclonal γδ T cells from peripheral blood of healthy donors and following 6-8 days of culture with Concanavalin A, FACS-sorted Vδ1 and Vδ2 cells were then stimulated with 500IU/ml of recombinant IL-2, 0.25μg/ml PHA and irradiated feeder cells.[76] The Vδ1 cells expanded by this method were cytotoxic against B-CLL cell lines.

Correia et al isolated γδ T cells by MACS positive selection and expanded Vδ1 cells with 1μg/ml of PHA and 100 IU/ml of recombinant IL-2.[165] The Vδ1 cells expanded by this method expressed high levels of the natural cytotoxicity receptors NKp46 and NKp44 with demonstrable cytotoxicity against primary B-CLL cells in a TCR-independent manner.

Following MACS-positive selection of γδ T cells from PBMCs, Wu et al expanded Vδ1 cells with recombinant IL-7 (20 ng/mL) and PHA (1 μg/mL).[166] The Vδ1+ cells obtained following 14 days of culture inhibited the human colon cancer cell line, HT29 in a xenograft mouse model.

More recently, Almeida et al published a Vδ1 expansion of MACS positively selected CD3+TCRαβ- cells from peripheral blood of healthy donors and CLL patients involving the use of a combination of cytokines: 100 ng/mL rIL4, 70 ng/mL rIFNγ, 7 ng/mL rIL21, and 15 ng/mL rIL1β; and a soluble antibody (70 ng/mL anti-CD3 mAb, clone OKT-

3) on Day 0 followed by 70 ng/mL rIL-15, 30 ng/mL IFNγ, and 1 μg/mL anti-CD3 mAb every 5-6 days.[167] The Vδ1+ cells which the authors named “DOT” cells were effective in inhibiting CLL growth in a xenograft mouse model.

Finally, monoclonal antibody activation via the TCR is an alternative strategy that has been employed for the expansion of Vδ1 T cells. Makkouk et al published an expansion method using immobilized agonistic anti-Vδ1, followed by retroviral transduction of a bicistronic CAR and αβ T cell depletion, achieving an average of 20,000-fold Vδ1 expansion with >80% purity.[168] However, a drawback of expansion via stimulation of the TCR is the potential for T cell exhaustion and functional impairment of the cell product.

Given the limitations of the various existing Vδ1 expansion methods, this part of the project aims to evaluate an expansion method that is both clinically relevant and reproducible. The secondary aim is to compare our novel method with previously published PHA-based Vδ1 expansion methods.

3.3 Chapter Objectives

1) To evaluate a novel method for the expansion of Vδ1 subset of γδ T cells using anti-CD3 and IL-15.
2) To assess the phenotypic and functional characteristics of IL-15 expanded Vδ1 γδ T cells.

3.4 Anti-CD3 (clone OKT3) and IL-15 based Vdelta1 Expansion Method

The Vδ1 expansion method is described in detail in the Materials and Methods section and published.[169] In brief, PBMCs were isolated from peripheral blood of healthy donors by the density gradient centrifugation method. Gamma Delta T cells were enriched following depletion of Alpha/Beta T cells and CD56+ cells by MACS. This was followed by incubation in complete media containing 1µg/ml of anti-CD3 mAb (OKT3) and 100ng/ml of IL-15. The media was refreshed every 2-3 days with complete media supplemented with 100ng/ml of IL-15. Vδ1 cell numbers and proportions were determined by flow cytometry.

3.5 Results

3.5.1 Donor Variation in Vdelta chain usage

There was a significant variation in the type of Vδ chain expressed by the gamma/delta T cells of donors. Vδ2 was the most commonly expressed delta chain type among PBMC donors. The median Vδ2/Vδ1 ratio was 2.1 with a range of 0.2 to 10.3 for a panel of 9 unique PBMC donors assessed (figure 3-1).

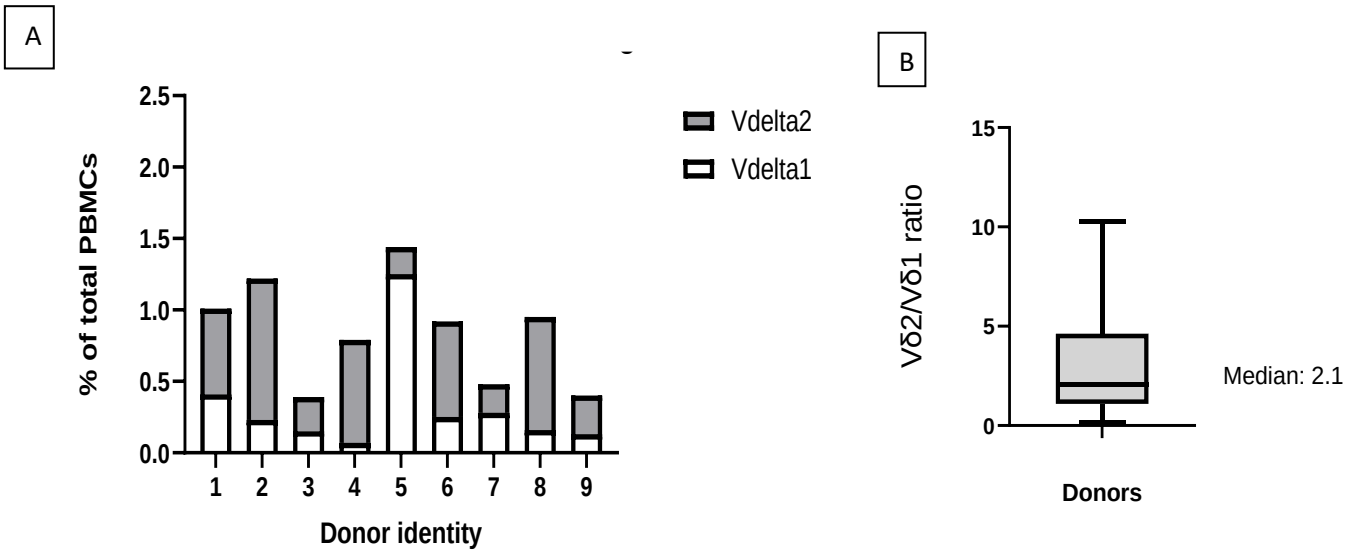

Figure 3-1: Donor variation in delta chain usage. (A) Gamma delta chain type as a percentage of total PBMCs (n=9) (B) Distribution of Vδ2/Vδ1 ratio among donors. Box represents median and interquartile range, whiskers represent maximum and minimum values.

3.5.2 Optimisation of anti-CD3 (OKT3) and IL-15 based Vdelta1 Expansion Method

3.5.2.1 Titration of CliniMACS TCR αβ antibody

To determine the saturating antibody volume for MACS depletion of α/β T cells, two incremental volumes of CliniMACS TCR α/β-biotin antibody (Miltenyi); 2µl per 10^6 PBMCs (1x volume) and 12µl per 10^6 PBMCs (6x volume) were assessed for residual αβ T cells post depletion. Although the comparison was limited due to low number of replicates, there was no statistically significant difference in residual αβ T cell content despite increased volumes of the depletion antibody (figure 3-2), suggesting that the 1x volume was a saturating volume and this was used for further depletions.

3.5.2.2 Comparison of combined versus sequential αβ TCR and CD56 depletions

As part of the optimisation step, depletion of αβ TCR followed by CD56+ cells (sequential depletion) was compared with both depletions in a single step (combined). There was no statistically significant difference in residual αβ T cell contamination following expansion for either method of depletion (figure 3-3). The combined depletion method was therefore adopted as it was more cost-effective and required less reagents.

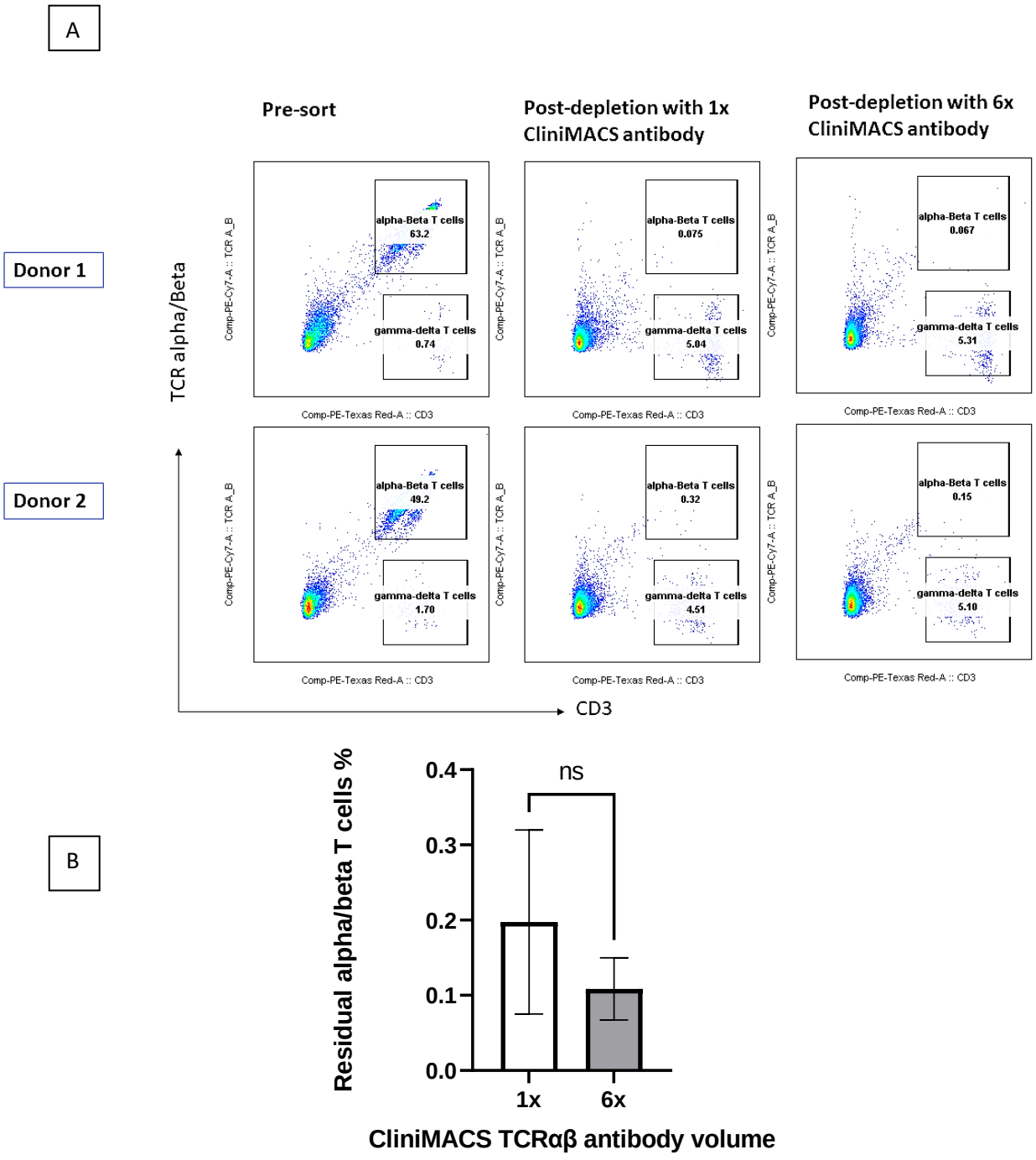

Figure 3-2: CliniMACS TCR α/β-biotin titration. (A) Flow cytometry plots showing residual αβ T cells following MACS depletion using two volumes of CliniMACS TCR α/β-biotin antibody showing similar depletion rates and enrichment of gamma delta T cells. To determine the optimal saturation volume of the CliniMACS TCR α/β-biotin antibody, MACS depletion of αβ T cells from peripheral blood of healthy donors (n=2) was performed using 2 µl per 10^6 PBMCs (1x antibody volume) and 12 µl per 10^6 PBMCs (6x antibody volume). Events were gated on live cells. (B) Graphical comparison of residual αβ T cells following MACS depletion using the CliniMACS TCR α/β-biotin antibody (n=2, error bars indicate Standard Error of Means (SEM), paired T test p=0.47, ns: non-significant).

A

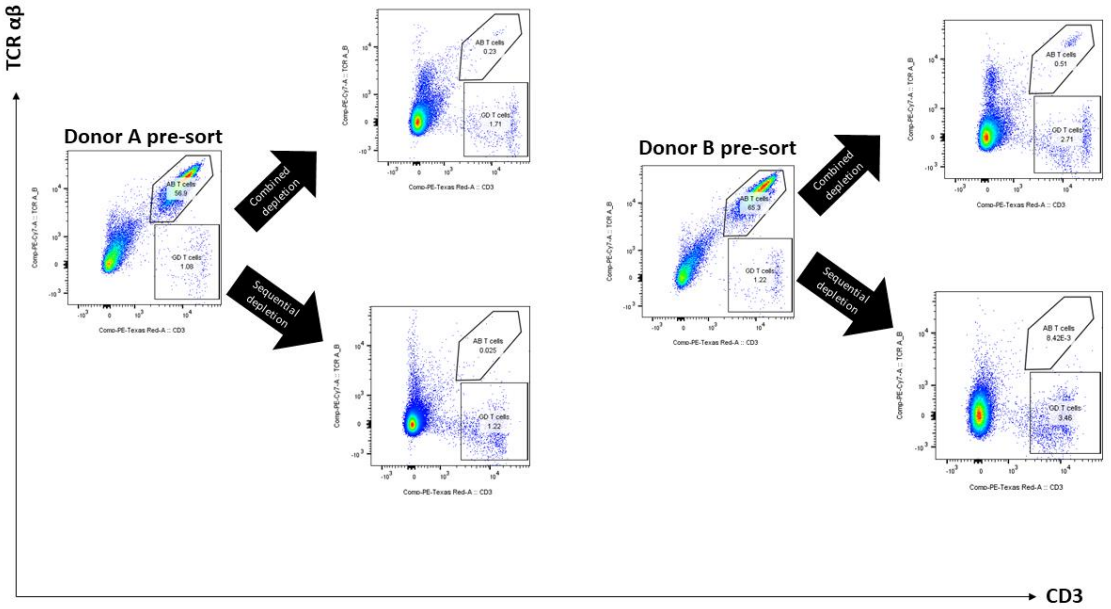

B

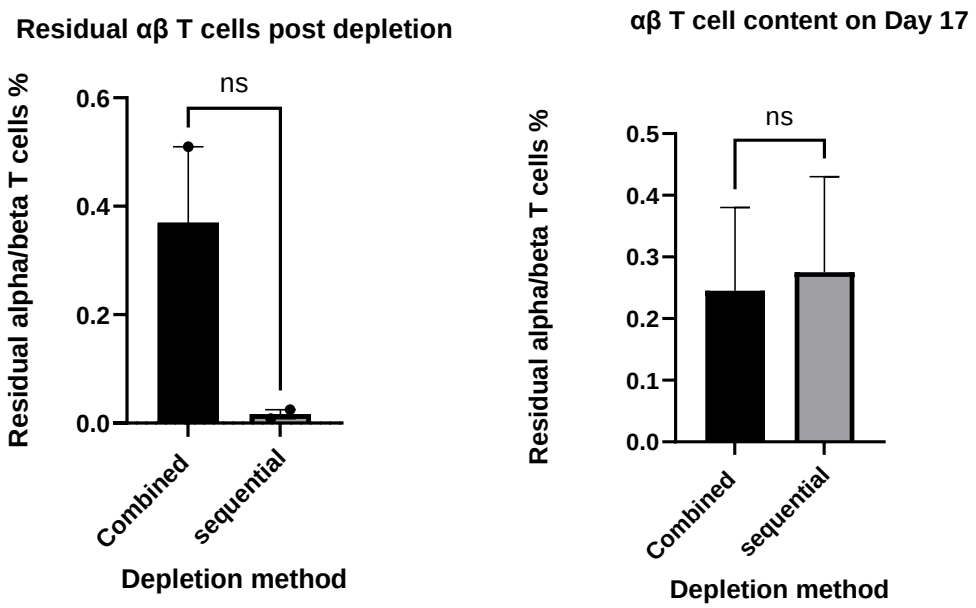

Figure 3-3: Comparison of αβ T cell depletion methods. (A) Flow cytometry dot plots showing depletion of αβ T cells by the combined method (αβ T cell and CD56+ depletion in a single step) or the sequential method (αβ T cell depletion followed by CD56+ depletion) for two representative donors. Events were gated on live cells. (B) Graphical comparison of residual αβ T cells determined by flow cytometry on day 0 following depletion (n=2, paired T test p=0.25) and residual αβ T cells in the same donors on expansion with IL-15 on day 17 (n=2, paired T test p=0.37) (error bars indicate SEM)

3.5.2.3 Optimisation of αβ T cell and CD56+ depletion

To achieve optimal depletion of αβ T cells and CD56+ cells, a double-combined depletion method was assessed i.e. the immunomagetically-labelled PBMCs were passed through two fresh MACS columns sequentially. Flow cytomery analysis showed that the αβ T cell depletion efficiency could be improved by this method (figure 3-4).

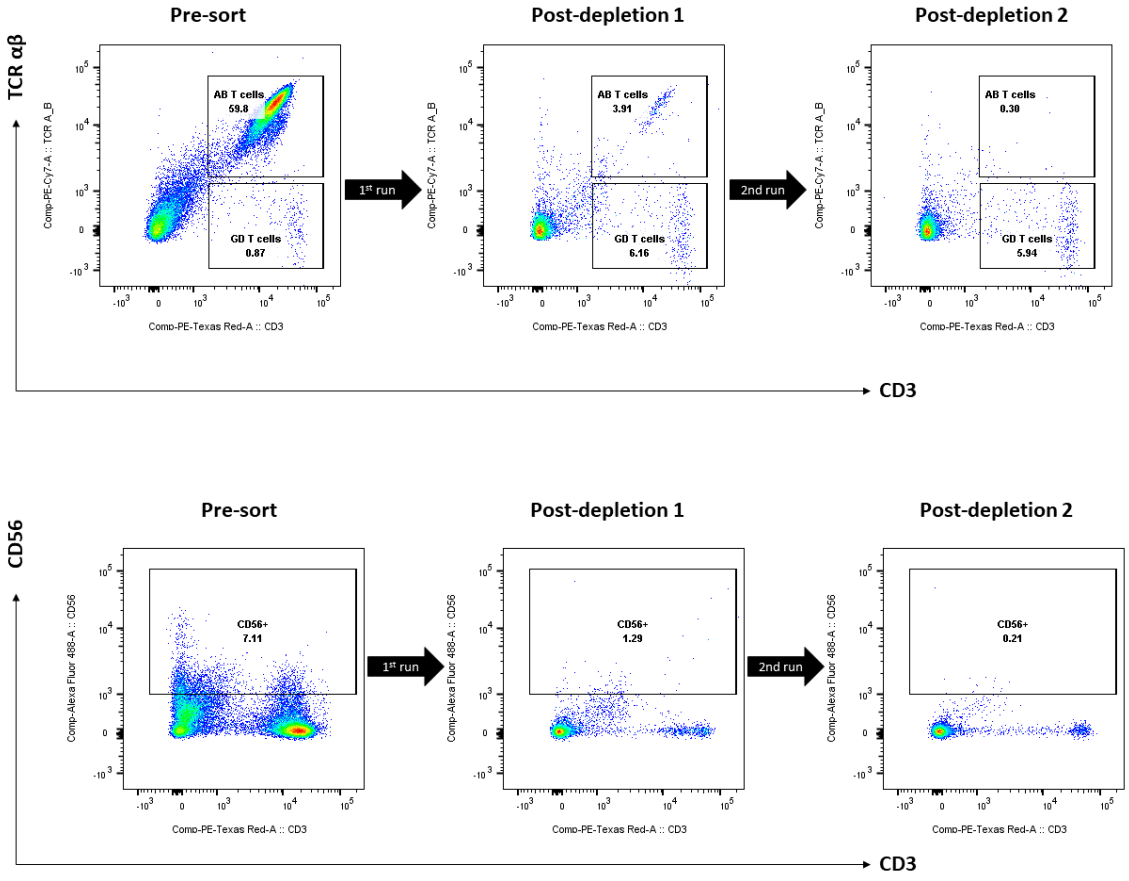

Figure 3-4: Optimisation of αβ T cell and CD56 depletions. Flow cytometry dot plots from a representative donor showing αβ T cell (top) and CD56+ (bottom) percentages before and after two sequential rounds of combined MACS depletions. PBMCs were incubated with biotinylated CD3 and anti-CD56 antibodies followed by incubation with anti-biotin microbeads. The labelled cells were passed through MACS depletion columns twice and residual αβ T cell and CD56+ cells were determined by flow cytometry after each depletion.

3.5.3 Comparison of anti-CD3 (OKT3) plus IL-15 versus PHA plus IL-7 expansion of Vδ1 T cells.

To compare our Vδ1 expansion method with a previously published method using 1µg/ml of PHA and 20ng/ml of IL-7[166], aliquots form two donors PBMCs were expanded in parallel to day 16. Stimulation with anti-CD3 (OKT3 clone) and IL-15 produced a higher yield of Vdelta1+ T cells on Day 16 compared with stimulation with PHA and IL-7 however, due to donor variability and possibly insufficient biological replicates, the difference was not statistically significant.

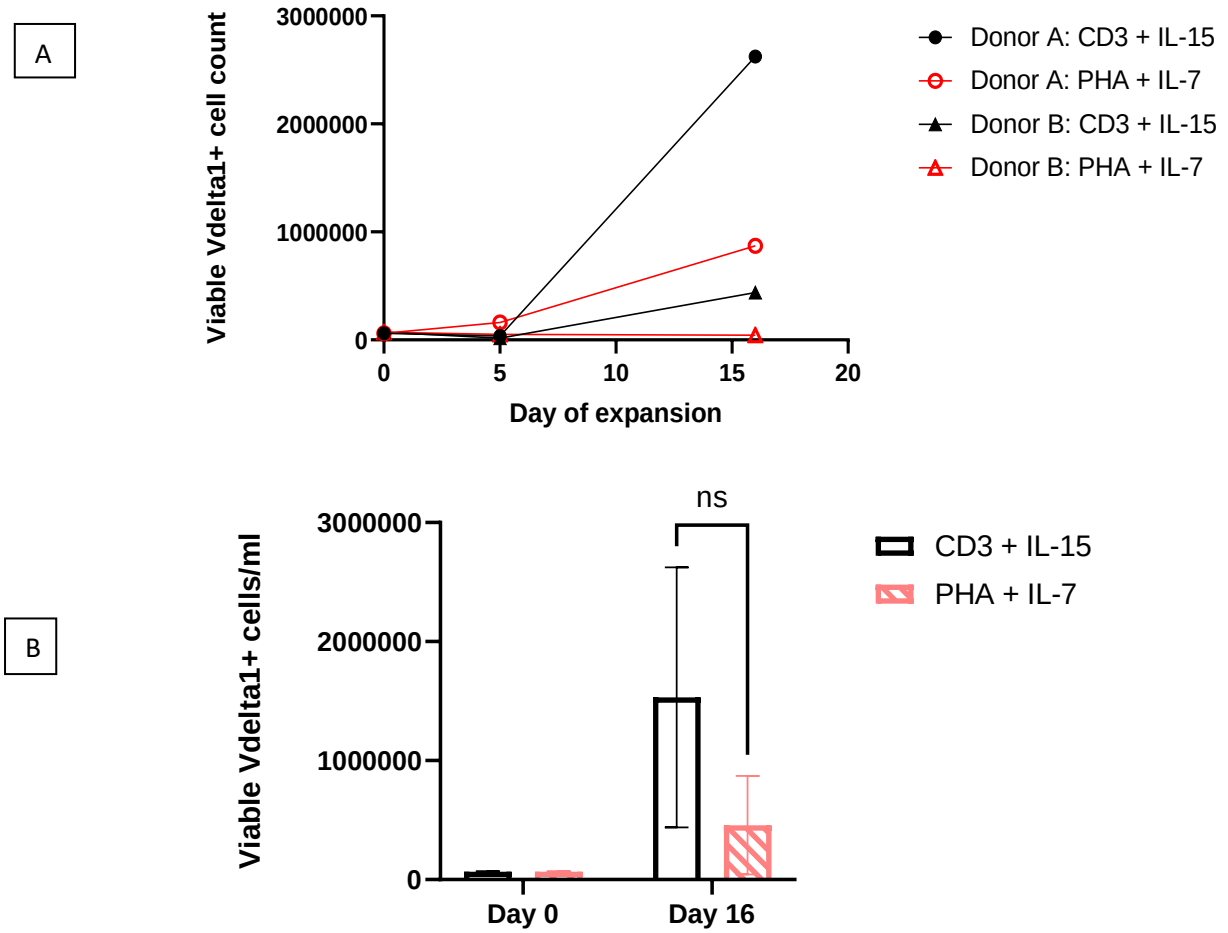

Figure 3-5: Comparison of Vdelta1 expansion methods. (A) Vδ1 expansion graphs for two donor PBMCs cultured with either 1µg/ml of anti-CD3 (clone OKT3) plus 100ng/ml of Interleukin-15 (IL-15) or 1µg/ml of phytohaemagglutinin (PHA) plus 20ng/ml of Interleukin-7 (IL-7). Identical numbers of PBMCs depleted of αβ T cells and CD56+ cells for each donor were expanded with the appropriate stimulant and cytokine for up to 16 days. Vδ1 cell numbers were determined by flow cytometry. (B) Comparison of Vδ1 expansion by stimulation method (n=2, unpaired t test, ns=non-significant p value). Error bars indicate standard error of means.

3.5.4 Comparison of anti-CD3 (OKT3) plus IL-15 versus PHA plus IL-2 expansion of Vδ1 T cells.

A similar parallel comparison was performed against a previously published PHA and IL-2 expansion method[75] using 3 donor PBMCs. Stimulation with anti-CD3 (OKT3 clone) and IL-15 was superior to stimulation with PHA and IL-2 in terms of Vδ1+ cell yield and fold-expansion (figure 3-6).

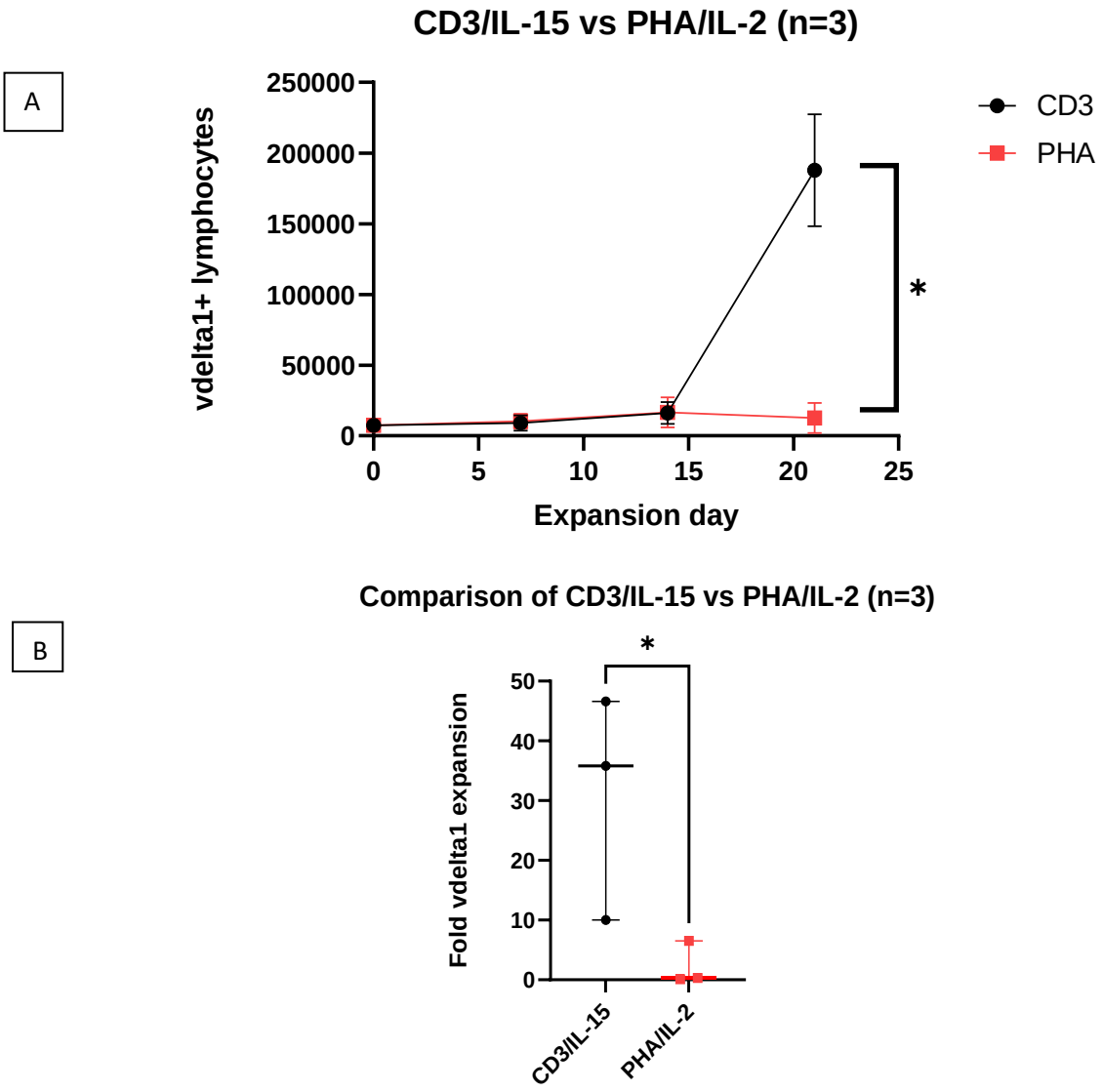

Figure 3-6: Comparison of Vdelta1 expansion methods. (A) Vδ1 expansion graphs for PBMCs (n=3) cultured with either 1µg/ml of anti-CD3 (clone OKT3) plus 100ng/ml of Interleukin-15 (IL-15) or 1µg/ml of phytohaemagglutinin (PHA) plus 200U/ml of Interleukin-2 (IL-2). Identical numbers of PBMCs depleted of αβ T cells and CD56+ cells for each donor were expanded with the appropriate stimulant and cytokine for up to 21 days. Vδ1 cell numbers were determined by flow cytometry (n=3, unpaired t test, *p<0.05). (B) Comparison of fold-change in Vδ1 cell numbers by stimulation method (n=3, unpaired t test, *p<0.05). Error bars indicate standard error of means.

3.5.5 CD3/IL-15 expanded cells upregulate markers of activation and cytotoxicity.

Expression of the activation marker, CD69, and the innate cytotoxicity receptor, NKG2D, were significantly upregulated following anti-CD3/IL-15 expansion compared with PHA/IL-2 expanded lymphocytes. A non-statistically significant increase in CD56 expression was similarly observed in CD3/IL-15 expanded cells (Figure 3-7). These findings suggest that CD3/IL-15 stimulation results in activated γδ T cells with potentially improved cytolytic properties.

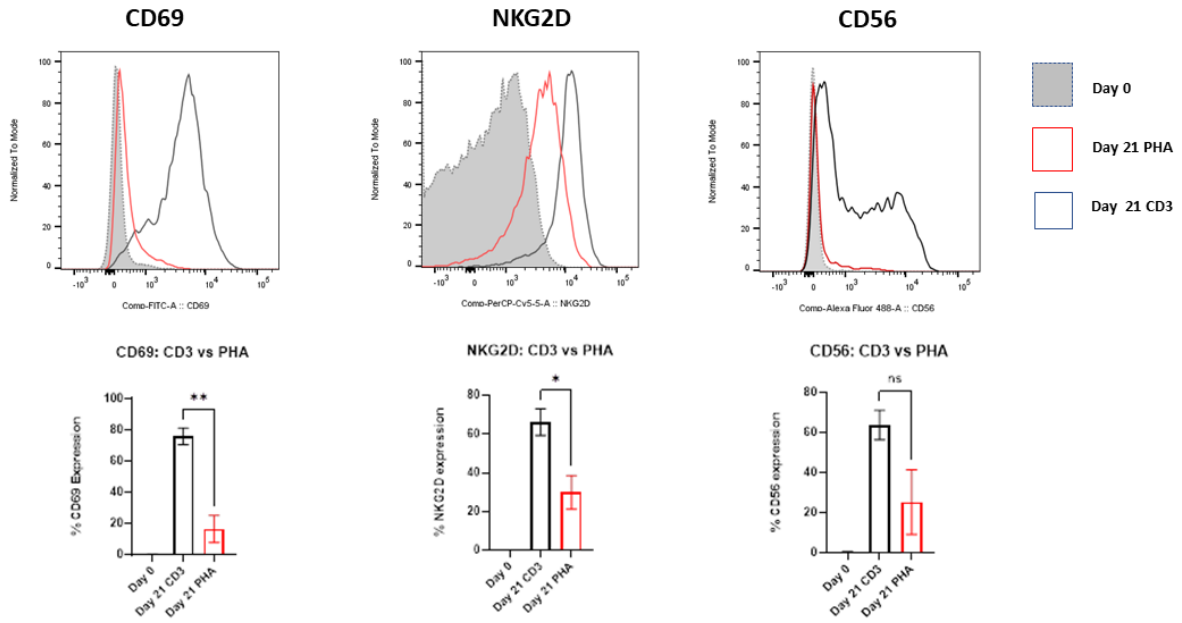

Figure 3-7: Expression of key cell surface markers on expanded T cells. Above: Flow cytometry histograms from a representative donor showing expression of CD69, NKG2D and CD56 prior to stimulation on Day 0 and following stimulation by anti-CD3 plus IL-15 or PHA plus IL-2 on Day 21. Events were gated on CD3+ live cells. Below: Graphical comparison of expression levels of CD69, NKG2D and CD56 (n=3, unpaired T test p values; ns = not significant, *p < 0.05, **p < 0.01). All error bars indicate standard error of means.

3.5.6 Expansion of cryopreserved PBMCs

To determine the feasibility of expansion of Vδ1 cells with anti-CD3 and IL-15 from frozen blood cells, PBMCs from three donors were cryopreserved for 14 days and subsequently expanded with anti-CD3 and IL-15 for 20 days. Figure 3-8 shows that expansion of Vδ1 T cells was feasible following a period of cryopreservation. Furthermore, there was no significant change in Vδ2/Vδ1 ratios following cryopreservation indicating the absence of unbalanced loss of either subset by the freeze-thaw process.

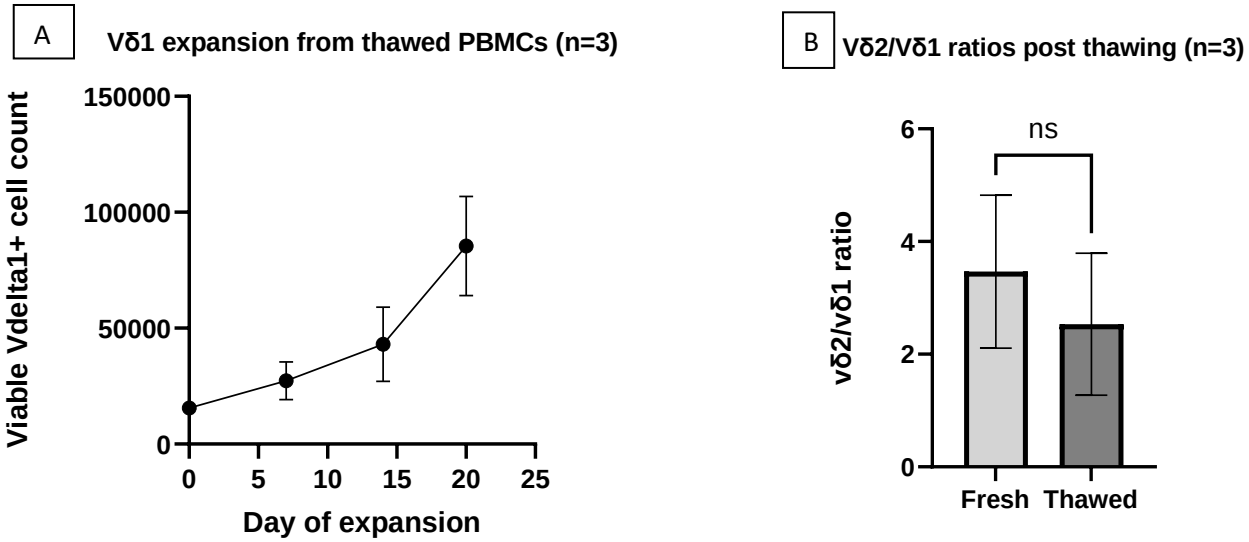

Figure 3-8: Properties of cryopreserved PBMCs. (A) Graphical representation of expansion of Vδ1 T cells following 14 days of cryopreservation and stimulation with anti-CD3 and IL-15. PBMCs (n=3) were isolated by density gradient centrifugation and cryopreserved for 14 days. The cells were subsequently thawed, depleted of αβ T cells and CD56+ cells and expanded with 1µg/ml of anti-CD3 (OKT3) and 100ng/ml of IL-15 for 20 days. Vδ1 T cell numbers were determined by flow cytometry on days 7, 14 and 20. (B) Graphical comparison of Vδ2/Vδ1 ratios of identical donors before and after cryopreservation (n=3, unpaired T test p=0.64). All error bars indicate SEM.

3.5.7 TCR alpha/Beta and CD56 depletion enriches Vδ1 T cells.

To determine the impact of initial CD56 and αβ T cell depletion on the respective PBMC components, a comparison of cell proportions was made by flow cytometry before and after depletion. The depletion of CD56+ and αβ T cells on Day 0 results in a relative enrichment of the Vδ1 T cell subset while reducing the NK cell content (figure 3-9A). Furthermore, αβ T cells, Vδ2, Vδ1, monocytes and NK cell proportions were serially measured at Day 0, 7 and 17 to determine the trajectory of expansion of these cells. Expansion with anti-CD3 (OKT3) and IL-15 for 17 days resulted in a statistically significant increase in Vδ1 T cells with a non-significant increase in NK and alpha/beta T cells (Figure 3-9B). The monocytic component was markedly reduced by day 17.

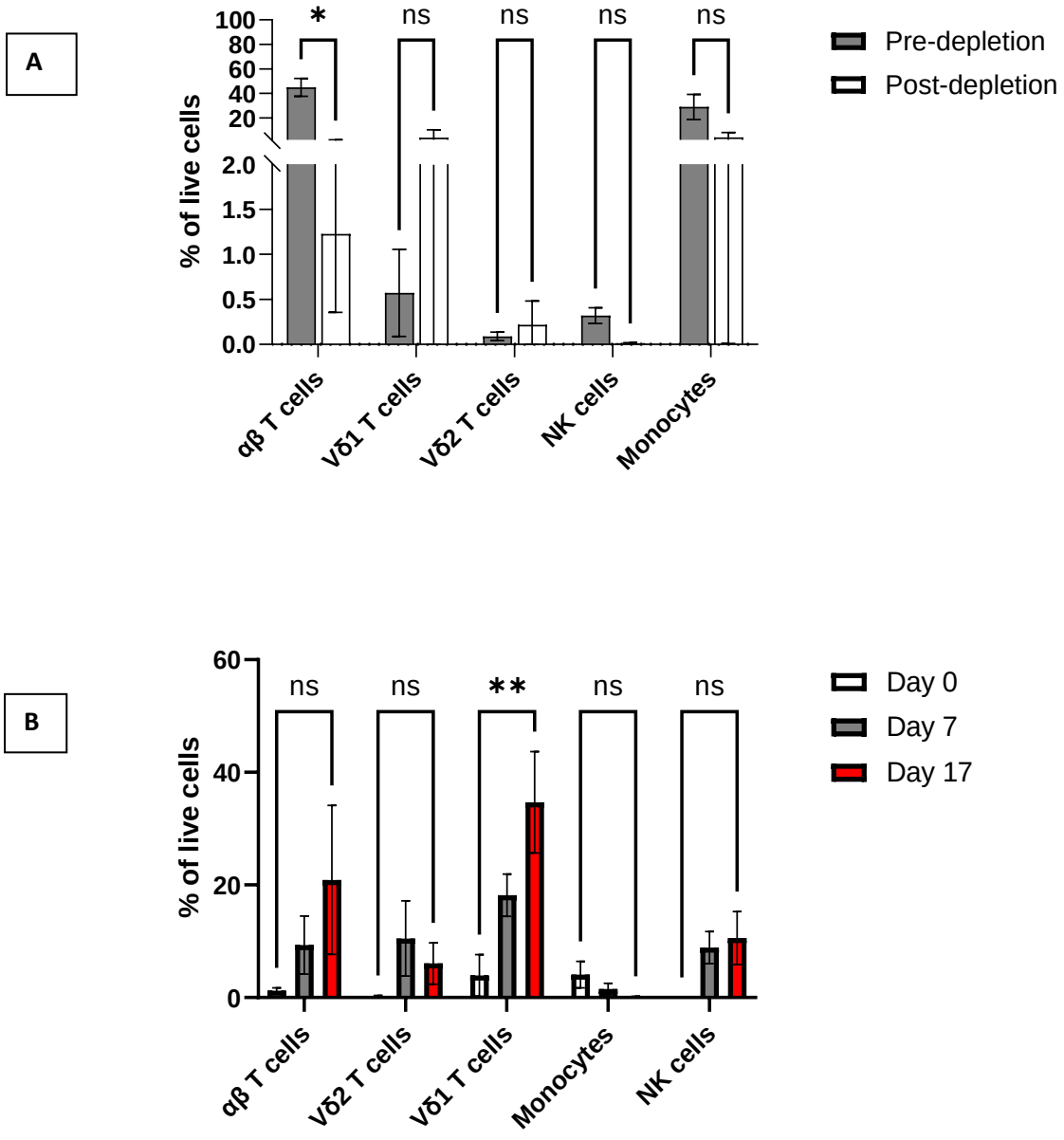

Figure 3-9: Cell components of OKT3/IL-15 expansion method. (A) Proportions of peripheral blood cell components before and after αβ T cells and CD56+ depletions as determined by flow cytometry (n=3, unpaired t test, *p<0.05). (B) Relative proportions of blood cells determined by flow cytometry on Days 0, 7 and 17 of expansion with IL-15 and anti-CD3 (OKT3 clone) (n=3, unpaired t test **p<0.01, ns=non-significant). All error bars indicate SE of means.

3.5.8 Vδ1 T cell purification by negative selection

In some experiments, a pure population of Vδ1+ T cells may be desirable therefore a purification step using immunomagnetic labelling was devised. A Vδ1+ T cell population of up to ~90% purity was obtained following MACS depletion of αβ T cells and Vδ2+ T cells using biotinylated antibodies against αβ and Vδ2 TCR respectively on day 16 of expansion (figure 3-10). These Vδ1+ cells were purified “untouched” i.e. isolated by negative selection without manipulation of the Vδ1 TCR.

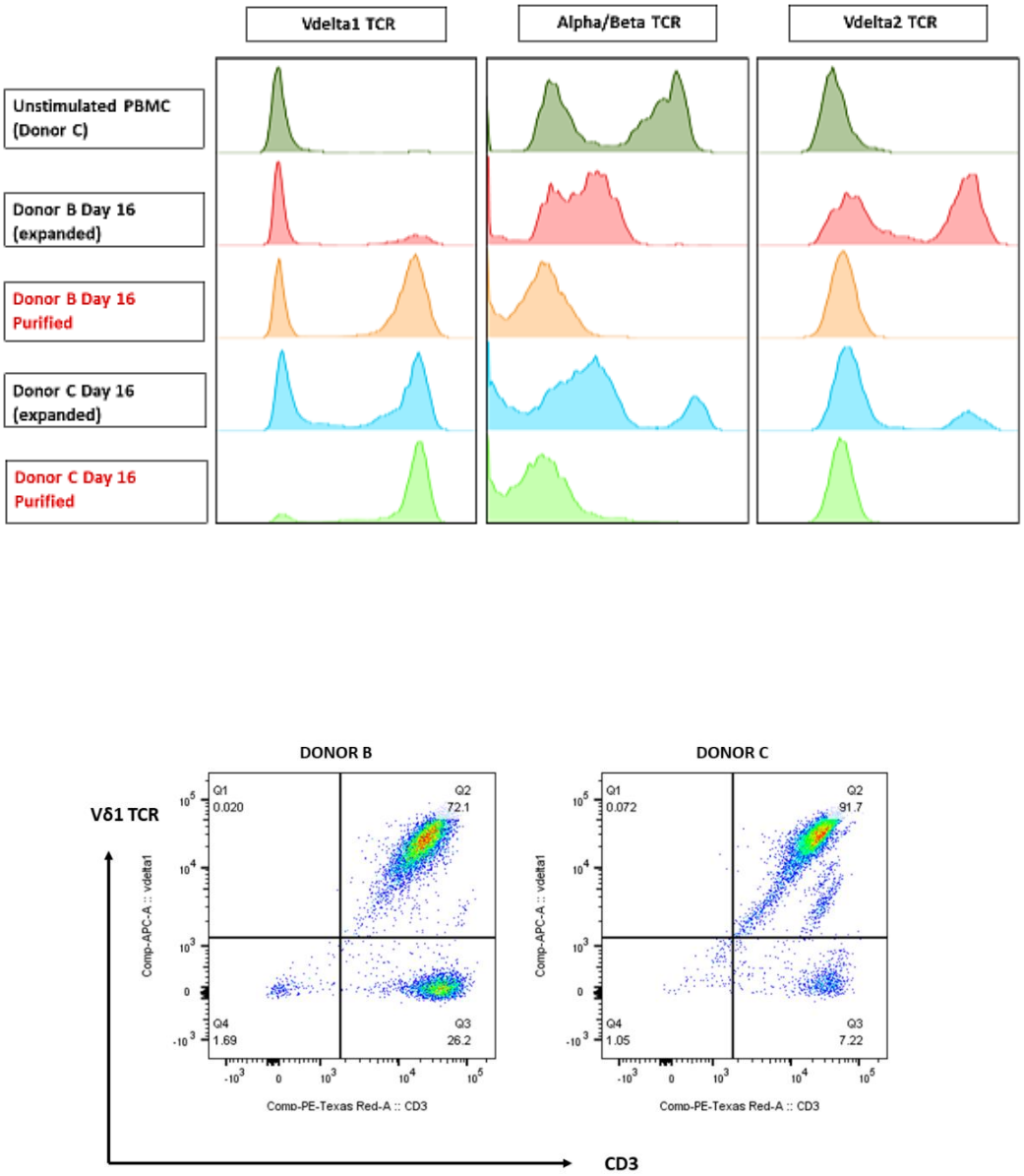

Figure 3-10: Vδ1 purification of expanded PBMCs. Above: Flow cytometry histograms showing Vδ1, Vδ2 and αβ T cell content for two representative donors following MACS purification on Day 16 of expansion. Below: Flow cytometry dot plots from the same donors showing Vδ1 purity following MACS purification. Events were gated on live cells. CD56 and αβ T cell depleted PBMCs were stimulated with 1µg/ml of anti-CD3 (OKT3) and 100ng/ml of IL-15 for 16 days followed by MACS-depletion of Vδ2 T cells.

3.5.9 Baseline Vδ2/Vδ1 ratios correlate with ratios after anti-CD3/IL-15 expansion.

To determine if the proportion of Vδ1 T cells at baseline correlated with Vδ1 proportions following expansion i.e. whether donors with lower Vδ2/Vδ1 ratios at baseline were better Vδ1 expanders following OKT3 and IL-15 stimulation, 11 independent donors were compared for Vδ2:Vδ1 ratios before and after stimulation. Indeed, the donor variability in delta chain usage at baseline was similarly reflected in the proportions of Vδ2/Vδ1 in the expanded T cell population. Overall, PBMC donors with higher proportions of Vδ1 T cells at baseline tend to be good expanders of the Vδ1 compartment following stimulation with anti-CD3 and IL-15. A positive correlation was observed between the Vδ2/Vδ1 ratio at baseline and following expansion (figure 3-11).

A

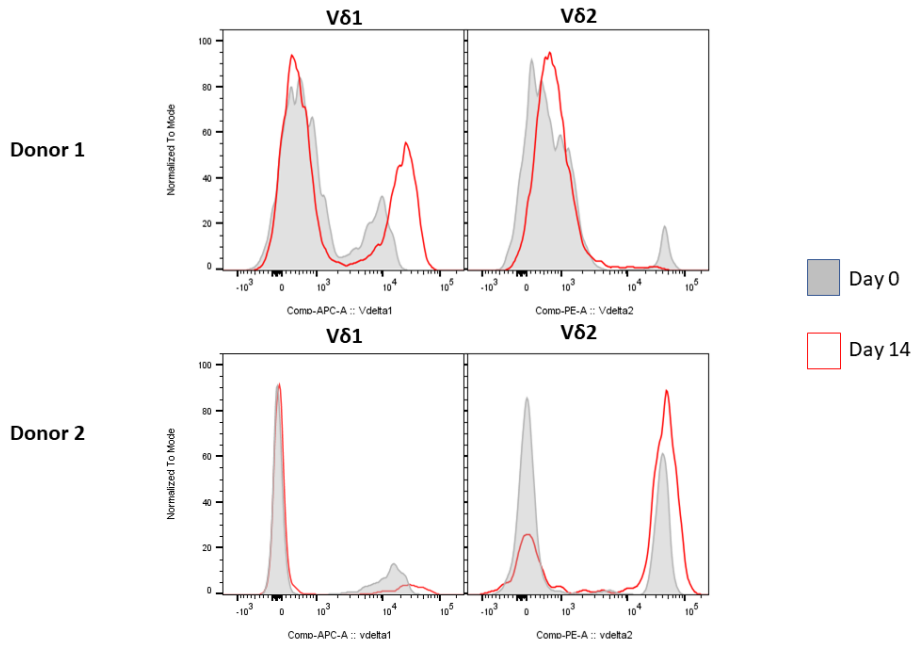

B

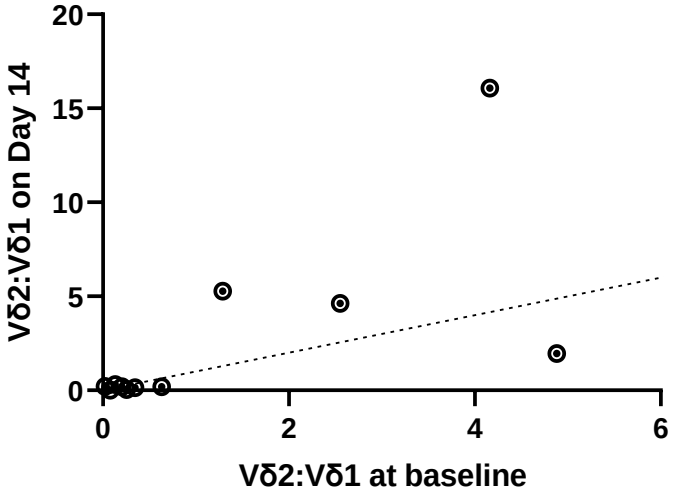

Figure 3-11: Donor variation in Vδ chain subtype expansion. (A) Flow cytometry histogram plots of two donors expanded with anti-CD3 and IL-15 showing donor variation in Vδ2/Vδ1 expansion. (B) Scatter plot showing correlation between Vδ2:Vδ1 ratios at baseline and 14 days after expansion with IL-15 (n=11, Pearson Correlation coefficient, r=0.6701, two-tailed p=0.0241).

3.5.10 Comparison of phenotypic properties between Vδ1 and non- Vδ1 T cells

Vδ1 T cells are thought to possess distinct functional properties compared with other T cell subsets and this may be reflected in the degree of expression of cell surface markers. Therefore, to compare expression levels of surface CD69, NKG2D, PD-1 and CD56 in Vδ1+ cells against other T cell subsets in the expanded cell population following OKT3/IL-15 stimulation, 3 donor PBMCs were assessed by flow cytometry in parallel and results showed significantly higher levels of NKG2D and PD-1 in Vδ1+ compared with Vδ1 negative T cells (figure 3-12). On the contrary, significantly higher CD56 expression was observed in co-expanded Vδ2+ T cells. There was no difference in expression levels of CD69 between Vδ1+ and Vδ1 negative T cells.

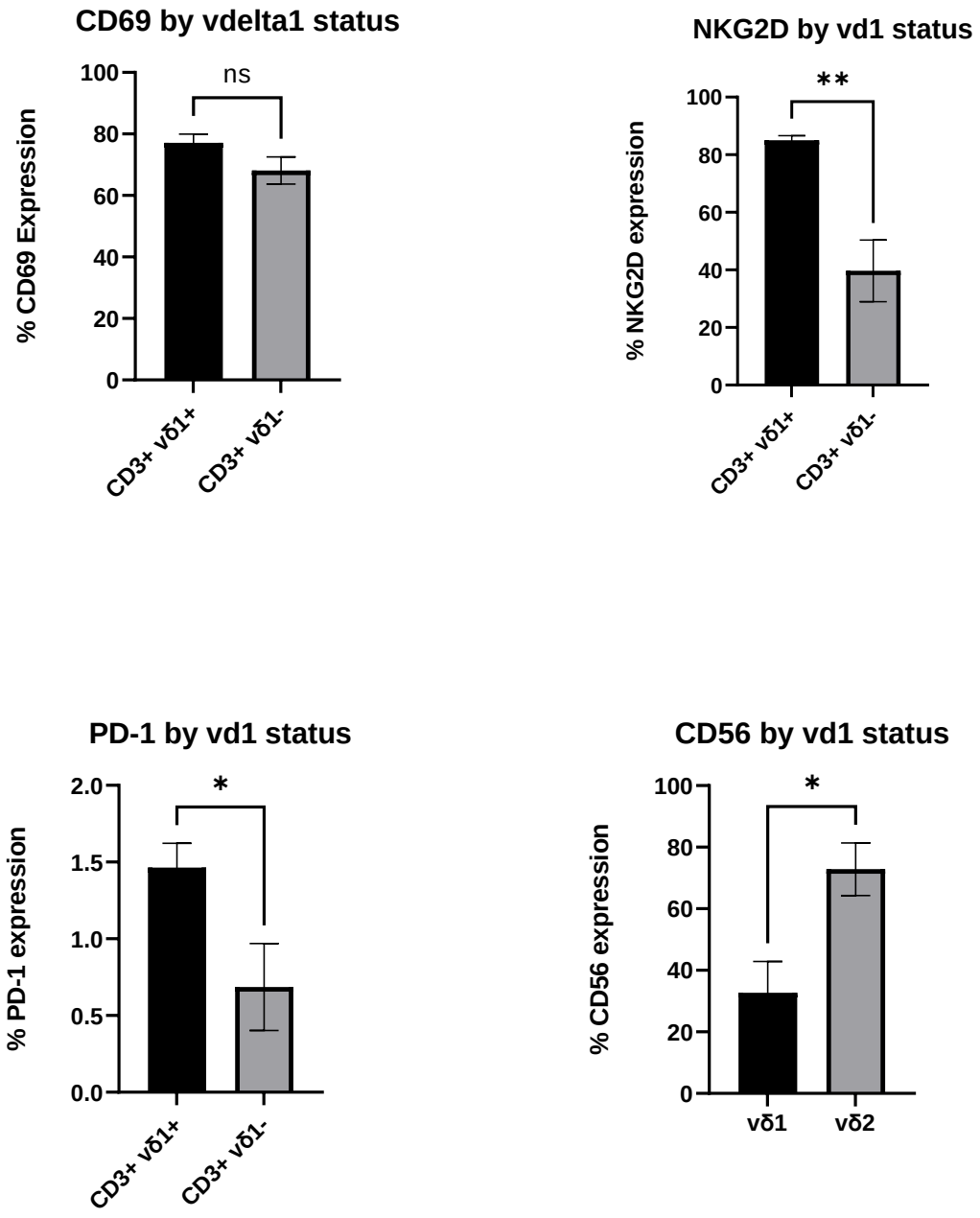

Figure 3-12: Comparisons of surface expression of markers on Vδ1 and non-Vδ1 T cells. Following expansion with OKT3 antibody and IL-15 for 20 days, expanded γδ T cells were assessed by flow cytometry for surface expressions of CD69, PD-1, NKG2D and CD56. Events were gated on CD3+live cells. [n=3, unpaired T test; p=0.13 (CD69), p=0.003 (NKG2D), p=0.04 (PD-1), p=0.04 (CD56)]. Error bars indicate SEM.

3.5.11 Phenotypic comparison T cells expanded from Fresh *versus* Thawed

To determine if a period of cryopreservation significantly impacts the phenotype of cells in the final expanded products, PBMCs from 3 independent donors were divided into two aliquots and half was immediately frozen (as described in Materials and Methods) and kept cryopreserved for 14 days. The other aliquot was expanded with OKT3/IL-15 without a period of cryopreservation. Following 14 days of cryopreservation, the other aliquots were thawed and expanded in an identical manner to the fresh samples. A qualitative comparison was then made to determine levels of expressions of key cell surface markers following expansion. Expression levels of CD69 and NKG2D were similar between Vδ1 cells expanded from either fresh or thawed PBMCs (figure 3-13). However, expansion of Vδ1 cells from thawed PBMCs was associated with increased PD-1 expression at day 20.

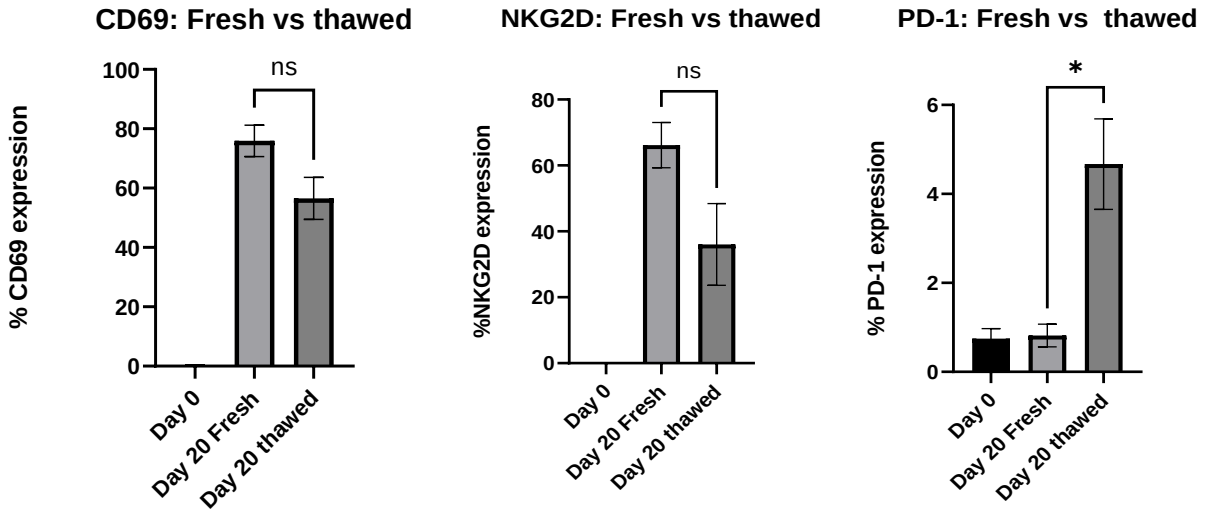

Figure 3-13: Comparison of surface expression of activation/exhaustion markers on Vδ1 T cells expanded from fresh and thawed PBMCs. PBMCs were expanded with anti-CD3/IL15 either freshly from isolation or following 14 days of cryopreservation and were subsequently assessed by flow cytometry for cell surface markers after expansion for 20 days. Events were gated on Vδ1+ live cells. [n=3, unpaired T test; p=0.09 (CD69), p=0.1 (NKG2D), p=0.02 (PD-1)]. Error bars indicate SEM.

3.5.12 Differentiation Phenotypes of expanded γδ T lymphocytes

Immunophenotypic analysis of differentiation markers reveal significant differences in the profiles of Vδ1 cells by expansion method (figure 3-14A). CD3 (OKT3) stimulated cells resulted in significantly more CCR7negCD45RA+ cells than with PHA stimulation (figure 3-14B). PHA-expanded Vδ1 cells were predominantly of CCR7negCD45RAneg phenotype. Similar differences were observed between Vδ1+ and Vδ1 negative T cells co-expanded by CD3 stimulation, with significantly higher proportions of CCR7negCD45RAneg populations in the latter (figure 3-15A). Expansion of cryopreserved PBMCs result in lower proportions of Vδ1+ cells which are CCR7negCD45RApos (figure 3-15B).

A

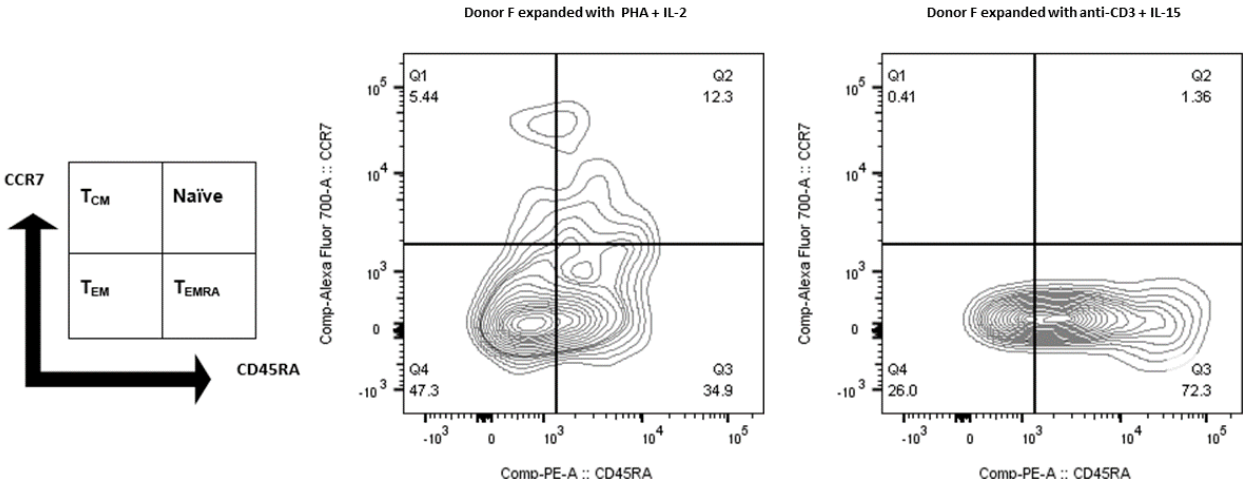

B

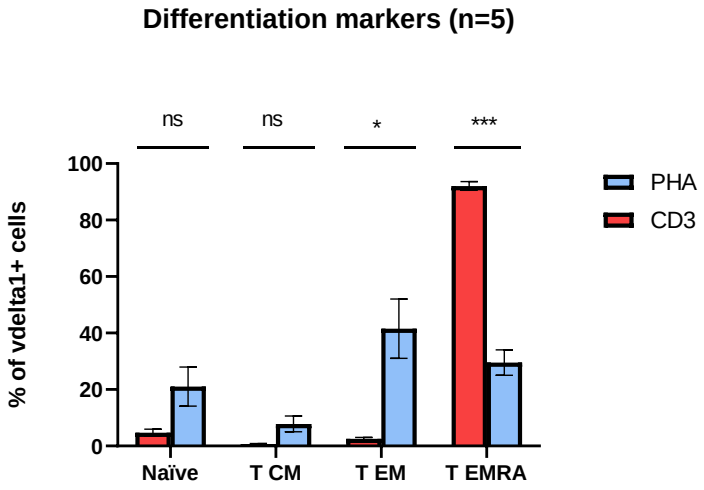

Figure 3-14: Expression of differentiation markers on γδ T cells. (Left) Schematic illustration of differentiation stages as determined by surface expression of CD45RA and CCR7 assessed by flow cytometry. (Right) Flow cytometry contour plots of a representative donor showing differences in expression of differentiation markers by stimulation type (PHA/IL-2 vs anti-CD3/IL-15) on Day 21. Events were gated on CD3+ live cells. The canonical classification of differentiation phenotypes which have been defined for αβ T cells have been used here although these may not correlate with γδ differentiation phenotypes.

A

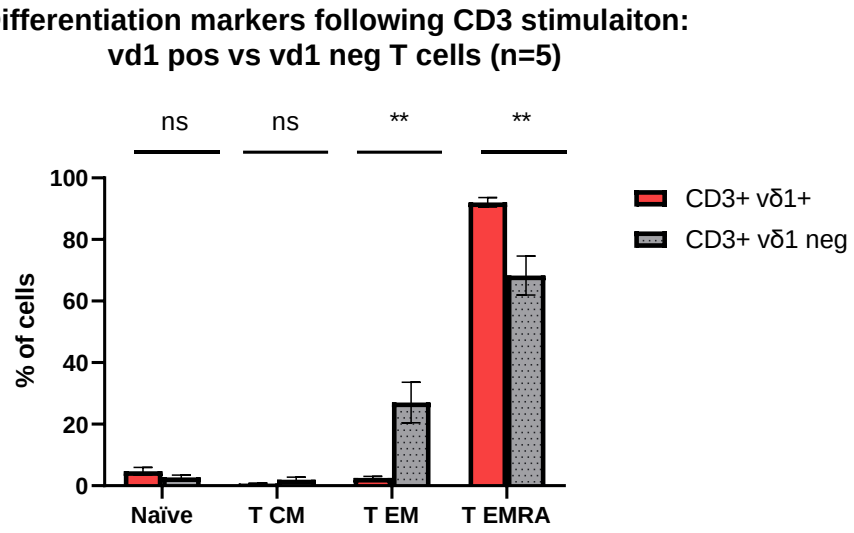

B

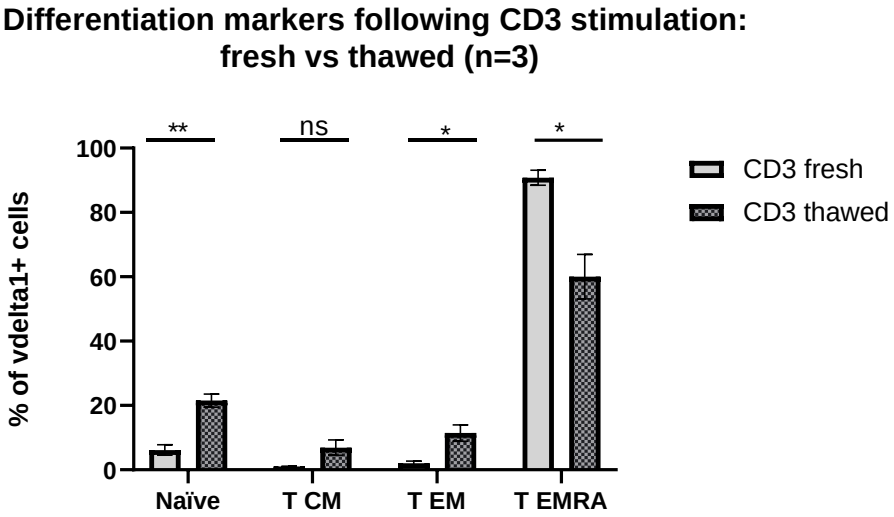

Figure 3-15: Comparison of differentiation markers at Day 21. A) Expression of differentiation markers by method of expansion [n=5, unpaired T test]. B) Comparison of differentiation markers between Vδ1+ and Vδ1- T cells [n=5, unpaired T test]. C) Comparison of differentiation markers between PBMCs expanded from fresh vs freeze-thawed [n=3, unpaired T test]. Events were gated on CD3+ live cells. All error bars indicate SE of mean. ns = not significant, *p < 0.05, **p < 0.01, ***p < 0.001. The canonical classification of differentiation phenotypes which have been defined for αβ T cells have been used here although these may not correlate with γδ differentiation phenotypes.

3.5.13 Anti-tumour activity of IL-15 expanded Gamma Delta T cells

To demonstrate the ability of unmodified, Vδ1-enriched γδ T cells to eliminate tumour targets, a 4-hour chromium-51 cytotoxicity assay was set up with expanded γδ T cells against cancer cell lines at increasing effector/target ratios. Indeed, IL-15 stimulated γδ T cells demonstrated dose-dependent cytotoxicity against haematological and solid tumour cell lines (Figure 3-16).

Similarly, CD107a degranulation by expanded γδ T cells, a surrogate marker of cytotoxicity, was significantly increased in response to the U87 cell line with similar (but non-significant) responses against other cancer cell lines (Jurkat and LAN1) but not in response to allogeneic PBMCs (Figure 3-17).

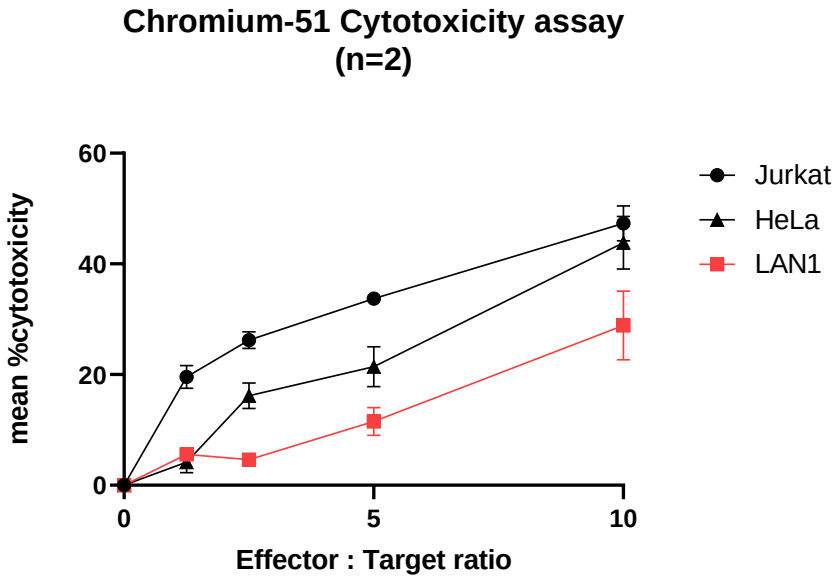

Figure 3-16: Chromium-51 cytotoxicity assay of unmanipulated γδ T cells against cancer cell lines. Graphical representation of results showing dose-dependent cytotoxicity of IL-15 stimulated, gamma delta T cell-enriched PBMCs against cancer cell lines. Jurkat, HeLa and LAN1 cell lines were labelled with Chromium-51 and subsequently co-cultured with expanded PBMCs (n=2) at effector/target ratios of 10:1, 5:1, 2.5:1 and 1.25:1 for 4 hours. Specific cytotoxicity was derived from the scintillation counts from released radioactive chromium and normalised to spontaneous chromium release (control) and maximum release with 1% Triton-X. Error bars indicate standard error of means.

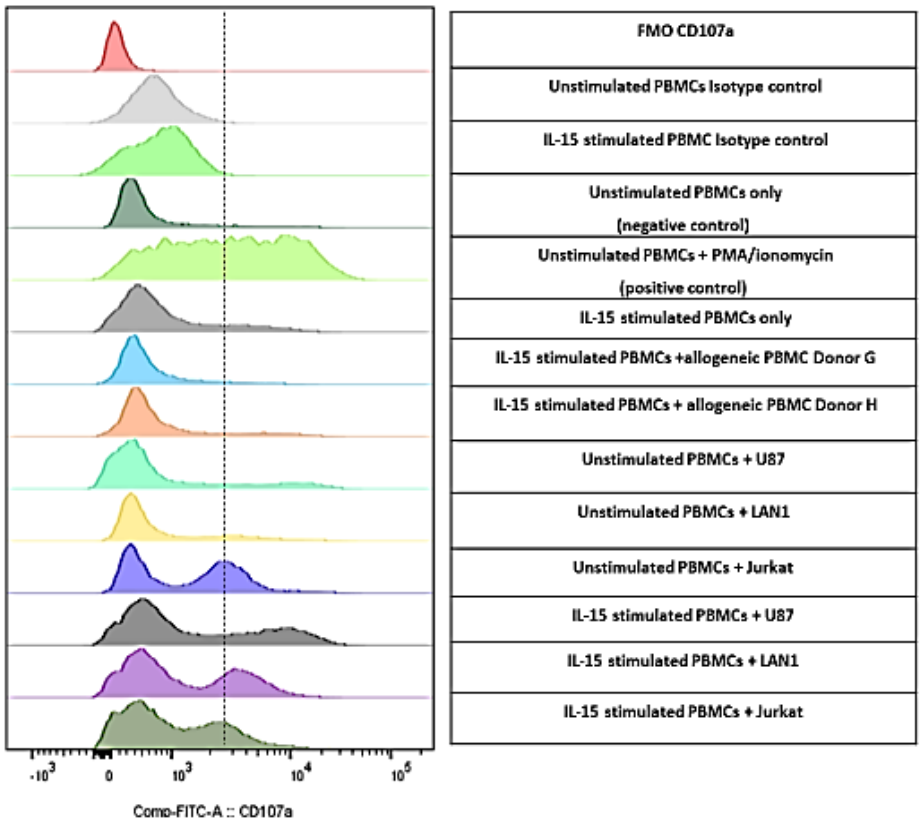

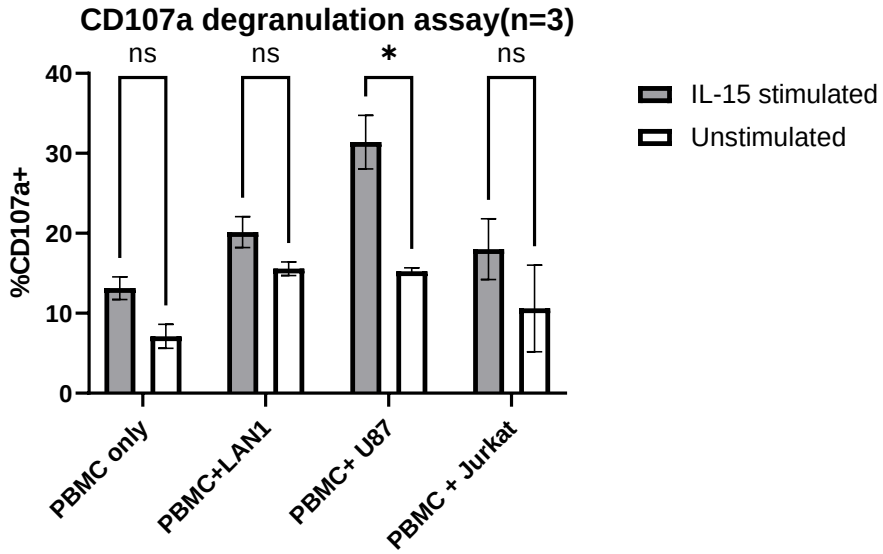

Figure 3-17. CD107a degranulation assay of unmanipulated γδ T cells. Above: Flow cytometry histograms for a representative donor showing the CD107a degranulation assay results for various co-culture conditions in 1:1 ratio with tumour cell lines (or appropriate controls). CD107a degranulation is evidenced by a shift of the histogram to the right in the positive control and in response to tumour cell lines but not against allogeneic PBMCs. Events were gated on live cells. IL-15 stimulated cells were enriched for gamma delta T cells by depletion of alpha-beta T cells and CD56+ cells, then stimulated with 100ng/ml of IL-15 for 21 days prior to co-culture. Unstimulated PBMCs were maintained in complete media for 21 days and either stimulated with Phorbol 12-myristate 13-acetate (PMA) and ionomycin (positive control) or co-cultured directly with tumour cell lines; U87, LAN1 and Jurkat. Below: Proportion of cells positive for CD107a as a surrogate for cytotoxic cell degranulation obtained by flow cytometry following co-culture with cancer cell lines, LAN1, U87 and Jurkat. Events were gated on live cells (n=3, unpaired t test, ns = not significant, *p < 0.05). All error bars indicate SE of means.

3.5.14 Expanded cells become dependent on IL-15

To determine if OKT3/IL-15 expanded γδ T cells could be maintained in culture without IL-15, an IL-15 withdrawal experiment was performed after an initial 14-day expansion period with IL-15 containing media. Cell viability and Annexin V binding were assessed at 48- and 96-hours post IL-15 withdrawal. The results showed a significant reduction in cell viability and increased Annexin V binding at 96 hours which was not rescued by addition of IL-2 (figure 3-18).

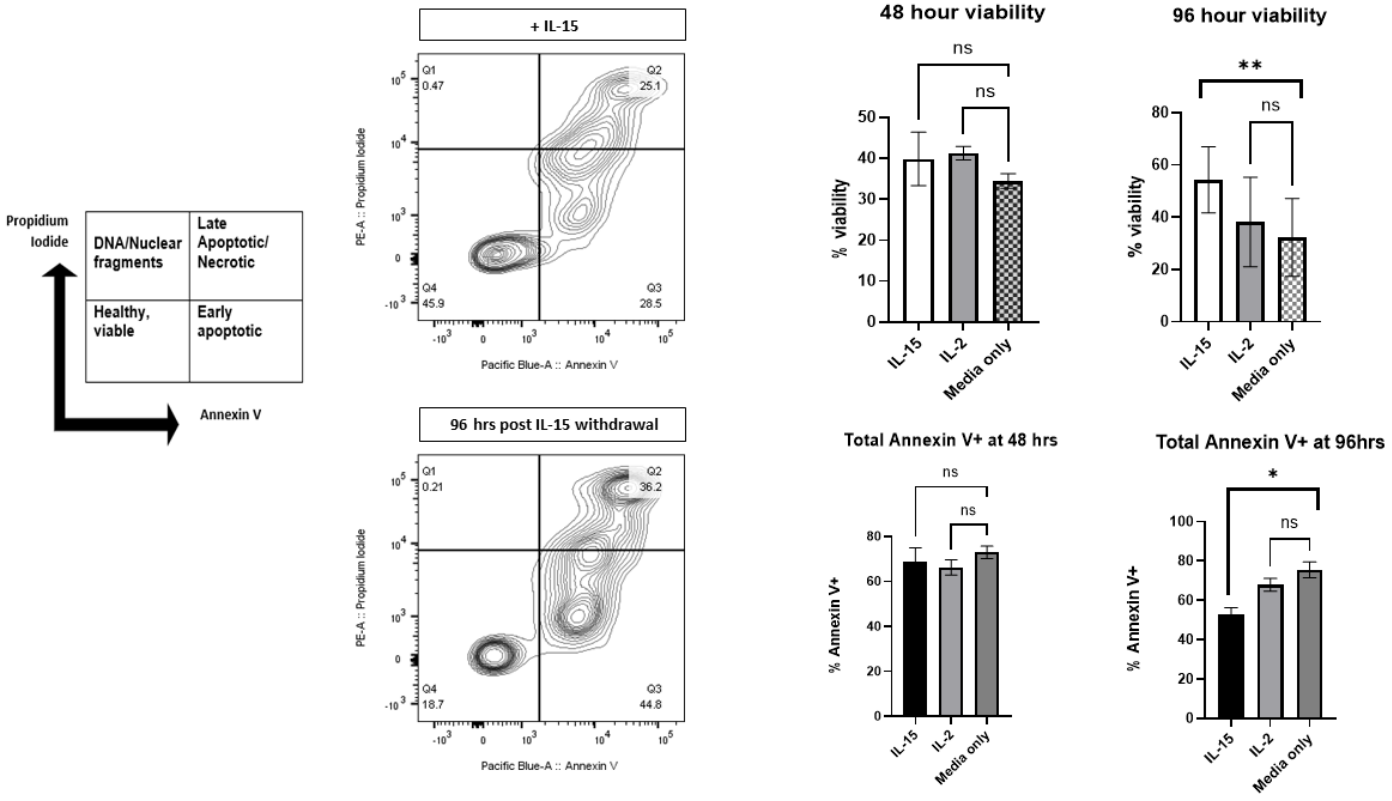

Figure 3-18. IL-15 deprivation experiment. Left: Schematic figure showing the populations represented in a typical Propidium Iodide versus Annexin V plot and flow cytometry contour plots of a representative sample showing proportions of apoptotic/necrotic cells in control cells maintained in 100ng/ml of IL-15 and 96 hours after Il-15 withdrawal. The cells were initially expanded in IL-15 containing media for 14 days prior to IL-15 withdrawal. Events were gated on single cells. Right (above): Comparison of cell viability following PBMC culture in IL-15, IL-2 or complete media without cytokines, determined at 48- and 96-hours post-media change. Right (below): Comparison of Annexin V+ percentage following PBMC culture in IL-15, IL-2 or complete media, 48- and 96-hours post-media change. Cells were expanded for 14 days prior to IL-15 withdrawal. All error bars indicate SE of means. ns = not significant, *p < 0.05, **p < 0.01.

3.6 DISCUSSION

Gamma Delta T cells have numerous properties which are desirable for cancer immunotherapy. The ability of these cells to recognize and eliminate tumours has been demonstrated by various *in vitro* and murine experiments but no significant clinical translation has occurred over the past couple of decades. Furthermore, γδ T cells, particularly Vδ1 T cells, are rare in peripheral blood hence a highly efficient expansion method would be required to achieve sufficient cell numbers required for clinical use. Limited knowledge of the natural ligands of the Vδ1 TCR also makes identification of appropriate stimulants/agonists difficult. Furthermore, since many TCR agonist are shared by multiple T cell types, purity is often an issue. Therefore, αβ T cell depletion or positive selection of γδ T cells is often required prior to expansion. As positive selection or cell sorting often requires TCR binding with a monoclonal antibody, this skews the phenotypes of the eventual cell product and may affect their functional properties. This makes the novel Vδ1 expansion method described in this chapter particularly attractive as direct manipulation of the Vδ1 TCR is avoided. Moreover, unlike other expansion protocols requiring IL-2 stimulation, this method utilizes IL-15 which, like IL-2, stimulates cytotoxic cells but avoids IL-2 mediated enhancement of regulatory T cells (Tregs).[170]

The predominantly MHC-independent mode of antigen recognition by γδ T cells makes allogeneic use of these cells particularly attractive as they are unlikely to cause a graft-versus-host reaction. Therefore, the highly desired “off-the-shelf” cell product is indeed feasible with γδ T cells. Adoptive transfer of lymphocytes such as Chimeric Antigen Receptor (CAR) T cells often requires isolation of PBMCs by apheresis followed by T cell expansion and CAR transduction before re-infusion to the patient. This process often takes several weeks and cell expansions are not always successful.

Furthermore, due to the immune dysfunction often associated with cancers and the effects of prior lymphotoxic therapies, expansion of T cells may be difficult or unsuccessful in some cancer patients. Therefore, an allogeneic product which does not trigger GVHD would be particularly beneficial for this group of patients.

While the combination of ZOL and IL-2 expands Vγ9δ2 cells, most Vδ1 expansion methods use T cell mitogens such as phytohaemagglutinin (PHA) which is a lectin extracted from red kidney beans.[171] While its exact mechanism of T cell activation is not completely understood, the PHA-L subunit (leucoagglutinin), agglutinates lymphocytes by binding to oligosaccharides as well as adenine and related ligands.[172] It has been shown that PHA binds to a component of the CD3 complex[173] which together with the γδ chains, forms the γδ TCR complex. While PHA binding to glycosylated components of the CD3 complex may explain T cell activation, this does not sufficiently explain the preferential expansion of Vδ1 cells observed under certain conditions. Apart from the structural differences between the αβ and γδ heterodimers, there are qualitative and quantitative differences in the CD3/TCR complex between the two lymphocyte subsets.[174] For instance, γδ T cells express approximately two-fold more TCR on the cell surface than αβ T cells.[175] This may account for the preferential expansion of certain subsets following PHA stimulation.

In this project, a novel Vδ1 expansion method which relies on stimulation with a monoclonal CD3 antibody and IL-15 has been compared with PHA expansion with either IL-2 or IL-7. The CD56 depletion step is necessary for the reduction of NK cells which would otherwise compete with γδ T cells following stimulation with IL-15. The combined αβ T cell and CD56+ depletion step was shown to be at least non-inferior to sequential depletions (αβ T cell followed by CD56+ depletion) in terms of fold expansion of Vδ1+ T cells (figure 3-3A and 3-3B).

CD3 and IL-15 stimulation produced superior Vδ1 expansion compared with PHA plus either IL-7 (figure 3-5) or IL-2 (figure 3-6). However, significant donor variation was observed in terms of fold expansion of Vδ1+ cells for either method. In general, donors with reduced Vδ2/Vδ1 ratios (i.e. more Vδ1 than Vδ2 T cells) at baseline were also good Vδ1 expanders (figure 3-11). It is therefore probable that Vδ1 cells are already primed for expansion in these patients presumably due to donor-related factors such as prior exposures to specific antigens. As the blood donors in this project were completely anonymised, it was unfortunately not possible to obtain relevant demographic data about donors.

While no direct experimental comparison was made with the DOT protocol by Almeida et al,[167] the anti-CD3/IL-15 method described in this chapter offers several advantages including simplicity and cost effectiveness. The published phenotypic analysis of the DOT cells similarly showed upregulation of key surface markers including CD69, CD56 and NK receptors on Vδ1 T cells. However, the DOT protocol requires a cocktail of cytokines and a 2-step process which will be expensive for clinical-scale expansion of Vδ1 T cells compared with the simple CD3/IL-15 method. While experimental data has shown potent anti-cancer properties for Vδ1 T cells expanded by both methods, TCR repertoire analyses could further elucidate the differentiation stages of the cells and predict efficacy. This could potentially be employed in selecting ideal donors for manufacture of cell therapy products for off-the-shelf use.

Furthermore, it is clinically relevant that Vδ1 T cells were successfully expanded with the CD3/IL-15 method following a 14-day period of cryopreservation (Figure 3-8A). The Vδ2/Vδ1 ratio post-thaw was comparable to the ratios measured following fresh PBMC isolation for each donor (Figure 3-8B) indicating that neither of the two major γδ subsets was lost following thawing. This is particularly beneficial for clinical

translation as cryopreservation is often required during the cell manufacture process. No differences were observed between T lymphocytes expanded from fresh or thawed PBMCS with respect to CD69 or NKG2D expression however a higher proportion of thawed cells expressed PD-1 on expansion with CD3/IL-15 (figure 3-13). As there were no significant differences in expansion, it is likely that PD-1 expression in this context reflects activation rather than exhaustion. T lymphocytes expanded from thawed PBMCs also differed from those expanded from fresh PBMCs in having lower proportions of T_{EMRA} and more Naïve T cells. (figure 3-16C) The significance of these observed minor differences between fresh and thawed PBMC expansions is uncertain and may require further analyses using a larger number of PBMC donors. Furthermore, the classification of differentiation phenotypes has been validated for αβ T cells and its extrapolation for γδ T cells is controversial.

By including a purification step which depletes Vδ2+ and αβ T cells, it was possible to obtain a Vδ1 cell purity of up to 90% (Figure 3-10). This population consists of unmanipulated Vδ1 cells as they are purified by negative selection. These cells would be particularly useful for future functional experiments where a pure Vδ1 population is desired. However, in the clinical context, it is unlikely that an ultra-pure Vδ1 T cell product would offer significant advantages over a mixed Vδ2/Vδ1 cell product.

Following CD3/IL-15 expansion, T lymphocytes expressed significantly higher levels of the activation marker CD69 and the cytotoxicity receptor NKG2D (figure 3-7) compared with PHA/IL-2. Similarly increased levels of CD56 were observed with CD3/IL-15 but the difference was not statistically significant (figure 3-7).

For T lymphocytes expanded by CD3/IL-15 (Figure 3-12), there was no difference in CD69 expression between Vδ1+ and Vδ1- (which were mainly Vδ2+) T lymphocytes.

However, a significantly higher proportion of Vδ1+ lymphocytes expressed NKG2D and interestingly, PD-1. Previous studies have similarly shown higher PD-1 expressions on Vδ1 compared with Vδ2 T cells[73,89] however, despite the expression of PD-1, Vδ1 T cells maintain a highly cytolytic profile without features of exhaustion. Although PD-1 has been thought to be a marker of T cell exhaustion, recent studies have shown that it is often upregulated in activated T cells and therefore, in certain contexts, may be a marker of activation.[176] Furthermore, cytokines such as IL-15 can directly induce PD-1 expression on T cells.[177]

To determine disparities in the differentiation phenotypes resulting from expansion with either CD3/IL-15 or PHA/IL-2, expression of the cell surface markers CCR7 and CD45RA were compared (Figure 3-14). In contrast to CD3/IL-15 expanded cells which were predominantly CCR7negCD45RA+, T lymphocytes expanded with PHA/IL-2 were mainly CCR7negCD45RAneg (Figure 3-14A). It must be mentioned that while the classification of T cell memory phenotypes based on expression of the cell surface markers CD45RA and CCR7 (or CD27) has been extensively characterised for αβ T cells, it is unclear if this equally applies to γδ T cell maturation as published data is limited.

Furthermore, CD3/IL-15 expanded T lymphocytes demonstrated dose-dependent cytotoxicity against a range of human cancer cell lines (figure 3-16). This was assessed directly by specific cytotoxicity via the chromium release assay. Cytotoxicity was also indirectly assessed by CD107a degranulation and there was an increase in response to cancer cell lines, statistically significant for the glioblastoma cell line, U87 (figure 3-17). Reassuringly, there was no appreciable CD107a degranulation response against allogeneic PBMCs.

A progressive reduction in cell viability and an increase in the proportion of apoptotic T cells was observed following withdrawal of IL-15 after an initial 14-day period of expansion with IL-15 (Figure 3-18). Furthermore, replacing IL-15 with IL-2 was not sufficient to prevent apoptosis. It therefore appears that these cells specifically require IL-15 for continued proliferation and survival. Strategies to overcome this IL-15 dependence such as ectopic activation of the JAK/STAT pathway will be explored in the course of this research.

3.6.1 Conclusion and future research

In summary, CD3/IL-15 stimulation is an effective method of expansion of Vδ1+ γδ T cells, providing superior fold expansions and cell quality compared with PHA-based expansions. The expanded Vδ1 γδ T cells expressed high levels of cytotoxicity markers and demonstrated specific cytotoxicity against human cancer cell lines. However, as lymphocytes generally require stimulation for ongoing proliferation and survival, further experiments will focus on fine-tuning the cancer targeting properties of these cells by transduction of a B7-H3 specific CAR while exploring strategies for enhancing persistence of these cells with manipulation of the JAK/STAT pathway.

Chapter IV: INVESTIGATION OF THE EFFICACY OF B7-H3 SPECIFIC CHIMERIC ANTIGEN RECEPTOR (CAR) GAMMA DELTA T CELLS

4.1 Introduction

In the previous chapter, the antitumour properties of IL-15 stimulated γδ T cells were demonstrated against a range of haematological and solid tumour cell types. The sensing of malignantly transformed or “stressed” cells by γδ T cells is mediated via a myriad of innate receptors and the γδ TCR. However, genomic instability often results in the emergence of malignant clones which can evade immune control by downregulating stress signals. Transduction of a chimeric antigen receptor (CAR) to γδ T cells ensures redirection of antitumour activity against target cells bearing the antigen. Furthermore, γδ T cells are excellent effector cells for CAR T cell therapy as the absence of MHC-restricted activation potentially avoids the development of graft versus host disease when infused into an allogeneic recipient. This would allow the development of an off-the-shelf product which would be extremely beneficial to patients who fail T cell harvest and significantly reduce time to treatment commencement.

CAR therapy can be considered a form of gene therapy where instead of correcting a gene defect, immune cells are genetically modified to more efficiently target a cell bearing an antigen of interest. The generation of CAR cells involves the expression of a synthetic receptor on native immune cells and several methods have been devised to achieve this.

4.2 CAR expression methods

4.2.1 Viral vectors

Viral vectors are the most common methods for CAR engineering and form the basis of current FDA-approved CAR T cell products. This method involves the use of retroviral or lentiviral vectors to integrate the DNA encoding the CAR into the immune effector cell. While both viral methods can efficiently transduce T cells, significant differences exist between lentiviral and gamma-retroviral vectors. While lentiviruses can transduce both resting and dividing cells, gamma-retroviruses generally transduce dividing cells more efficiently.[178] This difference is thought to be due to the fragmentation of the nuclear envelope during cell division which permits integration of retroviruses into the host's genome. Lentiviruses have evolved a more efficient integration mechanism which can traverse an intact nuclear membrane.[179]

Furthermore, gamma retroviral vectors in contrast to lentiviral vectors have a propensity to integrate into gene promoters hence the latter are considered to be safer with regards to the potential for oncogenic transformation.[180] Therefore, most clinical CAR products are generated with lentiviral vectors however the mutagenic risk is still not completely eliminated.

4.2.2 Non-viral vectors

The mutagenic risk of viral vectors has led to the exploration of non-viral based methods. These include Sleeping Beauty (SB) and PiggyBac (PG) transposon-based methods[181] as well as electroporation.[182] Novel methods such as the use of lipid nanoparticles are also being explored to deliver mRNA into the nucleus of the host cell.[183] While these methods offer the advantage of being safer and cheaper than

viral-based gene delivery methods, lower transduction efficiency and low cell viability (in the case of electroporation) are significant drawbacks.

A detailed literature review and introduction to CAR therapy has been presented in Chapter I. In this chapter, the antitumour functions of Vδ1-enriched γδ T cells transduced with a second-generation B7-H3-specific CAR bearing the CD28 co-stimulatory domain will be investigated. The functional readouts will be cytotoxicity, cytokine production and proliferation in response to antigen-expressing targets. In addition, Vδ1.CAR T cell function in the absence of the stimulating cytokine, IL-15, will be explored.

4.3 Chapter Objectives

1. To characterise the antitumour effects of Vδ1-enriched γδ T cells transduced with a B7-H3 specific CAR.
2. To determine if CAR signalling compensates for the loss of stimulatory effects of IL-15 following cytokine withdrawal.

4.4 Methods

4.4.1 Gamma retrovirus production

A second-generation CAR specific for human B7-H3 by virtue of a novel scFv termed TE9 and encoding the RQR8 safety switch and CD28 co-stimulatory domain (TE9 CD28z) was cloned into the SFG gamma retrovirus vector in the Anderson laboratory.[184] **Figure 4.1** shows a schematic illustration of the structure of the CAR. RD114 pseudotyped retroviral particles were produced by triple transfection using gag-pol, env (RD114) and TE9 CD28z CAR plasmids (all obtained from the Anderson lab team) in HEK293T cell line. Virus supernatants were harvested at 48 and 72 hours, both supernatants were combined and either used directly for transduction of Vδ1 enriched gamma-delta T cells or snap-frozen for future use. The procedures for retrovirus production are described in detail in the Materials and Methods chapter.

4.4.2 Transduction of Vδ1-enriched gamma delta T cells with B7-H3 specific CAR

Following initial depletion of αβ T cells and CD56+ cells, PBMCs were stimulated with 1µg/ml of anti-CD3 (Miltenyi) and 100ng/ml of IL-15 (Peprotech). The cell medium was changed on Day 3 and replaced with fresh complete medium supplemented with 100ng/ml of IL-15. The resulting Vδ1 T cell-enriched cells were counted and 0.5 $x10^6$ γδ T cells in 500 µl volume were plated in 24-well plates coated with RetroNectin (Takara). A 1.5 ml volume of B7-H3 CAR virus supernatant was added to the cell suspension and incubated for 48 hours at 37^oC and 5% CO_2. Transduction efficiency was assessed by the proportion of cells positive for CD34 via

flow cytometry. After 48 hours of incubation with the retrovirus supernatant, the cells were washed and resuspended in complete media with 100ng/ml of IL-15 and expanded every 2-3 days with fresh complete media with 100ng/ml of IL-15.

4.4.3 Flow cytometry for intracellular antigens (including cytokines)

For the detection of intracellular cytokines, Vδ1 T cell-enriched PBMCs were first co-cultured with the appropriate target or stimulant. After the first hour of stimulation, the culture plates were retrieved and a 1:1000 solution of monensin (Biolegend) was added to the culture medium to inhibit protein transport and to enable accumulation of cytokines within the Golgi complex. This was followed by another 3-4 hours of incubation at 37 ^{o}C and 5% CO_2. The cells were subsequently washed and resuspended in cell staining buffer (Biolegend) and incubated at 4^{o}C with antibodies specific for cell surface markers such as CD3 and a fixable viability dye for 20 minutes. Thereafter, the cells were washed, resuspended in fixation buffer (Biolegend) and incubated at room temperature for 20 minutes. Afterwards, the cells were centrifuged at 300x*g* for 5 minutes and resuspended in permeabilization buffer (Biolegend) followed by the addition of antibodies specific for intracellular antigens. After incubation for 20 minutes at room temperature, cells were washed once with permeabilization buffer and resuspended in cell staining buffer. Flow cytometry acquisition was with the LSRII instrument (BD Biosciences) and subsequent analysis was with the FlowJo software version 10.7.1 (BD Life Sciences).

4.4.4 ELISA assay for cytokine quantification

Following co-culture of CAR-transduced and untransduced PBMCs with cancer cell lines, the supernatants were carefully collected and cytokine production quantified using the Deluxe IL-2 and Interferon-γ ELISA kits (Biolegend) following the manufacturer's protocol. In brief, 96 well plates were first coated with a capture antibody and incubated at 2-8^{o}C overnight. The plates were subsequently washed and following a blocking step, samples and known standards were added to triplicate wells and incubated for 2 hours. A detection antibody was added followed by Avidin-HRP and TMB substrate. The reaction was terminated with a stop solution after 30 minutes and absorbance was read at 570nm and 450nm on a SpectraMax i3x Microplate Reader (Molecular Devices, San Jose, California, USA).

4.4.5 Cytotoxicity assays

The Chromium-51 and CD107a assays cytotoxicity assays were performed as described in the Materials and Methods chapter.

4.4.6 Cell Trace Violet Proliferation assay

Stimulated PBMC suspensions were centrifuged at 300x*g* for 5 minutes. The cell pellet was resuspended in 1:1000 dilution of CellTrace^{TM} Violet (Thermofisher) staining solution and incubated at 37^{o}C for 20 minutes. Complete cell culture media was subsequently added to stop the reaction and incubated at 37^{o}C for 5 minutes. The cells were then pelleted and resuspended in the respective culture media condition. The labelled cells were maintained in culture for 5-7 days at 37^{o}C and 5% CO_2. Flow cytometry acquisition was on the LSRII instrument and CellTrace^{TM} Violet

fluorescence was read at 405nm excitation and 450nm emission (Pacific Blue) channel after exclusion of dead cells with a viability dye.

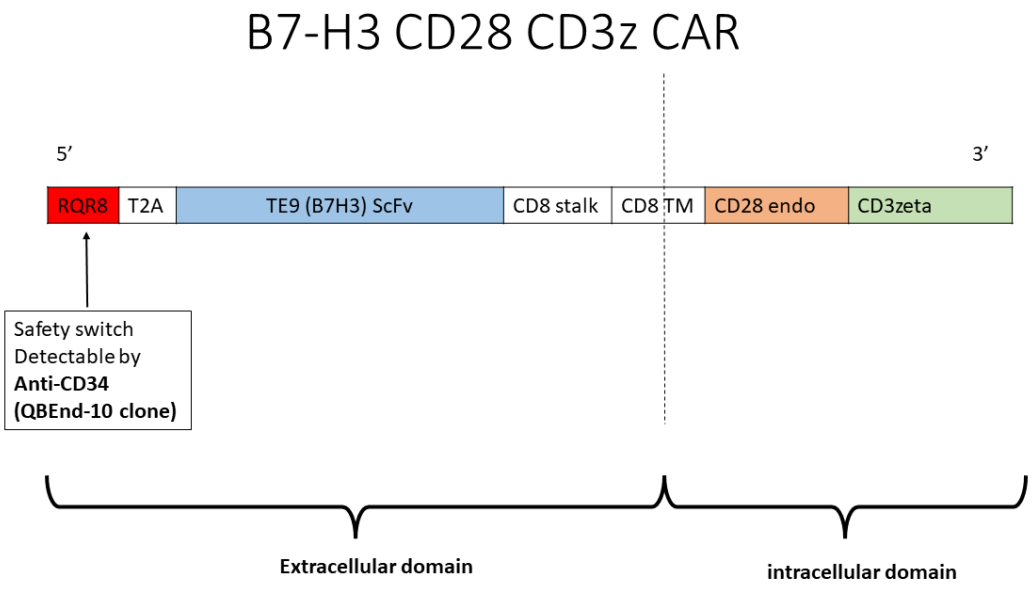

Figure 4-1: Structure of the B7-H3-specific CAR (TE9-28z). A schematic illustration showing the structure of the B7-H3-specific chimeric antigen receptor. The extracellular domain consists of the RQR8 safety switch separated from the ScFv by a self-cleaving T2A sequence. A CD8 stalk separates the ScFv from the intracellular CD28 co-stimulatory domain and CD3zeta signalling domain. The RQR8 safety switch also allows detection of CAR expression by surface staining for CD34 with a monoclonal antibody against CD34 (QBend/10 clone).

4.5 Results

4.5.1 B7-H3 is expressed on a range of cancer cell lines but not on PBMCs.

To determine the degree of B7-H3 expression, cell lines were incubated with a phycoerythrin (PE)-conjugated antibody against human B7-H3 and expression levels were determined by flow cytometry. The highest expression was observed in LAN1 and U87 cell lines while HeLa, Siha and Caski had intermediate levels of expression (**figure 4-2A**). The Jurkat wild type cell line expressed B7-H3 at minimal levels while a Jurkat cell line engineered to express B7-H3 was also tested.

To determine whether PBMCs expressed B7-H3 and to determine if this was upregulated following stimulation, PBMCs were tested before and after stimulation with IL-15. The results showed no significant B7H3 expression either at baseline or following stimulation with IL-15 for 14 days (figure 4-2B).

4.5.2 CAR transduction efficiency

CAR transduction efficiency was routinely assessed by surface staining for the RQR8 suicide gene which is detectable by a monoclonal antibody against human CD34 (clone Qbend/10). To determine the optimal timing for retroviral transduction, CAR transduction efficiencies were compared at Day 3 and Day 7 of expansion with 3 independent donors respectively. Transduction of γδ T cells on Day 3 of expansion consistently yielded a higher proportion of CAR+ T cells (**figure 4-3A**) as opposed to transduction on Day 7 (**figure 4-3B**) although separate donors were assessed.

B7-H3 expression on cell lines and PBMCs

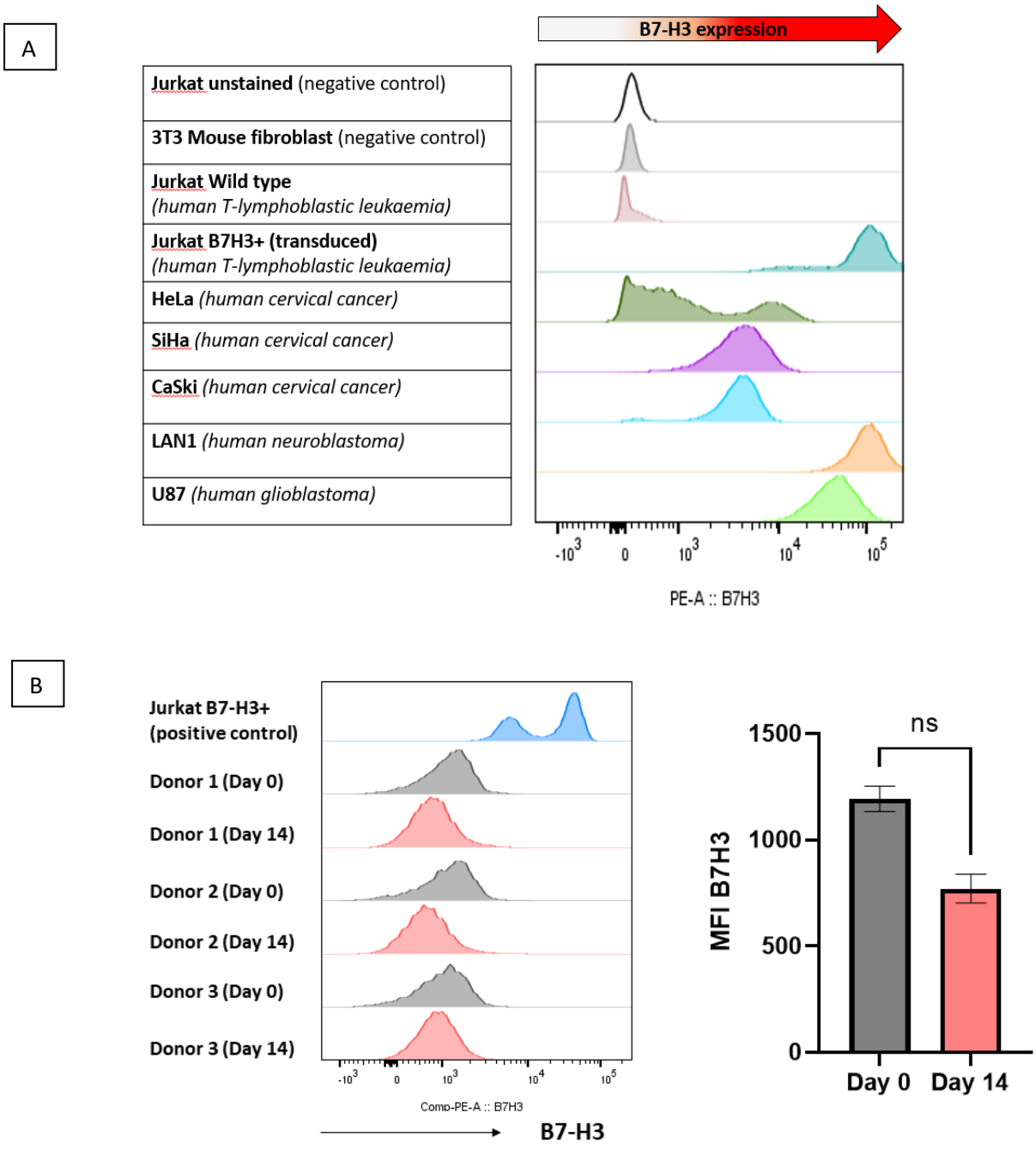

Figure 4-2: B7-H3 expression on cell lines and PBMCs. (A) Flow cytometry histogram plots showing surface B7-H3 expression on a range of cell lines. Events were gated on live cells. (B) Left: flow cytometry histograms (left) showing B7-H3 expression on freshly-isolated PBMCs (n=3) at baseline and 14 days after stimulation with 1µg/ml of anti-CD3 (OKT3 clone) and 100ng/ml of IL-15. Events were gated on CD3+ live cells. Right: Comparison of B7-H3 Median Fluorescence Intensities (MFIs) for PBMCs at baseline (Day 0) and Day 14 after stimulation with anti-CD3/IL-15 (n=3, paired t test, non-significant (ns) p-value >0.05). Error bars indicate standard error of means.

CAR Transduction efficiency

A

B

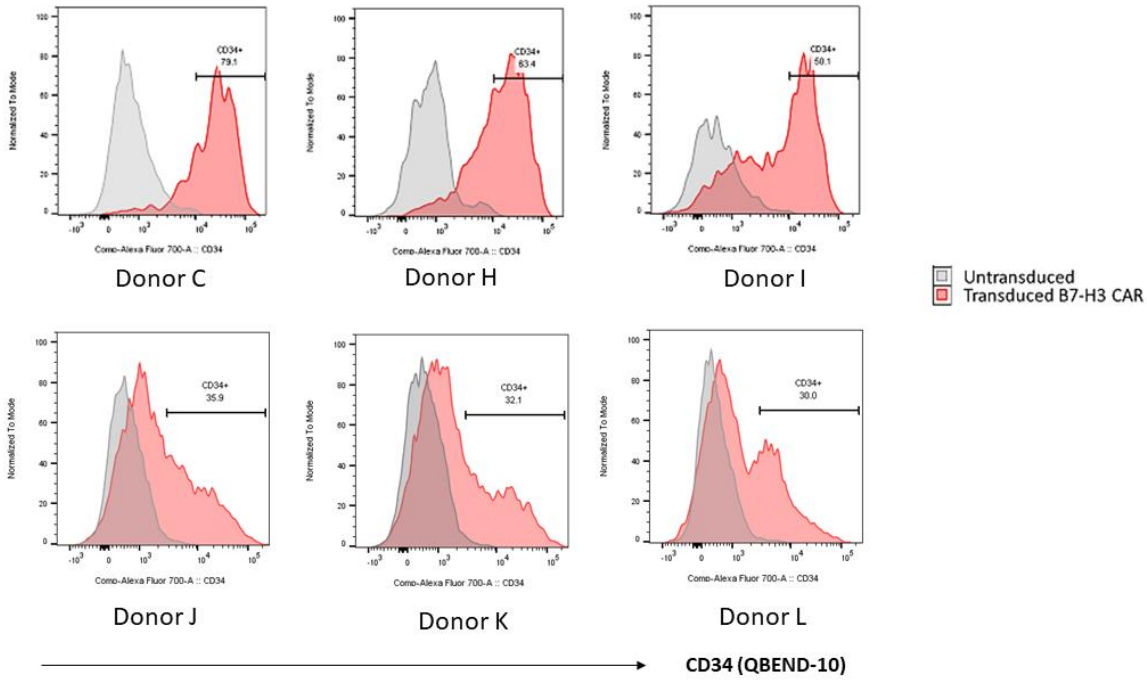

Figure 4-3: CAR expressions following retroviral transductions. (A) Flow cytometry histograms showing surface CD34 expression as a marker of CAR transduction efficiency. PBMCs from 3 separate donors depleted of αβ T cells and CD56+ cells were transduced on Day 3 with CAR-retrovirus supernatants and the culture media supplemented with 100ng/ml of IL-15. The cells were analysed by flow cytometry 48 hours after incubation at 37ºC. Events were gated on CD3+ live cells. (B) Flow cytometry histograms showing CAR transduction efficiencies 48 hours after transduction in a separate experiment. PBMCs from 3 independent donors depleted of αβ T cells and CD56+ cells were transduced on Day 7 with CAR-retrovirus supernatants with complete culture media supplemented with 100ng/ml of IL-15. Events were gated on CD3+ live cells.

4.5.3 CAR-transduced Vδ1 T cells upregulate activation markers.

To evaluate the expression of activation markers following CAR transduction, CAR+ and CAR- cells of the same donors were compared by flow cytometry on Day 10 post-transduction. CAR+ Vδ1 T cells had significantly increased CD69 expression (**figure 4-4).** Similarly, PD-1 expression was significantly upregulated in CAR+ Vδ1 T cells and this was consistent across all three donor pairs assessed. Interestingly, increased expression of the natural cytotoxicity receptor, NKG2D was also observed in CAR+ Vδ1 T cells.

4.5.4 Anti-tumour functions of CAR T cells are enhanced against B7-H3+ targets.

To investigate the anti-tumour degranulation responses of CAR-transduced cells in the presence of B7-H3+ cell lines, the CD107a (Lysosomal-associated membrane protein-1, LAMP-1) degranulation assay was used to compare pairs of CAR-transduced and untransduced donor γδ T cells. CD107a degranulation was significantly enhanced following co-culture with the B7-H3+ LAN1 and U87 cell lines but not with the B7-H3 Jurkat wildtype cell line (**figure 4-5).** Furthermore, there was significant intracellular accumulation of interferon-γ following co-culture with LAN1 with a similar but non-statistically significant increase with U87 **(figure 4-6)**. Intracellular granzyme B was expressed across all donor γδ T cells at high levels with no appreciable increase following co-culture with cancer cell lines **(figure 4-7)**.

.

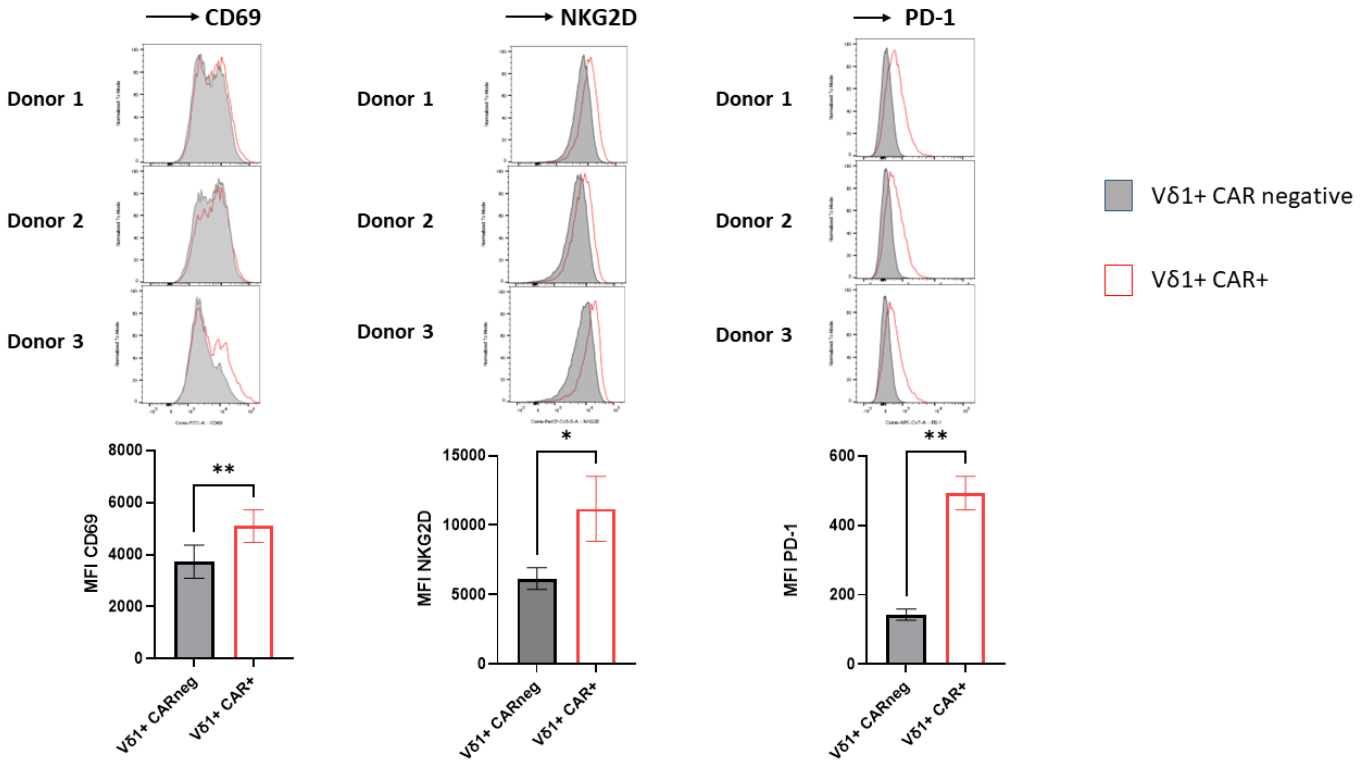

Figure 4-4: Phenotyping of CAR-transduced cells. Above : Flow cytometry histograms of B7-H3 CAR-transduced PBMCs comparing surface expressions of CD69, NKG2D and PD-1 on CAR-positive Vδ1 T cells and CAR-negative Vδ1 T cells for each donor on Day 10 following transduction with the CAR. Below: Graphical comparisons of median fluoresence intensities (MFIs) of CD69, NKG2D and PD-1 between CAR-positive and CAR-negative Vδ1 T cells. Events were gated on Vδ1 T cells and CAR positivity was determined by surface CD34 expression. (n=3, paired t test; *p<0.05, **p<0.01, error bars indicate standard error of means).

A

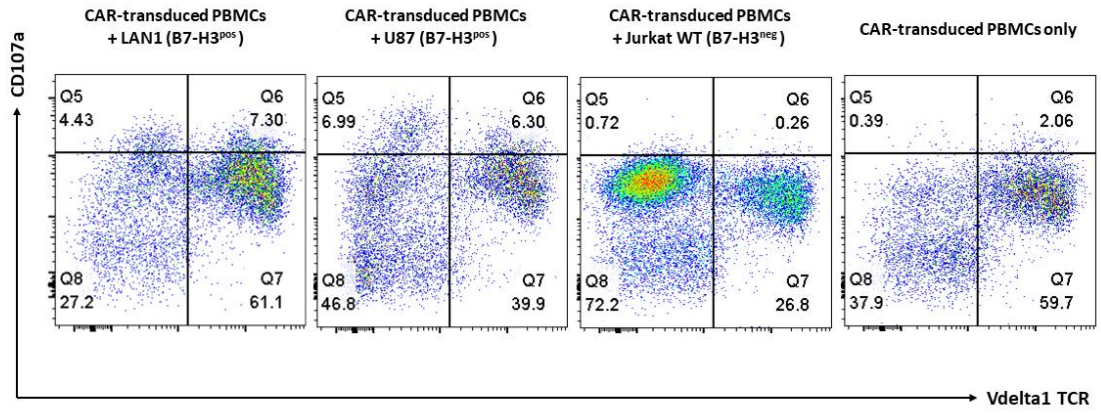

B

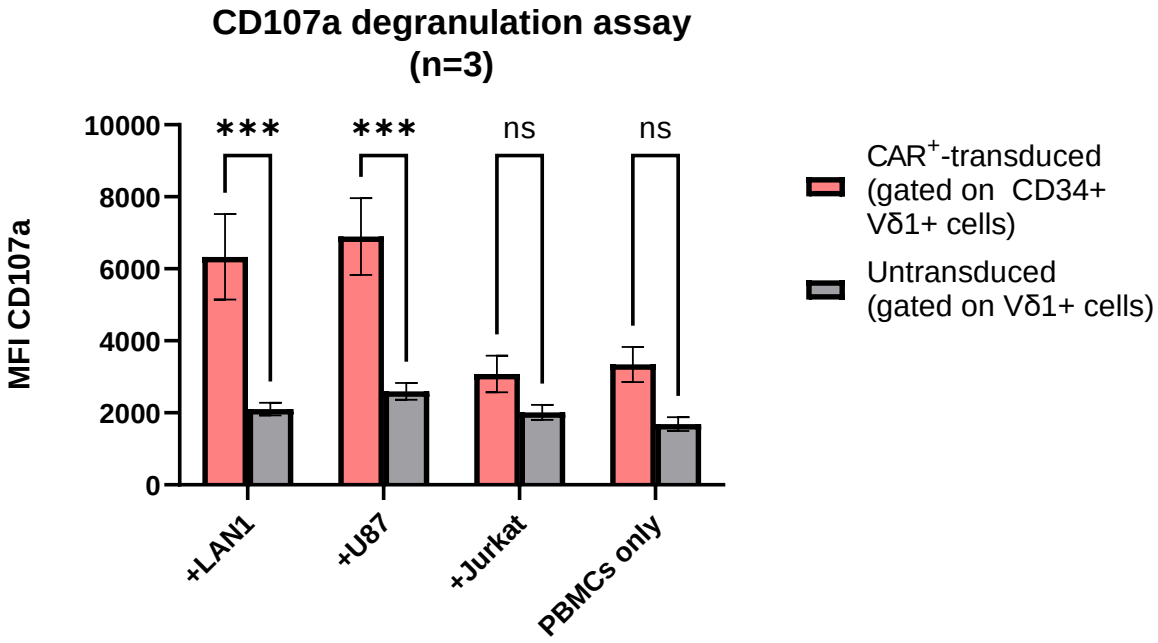

Figure 4-5: CAR CD107a degranulation in response to cancer cell lines. (A) Flow cytometry dot plots for a representative sample showing increased CD107a degranulation in response to B7-H3 positive cell lines. CAR-transduced PBMCs and respective negative controls from 3 separate donors were co-cultured for 5 hours with cancer cell lines in a 1:1 ratio. Cells were labelled with anti-CD107a at the start of the co-culture and 1x monensin was added after the first hour of co-culture. The cells were co-cultured in complete media supplemented with 100ng/ml of IL-15 and incubation was at 37^{o}C and 5% CO_2. Events were gated on live cells. (B) Comparison of Median Fluorescence Intensities (MFIs) of CD107a for the respective co-culture conditions. Events were gated on Vδ1+ live cells (n=3, 2-way ANOVA with multiple comparisons, ns=non-significant, ***p-value <0.001, error bars indicate standard error of means, Jurkat WT=wild-type).

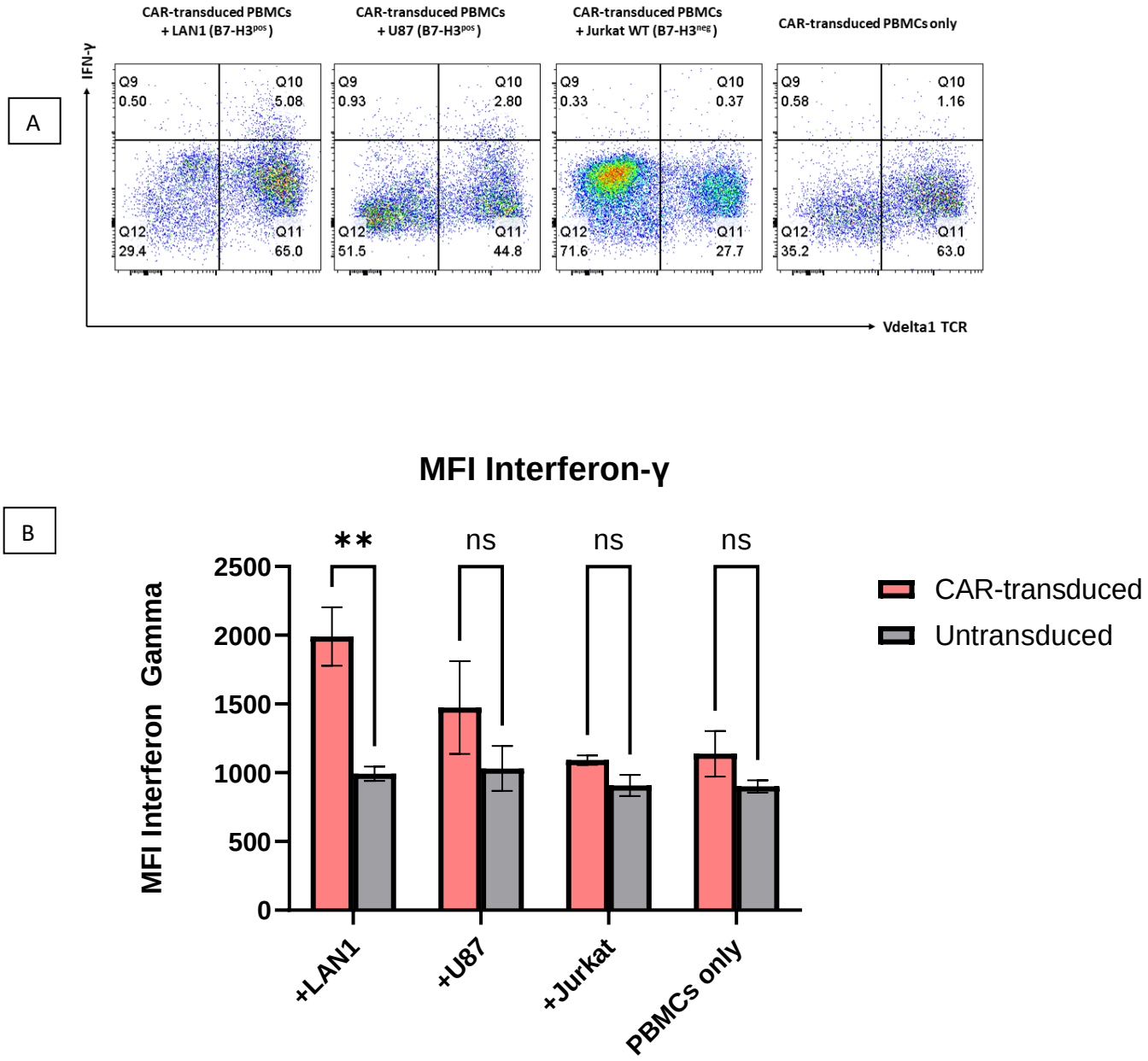

Figure 4-6: Intracellular Interferon-γ accumulation following co-culture with cancer cell lines. (A) Flow cytometry dot plots for a representative sample showing increased Interferon-γ (IFNγ) accumulation in response to the B7-H3 positive cell line, LAN1. CAR-transduced PBMCs and respective negative controls from 3 separate donors were co-cultured for 5 hours with cancer cell lines in a 1:1 ratio and treated with 1x monensin after the first hour of co-culture. The cells were maintained in complete media supplemented with 100ng/ml of IL-15 and incubation was at 37°C and 5% CO_2. Intracellular staining for IFNγ was done after fixation and permeabilization steps. Events were gated on live cells. (B) Comparison of Median Fluorescence Intensity (MFI) of intracellular IFNγ for the respective co-culture conditions. Events were gated on Vδ1+ live cells (n=3, 2-way ANOVA with multiple comparisons; **p-value <0.01, ns=non-significant, error bars indicate standard error of means, Jurkat WT=wild-type).

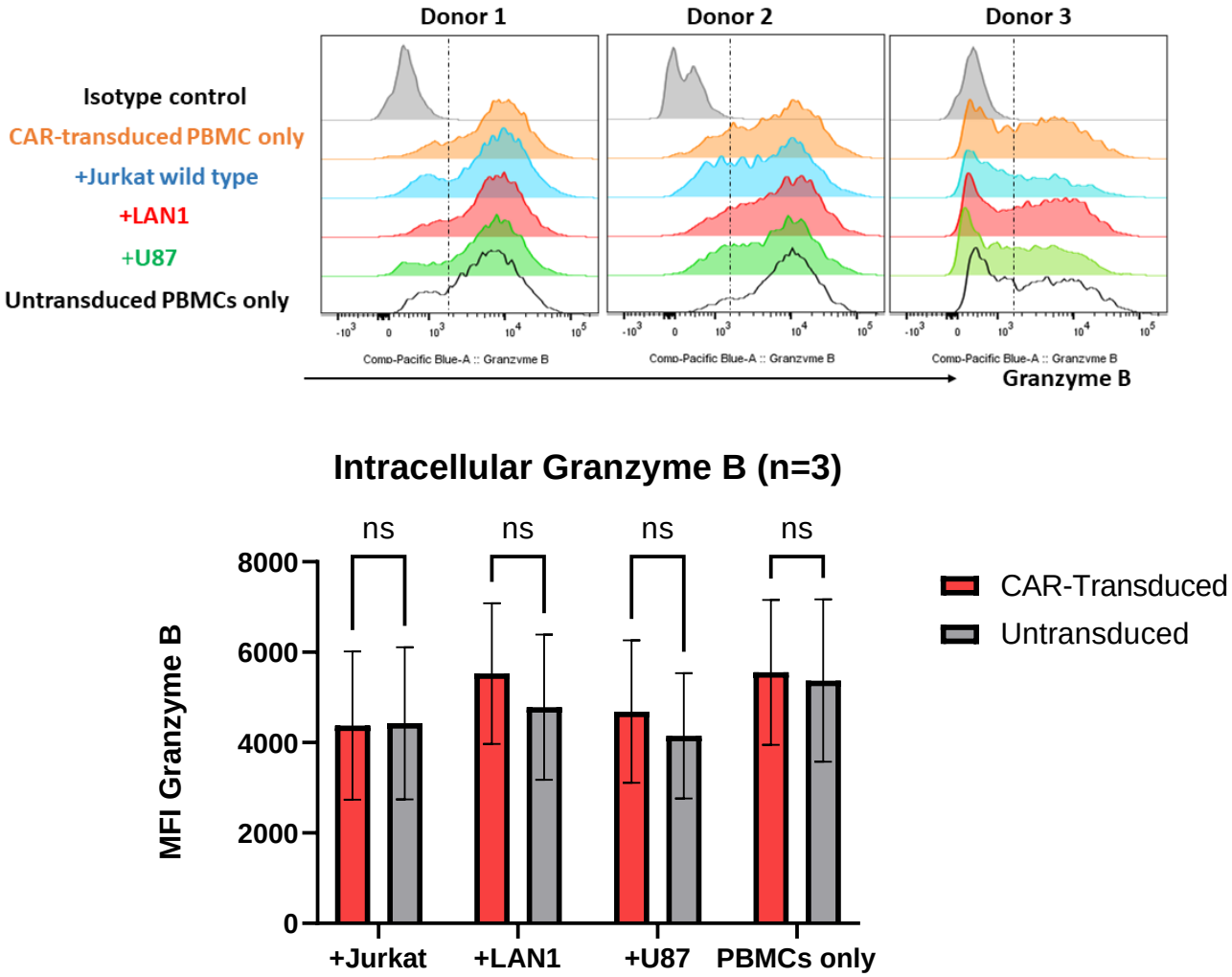

Figure 4-7: Intracellular Granzyme-B accumulation following co-culture with cancer cell lines. (A) Flow cytometry histograms for 3 separate donors showing that intracellular Granzyme B (GrB) accumulation is independent of the presence of CAR or antigen-positive targets. CAR-transduced PBMCs and respective negative controls from 3 donors were co-cultured for 5 hours with cancer cell lines in a 1:1 ratio and treated with 1x monensin after the first hour of co-culture. The cells were maintained in complete media supplemented with 100ng/ml of IL-15 and incubation was at 37^{o}C and 5% CO_2. Intracellular staining for GrB was done after fixation and permeabilization steps. Events were gated on Vδ1+ live cells. (B) Comparison of Median Fluorescence Intensity (MFI) of GrB for the respective co-culture conditions. Events were gated on Vδ1+ live cells (n=3, 2-way ANOVA with multiple comparisons; ns=non-significant, error bars indicate standard error of means).

4.5.5 No significant expression of intracellular IL17A in γδ T cells

Given the potentially pro-tumour properties of IL17A producing γδ T cells, IL17A accumulation in CAR-γδ T was assessed by intracellular flow cytometry staining at baseline and following co-culture with cancer cell lines. There was no appreciable expression of IL17A on Vδ1 T cells and no upregulation following co-culture with either B7-H3+ or B7-H3 negative cell lines (**Figure 4-8).**

4.5.6 γδ T cells do not respond to allogeneic PBMCs.

Given the significant anti-tumour responses of CAR-γδ T cells against tumour cell lines, it was important to determine if there were similar responses against allogeneic PBMCs. Therefore, a co-culture experiment was set up with CAR-γδ T cells against allogeneic PBMCs from 2 independent donors. CD107a degranulation as well as intracellular interferon-γ, Granzyme B and IL-17A were compared following co-culture with allogeneic PBMCs and there was no appreciable response to allogeneic PBMCs (**figure 4-9**).

4.5.7 IFNγ secretion by γδ.CAR T cells is significantly increased in the presence of B7H3 positive cell lines.

To determine if cytokine secretion by γδ.CAR T cells was influenced by the presence of the target antigen, a 24-hour co-culture experiment followed by cytokine quantification by ELISA was set up with both B7-H3+ and B7-H3 negative cell lines. A significant increase in Interferon-γ (IFNγ) was observed in the presence of B7-H3 positive U87, LAN1 and Jurkat B7H3+ but not to wildtype Jurkat (B7H3 negative). Interestingly, a significant increase in IFNγ was observed in CAR-transduced cells compared with untransduced, IL-15 stimulated γδ T cells even in the absence of

cancer cell lines (**figure 4-10A**). No appreciable IL-2 secretion was detected for γδ T cells by ELISA.

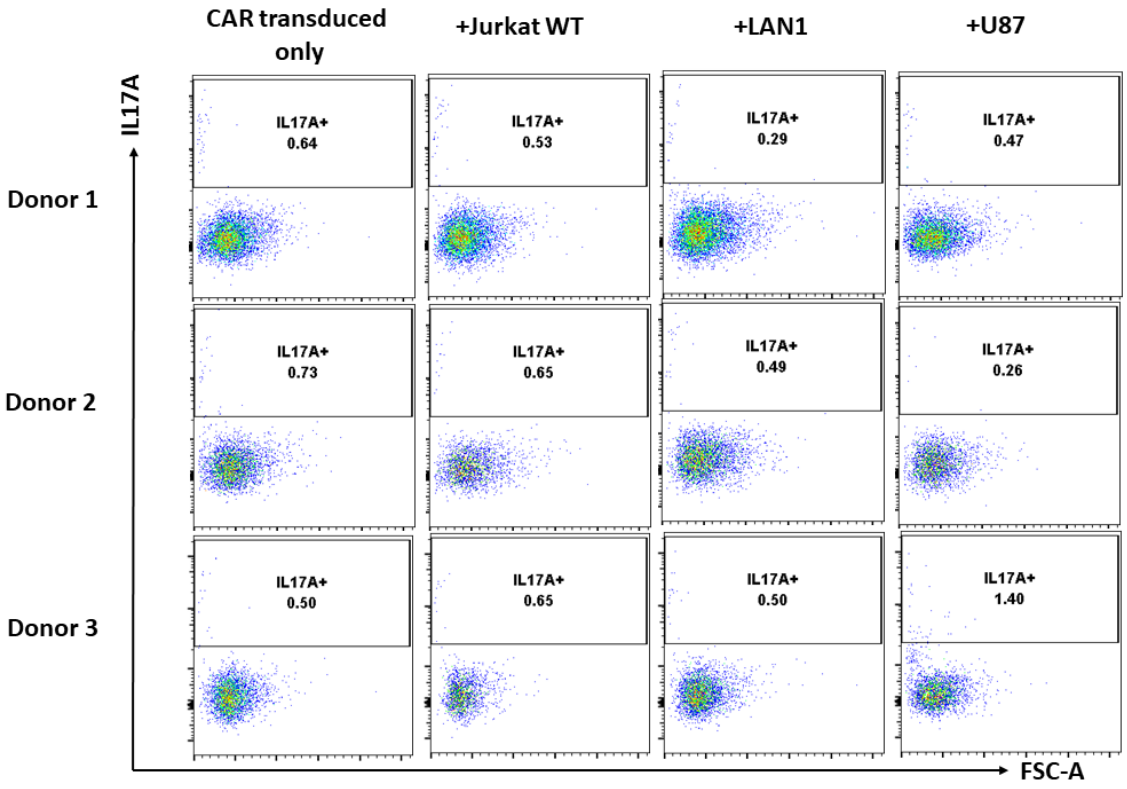

Figure 4-8: Intracellular IL17A accumulation. (A) Flow cytometry dot plots for 3 separate donors showing that intracellular IL17A accumulation is not increased following co-culture with cancer cell lines. CAR-transduced PBMCs and respective negative controls from 3 donors were co-cultured for 5 hours with cancer cell lines in a 1:1 ratio and treated with 1x monensin after the first hour of co-culture. The cells were co-cultured in complete media supplemented with 100ng/ml of IL-15 and incubation was at 37^{o}C and 5% CO_2. Intracellular staining for IL17A was done after fixation and permeabilization steps. Events were gated on Vδ1+ live cells.

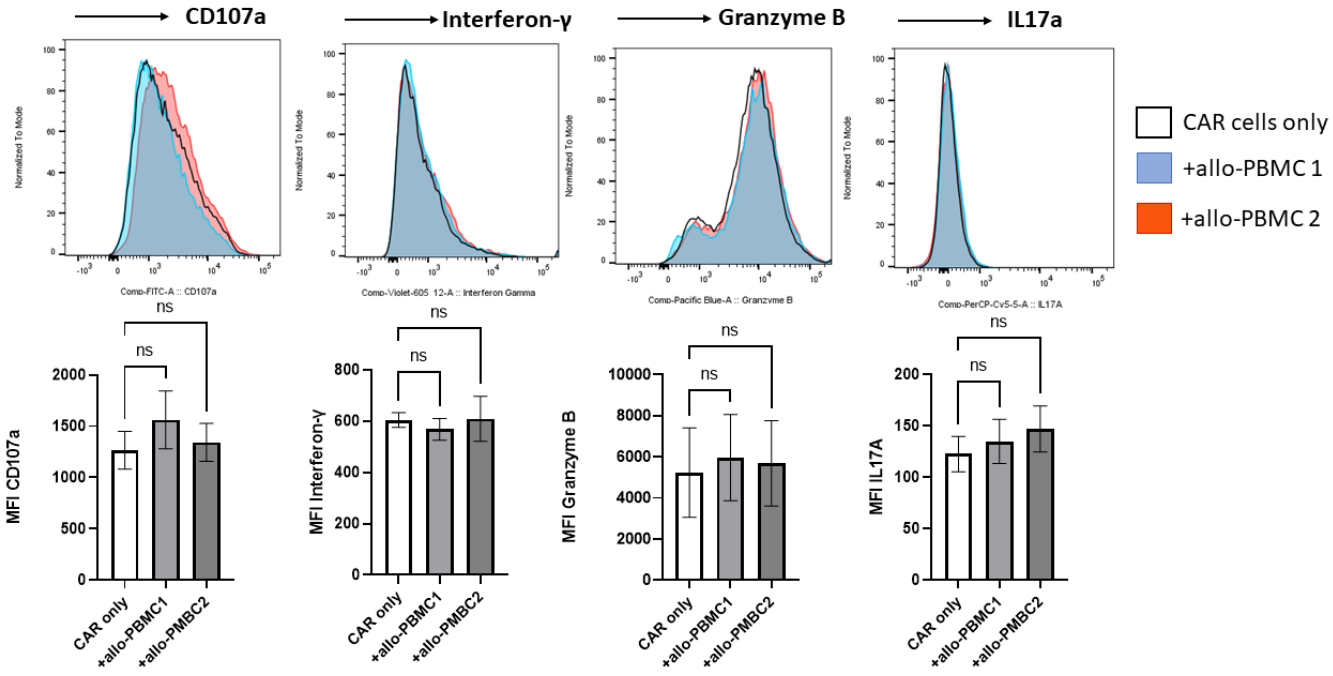

Figure 4-9: CAR co-culture with allogeneic PBMCs. (Above) Flow cytometry histogram plots of CD107a degranulation, intracellular interferon-γ, Granzyme B and IL17A for a representative donor showing that CAR-transduced T cells do not respond significantly to allogeneic PBMCs. CAR-transduced PBMCs and respective negative controls from 3 donors were co-cultured for 5 hours with allogeneic PBMCs(n=2) in a 1:1 ratio and treated with 1x monensin after the first hour of co-culture. The cells were maintained in complete media supplemented with 100ng/ml of IL-15 and incubation was at 37^{o}C and 5% CO_2. Intracellular staining for Interferon-γ, Granzyme B and IL17A was done after fixation and permeabilization steps. Events were gated on Vδ1+ live cells. (Below) Graphical comparisons of median fluorescence intensity (MFI) of CD107a, interferon-γ, Granzyme B and IL17A for the respective co-culture conditions. Events were gated on Vδ1+ live cells (n=3, 1-way ANOVA; ns=non-significant p value, error bars indicate standard error of means).

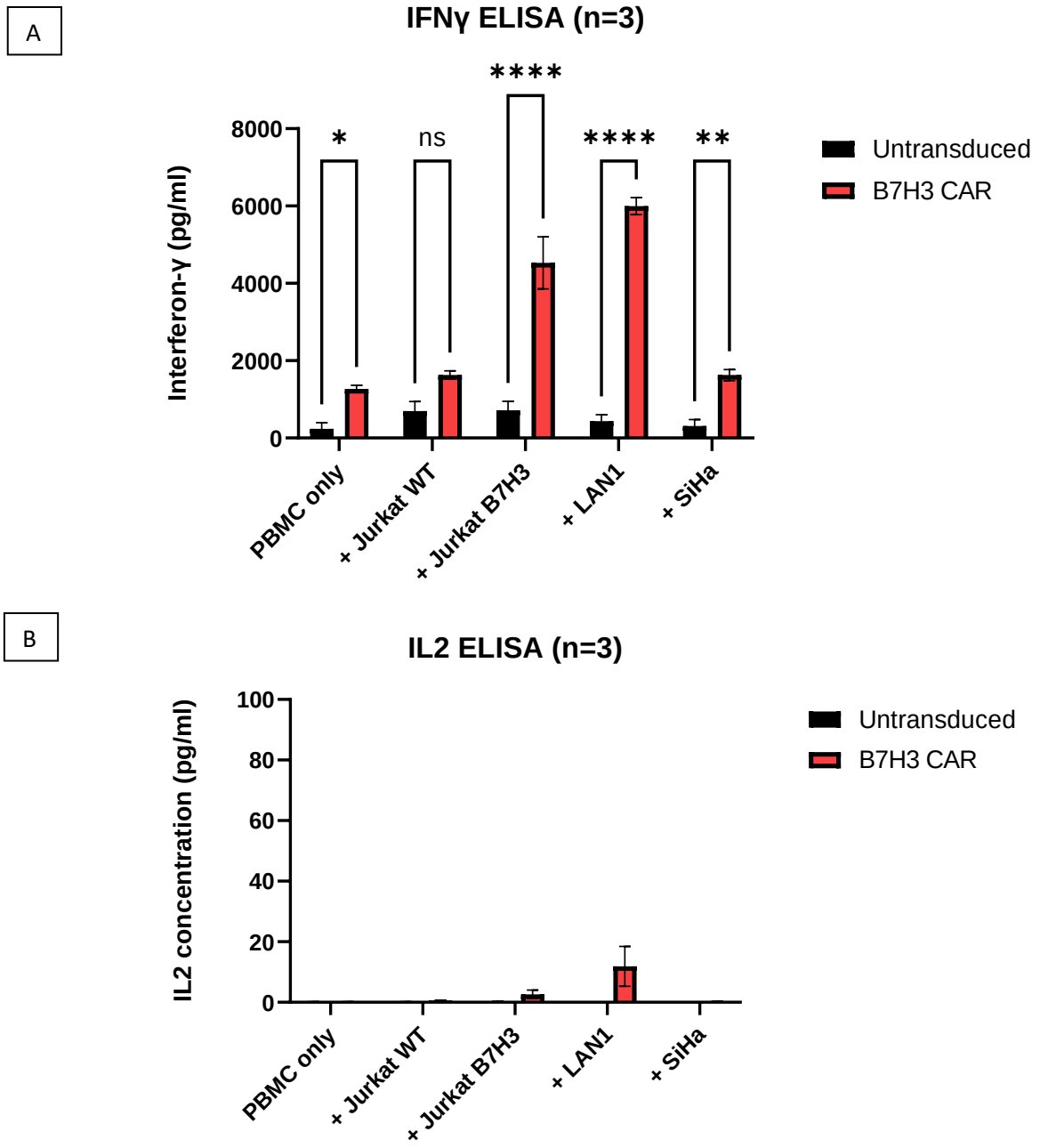

Figure 4-10: Cytokine secretion in response to cancer cell lines. (A) Interferon-γ secretion following a 24-hour co-culture of $2x10^5$ CAR-transduced and untransduced γδ T cells in 1:1 ratio with cancer cell lines in the presence of 100ng/ml of IL-15. The cell culture medium was subsequently harvested and analysed by ELISA for cytokine concentrations. The results show a significant increase in IFNγ secretion for CAR-transduced cells following co-culture with B7-H3 positive cell lines; LAN1, SiHa and B7-H3-expressing Jurkat cell line but not in response to the B7-H3 negative wild-type Jurkat cell line. (n=3, 2-way ANOVA; p values: *p <0.05, **p<0.01, ****p<0.0001, ns=non-significant). (B) IL-2 secretion as similarly measured by ELISA following co-culture of CAR-transduced and untransduced γδ T cells with cancer cell lines in the presence of IL-15. The results show minimal IL-2 secretion. All error bars indicate standard error of means.

4.5.8 CAR T cell cytotoxicity is enhanced against B7-H3 positive targets.

To demonstrate antigen-specific functional enhancement for γδ.CAR T cells, cytotoxicity was compared against Jurkat wildtype and the isogenic jurkat-B7-H3+ cell line. There was significant enhancement of cytotoxicity against the Jurkat B7-H3+ cell line in the presence of IL-15 in a 4-hour co-culture (**figure 4-11A**). To determine the effect of IL-15 withdrawal on the function of γδ.CAR T cells, the cytotoxicity experiment against Jurkat WT and Jurkat B7H3+ was repeated with the same donor γδ CAR T cells following 48 hours of IL-15 withdrawal from the cell culture media. The antigen-specific enhancement of cytotoxicity for γδ.CAR T cells was preserved following IL-15 withdrawal. (**Figure 4-11B**).

The cytotoxicity experiment, including short-term IL-15 withdrawal, was repeated for LAN1, HeLa, Jurkat WT and Jurkat B7-H3 using separate donors and including untransduced, IL-15-stimulated γδ T cells. The general trend was towards a reduction of cytotoxicity for untransduced cells in the absence of IL-15 which was not observed for CAR-transduced cells but in the case of Jurkat B7-H3, the influence of the CAR was not prominent as the curve was comparable to the untransduced condition in the presence of IL-15 (**figure 4-12**). A possible explanation could be that over-expression of B7-H3 in Jurkat B7-H3 cell line sensitizes it to γδ T cell killing via the alternative receptors. The general trend was for a reduction in cytotoxicity following IL-15 withdrawal for the untransduced γδ T cells. Therefore, IL-15 plays an important role in not only promoting proliferation and survival of γδ T cells, but also enhances cytotoxicity against cancer cell lines.

NKG2D is highly expressed on γδ T cells and has been shown to contribute to its cytotoxic potential. Therefore, to determine if NKG2D blockade affects CAR T cell

cytotoxicity, the 4-hour cytotoxicity experiment was repeated following incubation of CAR-transduced T cells with an NKG2D blocking monoclonal antibody. No significant difference in cytotoxicity was observed following NKG2D blockade (**figure 4-13**).

A

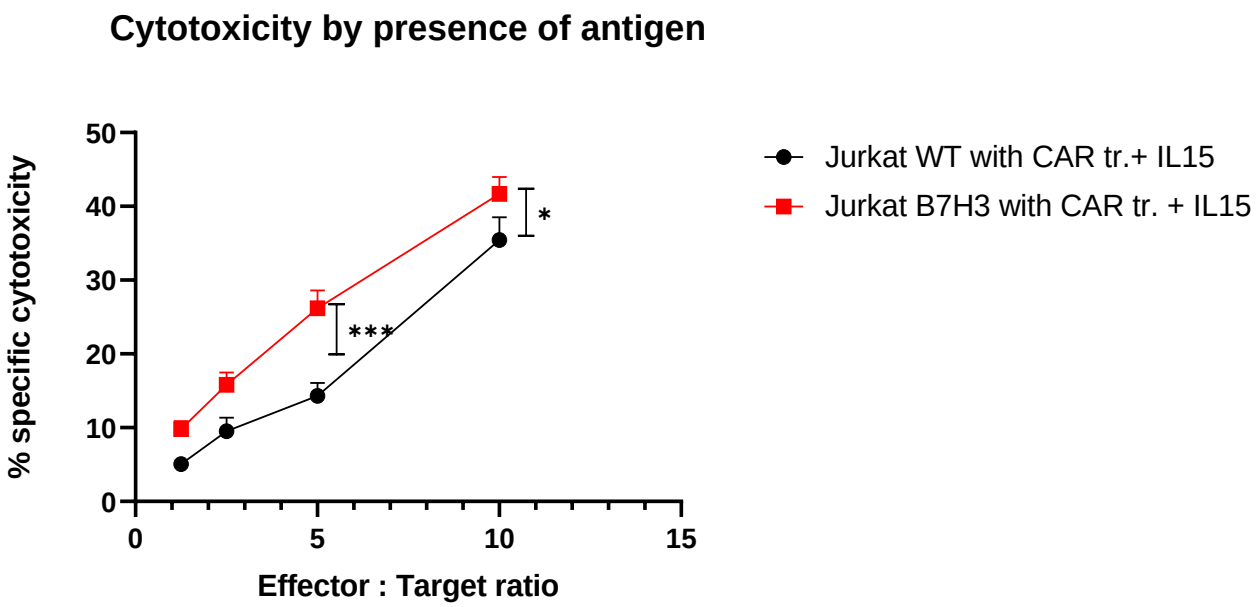

B

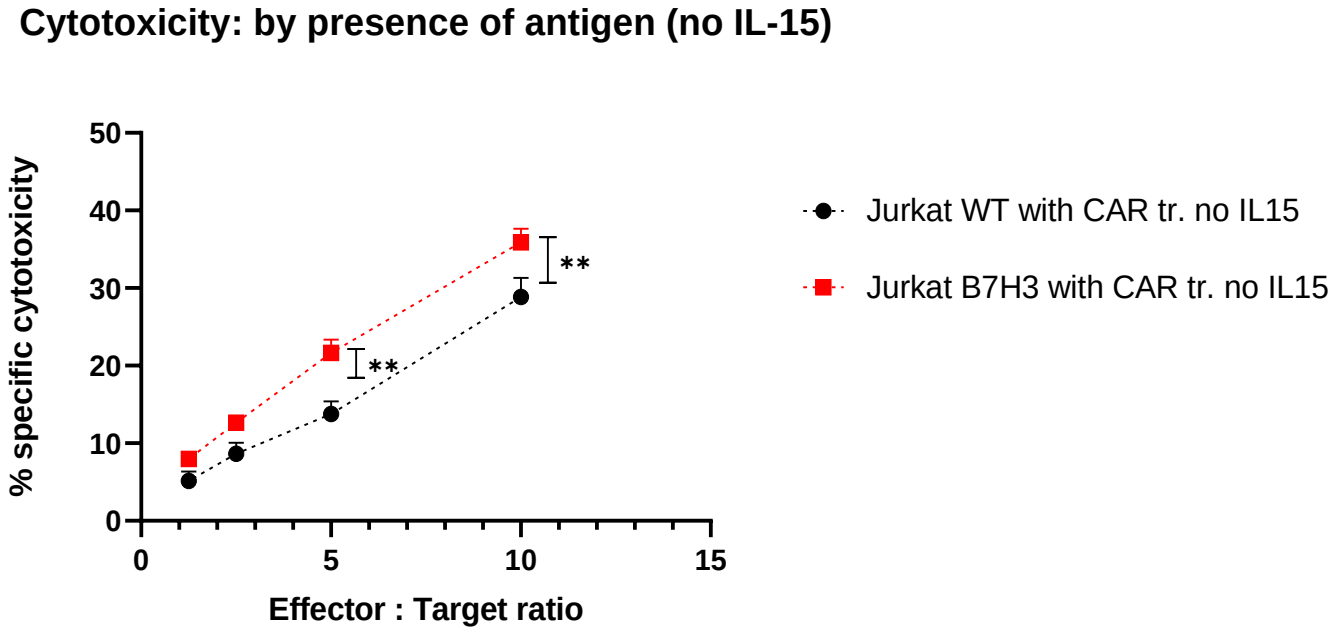

Figure 4-11: Antigen-specific cytotoxicity against Jurkat cell lines. (A) Graphical comparison of specific cytotoxicity of CAR-transduced γδ T cells (CAR tr.) against Jurkat wildtype (B7-H3 negative) and a B7-H3 expressing Jurkat cell line (Jurkat B7-H3) in the presence of 100ng/ml of IL-15. The graphs show significant enhancement of cytotoxicity for the transduced cells in the presence of the B7-H3 antigen. CAR-transduced cells and negative controls were incubated with Chromium-51-labelled cell lines and incubated for 4 hours at 37°C and 5% CO_2 in effector/target ratios of 10:1, 5:1, 2.5:1 and 1.25:1. The cell culture medium was subsequently harvested and cytotoxicity was determined by scintillation counts as a marker of radioactive chromium release. Specific cytotoxicity was normalised to the spontaneous chromium release (negative control) and maximum release (induced by 1% Triton-X100) values. (B) Graphical comparison of specific cytotoxicity of CAR-transduced γδ T cells from the same donors in the absence of IL-15. The effector cells were deprived of IL-15 for 48 hours before co-culture with the cell lines. All other experimental conditions were identical (n=4, 2-way ANOVA *p<0.05, **p<0.01, ***p<0.001 All error bars indicate standard error of means).

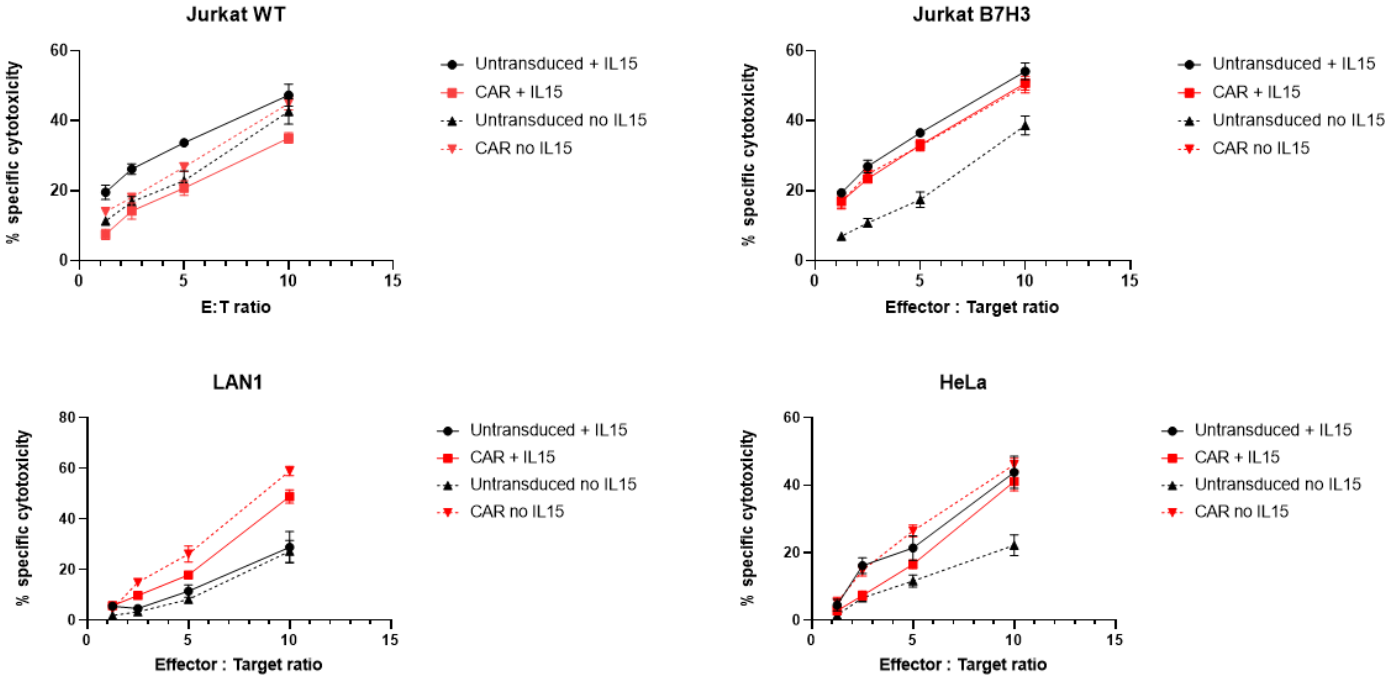

Figure 4-12: Antigen-specific cytotoxicity against tumour cell lines. (A) Graphical representations of the specific cytotoxicities of CAR-transduced and untransduced γδ T cells against B7-H3 negative Jurkat wildtype and B7-H3 positive Jurkat B7-H3, LAN1 and Hela cell lines with or without the presence of IL-15. Paired comparisons were made between specific cytotoxicity of CAR-transduced and untransduced γδ T cells for each donor PBMC/target pair. The graphs show enhancement of cytotoxicity for the transduced cells in the presence of the B7-H3 antigen which was maintained even in the absence of IL-15. CAR-transduced cells and negative controls were incubated with Chromium-51-labelled cell lines and incubated for 4 hours at 37°C and 5% CO_2. The cell culture medium was subsequently harvested and cytotoxicity was determined by scintillation counts as a marker of radioactive chromium release. Specific cytotoxicity was normalised to the spontaneous chromium release (negative control) and maximum release (induced by 1% Triton-X100) values. Where indicated, the culture medium was supplemented with 100ng/ml of IL-15 and for the IL-15 negative conditions, the cytokine was withdrawn 48 hours before the co-culture (n=2, 2-way ANOVA *p<0.05, **p<0.01, ***p<0.001 All error bars indicate standard error of means).

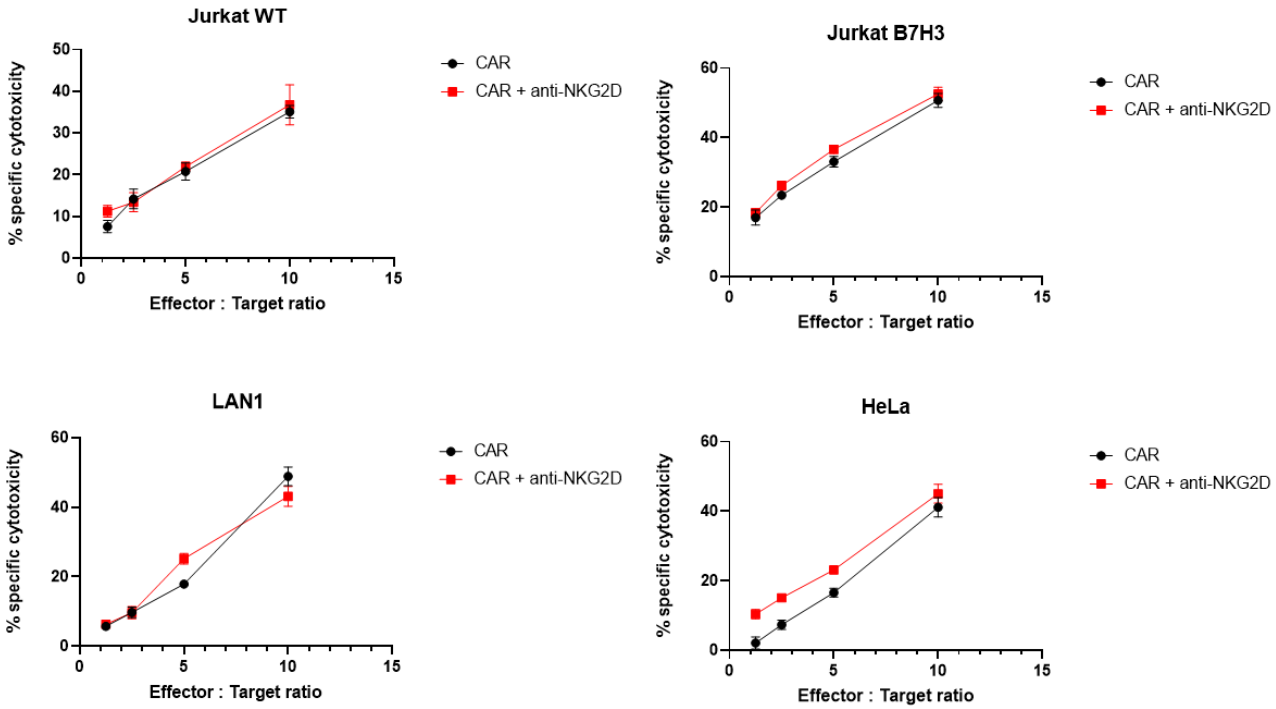

Figure 4-13: CAR Cytotoxicity in the presence of an NKG2D blocking antibody (A) Graphical representations of the specific cytotoxicities of CAR-transduced and untransduced γδ T cells against B7-H3 negative Jurkat wildtype and B7-H3 positive Jurkat B7-H3, LAN1 and Hela cell lines with or without the presence an NKG2D-blocking antibody. Paired comparisons were made between specific cytotoxicity of CAR-transduced γδ T cells with or without anti-NKG2D. For NKG2D receptor blocking, CAR-transduced cells were incubated for 30 minutes with 20µg/ml of purified anti-NKG2D (clone 1D11). The graphs show no significant difference in cytotoxicity despite the presence of the NKG2D-blocking antibody. The cell culture medium was supplemented with 100ng/ml of IL-15. Specific cytotoxicity was determined by chromium-51 release as previously described. (n=2, 2-way ANOVA *p<0.05, **p<0.01, ***p<0.001 All error bars indicate standard error of means).

4.5.9 IL-15 enhances proliferation and Interferon-γ secretion by γδ T cells

To determine the impact of IL-15 withdrawal on CAR T cell proliferation in co-culture conditions with Jurkat WT and Jurkat B7-H3+ cell lines, all cells were first expanded and maintained in IL-15 containing media. The cells were subsequently divided into two independent cultures. For one culture condition, IL-15 was withdrawn from the culture media for 48 hours prior to co-culture and the co-culture was incubated for 5 days. IL-15 deprived CAR-transduced cells were compared with IL-15 maintained CAR transduced cells via the CellTrace Violet proliferation assay. CellTrace Violet dilution (as assessed by reduction in median fluorescence intensity) was significantly enhanced in all the co-culture conditions with IL-15 indicating increased proliferation and this was independent of the presence of cancer cell lines (figure 4-14A & 4-14B). In the absence of IL-15, there was a trend towards increased proliferation in response to Jurkat B7H3+ in 2 of 3 donors i.e cells from Donor 1 had less proliferative capacity for all the conditions (apparent in the flow cytometry histograms) (figure 14-4A) hence the overall difference in median fluorescence intensities was not statistically significant. Similarly, IFNγ secretion was significantly enhanced by IL-15 (figure 4-14C) and antigen-specific induction of IFNγ secretion was maintained in the absence of IL-15. In summary, IL-15 independently drives the proliferation and Interferon-γ secretion by γδ T cells regardless of target engagement. The effect of CAR signalling on proliferation and IFNγ secretion becomes more obvious following IL-15 withdrawal.

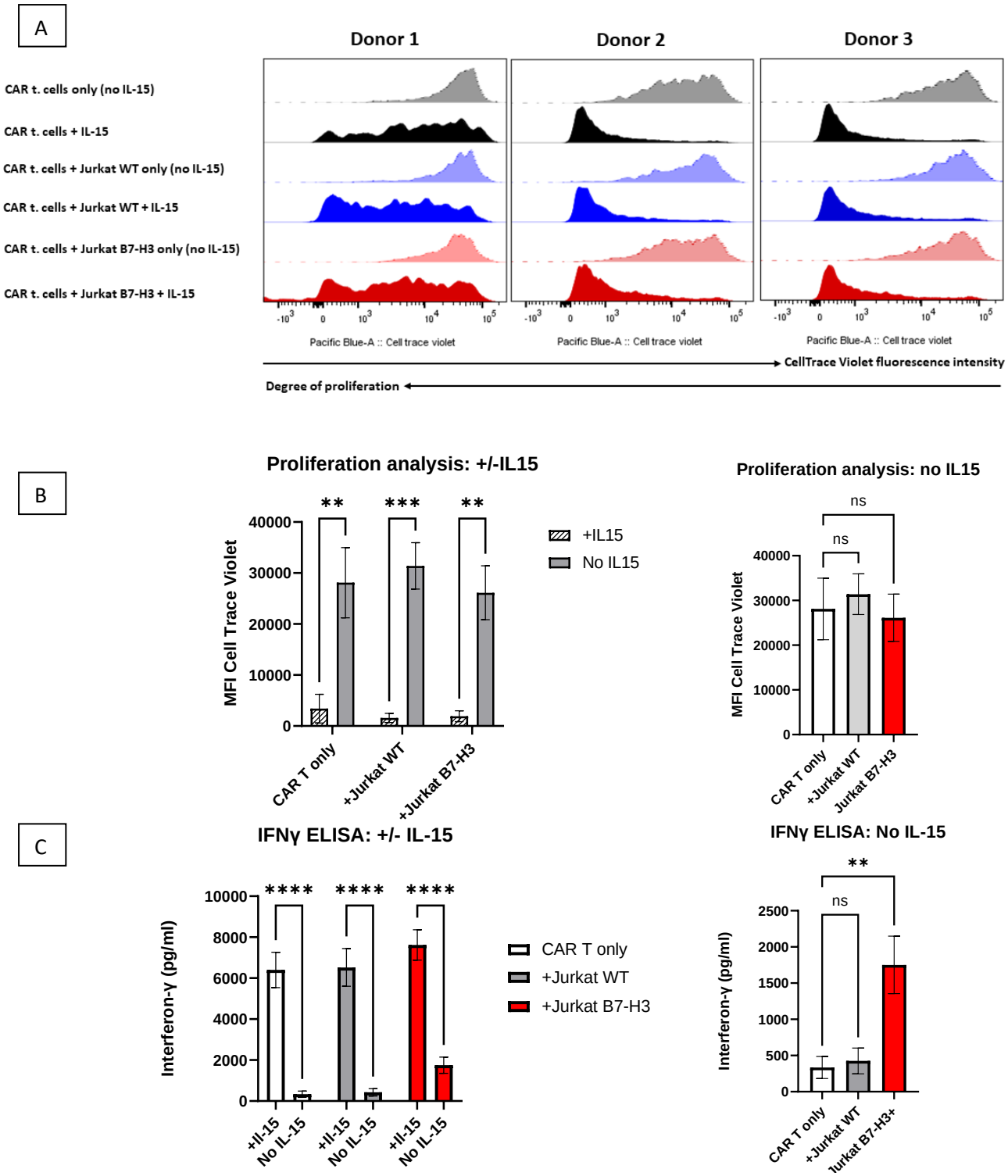

Figure 4-14: Effects of IL-15 deprivation on CAR T cells. (A) Flow cytometry histograms for three donors showing CellTrace Violet dilution as a marker of cell proliferation in the presence of Jurkat WT and Jurkat B7-H3+ with or without IL-15. The plots show enhancement of proliferation by the presence of IL-15. For the IL-15+ conditions, cells were maintained in cell media supplemented with 100ng/ml of IL-15 while the IL-15 deprived cells had cytokine withdrawn 48 hours prior to co-culture with cell lines. (B) Comparison of median fluorescence intensities of CellTrace Violet for the experimental conditions described in (A) Events were gated on CD3+ live cells. (n=3, 2-way ANOVA; ns=non-significant, **p<0.01, ***p<0.001, error bars indicate standard error of means). (C) Interferon-γ secretion determined by ELISA following 24 hours of co-culture with Jurkat WT or Jurkat B7-H3+ in the presence or absence of IL-15 (separate experiment). (n=4, 2-way ANOVA; ns=non-significant, **p<0.01, error bars indicate standard error of means)

4.5.10 Long-term co-culture of CAR-transduced T cells with cancer cell lines results in Vδ1 T cell expansion

CAR T cell proliferation is expected following target engagement therefore to compare Vδ1 T cell proliferation dynamics between CAR-transduced and untransduced conditions, Vδ1 cells were counted at the start (on Day 14 of expansion and Day 10 days post-CAR transduction) and at the end of a 7-day co-culture with cancer cell lines in the presence of IL-15. Vδ1 cell numbers were increased in the CAR-transduced conditions independent of the presence of cancer cell lines (**figure 4-15**). Furthermore, significantly more Vδ1 T cells were present in the co-cultures with the B7-H3-positive cell lines, LAN1 and SiHa, compared with the negative control (CAR T cells alone). For the co-cultures with untransduced T cells, the only statistically significant Vδ1 T cell expansion was observed with LAN1. In general, target engagement enhances CAR.Vδ1 T cell proliferation and the CAR-transduced population had significantly higher Vδ1 content after 7 days of co-culture with cancer cell lines.

4.5.11 PD-1 is significantly upregulated in Vδ2 CAR-transduced T cells.

To investigate differences in PD-1 expression between CAR-transduced Vδ1 and Vδ2 T cells and following long-term co-cultures with cancer cell lines in the presence of IL-15, both cell populations were compared by flow cytometry in a 7-day co-culture experiment. While a higher proportion of untransduced Vδ1 T cells expressed PD-1 at baseline compared to Vδ2 T cells, there was no significant PD-1 upregulation on transduced Vδ1 T cells following co-culture with cell lines (**figure 4-16A & B**). This was in contrast to CAR-transduced Vδ2 T cells which had significantly higher PD-1

expressions compared with transduced Vδ1 T cells and this was observed even in the absence of cancer cell lines (**figure 4-16C**).

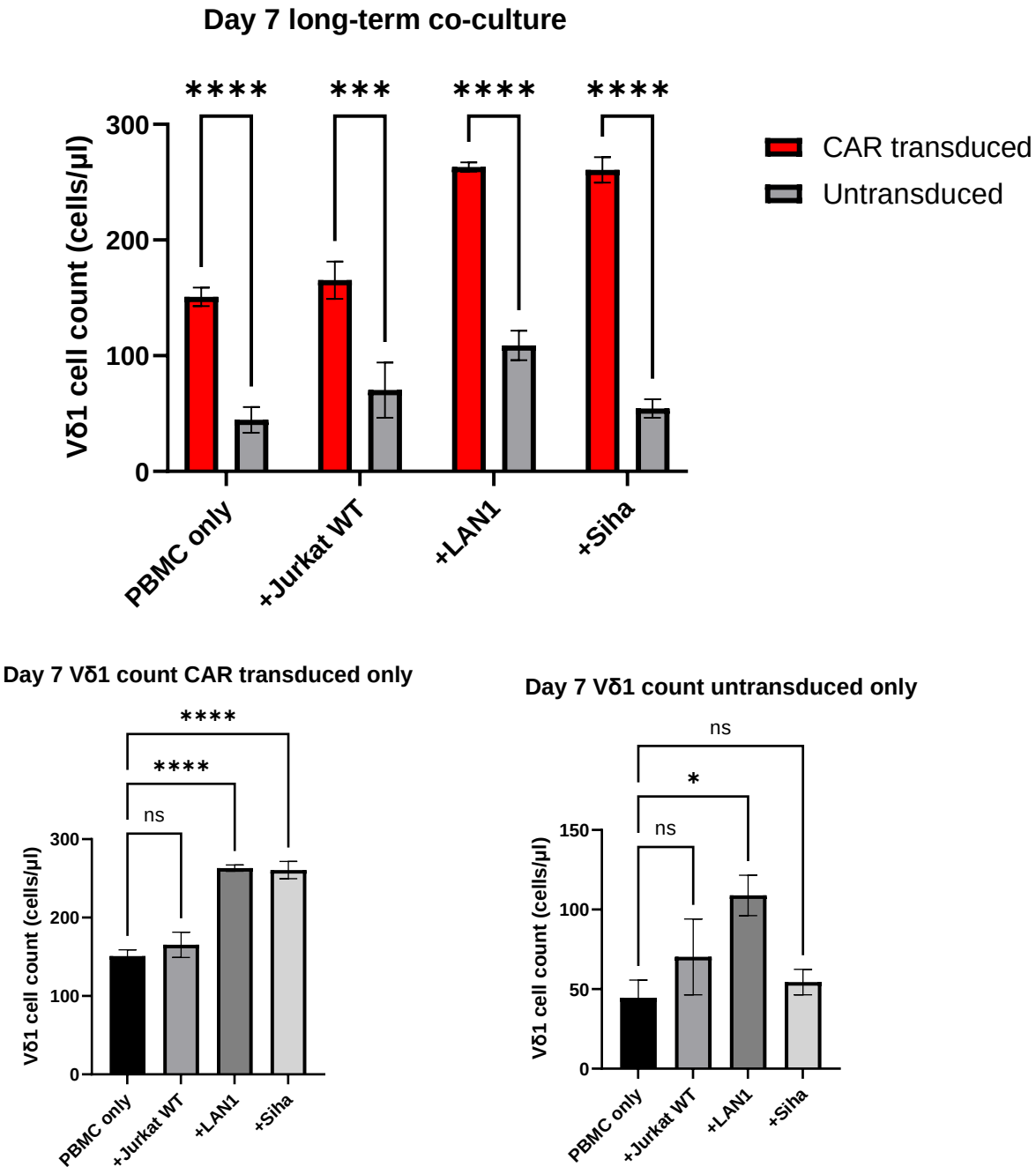

Figure 4-15: Proliferation of CAR-transduced Vδ1 T cells. PBMCs were first expanded with OKT3 and IL-15 until Day 14 when the long-term co-culture was set up. Following a 7-day co-culture of $2x10^4$ PBMCs with cell lines in 1:1 ratio, CAR-transduced (CAR t.) and untransduced cells were analysed by flow cytometry for Vδ1 cell counts. This experiment was performed in the presence of IL-15. Above: Graphical comparison of Vδ1 cell counts for the various co-culture conditions showing enhancement of Vδ1 proliferation in the CAR-transduced condition. Below: Comparisons of Vδ1 cell counts for transduced (left) and untransduced (right) conditions. Cell counts were normalised using counting beads. The cell culture medium was supplemented with 100ng/ml of IL-15 (n=4, 2-way ANOVA; ns=non-significant, *p<0.05, ***p<0.001, ****p<0.0001, all error bars indicate SEM).

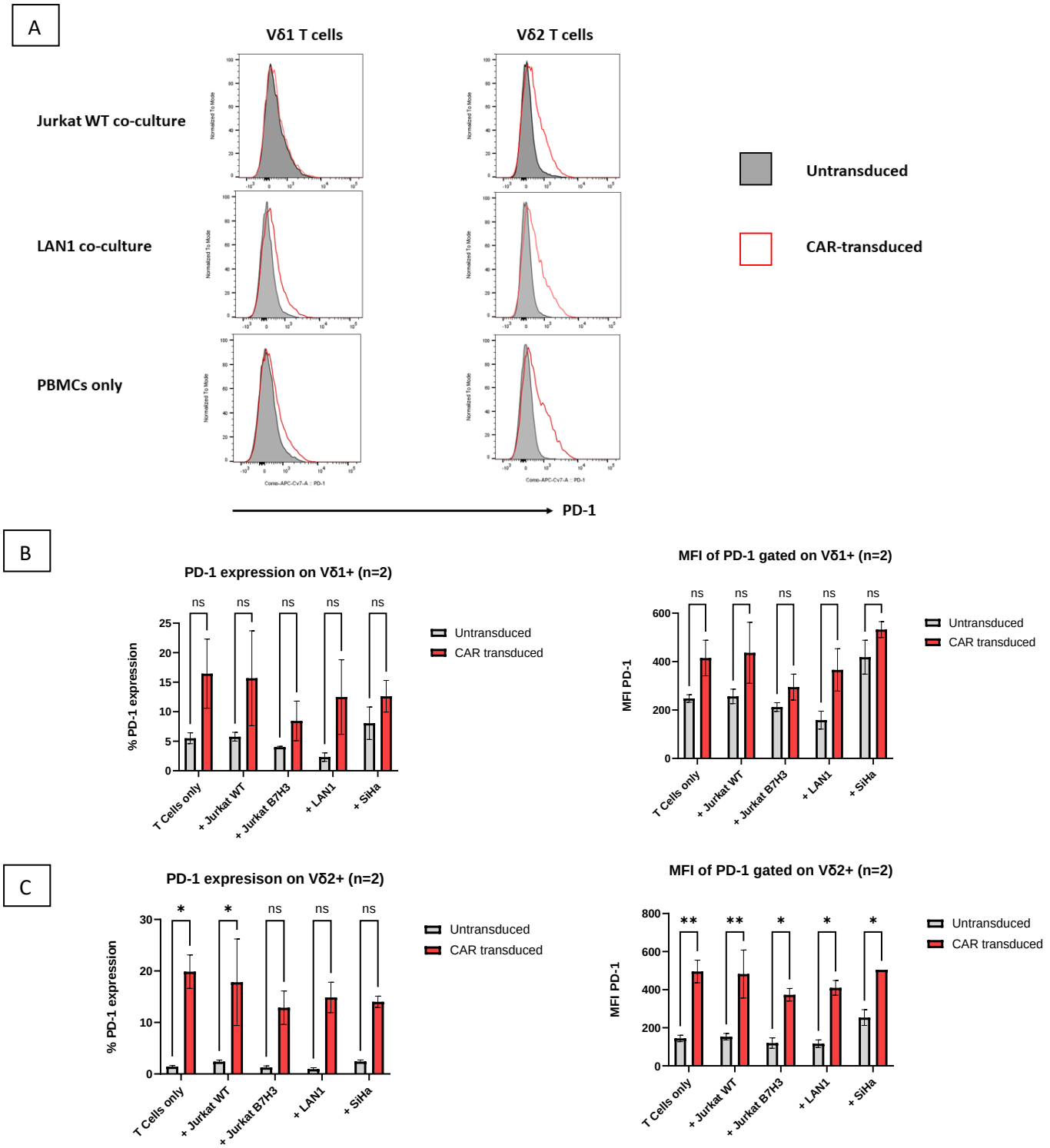

Figure 4-16: Induction of PD-1 expression on CAR transduced cells following long-term co-culture with cancer cell lines. Following a 7-day co-culture of 2x10^4 PBMCs with cell lines in 1:1 ratio, CAR-transduced (CAR t.) and untransduced cells were analysed by flow cytometry for PD-1 expression. (A) Flow cytometry histogram plots for a representative donor showing upregulation of PD-1 expression on CAR-transduced Vδ2 T cells regardless of the presence of cancer cell lines. Events were gated on Vδ1 T cells (left) and Vδ2 T cells (right) respectively. (B) Graphical comparison of PD1 expression (left) and median fluorescence intensities (MFIs) (right) gated on Vδ1 T cells for the various co-culture conditions showing no statistically significant upregulation of PD-1 (C) Graphical comparison of PD1 expression (left) and median fluorescence intensities (MFIs) (right) gated on Vδ2 T cells for the various co-culture conditions showing significant upregulation of PD-1 on CAR-transduced Vδ2 T cells. (n=2, 2-way ANOVA; ns=non-significant, *p<0.05, **p<0.01, all error bars indicate SEM).

4.6 Discussion

In the previous chapter, it was shown that CD3/IL-15 expanded γδ T cells possess significant anti-tumour properties but become dependent on IL-15 for ongoing proliferation and survival. In this chapter, the main objective was to demonstrate enhanced anti-tumour properties in CAR-transduced, CD3/IL-15 expanded γδ T cells. The secondary objective was to investigate if CAR transduction overcomes IL-15 dependence in these cells. The 2nd-generation B7-H3-specific CAR evaluated in this chapter encodes the RQR8 safety switch which enables detection of CAR+ cells by surface staining for CD34. In the clinical context, the inclusion of RQR8 in the CAR construct would permit functional depletion of CAR T cells in the event of intolerable side effects such as severe cytokine storm.[185]

The choice of B7-H3 as a target antigen for CAR-directed immunotherapy in solid tumours is both relevant and rational given the pattern of over-expression across a wide range of cancers. B7-H3 expression has previously been found to be inducible on some immune cells e.g. dendritic cells following stimulation[142] hence it was reassuring that there was no significant expression on PBMCs either at baseline or following stimulation with anti-CD3 mAb and IL-15 as the presence of B7-H3 on these cells would induce fratricide and significantly impair CAR T cell efficacy. The solid cancer cell lines tested were positive for B7-H3 to varying degrees.

The pattern of CD69 upregulation observed on CAR-transduced T cells in the absence of the target antigen most likely represents a relative state of activation. This is also more likely the case for the increase in PD-1 expression on CAR-transduced T cells. Indeed, the expression of PD-1 in an EGFRvIII-directed CAR T cell product was shown to be associated with improved glioblastoma progression

free survival in a Phase I clinical trial.[186] The associated upregulation of NKG2D was an interesting but unexpected finding as the innate receptor had not previously been shown to be upregulated in CAR T cells but it is likely that this finding also reflects activation of transduced cells.

Antigen-specific antitumour responses by CAR+ Vδ1 T cells were evidenced by increased CAR T cell degranulation in response to B7H3+ cancer cell lines and a similar induction of IFNγ secretion following co-culture with the glioblastoma cell line, U87. LAN1 cells also induced IFNγ secretion but due to donor variability, this increase was not statistically significant. Granzyme B was uniformly expressed in both untransduced and CAR-transduced γδ T cells regardless of the presence of the target antigen, most likely representing the innate cytolytic potential of these cells. Furthermore, in line with the MHC-unrestricted mechanism of γδ T cell activation, no significant responses were observed following CAR T cell co-culture with allogeneic PBMCs however, more research, including long-term *in vivo* and clinical studies will be required to fully understand γδ T cell reactions in the allogeneic setting.

Given recent interests in the IL17-producing γδ T cells (γδT17) which are proinflammatory and previously shown to promote tumour progression in murine models,[187,188] it was reassuring that there was no appreciable IL-17A expression on intracellular staining of Vδ1 T cells and there was no upregulation following co-culture with cancer cell lines. An important caveat to this observation is the fact that there was no positive control for the IL17A antibody. Furthermore, the cancer-promoting γδT17 function has not been demonstrated in a clinical context and in fact, on the contrary, γδ T cell infiltration within tumours has been associated with improved outcomes across a range of cancers.[88]

The role of IL-15 in activating and maintaining the cytolytic potential of γδ T cells has been well described[189–191] and in the previous chapter, the dependence of γδ T cells on IL-15 was demonstrated. Chromium-51 cytotoxicity data shown in this chapter (figures 4-11 and 4-12) suggest IL-15 independence for CAR transduced T cells. Interestingly, despite significant upregulation of NKG2D on CAR-transduced γδ T cells (figure 4-4), NKG2D blockade using a well-recognized blocking antibody did not affect CAR T cell cytotoxicity probably suggesting functional redundancy for NKG2D-mediated cytotoxicity in CAR transduced cells. Furthermore, in the presence of IL-15, γδ T cells produced significantly more IFNγ both in response to antigen-positive cell lines and in the absence of cancer cell lines (figure 4-10). On the contrary, without IL-15, the only significant increase in IFNγ was in response to the Jurkat B7-H3+ cell line, representing a CAR-specific response. A similar pattern was observed for IL-15-induced proliferative responses. It can therefore be argued that IL-15 induces background, non-antigen specific proliferation and IFNγ production in CAR-transduced γδ T cells. While non-specific cytokine secretion would be undesirable in the clinical context, the impact of reduced proliferative capacity in the absence of IL-15 warrants further investigation. Further experiments using serially diluted concentrations of IL-15 would shed more light on the impact of the cytokine on proliferation and determine if the effects are dose-dependent.

Long-term co-culture of CAR-transduced and untransduced γδ T cells with cell lines, in the presence of IL-15, showed significant persistence and expansion of the Vδ1 T cell subset. Interestingly, while Vδ1 T cells tend to express higher levels of PD-1 at baseline, a finding also observed in a study of tissue resident Vδ1 T cells[89], there was no significant upregulation of PD-1 following long-term co-culture. This was in contrast to the Vδ2 subset which consistently upregulated PD-1 in CAR transduced

cells (figure 4-16). These observations may lend credence to the suggestion that Vδ1 T cells may be resistant to activation-induced cell death as PD-1 upregulation following CAR transduction and target engagement is more likely to reflect T cell exhaustion in this context. However, further experiments with a higher number of donors are required before definitive conclusions can be made.

In summary, the B7-H3 specific (TE9 CD28z) CAR enhanced the anti-tumour functions of γδ T cells and conferred antigen-directed cytolytic capacity which was sustained in the absence of IL-15. CAR T cell proliferation and cytokine production were however significantly reduced following IL-15 withdrawal. Future research investigating additional strategies for overcoming the dependence of expanded γδ T cells on exogeneous IL-15 are justified.

CHAPTER V: OVERCOMING IL-15 DEPENDENCE IN GAMMA DELTA (γδ) T CELLS VIA STAT5 SIGNALLING

5.1 Introduction

5.1.1 The molecular basis of IL-15 biological functions

A lymphokine produced by the adult T-cell leukaemia (ATL) cell line, HuT-102 which enhanced the cytotoxic activity of large granular lymphocytes and induced T cell proliferation was first reported by Burton et al in 1994.[192] Almost simultaneously, another group of scientists identified the cytokine with similar properties to IL-2 which was named IL-15.[193]

IL-15 belongs to the common cytokine receptor chain (γ_c) family of cytokines. Other members include IL-2, IL-4, IL-7, IL-9 and IL-21.[194,195] The receptors of all the members of this cytokine family are heterotrimers comprising a common gamma (γ_c) subunit, an alpha (α) chain and a beta (β) chain. IL-2 and IL-15 share a common β subunit, IL-2/15Rβ [193] hence signal transductions by both cytokines via the receptor complexes share the same receptor kinases (Jak1 and Jak3) and transcription factor pathways.[196,197] Two forms of the IL-15 receptor have been identified; the high-affinity receptor comprises IL-15Rα, IL-2/15Rβ and γ_c while the intermediate-affinity receptor has only IL-2/15Rβ and γ_c subunits.[198] IL-15 and IL-2 compete for binding to the intermediate-affinity receptor thus providing an explanation for some of the similarities in function.[199] However, despite sharing similar functions in activating cytotoxic T cells, facilitating the proliferation of B and T cells and the maintenance of NK cells, IL-15 has some contrasting roles with IL-2. For example, unlike IL-15, IL-2 supports the maintenance of CD4+CD25+ regulatory T cells (Tregs)[200] and can trigger activation-induced cell death (AICD) via increased expression of the Fas

ligand (FasL)[201]. Significant differences also exist in the mode of presentation with IL-2 being predominantly secreted while IL-15 is mainly membrane bound and presented in *trans* on cells expressing IL-15Rα to target cells expressing lL-2/15Rβ and γ_c, notably NK cells and CD8+ memory T cells.[199,202,203] Furthermore, monocytes and macrophages are the main producers of IL-15 *in vivo* and unlike IL-2, IL-15 is not produced by activated T cells.[204]

Human IL-15 is a 114-amino acid four-helix bundle protein encoded by the *IL15* gene on chromosome locus 4q31.[205] IL-15 shares only 20.2% sequence identity with IL-2 with the most similar regions being the A, C and D helices which interact with IL-2/15Rβ and γ_c.[203]

The contrasting biological effects of IL-2 and lL-15 can be explained by a number of factors. First, the private, high-affinity α-subunit of the respective cytokine receptor is differentially expressed with IL-2Rα expressed mainly by activated T and B cells while IL15Rα is predominantly expressed by activated monocytes and dendritic cells.[195] Furthermore, there is experimental evidence that differential receptor internalisation occurs following receptor binding and alternative signalling pathways can be employed by IL-2 and IL-15-receptor interactions.[206]

5.1.2 IL-15 signalling via the JAK/STAT pathway.

The binding of IL-15 to its cognate receptor complex triggers a cascade of intracellular reactions which effectively transmit the IL-15 signal to the nucleus. The crucial proteins involved in the signal transduction of IL-15 include the Janus Kinases (JAKs) via the JAK/STAT pathway. Two of the JAK family of intracellular tyrosine kinases, JAK1 and JAK3, are involved in IL-15 signal transduction and are constitutively associated with the intracellular domain of the IL-15 receptor

complex.[207] Binding of the cytokine to the receptor complex induces activation of the JAK proteins by transphosphorylation thereby enhancing their catalytic activity.[208] Activated JAK proteins in turn phosphorylate specific tyrosine residues on the intracellular tails of the cytokine receptors which act as docking sites for transcription factors of the Signal Transducers and Activators of Transcription (STAT) family.[209] Selective associations exist between specific JAK proteins and the various subunits of the IL-15/IL-2 receptor complex. For example, in lymphocytes, JAK1 associates with the IL-2/15Rβ subunit while JAK3 associates with γ_c.[210] While the clinical significance of this selective association is unclear, it provides a potential mechanism for distinct physiological effects based on differential receptor expressions.

The canonical JAK/STAT signalling pathway requires four basic components: cytokine, receptor, JAK and STAT. The JAK/STAT pathway and its regulatory mechanisms are summarised in Figure 5-1. Transcription factors of the STAT family are vital for the transduction of IL-15 signals to the nucleus. Seven members of the STAT family have been identified-STAT1, STAT2, STAT3, STAT4, STAT5A, STAT5B and STAT6.[211–214] The basic structure of the STAT protein comprises a carboxyl-terminus transactivation domain preceded by a highly-conserved Src-homolog 2 (SH2) domain with a tyrosine residue which becomes phosphorylated situated between the two domains.[212] The SH2 domain is involved in STAT dimerization and activation and this is the site of many pathogenic point mutations.[215] The other domains include the DNA binding domain which binds to regulatory regions of the target gene, a highly-conserved linker domain, a coiled-coil domain and the amino terminal domain.[211]

STAT5A and STAT5B, though encoded by two separate genes on chromosome 17 in humans, share 90% sequence identity.[216] Both STAT5A and STAT5B are

generally thought to perform the same roles and thus are functionally redundant but evidence for differential biological effects exist and these are thought to, at least partly, be due to differences in their respective DNA binding sites.[217,218]

For IL-15 signal transduction in lymphocytes, STAT3 and STAT5 are phosphorylated by activated JAK1 and JAK3 respectively.[219] JAK-mediated phosphorylation of specific tyrosine residues on the STAT protein results in dimerization and activation with subsequent translocation to the nucleus where they bind to regulatory regions of genes to activate or repress transcription (figure 5-1).[220] Examples of genes regulated by STAT5B include those involved in T cell activation and proliferation as well as survival and apoptosis.[221]

As the JAK/STAT pathway influences crucial biological processes, strict regulatory mechanisms exist (summarised in figure 5-1). The regulatory proteins involved in the control of the JAK/STAT pathway include the Suppressor of Cytokine Signalling (SOCS) family which are themselves induced by activated STAT-mediated transcription.[222] SOCS proteins block STAT recruitment to the receptor and impair the catalytic activity of JAKs by binding to the phosphorylated tyrosine of activated JAK.[223,224] Another negative regulator of the JAK/STAT pathway is the Protein Tyrosine Phosphatases (PTP) family of proteins which include CD45, a receptor which is highly expressed by haemopoietic cells, and SH2 domain containing Phosphatases 1 and 2 (SHP1 and SHP2).[223] These proteins dephosphorylate a wide range of substrates including JAKs, effectively switching off the activity of proteins which are activated by phosphorylation.[225] Furthermore, Protein Inhibitors of Activated STAT (PIAS), constitutively expressed negative transcriptional regulators of the JAK/STAT pathway, inhibit the functions of STAT by binding to dimers to block DNA binding and promote sumoylation.[226]

Besides the canonical JAK/STAT pathway, other functions have been described for STAT proteins which cannot be explained by the interactions described above. These complex non-canonical pathways include direct actions by unphosphorylated STATs, mitochondrial modulation and heterochromatin stabilization.[227,228]

Furthermore, STAT proteins can be activated by other receptor tyrosine kinases besides JAK. Epidermal Growth Factor Receptor (EGFR) has been shown to phosphorylate STAT3 [229] and Platelet Derived Growth Factor Receptor (PDGFR) mediated phosphorylation activates STAT1, STAT3 and STAT5.[230] Moreover, the crosstalk between the JAK/STAT and other signal pathways via STAT-mediated induction of key proteins potentially increases the range of biological effects and thus therapeutic inhibitors of the JAK/STAT pathway could influence other signal transduction pathways.

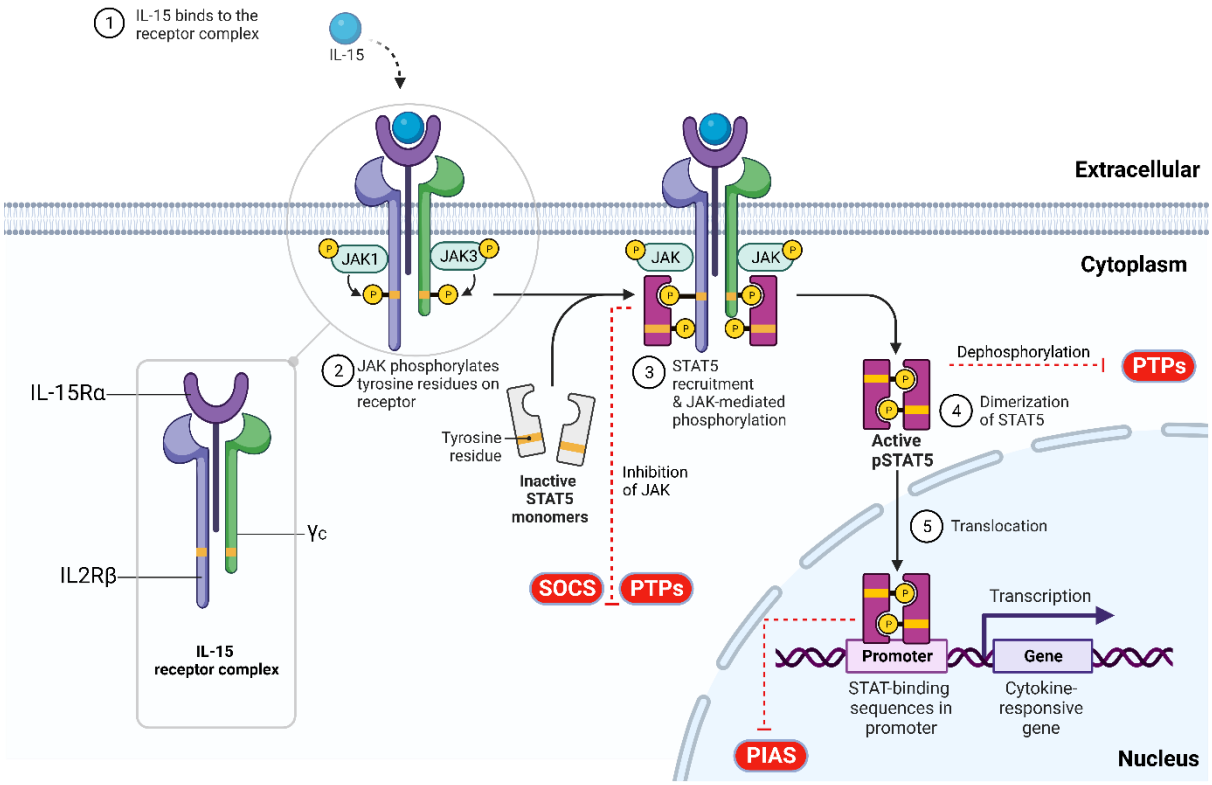

Figure 5-1. IL-15 signal transduction via the canonical JAK/STAT pathway. A simplified schematic representation of the role of the JAK/STAT pathway in IL-15 signalling. The IL-15 receptor complex comprises the high-affinity IL-15Rα subunit, the IL2/15Rβ and the common gamma chain (γ_c). Janus Kinases, JAK1 and JAK3, are associated with IL2/15Rβ and γ_c respectively. Following cytokine binding to the receptor complex, JAK proteins are activated by autophospholylation leading to phosphorylation of tyrosine residues on the intracellular domains of the receptor chains. Signal Transducers and Activators of Transcription (STAT) proteins are recruited to the docking sites on the receptors where they are phosphorylated. Note that for simplicity, STAT5 is shown as the only STAT molecule involved in the pathway whereas STAT3 is also known to be involved IL-15 signalling. The active phosphorylated STAT (pSTAT5) dimerizes and translocates to the nucleus where it binds to the promoter region of target genes to activate DNA transcription. The JAK/STAT pathway is regulated via several mechanisms including the Suppressor of Cytokine Signalling (SOCS) family of proteins which inhibit recruitment of STAT to the receptor and inhibit JAKs. Other negative regulators include Protein Tyrosine Phosphatases (PTPs) which mediate dephosphorylation of pSTAT5 and JAKs. Protein Inhibitors of Activated STAT (PIAS) are a family of proteins which interact with dimerized STAT to block their DNA-binding activity. Black solid lines represent activation processes while red broken lines indicate regulatory/inhibitory mechanisms. Modified from Morris *et al* and Hu *et al*[209,211] This figure was created with biorender.com.

5.2 Clinical correlations of JAK/STAT alterations

Since the JAK/STAT pathway regulates a broad range of cellular processes, alterations in key components have been implicated in both benign and malignant conditions. For instance, the JAK2 V617F somatic mutation induces a conformational change in the protein which drives constitutive tyrosine kinase activity and downstream signalling independent of ligand binding.[231] JAK2 V617F is a driver mutation in myeloproliferative neoplasms for which an inhibitor, ruxolitinib is currently a licenced treatment.[223] Gain-of-function mutations in JAK1 have also been associated with acute lymphoblastic leukaemia (ALL).[232]

A germline loss-of-function mutation in STAT5B resulting in substitution of proline for alanine at position 630 (A630P) was reported in a patient who had presented with growth failure and features of growth hormone insensitivity.[233] Several activating mutations in the SH2 domain of STAT5B have also been associated with haematological malignancies with the N642H missense mutation linked with aggressive Large Granular Lymphocytic leukaemia (LGL), ALL and γδ T cell lymphomas.[234] Experimental evidence suggests that the aggressive phenotype conferred by this mutation is due to prolonged STAT phosphorylation and dimerization resulting in constitutive activation.[235]

Several inhibitors of STAT proteins are being investigated in early phase clinical trials but given the far-reaching effects of STAT proteins, significant toxicities would be expected from non-specific inhibition of these proteins.

To investigate the biological effects of constitutively active STAT mutations, several groups have generated point mutations in STAT5 in experimental models.[236] Cytokine-independent proliferation and enhanced survival are predictable consequence of constitutive activation of STAT5B and in this chapter, a novel mechanism to overcome IL-15 dependence in γδ T cells via constitutive activation of STAT5B will be investigated.

5.3 Chapter Objectives

1. To investigate the role of STAT5B in IL-15 signalling in γδ T cells.
2. To determine the role of constitutive activation of STAT5B in overcoming IL-15 dependence in γδ T cells.

5.4 Methods

5.4.1 Cloning of STAT5B constructs

The complementary DNA (cDNA) sequence for human STAT5B was obtained from the ESEMBL genome browser.[237] To create the mutant plasmid, the nucleotide sequence AAT was replaced with CAT at position 1924 of the STAT5B cDNA sequence thus encoding the N642H point mutation. Plasmid gene blocks for STAT5B wildtype (WT) and STAT5B N642H, flanked by NcoI and MluI restriction sites were synthesized by Invitrogen (Thermofisher). The synthesized gene blocks were inserted into pMK-RQ vectors encoding the kanamycin resistance gene, KanR. Gene block plasmid purification and concentration was achieved by midi-prep bacterial cultures using 50 µg/ml Kanamycin selection agar plates and LB broth (see detailed descriptions of bacterial transformation and plasmid purification in the Materials and Methods chapter).

To clone the STAT5B constructs into the SFG γ-retrovirus vector backbone, the TE9 CAR and STAT5B plasmid gene blocks were first digested with MluI and NcoI restriction enzymes (Thermofisher). The 2.5kb STAT5B fragments were ligated to the 7.7kb SFG vector backbone encoding RQR8 from the digested TE9 CAR plasmid and ampicillin resistance gene. Competent *E.coli* were transformed with the ligated plasmid encoding RQR8 and STAT5B WT or N642H mutant. Multiple bacterial clones were subsequently selected from the ampicillin selection plates and miniprep cultures were prepared followed by plasmid purification. The sequence integrity of the purified plasmid clones were confirmed by Sanger sequencing (Cambridge Bioscience, Cambridge UK). The cloning strategy is summarized in figure 5-2.

Simulation of agarose gel electrophoresis patterns was performed using the SnapGene® software version 5.2.2 (Dotmatics, Boston, USA).

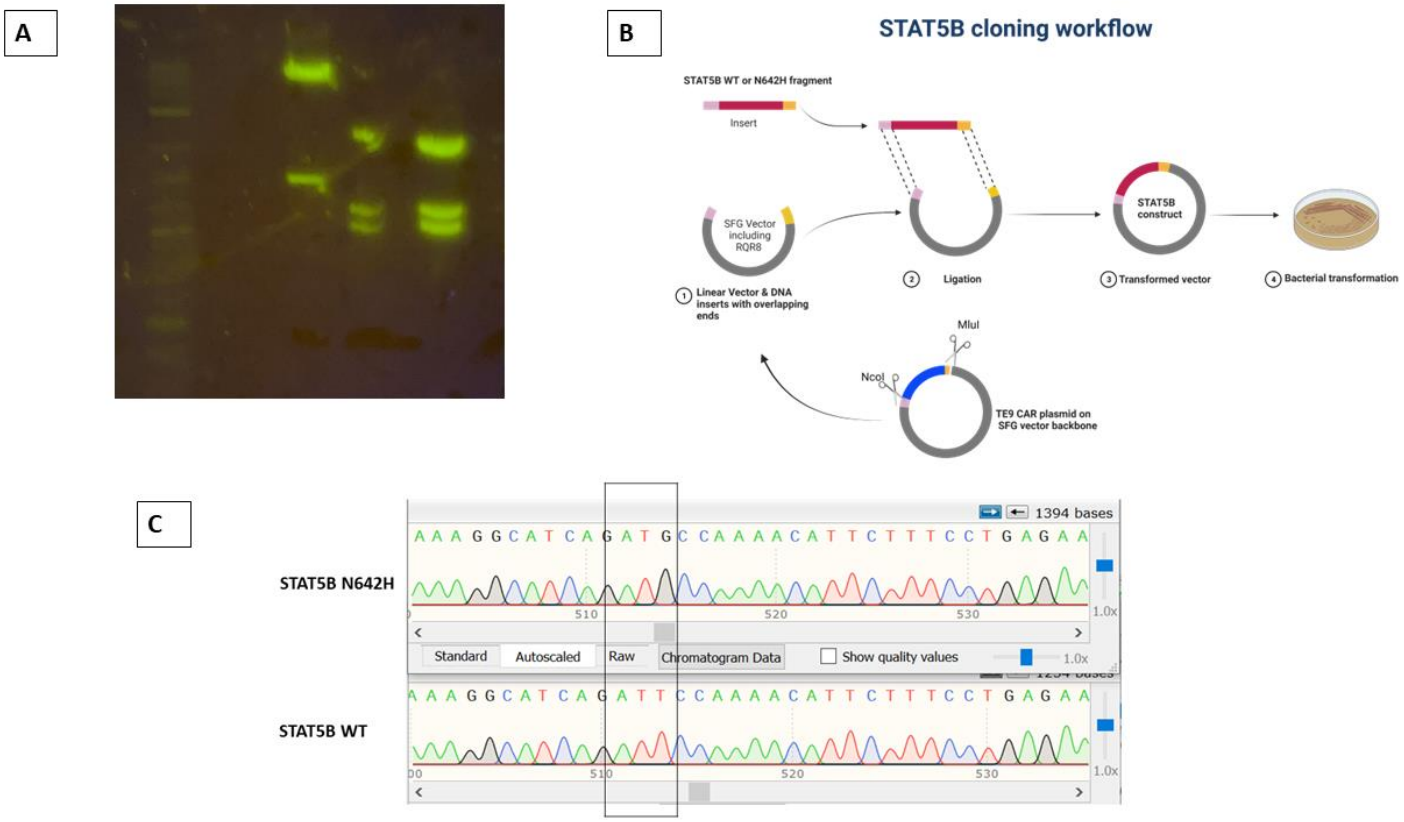

Figure 5-2 Cloning of *STAT5B* constructs. (A) Agarose gel electrophoresis photograph following restriction digestion of TE9 CAR (lane 2), *STAT5B* WT (lane 3) and *STAT5B* N642H (lane 4) with NCoI and MluI restriction enzymes. A 1kb DNA ladder (Thermofisher) is shown in Lane 1. The 2.5kb *STAT5B* WT and *STAT5B* N642H fragments as well as the 7.7kb SFG vector fragments were excised from the agarose gel and purified. (B) Schematic representation of the cloning strategy. The TE9 CAR was digested with NcoI and MluI restriction endonucleases removing the ScFv but retaining RQR8 in the vector backbone. *STAT5B* WT and N642H gene block fragments with complementary ends were ligated to the vector backbone followed by bacterial transformation and antibiotic selection of clones. (C) Sanger sequencing results of the cloned plasmids showing the T>G point mutation in codon 642 representing the *STAT5B* N642H mutation. The reverse complement of the coding strand sequence is shown here.

5.4.2 Transduction of PBMCs with *STAT5B* constructs

Following production of retroviral particles as previously described in the Materials and Methods Chapter, non-tissue-culture-treated 24-well plates (Falcon) were first coated with a 10 µg/ml solution of RetroNectin (Takara) and incubated at room temperature for 2 hours or overnight at 4^{o}C. Thereafter, 5 x 10^5 PBMCs were plated in 500 µl volume per well and 1.5 ml of retrovirus supernatant was added to each well. The culture plates were centrifuged at 1000 x *g* for 40 minutes and subsequently incubated at 37^{o}C and 5% CO_2 for 48 hours. Transduction efficiency was assessed by flow cytometry detection of surface CD34, 48 hours after transduction.

5.4.3 IL-15 withdrawal experiments

STAT5B-transduced PBMCs and the respective negative controls were initially expanded with complete media supplemented with 100 ng/ml of IL-15. For the determination of cell viability following withdrawal of IL-15, the PBMCs were counted, washed and resuspended in fresh complete media without IL-15 for 48 hours. PBMCs for each donor and experimental condition were plated in identical numbers. Duplicate wells were harvested every 3 days and viable cells were enumerated by flow cytometry following exclusion of dead cells with a viability dye and normalisation with counting beads (Biolegend).

5.4.4 Detection of CAR+ Cells using recombinant B7-H3 protein

The lyophilised recombinant his-tagged B7-H3 protein (Biotechne) was first resuspended with PBS to a stock concentration of 100µg/ml. The stock solution was aliquoted into smaller volumes and stored at -20^{o}C. For the detection of the B7-H3 specific CAR, transduced cells were incubated with 2µl of the stock solution of B7-

H3-his tagged protein per 10^6 PBMCs at 4^{o}C for 30 minutes. Following a wash step, the secondary staining for the his-tag was performed as follows; the cells were resuspended in cell staining buffer and incubated for 30 minutes with 1 µg of PE-tagged anti-His (Biolegend) per 10^6 PBMCs. Surface expression of the CAR was determined by flow cytometry detection of the his-tag.

5.4.5 Deletion of RQR8 from TE9 CAR construct

To allow co-transduction of the TE9 CAR with *STAT5B* constructs, deletion of RQR8 from the TE9 CAR was performed by mutagenesis PCR as follows. The TE9 CAR plasmid encoding RQR8 was first diluted to a concentration of 10 ng/µl followed by exponential amplification by PCR using the following mutagenic primers.

Forward: 5’ AGAGCCGAGGGCAGAGGC 3’

Reverse: 5’ GTTGGCAGTCTAGAGGATGGTCC 3’

The mutagenesis PCR was performed with the Q5 site-directed mutagenesis kit (New England Biolabs) with the PCR reaction components shown in Table 5-1 and PCR conditions as summarised in Table 5-2.

PCR Components	**Volume**
Q5 Hot Start High-Fidelity 2x Master Mix	12.5 µl
10 µM Forward Primer	1.25 µl
10 µM Reverse Primer	1.25 µl
Template DNA (10ng/µl)	1 µl
Nuclease-free water	9 µl
Total	**25µl**

Table 5-1. Components of the site-directed mutagenesis PCR

Step	Temperature	Time
Initial Denaturation	98ºC	30 seconds
25 cycles	98ºC	10 seconds
	70ºC	30 seconds
	72ºC	3 minutes
Final Extension	72ºC	2 minutes
Hold	10ºC	Indefinite

Table 5-2. Mutagenesis PCR conditions

Following the mutagenesis PCR, the amplified product was subjected to the KLD (kinase, ligase and Dpnl) reaction to circularize the DNA with the reaction components as shown in Table 5-3.

KLD Reaction Components	Volume
PCR Product	1 µl
2x KLD Reaction Buffer	5 µl
10x KLD Enzyme mix	1 µl
Nuclease-free water	3 µl
Total	**10µl**

Table 5-3. Components of the KLD reaction

The final step was transformation of 5-alpha Competent *E. coli* cells (New England Biolabs) on ice as previously described in the Materials and Methods Chapter. The transformed bacteria were plated on ampicillin-treated agar plates and incubated overnight. Ten clones were subsequently harvested from the agar plates and the

DNA was purified by the miniprep method (see Materials and Methods Chapter). A restriction digestion step with MluI and MreI restriction enzymes (Thermofisher) was performed to screen the clones for the absence of RQR8 (Figure 5-3). Clone 1 was chosen and the DNA sequence was confirmed by Sanger sequencing (Source Bioscience, Cambridge UK).

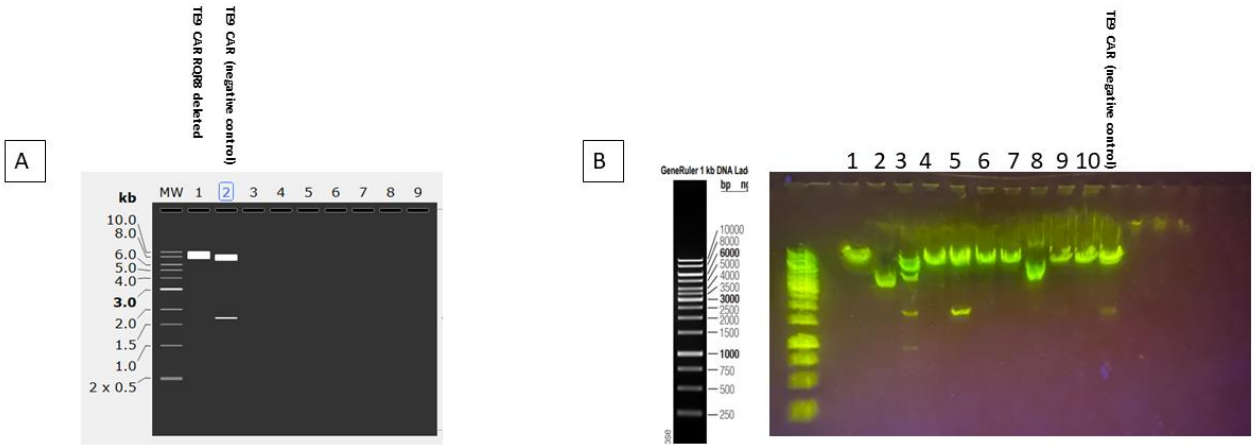

Figure 5-3 Screening restriction digestion. (A) Snapgene® software simulation of restriction digestion of RQR8-deleted TE9 CAR and the original TE9 CAR plasmids with MreI and MluI. (B) Photograph of 1% agarose gel electrophoresis following a screening restriction digestion with MreI and MluI of RQR8-deleted clones 1-10 and the original TE9 CAR (negative control). Clone 1 was sent for Sanger sequencing to confirm the DNA sequence.

5.4.6 Double transduction with TE9 CAR and *STAT5B* N642H

Non-tissue-culture-treated 24-well plates (Falcon) were first coated with a 10 µg/ml solution of RetroNectin (Takara) and incubated at room temperature for 2 hours or overnight at 4^{o}C. Thereafter, 2.5 x 10^5 PBMCs to be transduced were plated in 500 µl volume per well and 750 µl each of *STAT5B* N642H and TE9 CAR (RQR8-deleted) virus supernatants were added to each double-transduced well. The culture plates were centrifuged at 1000 x *g* for 40 minutes and subsequently incubated at 37^{o}C and 5% CO_2 for 48 hours. Transduction efficiency was assessed by flow cytometry 48 hours after transduction. The proportion of CAR-positive cells was determined by secondary staining for the His-tag following incubation with a His-tagged recombinant B7-H3 protein while the *STAT5B* N642H positive cells were identified by detection of RQR8 by surface CD34.

5.4.7 Phospho-STAT5 flow cytometry optimisation

To determine the optimal duration of incubation of PBMCs for detection of phospho-STAT5 (pSTAT5) by flow cytometry, 0.5 million unstimulated donor PBMCs from a single donor were washed with PBS and resuspended in 100 µl of PBS supplemented with or without 100 ng/ml of IL-15. Each aliquot was incubated for either 30 or 60 minutes at 37^{o}C. Subsequent sample preparation steps were on ice following the instructions of the Transcription Factor Phospho Buffer kit (BD Pharmigen). In brief, following incubation, cells were washed twice with excess PBS by centrifuging at 1000 x *g* on an Eppendorf Centrifuge 5415R for 1 minute each time. Antibodies against surface antigens and a fixable viability dye were added and incubated on ice for 20 minutes. Following a wash step, cells were resuspended with 1xFix/Perm buffer incubated on ice for 50 minutes. The cells were subsequently washed with the 1xTranscription factor permeabilization (TFPerm) wash buffer and resuspended in Perm buffer III and incubated on ice for 20 minutes. This was followed by a wash step. The cell pellet was resuspended in 100 µl of 1xTFPerm wash buffer and 1µg/million cells of phosphoSTAT5 PE antibody (Biolegend) was added followed by incubation for 40 mins on ice. Cells were washed in 1xTFPerm wash buffer and resuspended in Cell staining buffer (Biolegend). Acquisition was on LSRII cytometer (BD bioscience). The result of the pSTAT5 optimisation experiment is summarised in Figure 5-12.

5.5 Results

5.5.1 *STAT5B* transduction enhances PBMC proliferation and survival.

To track the growth dynamics of *STAT5B*-transduced PBMCs, the proportion of *STAT5B*-transduced cells was assessed by flow cytometry for CD34 expression (which is co-expressed with both mutant and wildtype *STAT5B* constructs) on Days 2, 5 and 9 following retroviral transduction. Both *STAT5B* wildtype (WT) and *STAT5B* N642H mutant transduced PBMCs selectively expanded from an average of 17% and 20% respectively on Day 2 to 54% and 47.9% on Day 9 (Figure 5-4).

To interrogate the impact of *STAT5B* overexpression on activation and exhaustion markers, expressions of CD69 and PD-1 were compared between *STAT5B*-transduced cells against unstimulated and non-transduced PBMCs. The analysis showed upregulation of both markers in *STAT5B* WT and *STAT5B* N642H-transduced cells compared to unstimulated PBMCs. Expression levels of CD69 and PD-1 were however similar to those of untransduced, IL15-stimulated PBMCs (Figure 5-5).

To determine the effect of *STAT5B* transduction on apoptosis following IL-15 withdrawal, *STAT5B* WT and *STAT5B* N642H transduced PBMCs were deprived of IL-15 for 48 hours and the proportions of viable, non-apoptotic cell proportions were compared with untransduced PBMCs subjected to the same conditions. There was a relative increase in viable (Annexin V negative, Propidium Iodide negative) cell proportions in the *STAT5B* transduced cells however, this difference was not statistically significant (Figure 5-6). To evaluate whether significant differences in cell death protection could be observed following longer periods of IL-15 deprivation, a further experiment was performed to enumerate viable PBMCs following IL-15 deprivation for up to 9 days. In the absence of IL-15, there was a marked decline in

cell viability by Day 9 for untransduced PBMCs while *STAT5B* N642H-transduced PBMCs maintained the highest viability (Figure 5-7). In contrast, cell viability was generally maintained in the presence of IL-15 with the highest proportion of viable cells in the *STAT5B* WT transduced cells. These results were in keeping with the CellTrace proliferation assay results which showed a trend towards enhancement of proliferation (as determined by CellTrace Violet dye dilution) for *STAT5B* mutant transduced cells maintained in IL-15 although the difference in proliferation was not significant due to marked donor variability; Donor 2 demonstrated reduced proliferative capacity across all experimental conditions (figure 5-8).

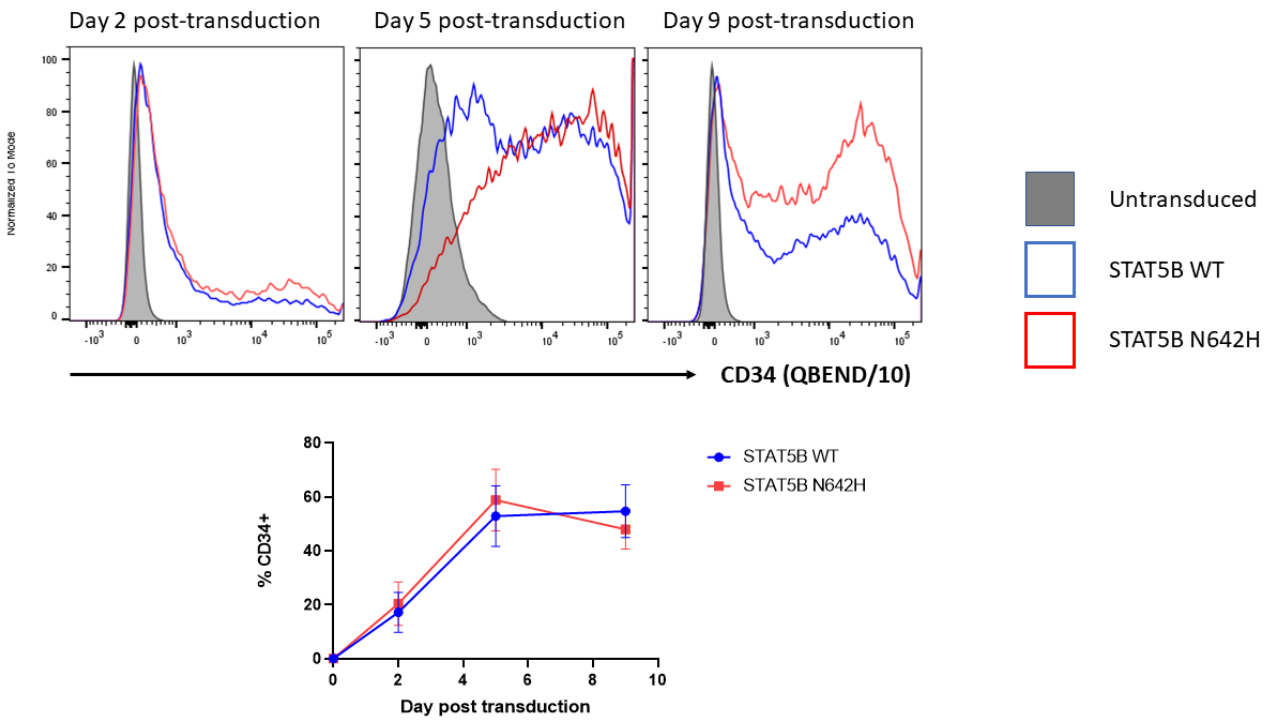

Figure 5-4: Expansion of STAT5B-transduced cells. (Above) Flow cytometry histograms for a single donor assessed on days 2, 5 and 9 after transduction with *STAT5B* wildtype (WT) and *STAT5B* N642H showing progressive enrichment of *STAT5B*-transduced cells. Cells were maintained in complete media supplemented with 100ng/ml of IL-15. *STAT5B*-transduced cells were identified by positive staining for CD34. Events were gated on live cells. Below: Graphical representation of the proportions of *STAT5B*-transduced cells positive for CD34 assessed on days 2, 5 and 9 after transduction (n=3, error bars indicate standard error of means).

Phenotyping of *STAT5B*-transduced cells

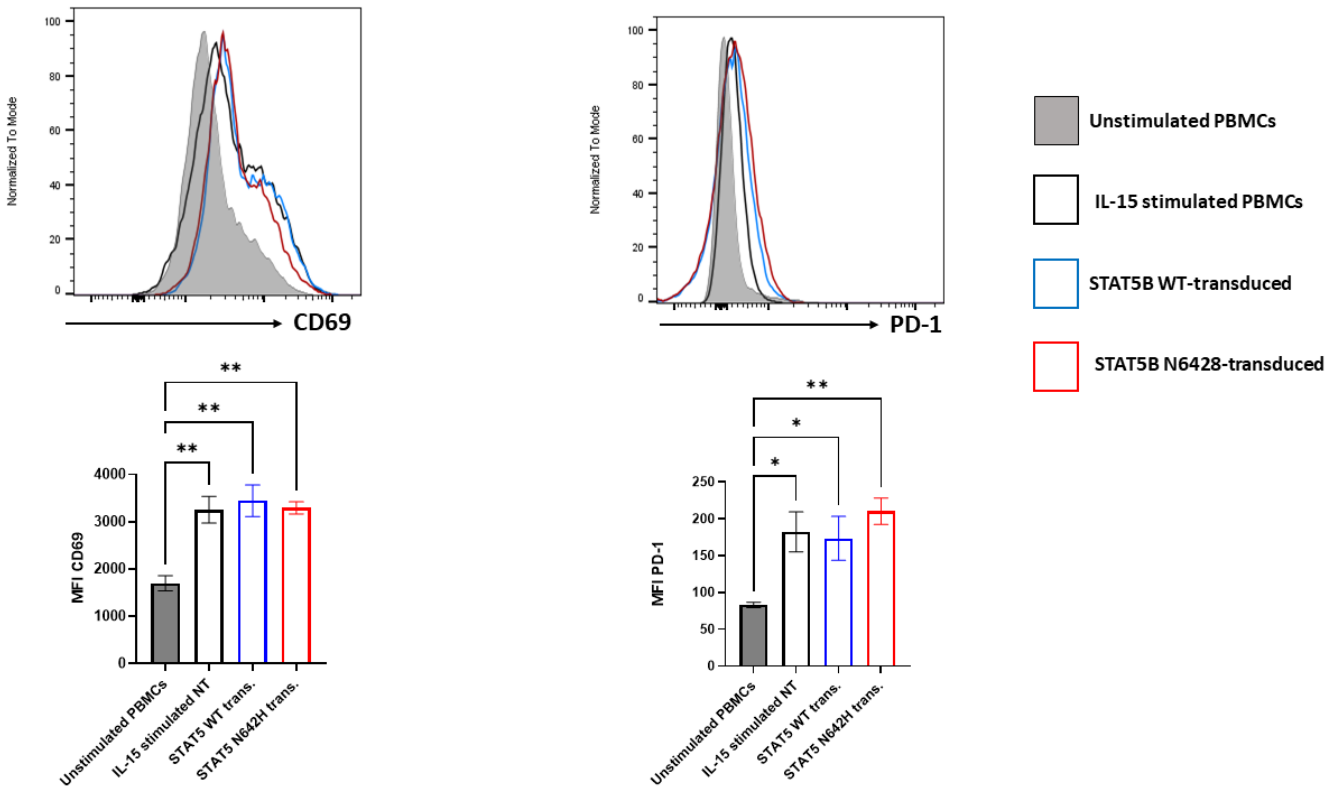

Figure 5-5: Expression of CD69 and PD-1 on *STAT5B*-transduced cells. Above: Flow cytometry histograms for a representative donor showing surface expressions of CD69 and PD-1 respectively. Cells were assessed on Day 5 following transduction. Events were gated on CD34+ cells and live T cells (for untransduced conditions). Below: Graphical comparisons of median fluorescence intensities of CD69 and PD-1 respectively for the same donor cells transduced with *STAT5B* wildtype (WT), *STAT5B* N642H as well as IL-15 stimulated untransduced and unstimulated PBMC controls (n=3, 1-way ANOVA; *p<0.05, **p<0.01, error bars indicate standard error of means).

Apoptosis assay of STAT5-transduced cells

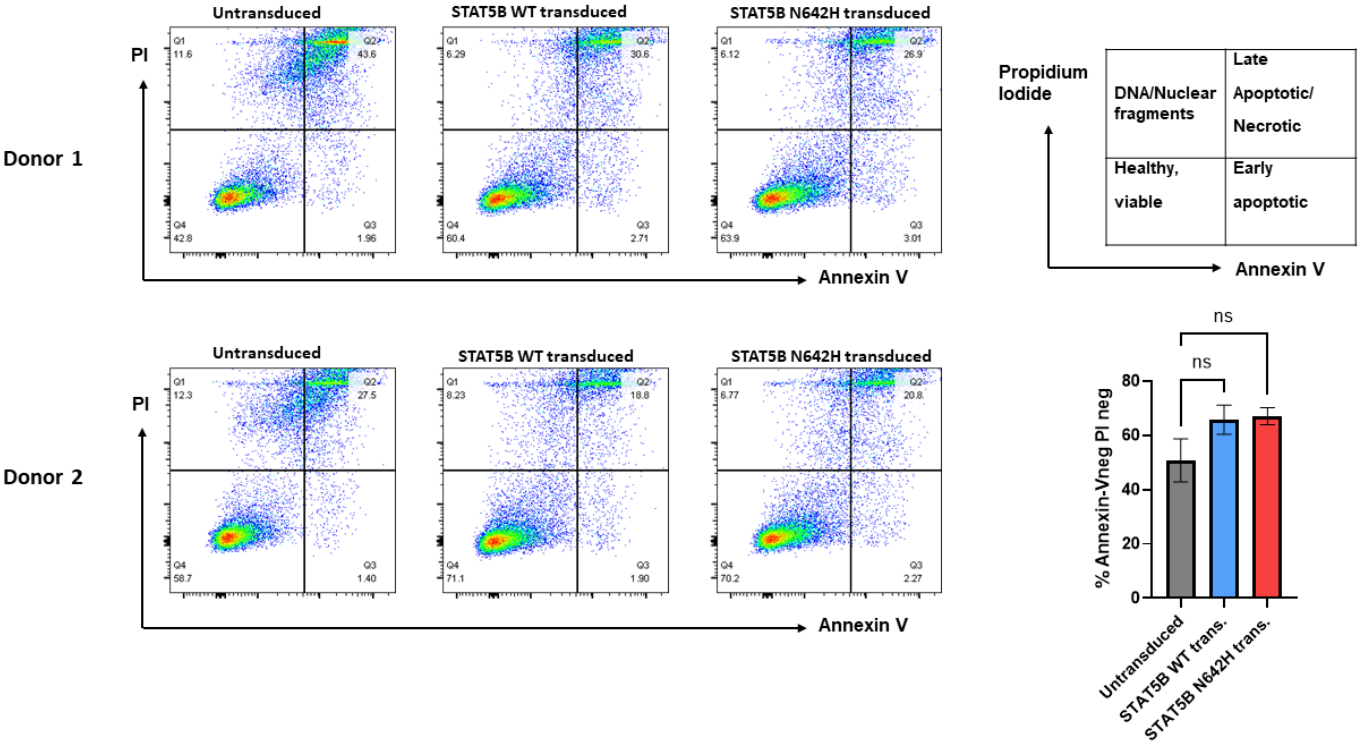

Figure 5-6: Apoptosis Assay of *STAT5B*-transduced PBMCs (Left) Flow cytometry dot plots for two representative donors showing Annexin-V and Propidium iodide (PI) staining following 48 hours of IL-15 deprivation. All cells were initially expanded in complete media supplemented with 100 ng/ml of IL-15 and were subsequently washed and cultured in complete media without IL-15 for 48 hours prior to flow cytometry analysis. Events were gated on single cells. Above, right: Schematic illustration of the respective cell populations represented in a typical Annexin V *vs* PI flow cytometry plot. Below, right: Graphical comparison of percentage of Annexin-V negative, PI negative (viable) cells for each condition (n=2, 1-way ANOVA; ns=non-significant, error bars indicate standard error of means).

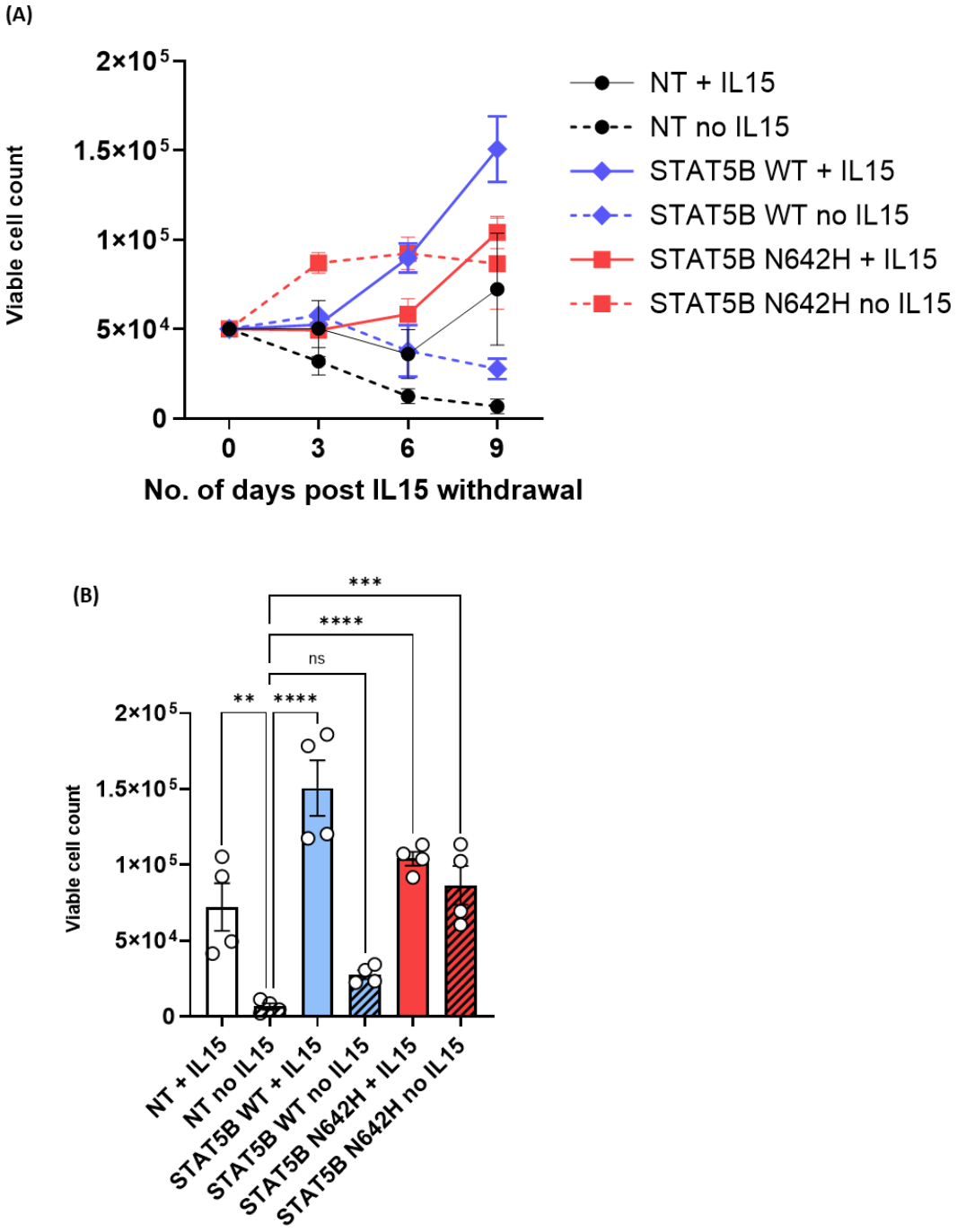

Figure 5-7: Cell viability of *STAT5B*-transduced PBMCs (A) Viable cell counts for *STAT5B* wildtype (WT) and *STAT5B* N642H-transduced PBMCs and their respective controls assessed on Days 3, 6 and 9 post-IL-15 withdrawal. Cells were counted at the start of the experiment and $5x10^4$ cells were plated in six replicate wells for each donor condition. On days 3, 6 and 9, duplicate wells from each donor condition were retrieved and viable cells were enumerated by flow cytometry normalised with counting beads. All cells were initially expanded in complete media supplemented with 100ng/ml of IL-15 and were subsequently washed and cultured in complete media without IL-15 where appropriate. All events were gated on live cells. (B) Graphical comparison of viable cell counts on Day 9 following IL-15 withdrawal (n=2, 1-way ANOVA; **p<0.01, ***p<0.001, ****p<0.0001, ns=non-significant, error bars indicate standard error of means, NT=non-transduced).

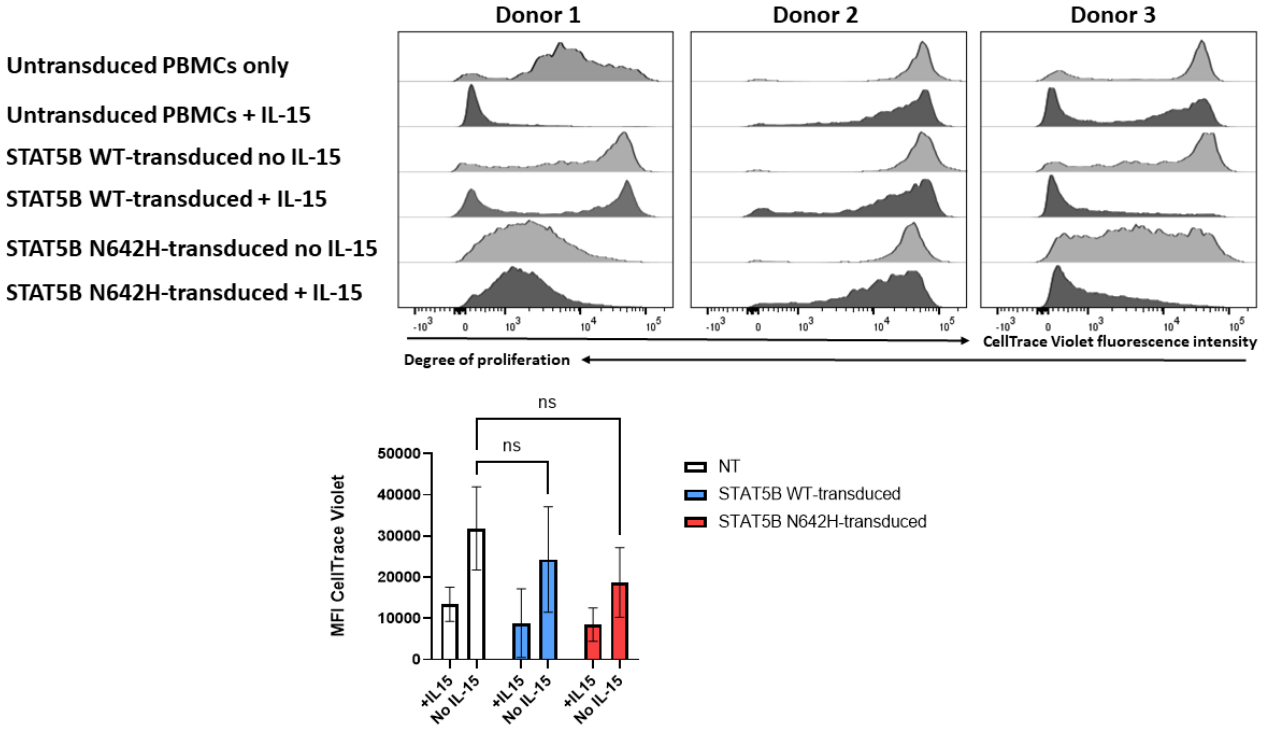

Figure 5-8: Role of IL-15 in *STAT5B* transduced cell proliferation: Above: Flow cytometry histograms from three independent donors comparing CellTrace Violet fluorescence intensities for untransduced (NT), *STAT5B* wild type (WT) and *STAT5B* N642H-transduced PBMCs with and without IL-15. All cells were initially expanded in complete media supplemented with 100 ng/ml of IL-15, subsequently washed and, where appropriate, cultured in complete media without IL-15. Events were gated on live cells. Below: Graphical representation of CellTrace Violet median fluorescence intensities (MFIs) for the respective experimental conditions (n=3, 2-way ANOVA; ns=non-significant, error bars indicate standard error of means, NT=non-transduced)

5.5.2 *STAT5B*-transduced γδ T cells retain anti-tumour properties.

To determine if the anti-tumour properties of *STAT5B*-transduced γδ T cells were retained following transduction and the influence of IL-15 on these properties, a CD107a degranulation assay was performed comparing degranulation by *STAT5B* WT, *STAT5B* N642H and TE9 (B7-H3 targeting) CAR transduced PBMCs against LAN1 targets (B7-H3+) both with and without IL-15. In general, CD107a degranulation was slightly enhanced in the presence of IL-15 for all conditions regardless of the presence of targets. The only statistically significant increase in CD107a degranulation against the B7-H3 positive LAN1 target was by the TE9 CAR transduced γδ T cells and this was maintained in the absence of IL-15 (Figure 5-9).

Furthermore, Interferon-γ (IFNγ) secretion was assessed in response to tumour targets with and without IL-15 and there was enhancement by IL-15 of IFNγ secretion for *STAT5B*-transduced PBMCs but IFNγ secretion was minimal in the absence of IL-15 (figure 5-10). The IL15-induced IFNγ secretion by *STAT5B*-transduced PBMCs was independent of the presence of cancer targets. In contrast, following IL-15 withdrawal, TE9 CAR transduced cells maintained antigen-specific IFNγ secretion against Jurkat B7H3 cells even in the absence of IL-15. This result suggests that IFNγ secretion by CAR-transduced cells in response to target antigen expressing cell lines is independent of IL-15 stimulation.

Furthermore, both *STAT5B* WT and *STAT5B* N642H transduced γδ T cells demonstrated comparable dose-dependent specific cytotoxicity against both Jurkat WT and Jurkat B7-H3 and this was not affected by IL-15 withdrawal (figure 5-11).

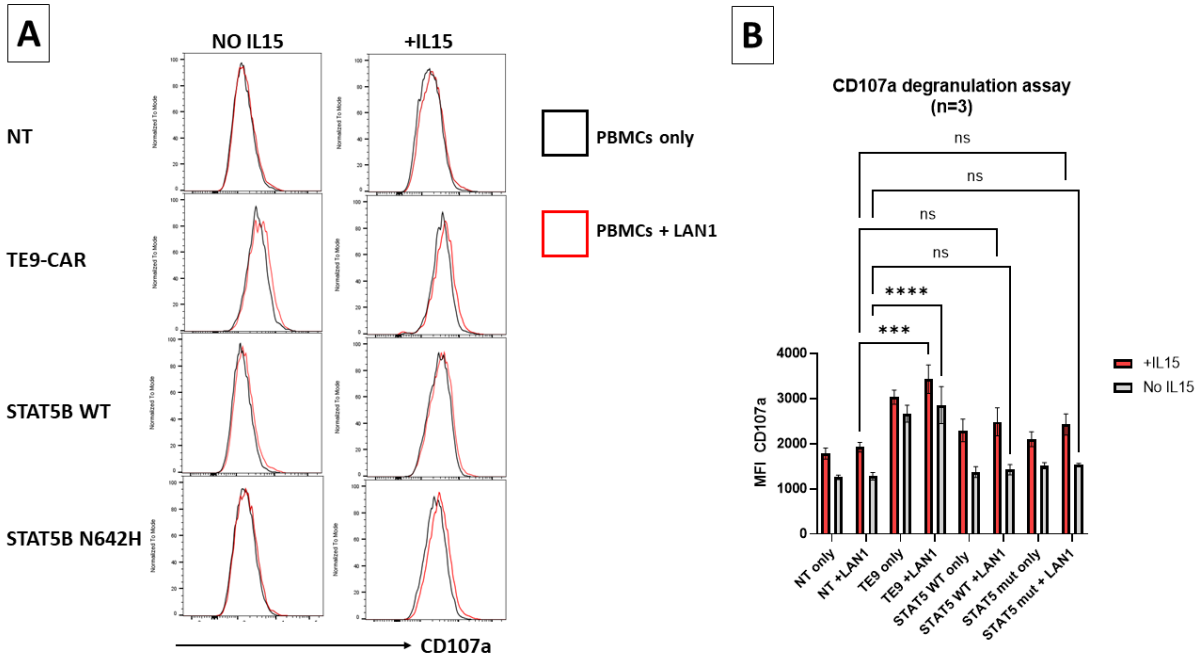

Figure 5-9: CD107a degranulation assay of *STAT5B* transduced PBMCs (A) Flow cytometry histograms from a representative donor comparing CD107a fluorescence intensities for untransduced (NT), TE9 CAR, *STAT5B* wild type (WT) and *STAT5B* N642H-transduced PBMCs with and without IL-15. Overlaid on the histogram for PBMCs alone (black line) is the histogram for CD107a fluorescence following co-culture with LAN1 cell line (red line) for 4 hours at 37ºC. All cells were initially expanded in complete media supplemented with 100 ng/ml of IL-15, subsequently washed and, where appropriate, cultured in complete media without IL-15 48 hours before the co-culture experiment. Events were gated on Vδ1+ T cells. (B) Graphical representation of CD107a median fluorescence intensities (MFIs) for the respective experimental conditions (n=3, 2-way ANOVA; ***p<0.001, ****p<0.0001, ns=non-significant, error bars indicate standard error of means, NT=non-transduced)

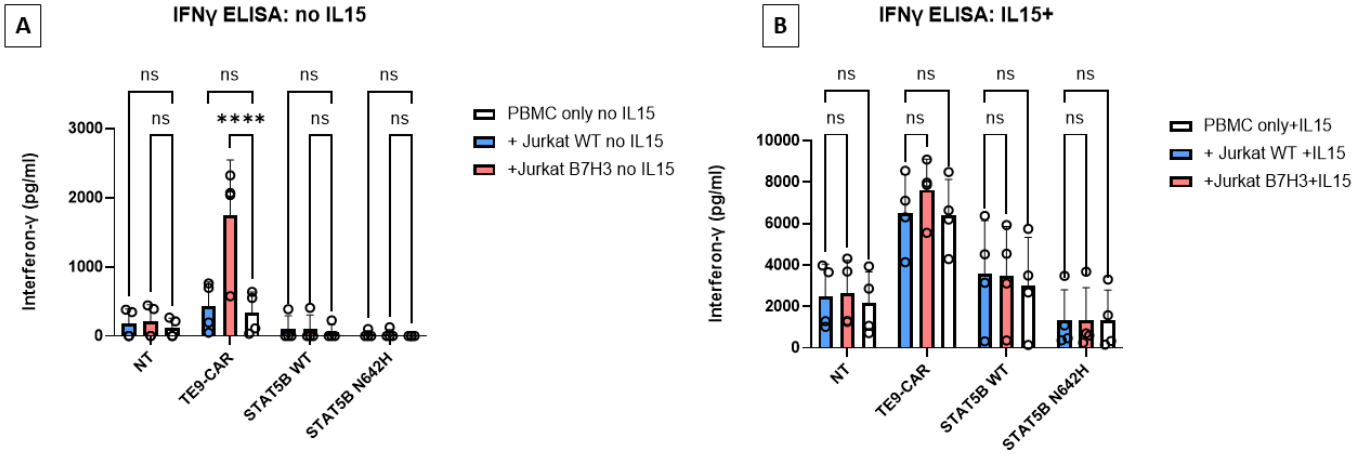

Figure 5-10: Comparison of Interferon-γ secretion (A) Graphical comparison of interferon-γ (IFNγ) secretion as measured by ELISA following a 24-hour co-culture experiment with $2x10^5$ *STAT5B* WT, *STAT5B* N642H or TE9 CAR-transduced PBMCs plated in 1:1 ratio with either Jurkat wildtype or Jurkat B7H3+ cell lines in the absence of IL-15. (B) Graphical comparison of interferon-γ (IFN-γ) secretion as measured by ELISA following a 24-hour co-culture experiment with $2x10^5$ *STAT5B* WT, *STAT5B* N642H or TE9 CAR-transduced PBMCs plated in 1:1 ratio with either Jurkat wildtype or Jurkat B7H3+ cell lines in the presence of 100ng/ml of IL-15. (n=4, 2-way ANOVA; ****p<0.0001, ns=non-significant, error bars indicate standard error of means, error bars indicate standard error of means, NT=non-transduced)

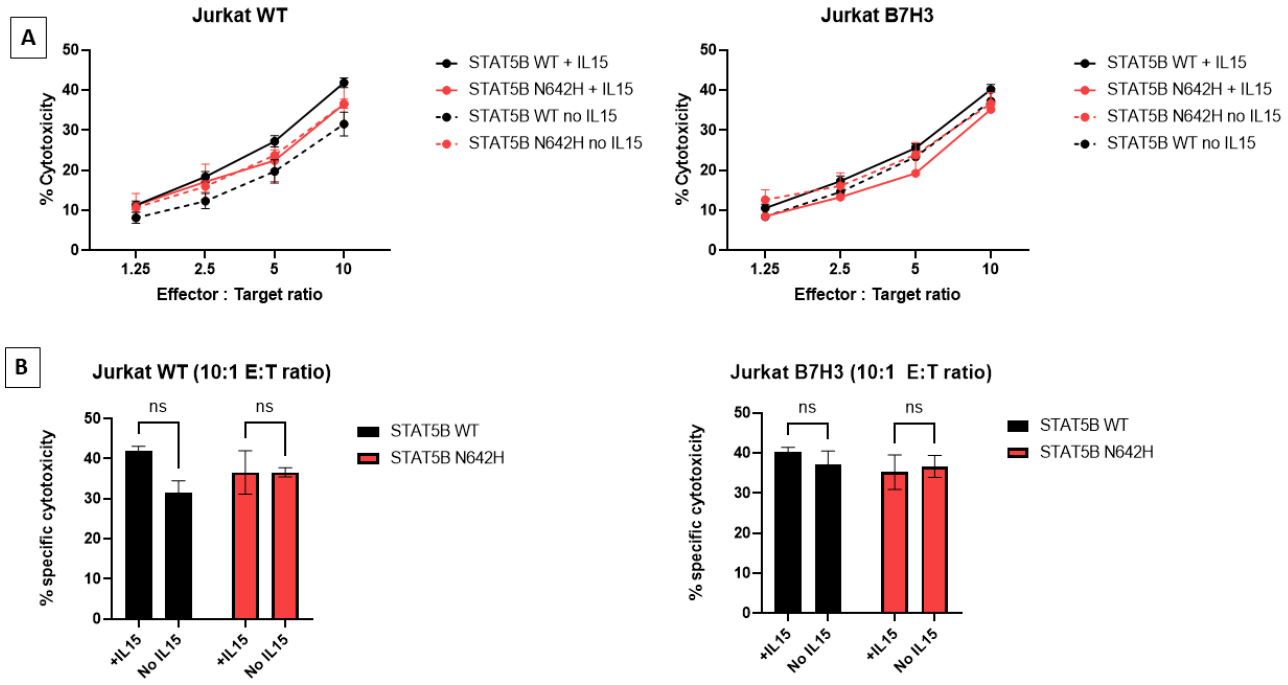

Figure 5-11: Cytotoxicity of *STAT5B*-transduced cells. (A) Graphical representations of the specific cytotoxicities of *STAT5B* wildtype (WT) and *STAT5B* N642H-transduced γδ T cells against B7-H3 negative Jurkat wildtype and B7-H3 positive, Jurkat B7-H3 cell lines with and without the presence of IL-15. Paired comparisons were made between specific cytotoxicity of *STAT5B*-transduced and untransduced γδ T cells for each donor PBMC/target pair. (B) Graphical comparisons of specific cytotoxicities at E:T ratios of 10:1 for *STAT5B* WT and *STAT5B* N642H-transduced γδ T cells against Jurkat WT and Jurkat B7-H3 cell lines. The graphs show no significant difference in cytotoxicity for *STAT5B* WT and *STAT5B* N642H-transduced γδ T cells against both cell lines in the absence of IL-15. *STAT5B*-transduced cells and negative controls were incubated with Chromium-51-labelled cell lines and incubated for 4 hours at 37°C and 5% CO_2. The cell culture medium was subsequently harvested and cytotoxicity was determined by scintillation counts as a marker of radioactive chromium release. Specific cytotoxicity was normalised to the spontaneous chromium release (negative control) and maximum release (induced by 1% Triton-X100) values. Where indicated, the culture medium was supplemented with 100ng/ml of IL-15 and for the IL-15 negative conditions, the cytokine was withdrawn 48 hours before the co-culture (n=4, 2-way ANOVA ns= non significant, all error bars indicate standard error of means)

5.5.3 STAT5B N642H potentiates phosphorylation of STAT5

The mechanism behind the observed properties of *STAT5B*-transduced γδ T cells particularly in relation to IL-15 withdrawal was investigated by phospho-flow cytometry for intracellular phosphorylated STAT5 (pSTAT5). First, an optimisation experiment was performed to determine the optimal duration of PBMC incubation with IL-15 to induce STAT5 phosphorylation. The 60-minute incubation was determined as the optimal duration as it resulted in higher median fluorescence intensity for pSTAT5 (figure 5-12). This incubation duration was used for the subsequent pSTAT5 experiments.

To Investigate the relationship between intracellular pSTAT5 and IL-15, a cytokine dose-titration experiment for pSTAT5 was performed and the results revealed significant IL-15 dose-dependent enhancement of pSTAT5 for STAT5B N642H transduced Vδ1 T cells compared with the untransduced (Figure 5-13). To further investigate basal pSTAT5 in the absence of IL-15, comparisons were made between non-transduced, TE9 CAR, *STAT5B* WT and *STAT5B* N642H transduced in a separate experiment. The MFI of pSTAT5 was significantly higher in the absence of IL-15 for *STAT5B* N642H transduced compared with *STAT5B* WT or TE9 CAR transduced (figure 5-14) indicating that the presence of the N642H mutation potentiates phosphorylation of STAT5.

Phospho-STAT5 flow cytometry optimisation

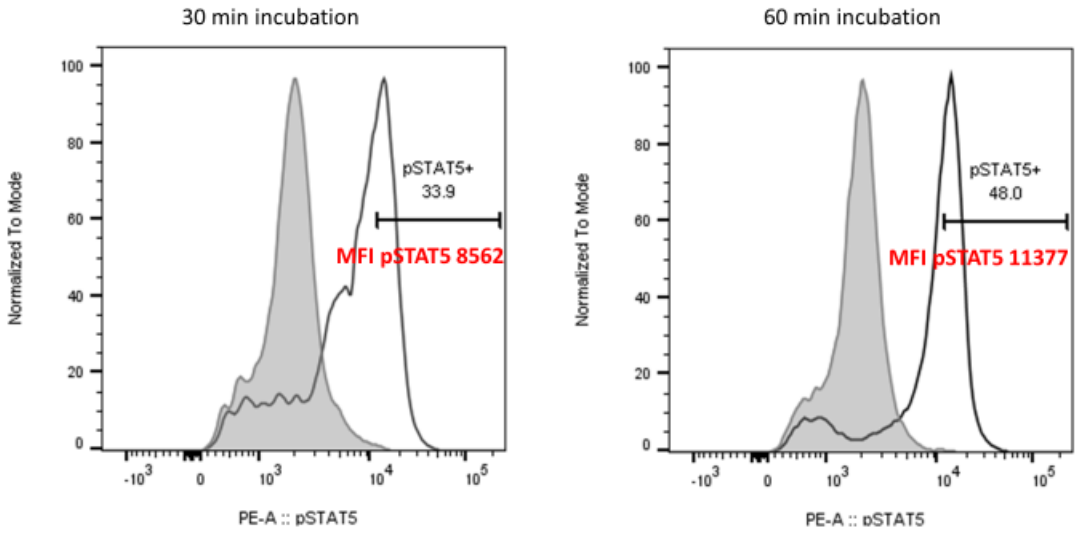

Figure 5-12: Phosphoflow cytometry experiment optimisation. Flow cytometry histogram plots showing intracellular phospho-STAT5 (pSTAT5) following a pilot experiment. Unstimulated PBMCs from a representative donor were incubated for either 30 or 60 minutes at 37°C in phosphate buffered saline (PBS) with and without 100ng/ml of Interleukin-15 (IL-15). Events shown were gated on CD3+ live cells and numbers indicate percentage of phospho-STAT5 (pSTAT5) positive cells and median fluorescence intensity (MFI). The grey histogram plots indicate IL-15 negative conditions. Phospho-STAT5+ gates were determined using the fluorescence minus one (FMO) control.

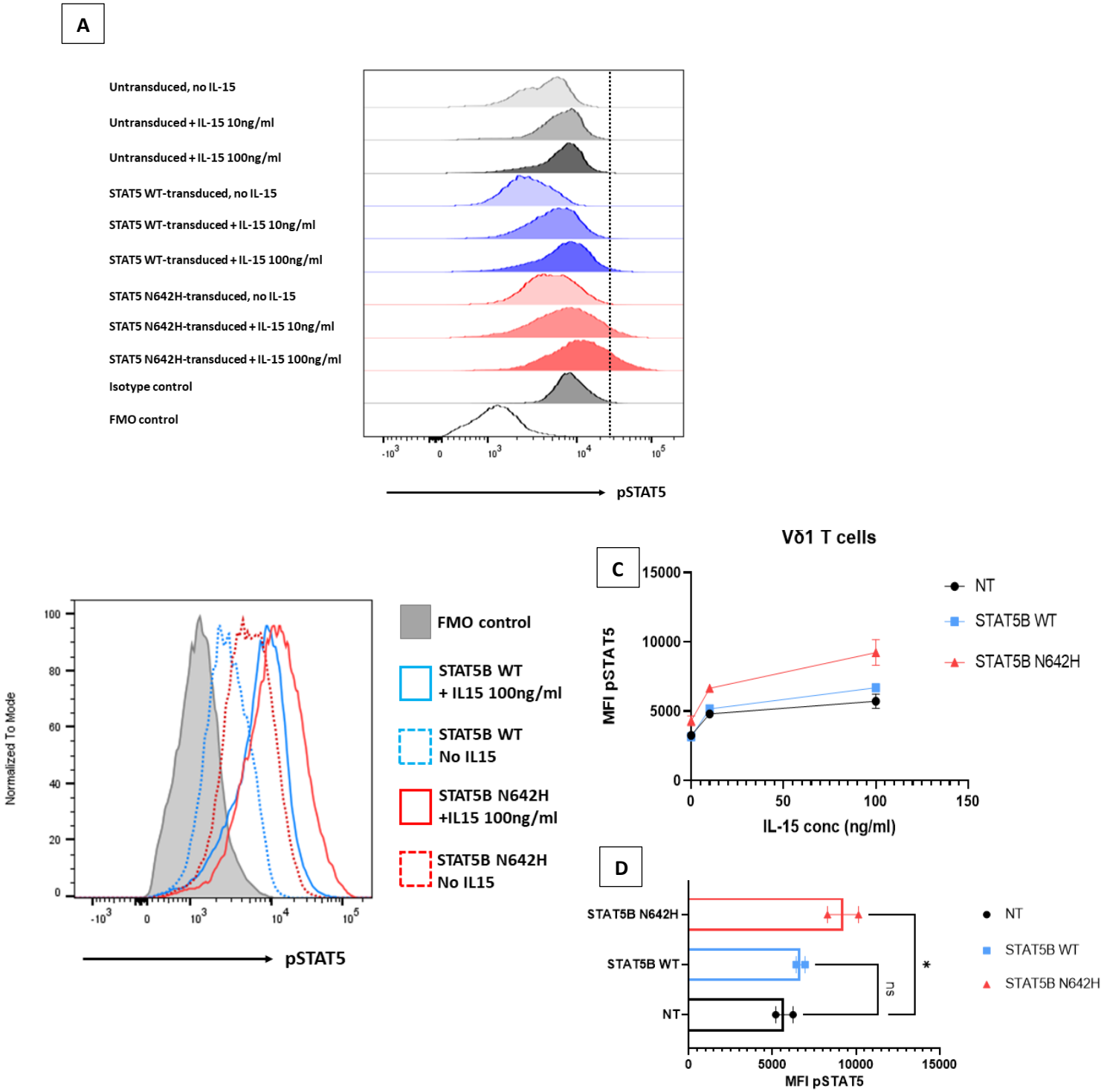

Figure 5-13: Phospho-STAT5 flow cytometry Experiment. (A) Flow cytometry histograms of phospho-STAT5 (pSTAT5) for a representative donor showing progressive increase in pSTAT5 fluorescence with increasing concentrations of IL-15. Cells were incubated at 37°C for 60 minutes before fixation and permeabilization for intracellular staining. Events were gated on CD3+ live cells. **(B)** Overlaid flow cytometry histograms from (A) comparing fluorescence intensities of phospho-STAT5 (pSTAT5) for STAT5B wild type (WT) and STAT5B N642H-transduced PBMCs with and without IL-15. All cells were initially expanded in complete media supplemented with 100ng/ml of IL-15, subsequently washed and cultured in complete media without IL-15 for the appropriate conditions. Events were gated on CD3+ live cells. **(C)** Graphical representation of pSTAT5 median fluorescence intensities (MFIs) for STAT5-transduced and untransduced Vδ1+ cells (n=2) at IL-15 concentrations of 0ng/ml, 10ng/ml and 100ng/ml. **(D)** Graphical comparisons of pSTAT5 MFI of Vδ1+ cells at IL-15 concentration of 100ng/ml for the respective experimental conditions. (n=2, 1-way ANOVA; *p<0.05, ns=non-significant, error bars indicate standard error of means, NT=non-transduced).

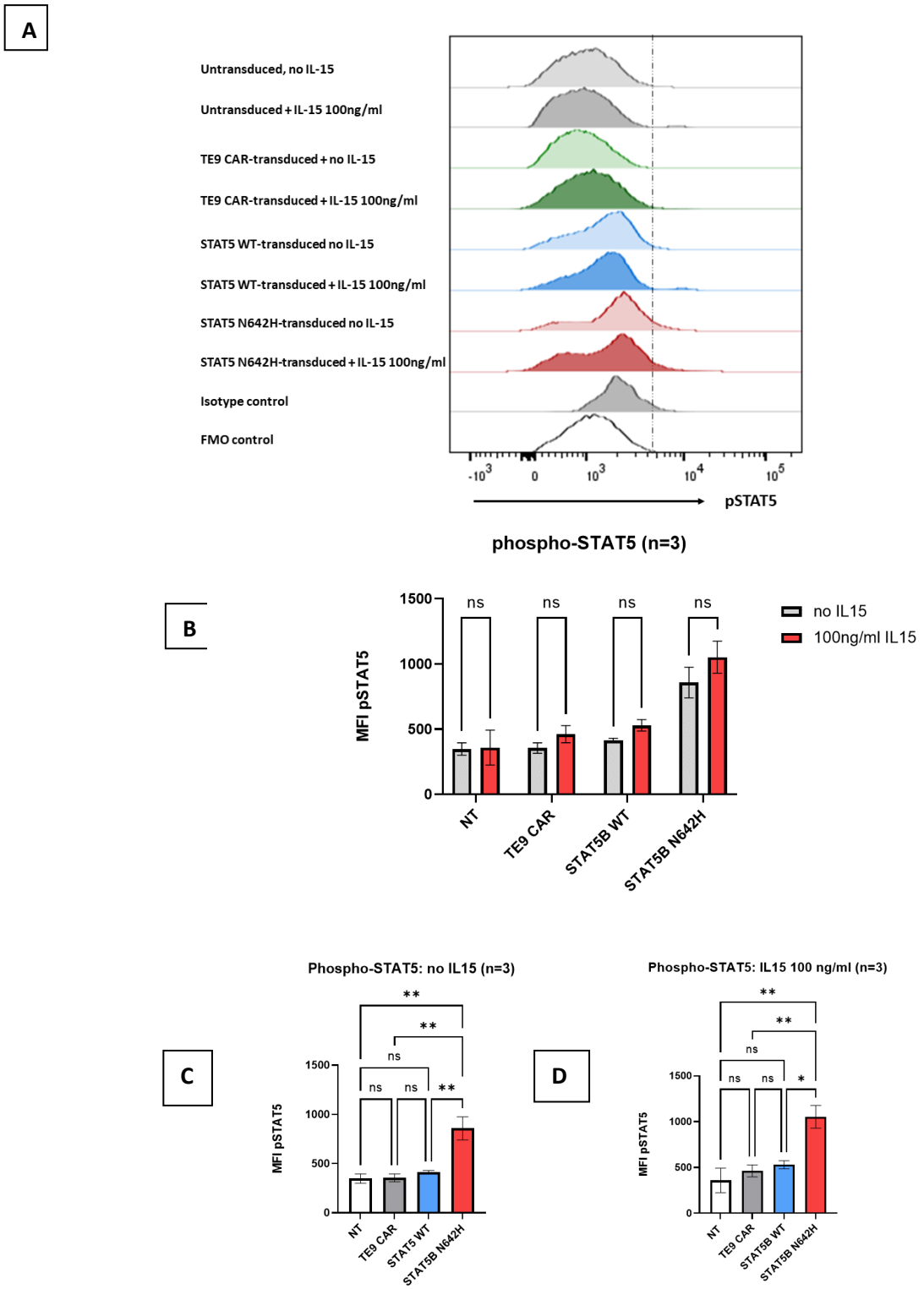

Figure 5-14: Phospho-STAT5 flow cytometry comparison: (A) Flow cytometry histograms from a representative donor comparing fluorescence intensities of phospho-STAT5 (pSTAT5) for untransduced (NT), TE9 CAR-transduced, *STAT5B* wild type (WT) and *STAT5B* N642H-transduced PBMCs with or without IL-15. All cells were initially expanded in complete media supplemented with 100ng/ml of IL-15, subsequently washed and, where appropriate, cultured in complete media without IL-15. Events were gated on CD3+ live cells. **(B)** Graphical representation of pSTAT5 median fluorescence intensities (MFIs) for the respective experimental conditions at IL-15 concentrations of 0ng/ml and 100ng/ml. The comparative analysis of pSTAT5 MFI are shown without IL-15 **(C)** and at IL-15 concentration of 100ng/ml **(D)** for the same experiment. Events were gated on CD3+ live cells. (n=3, 2-way ANOVA; *p<0.05, **p<0.01, ns=non-significant, error bars indicate standard error of means, NT=non-transduced)

5.5.4 TE9 CAR and *STAT5B* N642H "double transduced" γδ T cells

Given the antigen-specificity conferred by the second generation B7-H3 targeting TE9-28z CAR (referred to as simply TE9 CAR) and the IL-15 independent survival of STAT5B N642H, a double transduction strategy was devised to harness both desirable properties. First, γδ T cell enriched PBMCs were expanded with anti-CD3 and IL-15 as previously described. This was followed by transduction with both TE9 CAR (with RQR8 deleted) and *STAT5B* N642H (encoding RQR8 which is detectable by surface CD34 staining) retrovirus supernatants on Day 5. The double-transduced, CAR+CD34+ population which was assessed 48 hours post-transduction ranged from approximately 4% to 11% (figure 5-15a).

To determine antitumour responses to cancer cell lines, double-transduced cells were co-cultured with LAN1 (B7-H3 positive) and Jurkat WT (B7-H3 negative) in the absence of IL-15. While there was a trend towards higher MFIs for CD107a and intracellular IFNγ for these cells against LAN1 cells, the difference was not statistically significant (figure 5-15b). There was however significantly higher IFNγ secretion (compared with PBMCs alone) when double transduced PBMCs were cultured with Jurkat B7H3 in the absence of IL-15 (Figure 5-16) with a non-significant increase following co-culture with Jurkat WT. In the experimental conditions with IL-15, IFNγ secretion was almost uniformly increased irrespective of the presence of the target antigen, representing a non-specific response.

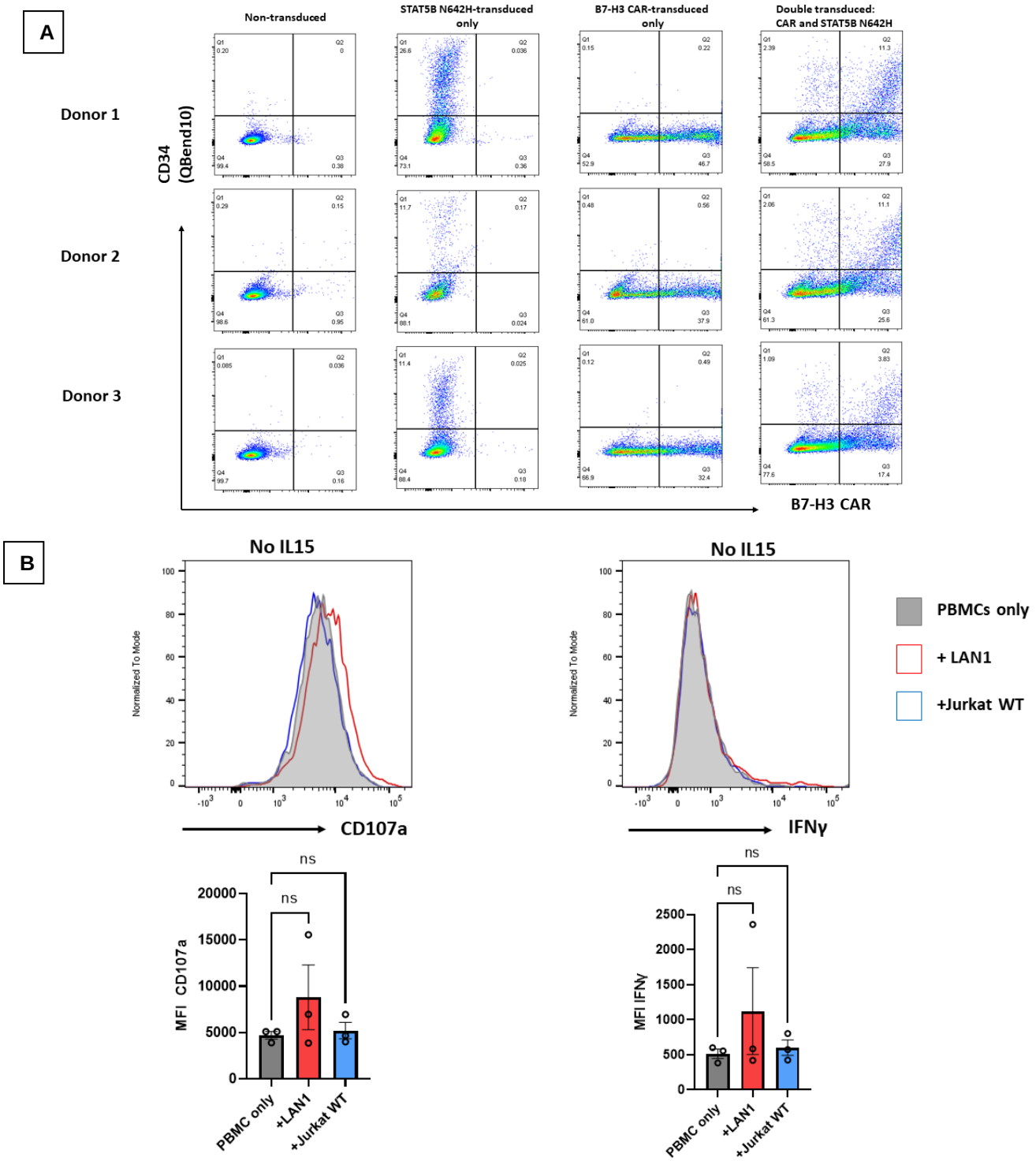

Figure 5-15: Antitumour responses of double transduced T cells. (A) Flow cytometry dot plots for three donors showing non-transduced (NT), *STAT5B* N642H-transduced, TE9 CAR-transduced and double (CAR and STAT5B N642H) transduced-PBMC populations. For the double transduced condition, PBMCs were transduced with equal proportions of TE9 CAR and *STAT5B* N642H retrovirus supernatants on Day 5 of PBMC expansion with 100ng/ml of IL-15. Events were gated on live cells. (B) Above: Flow cytometry histograms of **unsorted** double-transduced Vδ1 T cells from a single donor showing fluorescence intensities for CD107a (left) and Interferon-γ (right). Overlaid on the histograms for PBMCs alone (grey) are the histograms following co-culture with LAN1 (red line) and Jurkat wildtype (blue line) for 24 hours at 37ºC without IL-15. Below: Graphical representations of median fluorescence intensities (MFIs) for of CD107a (left) and Interferon-γ (right). All cells were initially expanded in complete media supplemented with 100ng/ml of IL-15 but the cytokine was withdrawn 24 hours before the co-culture experiment. Events were gated on Vδ1+ T cells (n=3, 1-way ANOVA; ns=non-significant, error bars indicate standard error of means).

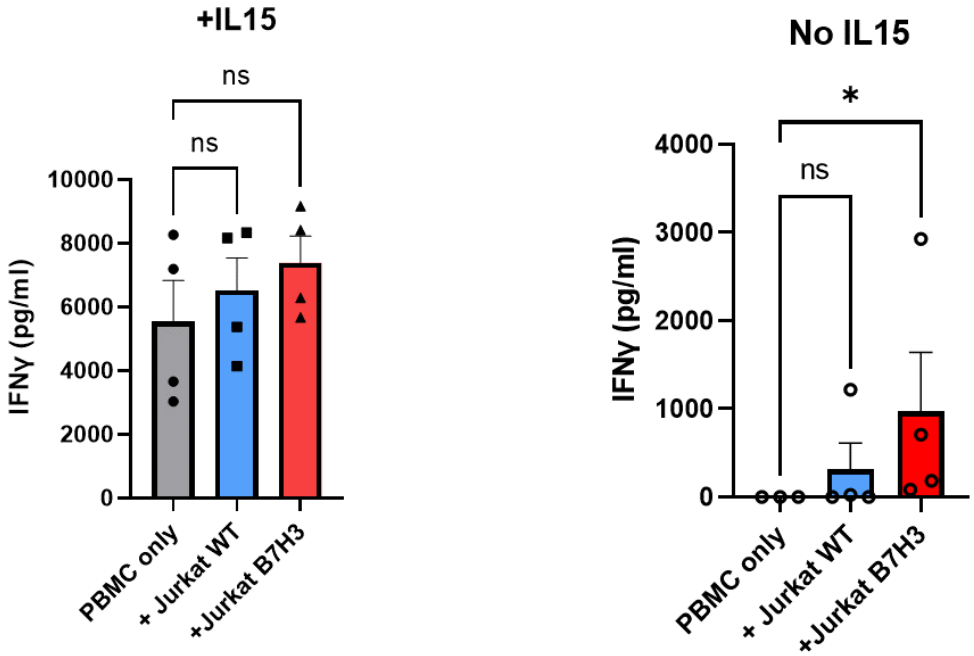

Figure 5-16: Interferon-γ secretion by double-transduced T cells. Graphical comparison of interferon-γ (IFN-γ) secretion as measured by ELISA following a 24-hour co-culture experiment with $2x10^5$ *STAT5B* N642H and TE9 CAR-transduced PBMCs plated in 1:1 ratio with either Jurkat wildtype or Jurkat B7H3+ cell lines with and without IL-15. Where appropriate, the complete medium was supplemented with 100ng/ml of IL-15 and in the IL-15 negative conditions, the cytokine was withdrawn 24 hours prior to the co-culture experiment. (n=4, Kruskal-Wallis test; *p<0.05, ns=non-significant, error bars indicate standard error of means, error bars indicate standard error of means).

5.6 Discussion

In the previous chapters of this thesis, the pivotal role of IL-15 in enhancing the anti-tumour properties of γδ T cells was elucidated. It was also shown that IL-15 stimulated γδ T cells become dependent on the cytokine for proliferation and survival. IL-15, like its common gamma chain (γc) counterpart IL-2, induces differentiation and proliferation of cytotoxic T cells and NK cells but unlike IL-2, it promotes persistence of CD8+ memory T cells and is less likely to activate regulatory T cells (Tregs) or initiate activation-induced cell death (AICD).[195] These properties of IL-15 initially renewed interest in the potential for use as an immunotherapeutic agent however clinical trial results have been disappointing. A Phase I clinical trial of intravenous recombinant IL-15 in patients with advanced cancers was associated with severe dose-limiting and sometimes unexpected adverse events such as gastrointestinal haemorrhage.[238] Clinical responses were modest with no patient achieving a partial response despite dramatic expansions of NK and CD8+ T cells. Given these findings, it is unlikely that co-administration of IL-15 with a cell therapy product would be tolerable hence the need for alternative strategies to maintain viability and persistence of γδ T cells while enhancing the function of these cells.

Downstream IL-15 signalling involves a cascade of signal transductions via transcription factors following activation of its receptors. Chief among the transcription factors involved in IL-15 signalling is STAT5B. Therefore, it is hypothesized that manipulation of the signalling pathway downstream of the ligand-receptor interaction, may overcome IL-15 dependence. To achieve this, the constitutively active *STAT5B* N642H point mutation was cloned into a retroviral vector and transduced to γδ T cell-enriched PBMCs. As *STAT5B* N642H has been

identified as a driver mutation in haematological malignancies[239–242], it was important to incorporate a suicide gene in the vector construct. RQR8, a compact suicide gene was co-expressed in the *STAT5B* N642H-transduced cells. It has been previously shown that cells expressing RQR8 can be efficiently deleted *in vivo* following administration of the anti-CD20 monoclonal antibody, Rituximab.[243] JAK inhibitors may also offer an alternative strategy for modulation of the proliferative potential of these *STAT5B*-transduced cells.[244] Therefore in the clinical context, the proliferative potential of *STAT5B* N642H transduced cells is subject to control where required but the rituximab-induced deletion of the STAT5B-transduced cells would need to be confirmed in an experimental *in vivo* model.

One of the functional consequences of *STAT5B* transduction was the promotion of proliferation as shown by selective expansion of transduced cells in the presence of IL-15 (figure 5-4) and this was similar for both *STAT5B* wild type and N642H mutant. A similar pattern was demonstrated in the CellTrace Violet proliferation assay (figure 5-8). In general, both *STAT5B* WT and *STAT5B* N642H transduced cells had enhanced proliferative capacity in the presence of IL-15 with the mutant retaining a greater degree of proliferation in the absence of IL-15 but this was diminished in the WT-transduced. The proliferation assay analysis comparing median fluorescence intensities however did not show a statistically significant difference between WT and mutant STAT5B due to marked donor-dependent variation in degree of proliferation for each experimental condition.

Furthermore, the initial signal of enhanced pro-survival capacity of T cells following STAT5B transduction was demonstrated in the Annexin V binding assay (figure 5-6) with a higher (but non-statistically significant) proportion of viable (Annexin V negative, PI negative) T cells in the *STAT5B* WT and N642H-transduced conditions

compared with the untransduced control following 48 hours of IL-15 withdrawal. As statistical significance of the difference in cell viability was not achieved after 48 hours of IL-15 withdrawal, it was hypothesized that a longer duration of cytokine withdrawal was required for a complete washout. Indeed, the 9-day IL-15 withdrawal experiment showed marked differences in cell viability between untransduced, WT and mutant *STAT5B* -transduced cells (figure 5-7). *STAT5B* N642H-transduced cells maintained viability independent of IL-15 for up to 9 days whereas there was a decline in the viability of *STAT5B* WT-transduced after Day 3. For the untransduced control, a marked reduction in cell viability was obvious with barely any viable cells remaining by Day 9. Therefore, it can be concluded that the N642H mutation overcomes IL-15 dependence for T cell survival. These results are in keeping with findings in a transgenic murine model of *STAT5B* N642H in which the mutation was found to render bone marrow (BM) cells hypersensitive to cytokine stimulation and were also capable of forming colonies in the absence of cytokine stimulation, an effect which was not seen in BM cells from *STAT5B* WT mice.[242] Given concerns about the potential for T cell exhaustion from hyperstimulation, it was reassuring to note that *STAT5B* WT and N642H transduced cells did not significantly upregulate PD-1 or CD69 expression compared with IL-15 stimulated, untransduced controls (figure 5-5).

While the pro-survival and mitogenic effects of the *STAT5B* N642H mutation on T cells have been described, little was previously known about its impact on the anti-tumour functions such as cytotoxicity and cytokine production. The 4-hour Chromium-51 assay for *STAT5B* WT and *STAT5B* N642H-transduced γδ T cell-enriched PBMCs co-cultured against Jurkat WT and Jurkat B7-H3 showed dose-dependent cytotoxicity which was maintained following IL-15 withdrawal (figure 5-

11). CD107a degranulation assay results showed a trend towards increased, albeit non-significant, responses for *STAT5B*-transduced cells in the presence of LAN1 cell line (figure 5-9). CD107a MFIs were slightly higher in the presence of IL-15 for all experimental conditions and unsurprisingly, a significant CD107a degranulation response was observed for the B7-H3 targeting TE9-28z CAR-transduced cells. Furthermore, IFNγ production by *STAT5B* WT and *STAT5B* N642H transduced γδ T cells was enhanced by IL-15 (figure 5-10) and the cytokine was barely detectable in co-culture with cancer cell lines in the absence of IL-15. Put together, these results suggest that STAT5B transduced T cells retain their capacity for anti-tumour cytotoxicity and cytokine production and while the former is not significantly diminished following IL-15 withdrawal, IFNγ secretion remains IL-15 dependent. A remarkable observation was that IFNγ secretion by TE9 CAR-transduced T cells remained significantly elevated in co-culture against Jurkat B7-H3 even in the absence of IL-15 thus indicating maintenance of CAR function independent of IL-15.

To dissect the underlying mechanism of the functional consequences of *STAT5B* N642H mutation on T cell function, a phosphoflow assay for pSTAT5 was designed which demonstrated potentiation of pSTAT5 in the N642H-transduced cells; pSTAT5 levels were significantly higher in a dose-dependent manner in *STAT5B* N642H-transduced cells (figure 5-13) and remained elevated following IL-15 withdrawal, a phenomenon that was not observed in the STAT5B WT or TE9 CAR-transduced cells (figure 5-14). It was therefore concluded that the N642H mutation results in persistence of the physiologically-active pSTAT5 following IL-15 withdrawal accounting for the observed pro-survival and proliferative effects of the *STAT5B* N642H mutation. However, it is likely that the induction of IFNγ secretion by IL-15 is via an alternative mechanism as it is not rescued by the N642H mutation.

A major cause of lack of CAR T cell efficacy in solid tumours is impaired T cell persistence. Since long term persistence of CAR T cells has been associated with clinical remission[245,246], improving CAR T cell persistence is of paramount importance. The antigen specificity of a CAR coupled with the pro-survival effects of *STAT5B* N642H offers a possible strategy for enhancing persistence. Transduction with both *STAT5B* N642H and TE9 CAR retroviruses yielded up to 11% of cells expressing both the CAR and CD34 (a surrogate marker for the STAT5B construct). This “double transduced” bulk γδ T cell population demonstrated antigen specific IFNγ secretion independent of IL-15 stimulation. However, since the cell populations were unsorted in the co-culture experiments, due to low cell numbers, it cannot be definitively concluded that the effects are attributable to the CAR+STAT5BN642H+ (double positive) population. While the CAR+STAT5B N642H+ population is relatively small, it is possible that engagement of the target antigen would result in expansion and enrichment of this population *in vivo*. Further optimisation and *in vivo* validation will be required to confirm the cytokine independence and long-term persistence of these cells. It was indeed difficult to obtain increased proportions of CAR+STAT5BN642H+ cells despite several attempts to optimise the retroviral transductions. A lentiviral transduction with a single construct which expresses the CAR alongside STAT5B N642H was also attempted but only transient expression was observed by flow cytometry. The possible explanations for this failure to optimally transduce PBMCs with both the CAR and *STAT5B* N642H include genotoxic stress from two retroviral transductions or hyperstimulation and exhaustion from dual signalling. To address these issues, further experiments including determination of exhaustion markers and viability of FACS-sorted double transduced γδ T cells may be necessary. An alternative strategy for ensuring T cell survival

which has been explored by other groups is the incorporation of an IL-15 transgene in the CAR construct. Furthermore, there is some evidence from the short term cytotoxicity and cytokine secretion that CAR-transduced cells maintain their function in the absence of IL-15 and there is a possibility that signalling via the CAR may, at least partially, rescue the effect of IL-15 withdrawal. This could be further explored in long-term co-cultures without IL-15 and in a mouse model.

In summary, manipulation of *STAT5B* signalling offers a novel strategy to overcome IL-15 dependence in γδ T cells as it has been demonstrated that transduction of a constitutively active STAT5B N642H mutant confers IL-15 independent proliferation and survival. However, further research is required to fully elucidate the impact on γδ T cell function in an *in vivo* model.

CHAPTER VI: INVESTIGATION OF A HYPOXIA-SENSING CHIMERIC ANTIGEN RECEPTOR (CAR)

6.1 Introduction

This chapter reviews the current literature on the consequences of hypoxia in tumour biology and proposes the hypothesis that tissue hypoxia in solid tumours could be harnessed in finetuning target engagement for cell-based immunotherapy.

6.1.1 Hypoxia in the tumour microenvironment

One of the major hallmarks of the solid tumour microenvironment is intratumoural hypoxia. The term hypoxia refers to a state of insufficient tissue oxygenation however, defining a threshold point is challenging because oxygen levels are generally lower even within healthy tissues, a physiological effect termed *physoxia*. In most *in vitro* experimental conditions, normoxia is defined as 21% Oxygen concentration (160 mmHg)-the oxygen saturation of inspired air- however, this is significantly higher than the physiologic oxygen levels within healthy tissues. For instance, oxygen concentration falls to 9.5% (70mmHg) in arterial blood and ranges from 3 to 7.4% (mean: 5%) within healthy peripheral tissues.[247][248] Despite significant heterogeneity within tumours, a consistent finding is that median oxygen levels within tumours are usually less than their normal tissue of origin and often below 2%. Pathological hypoxia is therefore defined as oxygen concentration below 1% (<8-10mmHg).[249][247][250] Intratumoural hypoxia is a consequence of the increased oxygen demand from highly proliferating cells and reduced oxygen supply from the dysfunctional tumour vasculature. While hypoxia is an almost universal

feature of untreated solid tumours, there is considerable heterogeneity in the degree of hypoxia between individual patients and cancer types with prostate and pancreatic tumours demonstrating more profound hypoxia. [247] Intratumoral hypoxia has been shown in several clinical studies to be associated with resistance to treatment modalities and poorer outcomes.[251–255]

Despite the recognition of the association between tumour hypoxia and resistance to radiotherapy by Gray et al in 1953[256] only recently has the crucial role of hypoxia in tumour biology been fully recognised. This was presumably due to the difficulty in measuring tissue oxygen levels in humans as only limited animal studies were possible. The development of invasive methods of measuring oxygen levels within tissues,[257] rekindled scientific interest in the role of intratumoral hypoxia in cancer as direct estimation of oxygen pressures within tumours and healthy tissues became possible. Further basic research in the last three decades has elucidated the role of the Hypoxia Inducible Factor (HIF) pathway in the cellular response to hypoxia and led to the recognition of hypoxia as a potent driver in malignancies, culminating in the award of the 2019 Nobel Prize in Physiology or Medicine to William Kaelin, Peter Ratcliffe and Gregg Semenza.[258]

6.2 Normal tissue adaptation to hypoxia and the role of HIF proteins

As tissues are often in a state of relatively low oxygen concentration, physiologic adaptative mechanisms have evolved. The chief regulatory mechanism of oxygen homeostasis is via the HIF pathway and the heterodimeric HIF proteins. The first recognition of a hypoxia-inducible factor, called Hypoxia Inducible Factor-1 (HIF-1) was by Semenza and Wang in 1992 [259] following the identification of a protein

complex which binds under hypoxic conditions to the enhancer region of the Erythropoietin (EPO) gene, resulting in transcriptional induction of EPO mRNA. Insight into the role of the HIF pathway has since evolved and it is now known that the Hypoxia Inducible Factors are heterodimeric proteins composed of α and β subunits belonging to the basic helix-loop-helix PAS family of proteins.[260] Oxygen-sensing behaviour of the HIF complex is conferred by the α-subunit and three isoforms have been identified; HIF-1α, HIF-2α and HIF-3α.[261,262] HIF-1α and HIF-2α are closely related in function but HIF-3α has been postulated to function as a negative regulator of HIF-1α.[263] HIF-1α synthesis can be stimulated by growth factors via activation of the phosphatidylinositol 3-kinase (PI3K) or mitogen-activated protein kinase (MAPK) pathways.[264] HIF-α stability is regulated by iron (Fe^{2+}), 2-oxoglutarate- and oxygen-dependent hydroxylases[265]; prolyl hydroxylase domain 1, 2 and 3 (PHD 1,2 and 3) and an asparaginyl hydroxylase also known as Factor inhibiting HIF (FIH). Under normoxic conditions, proteosomal degradation of HIF-1α is triggered following hydroxylation by the PHDs at two prolyl residues (Pro402 and Pro564) in its Oxygen Degradation Domain (ODD) via interaction with the von Hippel-Lindau (VHL) E3 ubiquitin ligase complex (summarised in figure 6-1).[266] FIH-mediated hydroxylation occurs at asparagine 803 (Asn803) in human HIF-1α and this inhibits interaction with the transcriptional coactivator p300.[267] Unlike the α subunit, HIF-1β (also known as Aryl receptor nuclear translator, ARNT) is constitutively expressed and dimerization with the α-subunit is permitted under hypoxic conditions as the hydroxylase activity is inhibited. The α/β HIF heterodimer translocates to the nucleus where it binds to hypoxia-responsive elements (HREs), DNA regulatory regions characterised by a consensus sequence 5'-RCGTG-3'[268], to

induce several target genes involved in angiogenesis, erythropoiesis, cell proliferation and metabolism such as *VEGF, EPO* and *GLUT-1*. [269–271]

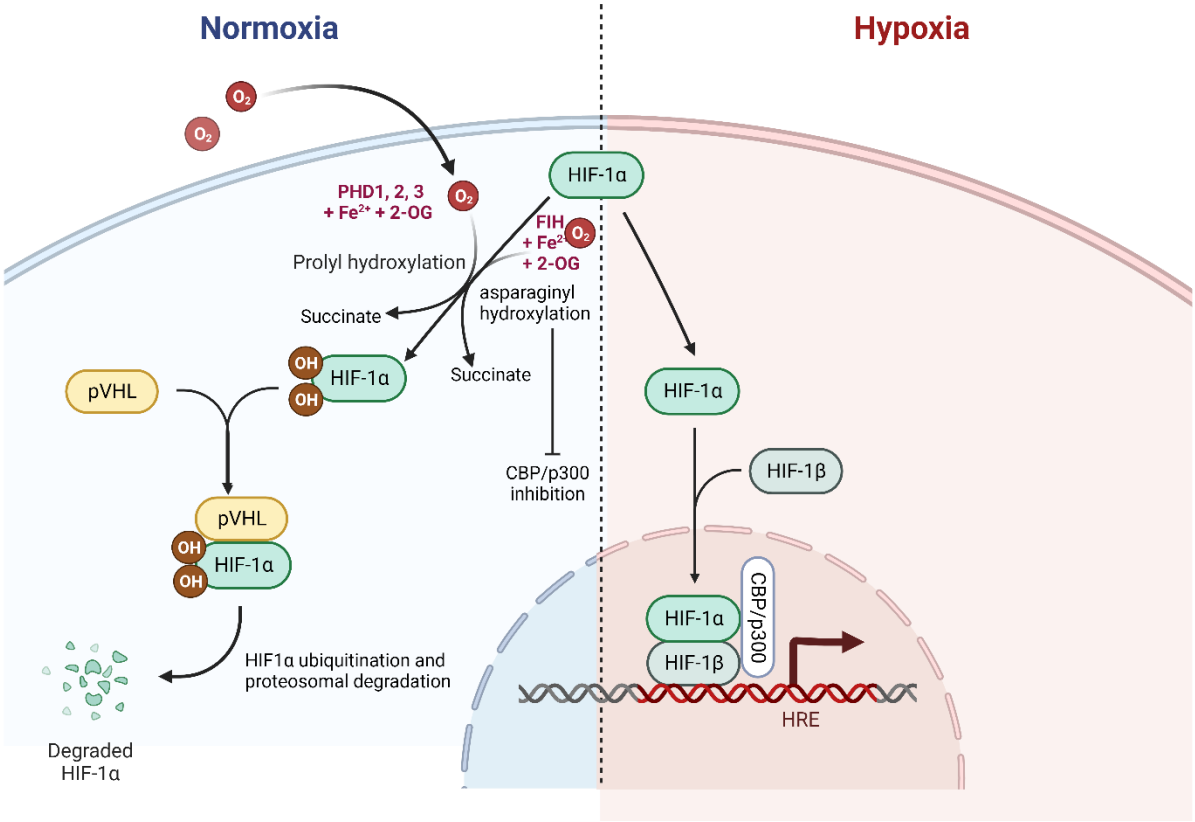

Figure 6-1: Physiological response to hypoxia via regulation of HIF-1α in human cells. The Hypoxia Inducible Factor-1α (HIF-1α) system is the chief regulator of cellular responses to hypoxia. Under normoxic conditions, HIF-1α is hydroxylated, an oxygen-sensitive reaction catalysed by prolyl and asparaginyl hydroxylases, which hydroxylate specific proline and asparagine on HIF-1α respectively. The reaction is dependent on Iron (Fe^{2+}) and 2-oxoglutarate (2-OG). The chief prolyl hydroxylases in human cells are prolyl hydrolase domain; PHD 1, 2 and 3 while the Factor inhibiting HIF (FIH) is responsible for asparaginyl hydroxylation. Hydroxylated HIF-1α associates with the Von Hippel Lindau protein (pVHL) and is degraded by the proteosome following ubiquitination. Under hypoxic conditions, hydroxylation of the HIF-1α subunit is inhibited and this permits dimerization with HIF-1β. The HIF heterodimer translocates to the nucleus where it interacts with the transcriptional coactivator, CBP/p300 to activate several target genes. HRE; Hypoxia responsive element. This figure was created with biorender.com.

6.3 Role of Hypoxia signalling in cancer

6.3.1 Effect of hypoxia on the tumour parenchyma

It has become apparent from recent understanding of the regulation of tissue responses to hypoxia in health and disease that hypoxia plays a key role in shaping the phenotypes of cancers and eventual response to therapy. It has previously been established that hypoxia is an almost universal finding in solid tumours and it is now being recognised that hypoxia also exerts a potent selective pressure on cancer cells resulting in clones with a more malignant phenotype.[272] A number of hypoxia adaptative mechanisms have been identified in cancer cells including constitutive stabilization of HIF-1α, gain of function mutations in oncogenes which upregulate HIF-1α and loss-of function mutations in tumour suppressor genes such as *VHL*. [271,273]

Overexpression of HIF-1α has been described across a wide range of solid tumours[274] and haematological malignancies such as acute myeloid leukaemia (AML)[275] and chronic lymphoid leukaemia (CLL)[276] where it is associated with poorer outcomes. The finding of increased HIF-1α expression in haematological malignancies, which are not frequently associated with hypoxia, suggests that oxygen-independent mechanisms also play important roles in the stabilization of the protein in cancer, these include post transcriptional modulation of VHL[277], activation of Protein Kinase C and upregulation of growth factors.[264,278] HIF-1α overexpression is associated with increased Programmed Death Ligand-1 (PD-L1) expression in certain cancers, indicating a cross-talk of the HIF and PD-1/PD-L1 pathways.[279,280] HIF-1α overexpression in some cancers has been linked to the upregulation of stem cell markers on cancer cells and acquisition of stemness indicating a role in tumour propagation.[281] Furthermore, cancer cell metabolism is markedly influenced by the

HIF pathway via induction of expression of key genes such as *LDHA*, *CA9* and *GLUT1*, resulting in the characteristic shift in cancer metabolism towards glycolysis and lactate production, widely known as the Warburg effect.[282–284]

6.3.2 Effect of hypoxia on the tumour microenvironment

The tumour microenvironment (TME) can be thought of as the chemical, physical and cellular milieu in which the malignant cells establish themselves and grow. This includes the non-malignant stromal cells, immune cells as well as the chemical factors and signalling molecules produced by the various cellular mediators. One of the best described HIF-mediated effects on the TME is the induction of angiogenesis via upregulation of pro-angiogenic factors such as VEGF, angiopoietin-2, Stromal derived factor 1 (SDF1)/CXCL12 and stem cell factor which induce neovascularisation within the tumour.[285] Paradoxically, tumour neovascularization is often dysfunctional and disorganised thereby resulting in hypoperfused regions, further contributing to the exacerbation of intratumoral hypoxia. HIF-regulated genes such as *CA9* and *PLOD2* have been implicated in extracellular matrix (ECM) remodelling in breast cancer, promoting tumour growth and is an independent predictor of shorter disease-free survival. [286]

Immune cell function within the TME has been of intense interest to researchers in recent years. It has been long established that cells of both the innate and adaptive immune systems can exert a range of functions in both controlling and promoting tumour progression. Hypoxia signalling plays an important role in modulating immune cell function within the TME. Neutrophils and macrophages are known to exhibit similar metabolic dependence on glycolysis as cancer cells and indeed, HIF-

1α has been shown to be essential for myeloid cell function as deletion results in impaired aggregation, motility and lactate production.[287] It has been proposed that the hypoxic TME promotes neutrophil adhesion to endothelial cells [288] and finetunes macrophage differentiation to the tumour-promoting M2-phenotype.[289] Natural Killer (NK) cell function is inhibited by downregulation of expression of MICA (an NKG2D ligand) on tumour cells.[290] Furthermore, antitumour cytotoxicity of NK cells is directly inhibited in the hypoxic TME by myeloid-derived suppressor cells recruited by HIF-mediated mechanisms.[291]

Experiments investigating cytotoxic T lymphocyte function under hypoxic conditions have shown an increase in cytotoxicity activity,[292] an effect explained by HIF-1 induced upregulation of perforin and granzymes.[293] However, despite the presence of tumour-infiltrating lymphocytes (TILs), many cancers still progress suggesting that the *in vivo* anti-cancer activity of lymphocytes is often limited. While TILs have been shown to be excluded from hypoxic regions of tumours, it is thought that the reason for this is not hypoxia *per se* but the adverse metabolic alterations that ensue, such as increased TME acidity from lactic acid production and glucose depletion by tumour cells. [294,295]It is now well established that regulatory T cells (Tregs) differentiation is promoted by HIF-mediated upregulation of Foxp3 transcription.[296,297] The immunosuppressive function of Tregs is well known and their induction within the TME promotes tumour escape from immune control. Tumour infiltrating myeloid derived suppressor cells (MDSCs) are another important component of the immunosuppressive TME. A study investigating tumour-infiltrating MDSCs in mice identified hypoxia-induced upregulation of PD-L1 mediated by direct HIF-1α binding to the HRE in the PD-L1 promoter.[298] Interaction of PD-L1 with the immune checkpoint receptor, PD-1, on activated T cells results in T cell dysfunction

and exhaustion and is a recognised mechanism for tumour escape from immune control.[299]

In summary, there is ample evidence that intratumoural hypoxia plays a significant role in promoting tumour progression by selecting tumour cells with the most malignant potential, remodelling the TME in favour of tumour progression and inhibiting antitumour immune responses. As considerable efforts are being made to identify vulnerabilities in cancer, hypoxia may provide a pivotal target for novel therapies.

6.4 Targeting hypoxia pathways in cancer

As the central role of intratumoral hypoxia in solid tumour biology has become apparent, there has been much interest in targeting key elements of the hypoxia-adaptation mechanism in cancer. Several ongoing clinical trials are investigating inhibitors of HIF proteins; EZN-2968, an oligonucleotide inhibitor of HIF-1α is being trialled for advanced solid tumours with liver metastases,[300]PT2385, a HIF-2α inhibitor is being investigated in patients with recurrent glioblastoma. Recently, a second-generation HIF-2α inhibitor, Belzutifan, was approved by the US Food and Drug Administration (FDA) for the treatment of renal carcinoma in Von Hippel-Lindau disease following objective responses in 49% of participants in the pivotal trial.[301] In addition, the anticancer effects of licenced drugs such as digoxin, a cardiac glycoside and topotecan, a topoisomerase I inhibitor are being investigated as they both inhibit HIF-1α accumulation.[286] Other strategies for hypoxia targeting include the use of prodrugs which are activated under hypoxic conditions.[302]

Exciting cell-based immunotherapy methods harnessing intratumoral hypoxia to finetune CAR expression have been recently reported. Juillerat et al engineered a novel CAR by fusing the oxygen sensitive domains of HIF-1α to the C-terminal and CAR expression was switched off under normoxic conditions and induced by hypoxia *in vitro*.[303] Kosti et al developed a dual oxygen-sensing ErbB-specific CAR by fusing a 203-amino acid ODD to the C-terminus and incorporating nine consecutive hypoxia-responsive elements in the long terminal repeat (LTR) enhancer region of the vector.[304] This strategy ensures enhancement of CAR expression in hypoxia and degradation under normoxic conditions. The CAR T cells suppressed tumour growth in a mouse model while limiting systemic toxicity.

6.5 Chapter Objectives

1. To develop a B7-H3 specific, hypoxia-inducible chimeric antigen receptor construct.
2. To test the hypothesis that incorporation of an Oxygen Degradation Domain (ODD) and Hypoxia Responsive Elements (HREs) in the B7-H3 CAR construct can confer hypoxia-responsive CAR expression in γδ T cells.

6.6 Methods

6.6.1 Cloning of the hypoxiCAR construct

A gene block plasmid encoding CD28-ODD flanked by Pfl23II and MluI restriction enzyme sites was synthesized by Thermofisher Scientific USA. The CD28-ODD plasmid and the plasmid encoding the TE9 CD28z CAR were digested with Pfl23II and MluI restriction enzymes (Thermofisher scientific, USA) following manufacturers' instructions (Figure 6-2). Restriction digestion was confirmed by gel electrophoresis on 1% agarose (Invitrogen, USA) with SYBR safe dye (Invitrogen, USA) added to visualise the DNA. Fragment sizes were estimated using a 1 kb DNA ladder (Thermofisher scientific, USA). The relevant gel segments were excised and purified using the Promega Wizard SV Gel and PCR clean-up kit (Promega Wisconsin, USA). Following purification of DNA, the 8.6 kbp fragment from the TE9 plasmid (vector) was ligated to the 1 kbp fragment from CD28-ODD (insert). Ligation of the vector and insert fragments in 3:1 molar ratios was done using the NEB Quick ligase kit (NEB Biolabs, USA). This was followed by bacterial transformation of competent *E.coli* (NEB biolabs, USA) with the ligation product using the heat-shock method previously described in the Materials and Methods Chapter. Transformed bacteria were inoculated on agar plates and following overnight incubation at 37^{o}C, single colonies were selected and incubated for 12 hours in LB broth (Thermofisher scientific, USA). Plasmid DNA purification was done using the NucleoSpin DNA purification kit mini-prep kit (Macherey-Nagel, Germany). Selection of clones encoding the correct ligated plasmid DNA was done following a screening restriction digest with MluI and Pfl23II enzymes (Thermofisher scientific, USA). This was subsequently confirmed by Sanger sequencing (Source Bioscience, Cambridge, UK). Following confirmation of the correct DNA sequence, the next step was removal

of one of the two XhoI restriction site at position 2474 by site-generated mutagenesis using the Q5 site-directed mutagenesis kit (NEB Biolabs, USA) and the following mutagenic primers (Integrated DNA Technologies, USA):

5’ ggcctagagcaggtgCAACTGCAGCAGTCAGGGG 3’ (forward)

5’ ggtgctgcctggcacCCACAGCAGCAGCACCCA 3’ (reverse)

Finally, a plasmid DNA based on the SFG retroviral vector backbone and encoding the Hypoxia-Responsive Element (HRE) enhancer, named P23 vector, was obtained from James Arnold (King’s College, London) and digested with NcoI and XhoI restriction enzymes (Thermofisher scientific, USA). The TE9-CD28z-ODD was also digested with NcoI and XhoI to obtain a 2kb DNA fragment encoding the TE9-CD3z-ODD. This was ligated to the P23 vector using the NEB Quick ligase kit (NEB Biolabs, USA) following manufacturer’s protocol. The final cloned DNA sequence was confirmed by Sanger Sequencing (Source Bioscience, Cambridge, UK) (illustrated in Figure 6-3).

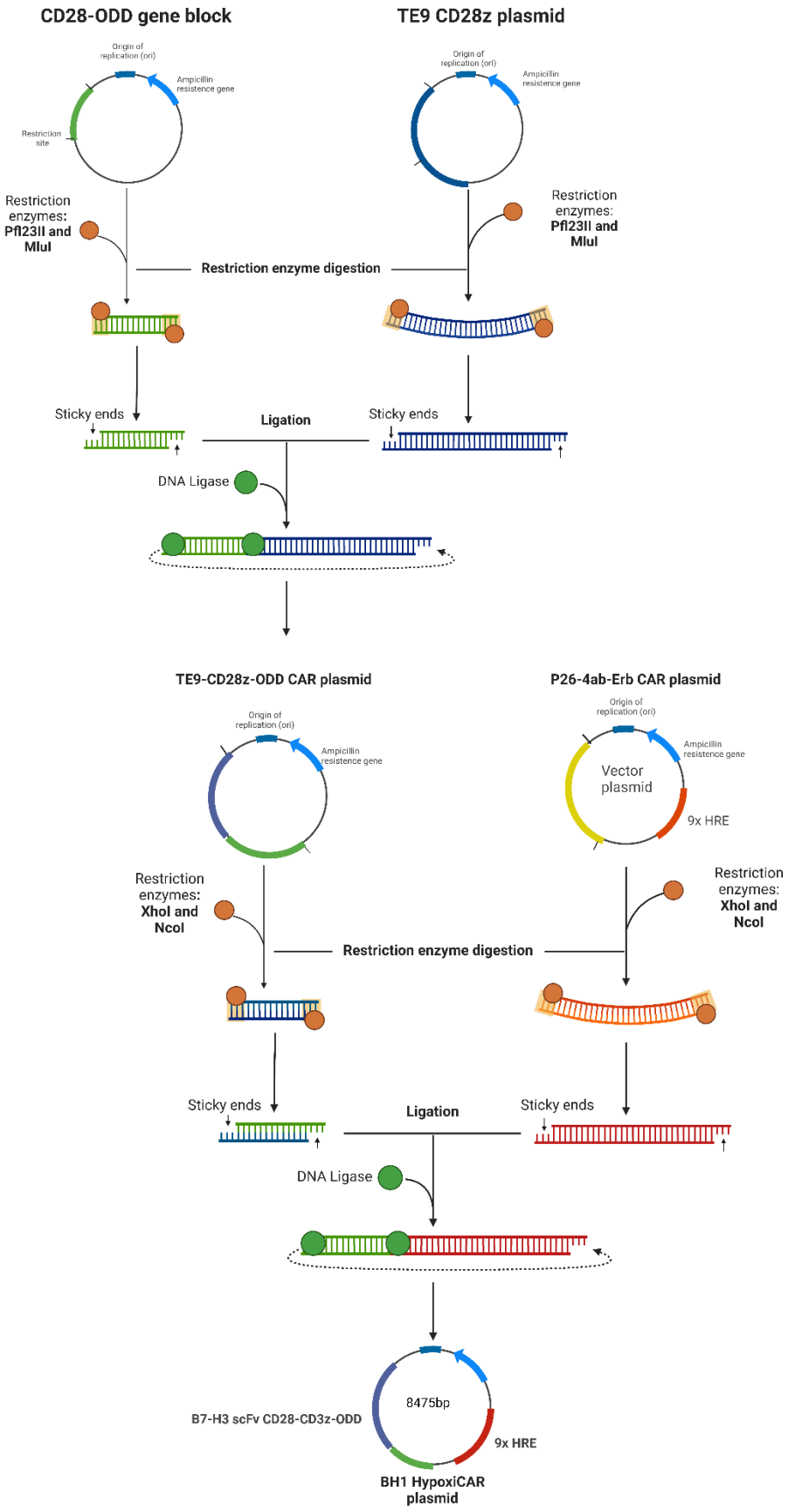

Figure 6-2: **B7-H3 HypoxiCAR (BH1) cloning strategy.**

6.6.2 Gamma-retrovirus production

A TE9 CD28z-ODD CAR specific for human B7-H3 was cloned into the SFG gamma retrovirus vector encoding a HIF1α promoter as described above. The resulting hypoxia-sensing construct was named BH1 CAR. Retroviral particles were produced by triple transfection using gag-pol, env (RD114) and BH1 CAR plasmids in HEK293T cell line. Virus supernatants were harvested at 48 and 72 hours and both supernatants were combined and either used directly for transduction of Vdelta1 enriched gamma-delta T cells or snap-frozen for future use.

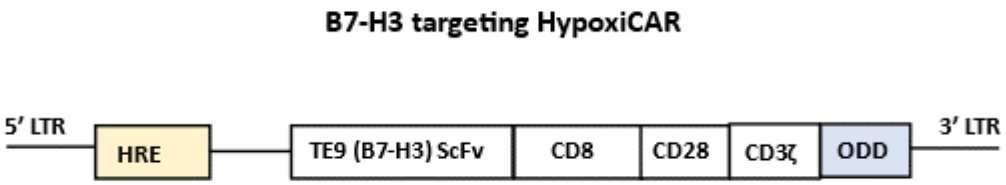

Figure 6-3: B7-H3 HypoxiCAR (BH1) construct. A schematic illustration of the B7-H3 specific hypoxiCAR. HRE; Hypoxia-responsive element, TM; transmembrane domain, ODD; Oxygen degradation domain

6.6.3 Transduction of PBMCs and Jurkat cell line

Peripheral Blood Mononuclear Cells (PBMCs) and Jurkat cells were counted and $5x10^5$ cells in 500 µl of complete media per well were plated on 24 well cell culture plates (Corning, New York, USA) coated with 10 µg/ml RetroNectin (Takara Bio, Japan). Thawed or freshly prepared retrovirus supernatants were added at 1.5 ml per well. Non-transduced conditions were also set up with complete media used instead of virus supernatant. The plates were centrifuged at 1000 x *g* for 40 mins in a 5920R centrifuge (Eppendorf; Hamburg, Germany) at room temperature. Each transduction was done in triplicate and each identical culture plate was incubated in a separate incubator. The plates were incubated at 37^{o}C and 5% CO_2 in three separate CellXpert C170i incubators (Eppendorf, Germany) with Oxygen saturations set at 21%, 5% and 1% (Figure 6-4). Transduction efficiency was assessed by flow cytometry following incubation for at least 48 hours.

6.6.4 Flow Cytometry for CAR expression

Following incubation, cells were resuspended, washed twice with Phosphate-buffered saline (PBS) (Sigma, USA) to remove residual supernatant and resuspended with Cell staining buffer (Biolegend, USA). The presence of the CAR was determined by binding of a his-tagged recombinant B7H3 protein (Biotechne, USA) detected by a PE-conjugated secondary antibody against the his-tag (Biolegend, USA). The Near-Infra Red viability dye (Thermofisher, USA) was used to exclude dead cells. Figure 6-6 shows the gating strategy for determining the CAR+ population.

6.6.5 Hypoxia-induction experiment

Following initial transduction under the respective Oxygen concentrations, both transduced and untransduced cells were harvested, washed twice and resuspended in complete media and subsequently incubated under new oxygen concentrations for at least 48 hours (Figure 6-5). CAR expression was subsequently determined by flow cytometry as described above.

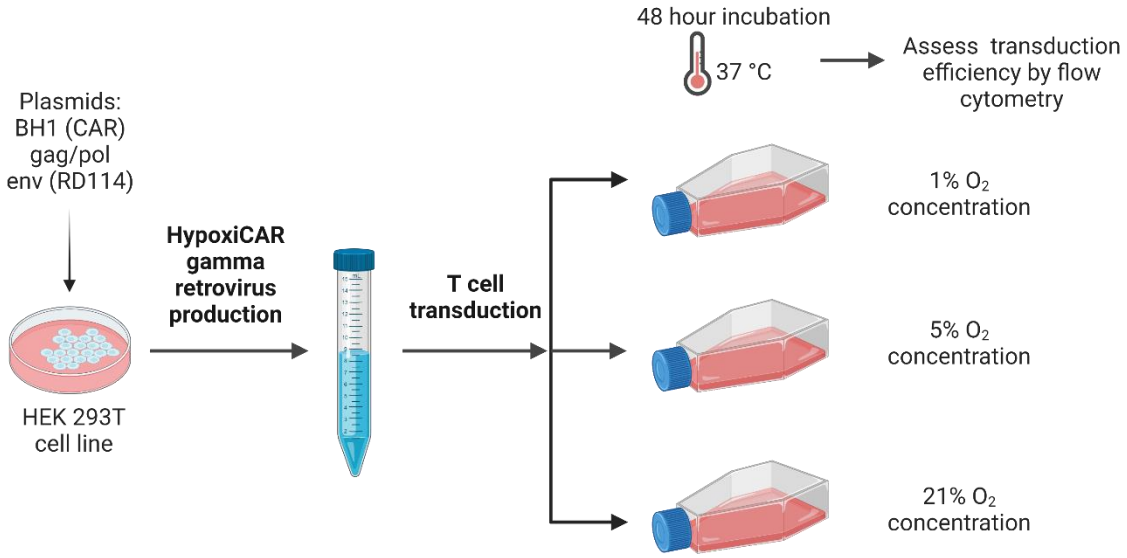

Figure 6-4: HypoxiCAR production and transduction. Gamma retroviral vector expressing the B7-H3 specific hypoxiCAR were produced by triple transfection of HEK 293T cells with plasmids BH1 (encoding the B7-H3 specific hypoxiCAR), gag/pol and RD114 envelope. Virus supernatants were harvested at 48 and 72 hours post-transfection. Interleukin-15 stimulated PBMCs and Jurkat cells were transduced in triplicate with the pooled retrovirus supernatants and incubated for at least 48 hours at Oxygen concentrations of 21%, 5% and 1%. CAR expression was assessed by flow cytometry. This figure was created with biorender.com.

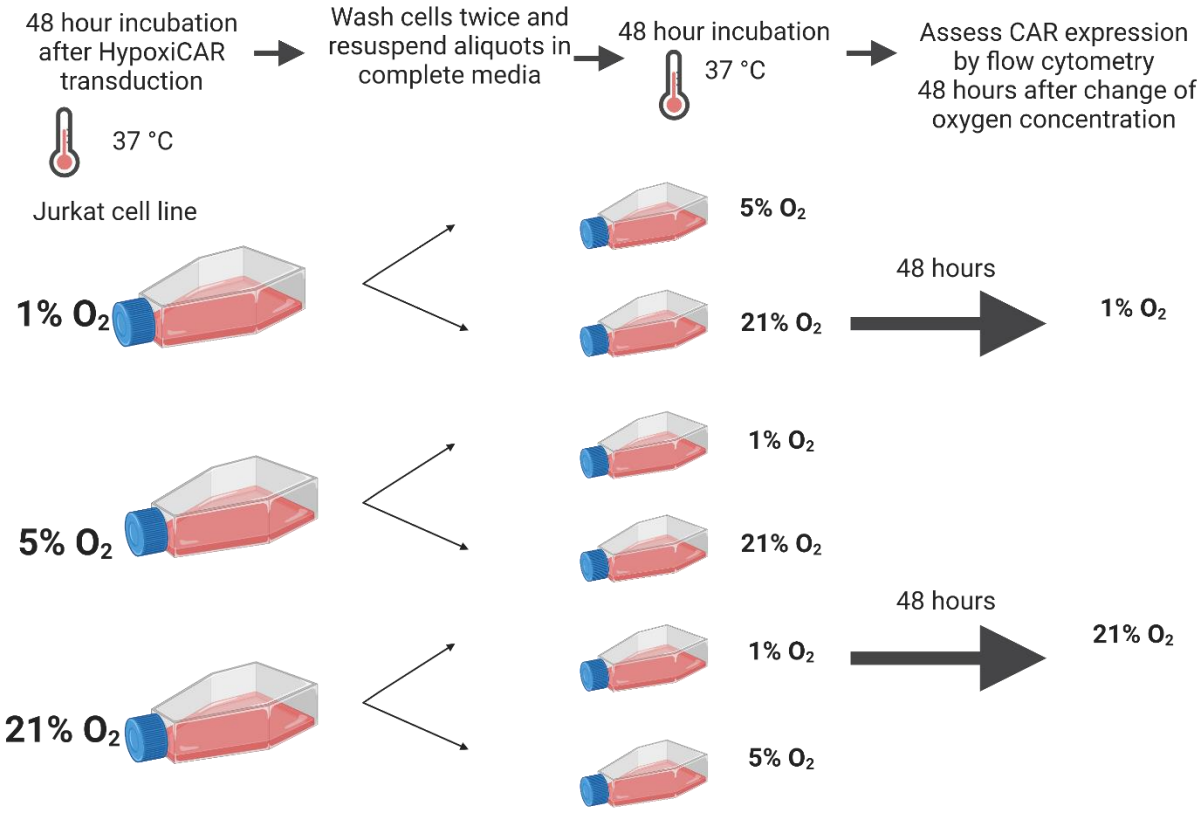

Figure 6-5: Hypoxia induction experiment. Jurkat cells were transduced in triplicate with the retroviral vector expressing the B7-H3 specific hypoxiCAR. Each replicate was maintained in 1%, 5% or 21% oxygen conditions for 48 hours. The cells were subsequently washed and resuspended in complete media and divided into two aliquots each incubated for 48 hours at different Oxygen concentrations. CAR expression was assessed by flow cytometry after 48 hours of incubation. The cells were subsequently returned to the original oxygen concentration at transduction and reassessed for changes in CAR expression. This figure was created with biorender.com.

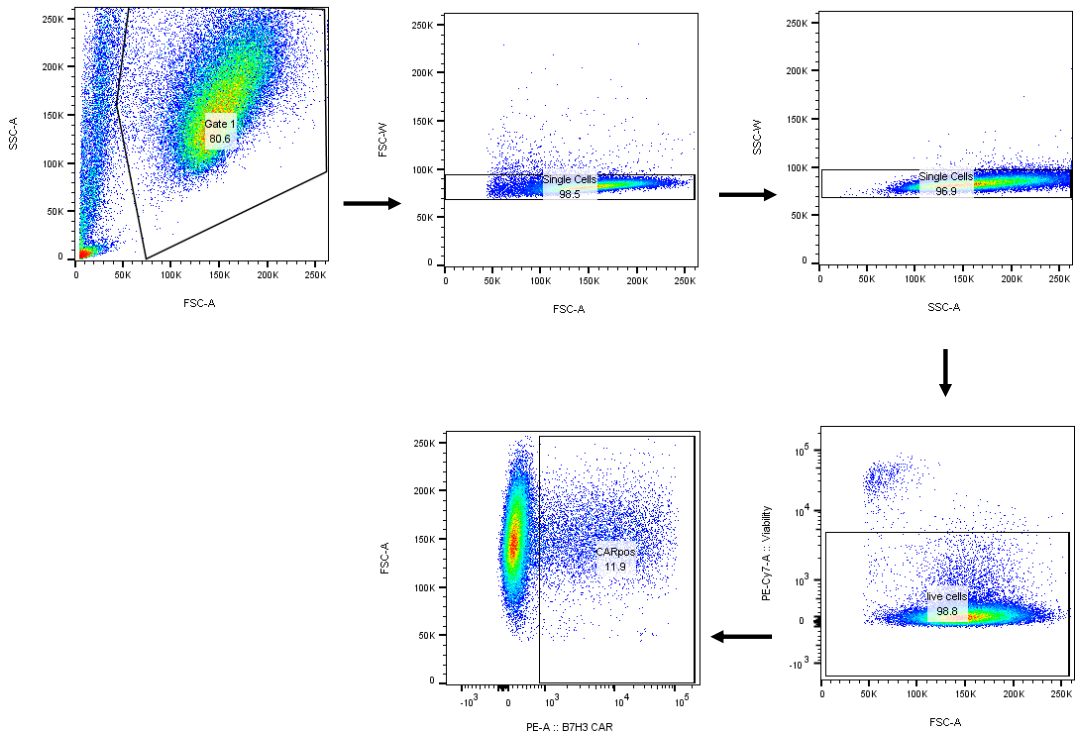

Figure 6-6: Typical gating strategy for HypoxiCAR transduction efficiency assessment by flow cytometry. Jurkat cells were used in this example. Gate 1 was created to exclude cellular debris and this was followed by doublet exclusion using forward and side scatter characteristics. Dead cells were excluded by the Near-Infrared viability dye and CAR positive events were gated using Fluorescence Minus One (FMO) controls.

6.7 RESULTS

6.7.1 CAR expression on PBMCs

Four donor PBMCs were expanded with IL-15 for 14 days. Figure 6-7 shows the respective T cell subsets at the time of hypoxiCAR transduction. In the four donor PBMCs transduced (figure 6-8), a significant increase in CAR expression was observed in the samples transduced and maintained in 1% Oxygen concentration. A slight increase in CAR expression was observed for the 5% Oxygen condition but this difference was not statistically significant when compared with the 21% Oxygen condition. CAR expression at normoxia (21% O_2) was negligible. Comparison of cell viability under the respective oxygen conditions showed a trend towards lower cell viability at 1% O_2 however, this difference was not statistically significant.

6.7.2 CAR expression on Jurkat cells

Jurkat cells were similarly transduced with the B7-H3 HypoxiCAR and the TE9 CD28z CAR (control) and the cells were maintained at Oxygen concentrations of 1%, 5% and 21%. A similar increase in CAR expression at 1% Oxygen was observed for the Jurkat cell line as for PBMCs although transduction efficiency was generally higher in PBMCs. No oxygen-dependent change in CAR expression was observed for the cells transduced with the non-hypoxia sensing TE9 CD28z control CAR (figure 6-9).

6.7.3 Hypoxia-inducible CAR expression on Jurkat cells

A significant upregulation of CAR expression was observed when HypoxiCAR-transduced Jurkat cells were transferred from normoxic conditions to 1% Oxygen concentration. Furthermore, when the cells were subsequently moved from 1% to

21% Oxygen, CAR expression diminished significantly, confirming the dual hypoxia-sensing mechanism of the HypoxiCAR (Figure 6-10).

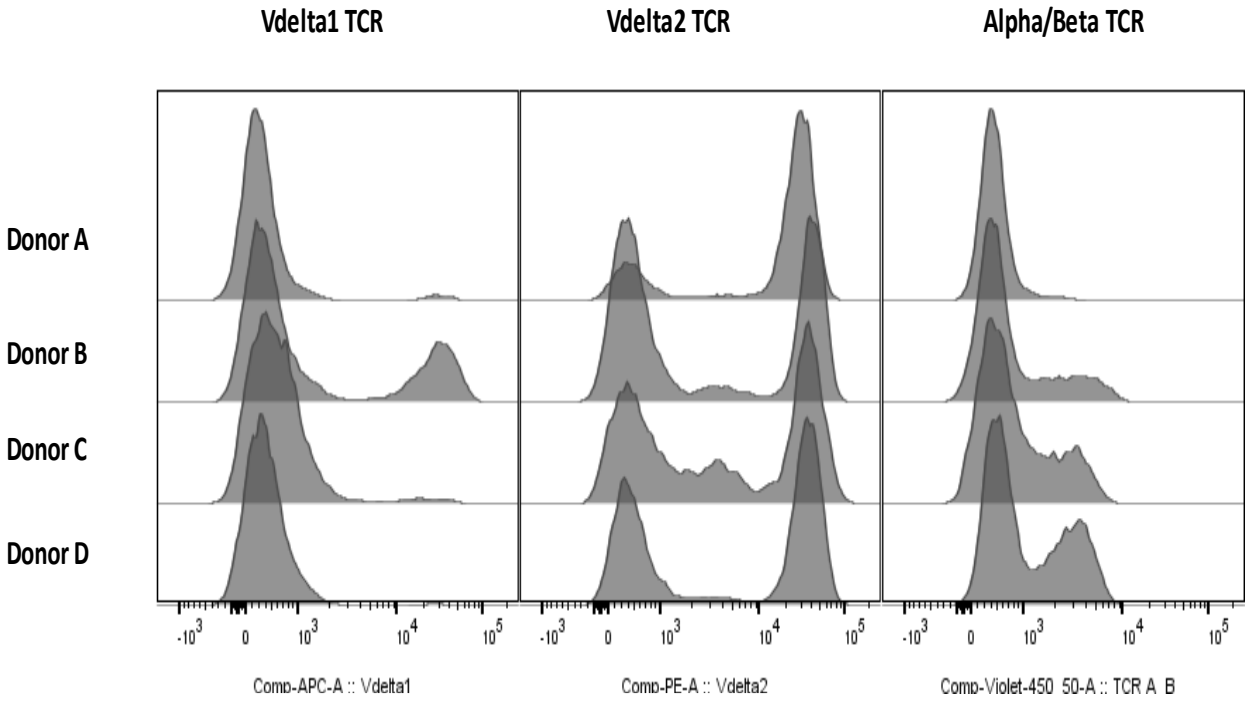

Figure 6-7: Flow cytometry histogram plots showing PBMC composition on Day 10 of expansion. Following depletion of Alpha/Beta TCR+ and CD56+ cells from peripheral blood of healthy donors, cells were stimulated with anti-CD3 (OKT3 clone) and IL-15 for 10 days prior to transduction with the hypoxiCAR retrovirus. Events were gated on CD3+ live cells

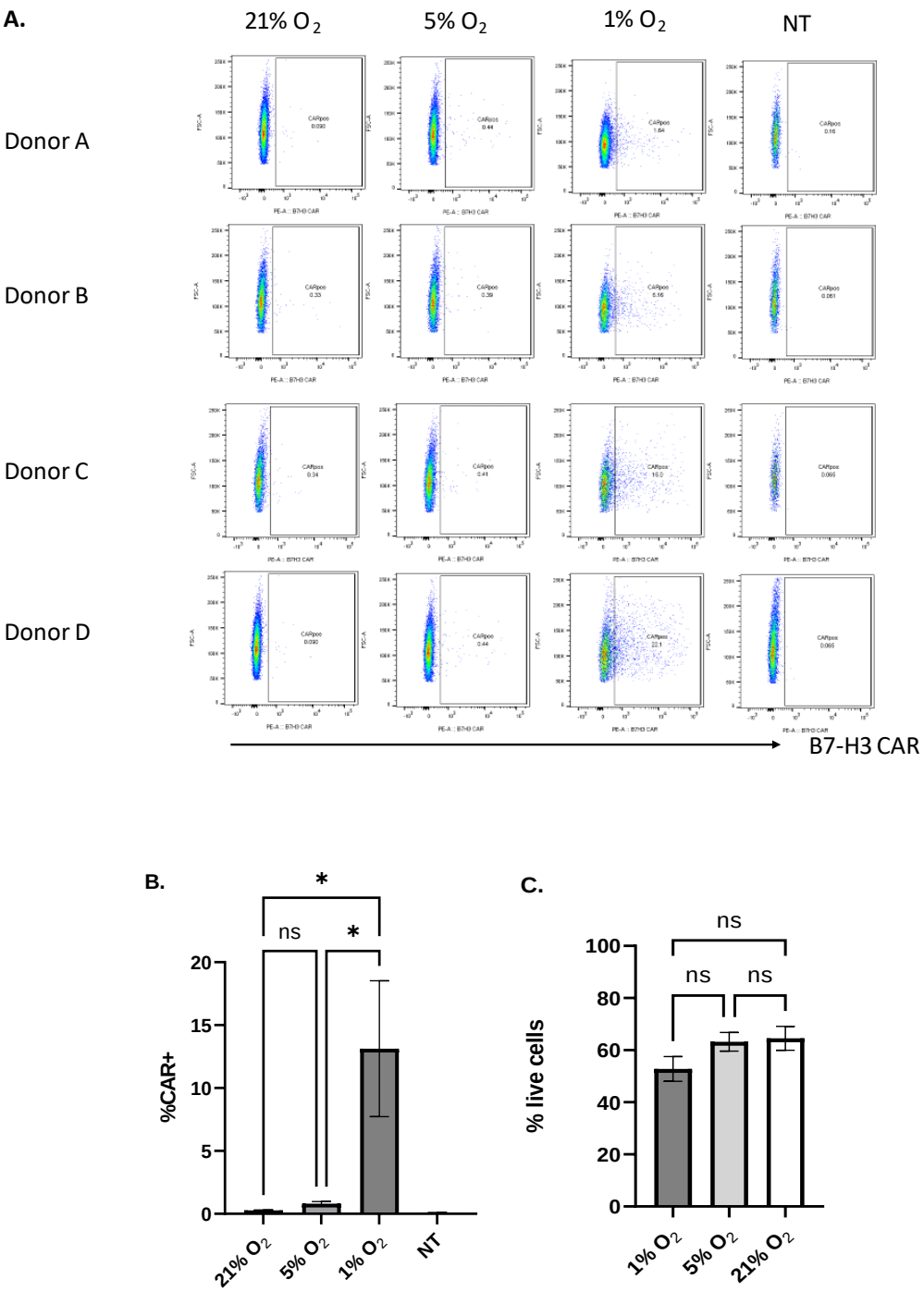

Figure 6-8: HypoxiCAR transduction efficiency at 72 hours. A. Flow cytometry plots showing transduction efficiencies. PBMCs (n=4) were acquired 72 hours following retroviral transduction and incubation in 21%, 5% and 1% Oxygen concentrations. Transduction efficiency was determined by the proportion of live cells positive for the B7-H3 specific CAR. PBMCs were stimulated with interleukin-15 for 5 days prior to viral transduction and maintained in IL-15 containing media. Events shown were gated on live cells. **B.** Graphical representation of CAR+ proportions following transduction under the respective Oxygen conditions (n=4, error bars indicate standard error of means, One way ANOVA statistical test with inter-group comparisons, *p < 0.05). **C.** Comparison of cell viability under the respective oxygen conditions. (n=4, error bars indicate standard error of means, One way ANOVA statistical test with inter-group comparisons, ns=not significant).

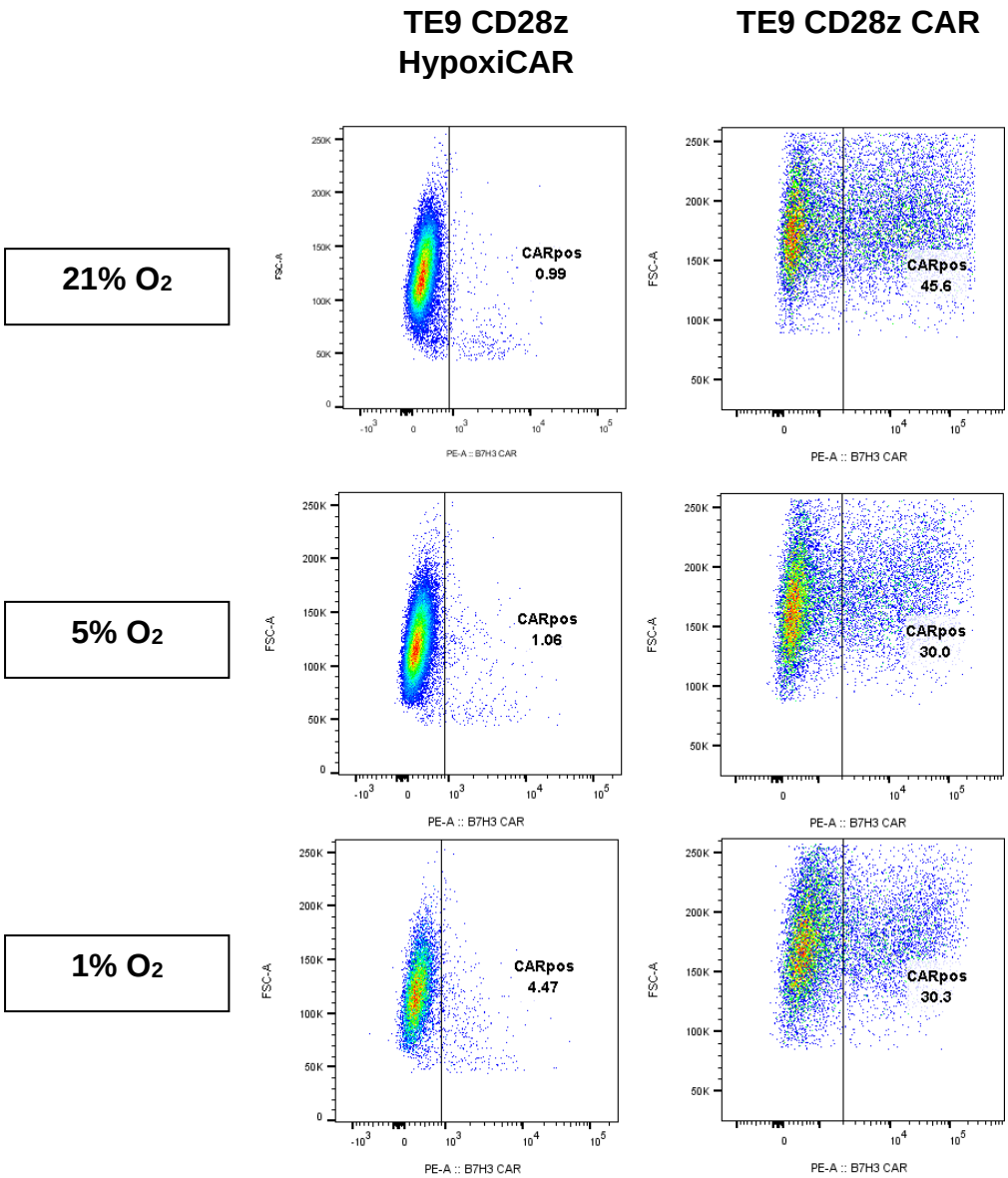

Figure 6-9: Flow cytometry plots showing CAR expression for HypoxiCAR compared with TE9 CD28z control CAR under normoxia and hypoxic conditions. Jurkat cells were transduced with retrovirus supernatants and assessed after 48 hours. Events were gated on live cells and numbers indicate percentage of CAR positive cells.

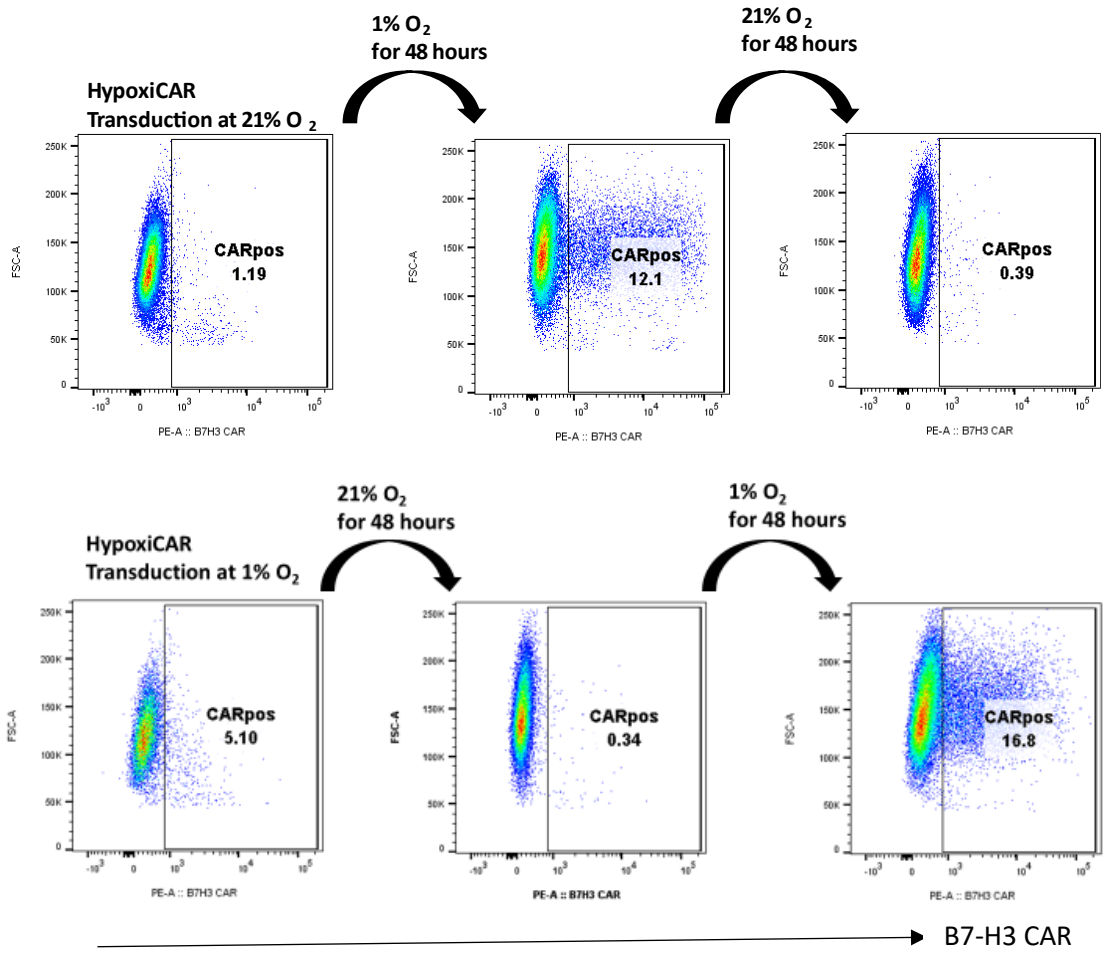

Figure 6-10: Hypoxia-inducible CAR expression. Dot plots showing upregulation of CAR expression under hypoxic conditions. Jurkat cells transduced with the BH1 hypoxiCAR under normoxic conditions were subsequently incubated in 1% Oxygen and vice versa. CAR expression was determined 48 hours after change of Oxygen conditions. Events were gated on live cells and numbers indicate percentage of CAR positive cells. Insert: Graphical representation of CAR+ proportions. Error bars indicate standard error of means.

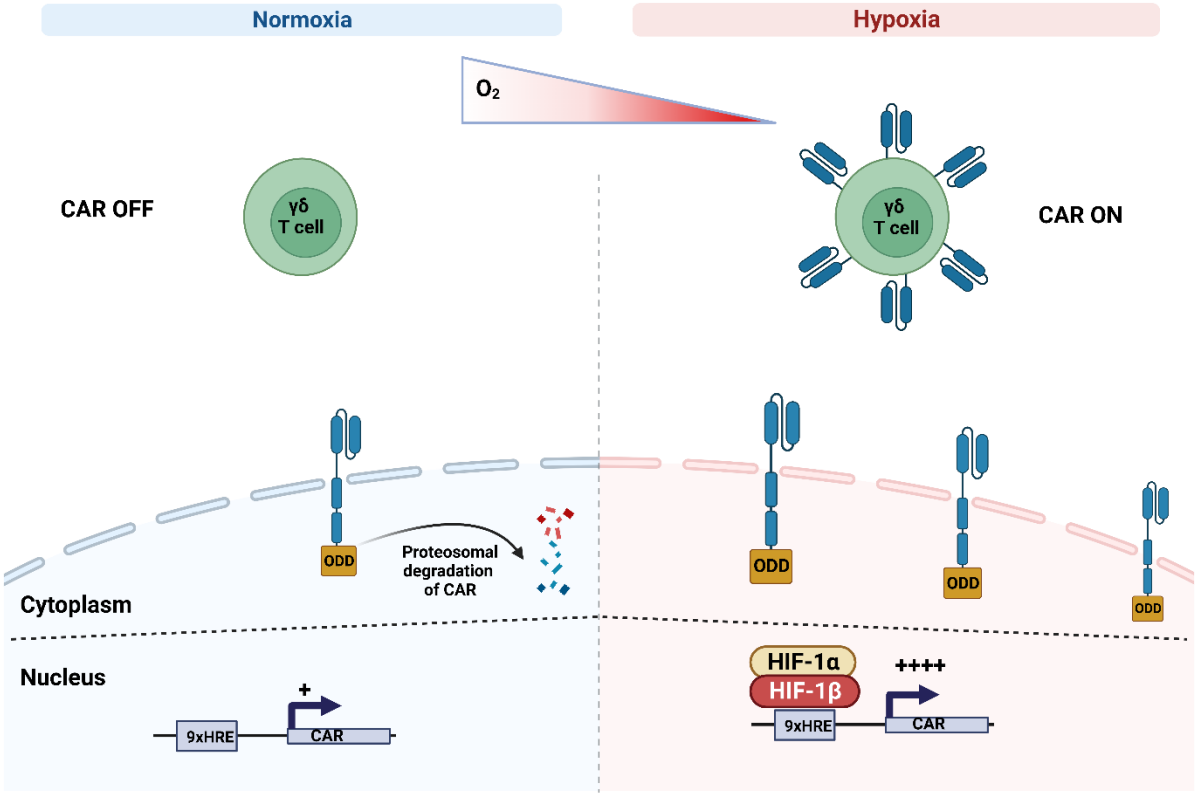

Figure 6-11: Dual Oxygen sensing mechanism of the hypoxiCAR. Under normoxic conditions, the oxygen degradation domain (ODD) marks the CAR for proteosomal degradation thereby switching off CAR expression. In hypoxia, the physiologically active HIF heterodimer enhances CAR expression by binding to the hypoxia responsive elements (HRE). This figure was created with biorender.com.

6.8 Discussion

Intratumoral hypoxia provides a barrier to immune control of solid cancers while exerting a potent selection pressure for malignant cells with the most invasive potential. Furthermore, hypoxia has been shown to promote malignant cell differentiation into a stem cell phenotype which is responsible for cancer propagation. Therefore, targeting the malignant cells in the hypoxic regions of the tumour would be a promising therapeutic strategy. To effectively target malignant cells for elimination, immune cells equipped with a chimeric antigen receptor specific for antigens expressed on the cancer cells have been successfully developed for haematological malignancies. Little success has been recorded so far for non-haematological malignancies due to the unique challenges of the solid tumour microenvironment including intratumoral hypoxia.

This project has demonstrated proof-of-principle for a dual oxygen-sensitive CAR specific for B7-H3. The CAR construct mimics the physiological HIF-mediated regulation of hypoxic responses by the incorporation of repetitive HRE sequences within the enhancer region of the vector resulting in marked upregulation of CAR expression under hypoxic conditions. Under normoxia, the HIF complex is unavailable to bind to the HREs while basal expression of the CAR is followed by degradation, effectively silencing the CAR (Figure 6-11). This hypoxia-sensitive CAR system ensures expression within the hypoxic TME while oxygen-induced degradation avoids on-target off tumour toxicity in healthy, normoxic tissues. In this work, gamma delta (γδ) T cells were the immune cells bearing the CAR. This offers a number of advantages: γδ T cells (as opposed to conventional αβ T cells) are activated via both their innate receptors and the γδ T cell receptor, some subsets of γδ T cells eg Vδ1 T cells are naturally tissue-resident and may be beneficial by

permitting sufficient intratumoral infiltration based on the tissue tropism of these cells.

In this study, the stringent dual oxygen sensing mechanism of the B7-H3 HypoxiCAR was confirmed by transducing Jurkat cells. The cells transduced and maintained in 1% oxygen had the highest level of CAR expression while in the cells maintained under normoxic conditions, CAR expression was negligible. To confirm that the negligible CAR expression on normoxic Jurkat cells was due to CAR degradation, rather than failure of CAR transduction, the cells were washed and transferred to hypoxic conditions and reassessed after 48 hours and a significant upregulation of CAR expression was observed (figure 6-10). The opposite effect was observed for the cells initially transduced under hypoxic conditions and subsequently exposed to normoxia. This provides proof of principle for the reversibility of CAR expression as the cells move from normoxia into the hypoxic TME and vice versa. Furthermore, since the CAR is degraded under normoxic conditions, this could be beneficial in avoiding tonic signalling and minimising T cell exhaustion during CAR T cell manufacture as the CAR is effectively silenced until the cells encounter the hypoxic TME.

A limitation of the dual-oxygen sensing CAR system is that tumour control in the non-hypoxic fraction of the tumour might be limited as CAR expression will be suppressed. However, CAR expression is significantly reduced but not completely absent in hypoxia and it is possible that the low-level expression in normoxia may be sufficient to engage residual antigen-expressing cancer cells. Furthermore, engagement of the γδ TCR and innate receptors on γδ T cells may be sufficient for tumour control in the normoxic areas. Alternative strategies include removal of the ODD from the CAR construct where target antigen expression in healthy tissues is

low enough to avoid significant off-tumour toxicity. Ultimately, the ideal test of HypoxiCAR induction in the hypoxic TME will be in an *in vivo* model therefore, further pre-clinical testing is required to address these questions.

In summary, this work has tested the principle that a B7-H3 targeting, dual oxygen sensing CAR could be harnessed in fine-tuning expression under hypoxic conditions in γδ T cells. Further *in vivo* work would be required to confirm tumour control in the hypoxic TME in a B7-H3-positive cancer model.

CHAPTER VII: CONCLUSION AND CLINICAL CORRELATES

7.1 Future perspectives

As the immense potential for γδ adoptive T cell therapy is being recognised, it is anticipated that there will be a dramatic increase in the clinical use of γδ T cell therapy products for a range of benign and malignant indications in the coming years.

The initial hurdle to clinical translation of γδ T cells has been the difficulty with clinical isolation and expansion of these cells. Being a rare cell population, highly efficient, Good Manufacturing Practice (GMP) grade expansion methods are required. Unlike previously published methods which require a cocktail of cytokines or mitogens, this research project has shown that the rare Vδ1 γδ T cell subset can be expanded from peripheral blood of healthy donors in a scalable and GMP-compliant manner using an antibody against CD3 and a single cytokine, IL-15. Another advantage of this method besides its simplicity, is the fact that the Vδ1 T cells were isolated "untouched", without direct engagement of the Vδ1 TCR thereby ensuring preservation of function. The expanded Vδ1 T cells were shown to be highly potent immune effector cells against cancer cell lines *in vitro*. It is anticipated that further preclinical and clinical translation will follow. While much emphasis has been placed on CAR development, it is expected that unmanipulated γδ T cells can be used as adoptive cell therapy given the potent antitumour properties conferred by the innate receptors in addition to the γδ TCR. The primarily non-MHC restricted mode of action makes γδ T cells attractive candidates for "off-the-shelf" use. In this scenario, donor γδ T cells are harvested from healthy donors, expanded and cryopreserved until required. This strategy not only minimizes the time to treatment commencement

(compared with engineering the patient's own cells) but also reduces overall cost as cells from a donor could be used for the treatment of multiple patients. Furthermore, the cell quality can be standardised using this approach. In contrast, the current method of autologous CAR T cell engineering is dependent on T cells from the patient which may be dysfunctional due to the immunosuppressive effects of the malignancy or as a consequence of previous lymphotoxic treatments. While no allogeneic γδ CAR T cell trials have been published for solid tumours, a conference abstract published recently showed safety and encouraging signals of efficacy for allogeneic anti-CD20 γδ CAR T cell against CD20 expressing B cell malignancies.[305] Furthermore, proof of feasibility of the off-the-shelf approach was demonstrated, albeit with another immune effector, by anti-CD19 Natural Killer (NK) CAR cells in HLA-mismatched patients with relapsed/refractory B-cell malignancies.[126]

While this study has shown that a higher baseline proportion of Vδ1 T cells (relative to Vδ2) is associated with proportionate Vδ1 expansions, future clinical γδ T cell research priorities should focus on identifying further biomarkers that predict which donor γδ T cells are likely to be excellent Vδ1 expanders. Once identified, a small donor pool of excellent γδ T cell expanders could be maintained for donation of PBMCs for the large-scale manufacture of γδ T cell products.

It is apparent that fundamental biological differences exist between Vδ1 and Vδ2 γδ T cells besides the structure of the TCR. For instance, this project has shown differences in surface expression of key markers such as PD-1 and CD56 between the two γδ T cell subsets. Recently, an extensive phenotypic and transcriptomic characterisation of human Vδ1 and Vδ2 T cells similarly showed significant differences between the two subsets.[306] The consequences of these differences are

not certain and therefore warrant further investigation. In addition, while much is now known about the mechanism of recognition of phosphoantigens by Vγ9δ2 TCR, knowledge of the natural ligands of the Vδ1 TCR remains limited. Identification of Vδ1 TCR ligands could potentially enable novel expansion methods for these cells. It is also not known if Vδ1 T cells in the peripheral blood differ from tissue-resident Vδ1 T cells therefore, further research addressing these fundamental questions in Vδ1 T cell biology would be beneficial in optimising future clinical applications.

Furthermore, this research has evaluated the *in vitro* efficacy of a novel B7-H3 scFv binder, TE9, in a 2nd generation CD28z CAR configuration. For the first time, Vδ1 T cells were successfully transduced to express the B7-H3 specific CAR with subsequent demonstration of enhanced activity against antigen-positive cancer cell lines. B7-H3 is an attractive solid tumour target for a number of compelling reasons. First, as an immune checkpoint molecule, its overexpression in cancers is immunoinhibitory and hence tumours overexpressing B7-H3 are more aggressive and confer a poorer prognosis. Therefore, targeting the antigen would potentially improve outcomes by switching off the inhibitory signal and by recruiting other immune cells towards the tumour microenvironment. Furthermore, B7-H3 is only minimally expressed in healthy tissues and in this project, it was shown that healthy PBMCs do not express B7-H3 at baseline or after stimulation with IL-15. Therefore, the risk of on-target, off tumour toxicity is not expected to be considerable. As reviewed in Chapter I, a monoclonal antibody against B7-H3 has been tested in early clinical trials and shown to be safe. As B7-H3 is overexpressed across a wide range of solid tumours, B7-H3 targeting γδ.CAR T cells can be adapted for the treatment of several malignancies ranging from prostate cancer to childhood tumours such as neuroblastoma. Coupled with the potential for off-the shelf use, B7-H3 targeting

γδ.CAR T cells will prove to be highly cost-effective as a single donor's cells could be used to treat multiple patients with different tumour types. Further experimental studies could investigate the function of the B7-H3 CAR in 3rd generation and T cells redirected for universal cytokine-mediated killing (TRUCK) formats, the latter could provide transgenic IL-15 for the maintenance of cell viability and enhancement of cytolytic functions. However, a possible complication of the TRUCK CAR is uncontrolled lymphoproliferation which could be mitigated by incorporation of an inducible suicide gene.

While γδ T cells expanded with IL-15 demonstrated potent antitumor properties, it was noted that they become dependent on IL-15 for survival. To overcome this cytokine dependence, the strategy of manipulation of the JAK/STAT pathway downstream of the IL-15 receptor was explored via transduction of a constitutively active *STAT5B* mutation. This resulted in maintenance of IL-15 independent γδ T cell survival and proliferation via potentiation of pSTAT5. Further work, including evaluation of this strategy in an *in vivo* model would be necessary. Since *STAT5B* N642H is a driver mutation in certain haematological malignancies, stringent *in vivo* testing would be required to ensure that cell proliferation can be terminated, when required, by activation of the RQR8 suicide gene. Alternative strategies to overcome IL-15 dependence should also be investigated. These strategies include the incorporation of a transgene encoding IL-15 to maintain cell viability and survival, membrane-tethered IL-15 to provide local cytokine stimulation without significant systemic effects and transduction of a constitutively active IL-15 receptor.

Following the proof-of-concept demonstration of hypoxia-inducible CAR expression, *in vivo* testing in a murine solid tumour model would confirm the enhanced efficacy within the hypoxic tumour microenvironment and the avoidance of on-target, off-

tumour toxicities. The addition of a cytokine transgene in the hypoxiCAR construct just distal to the ODD would induce cytokine secretion to facilitate the non-CAR mediated cytotoxic function of the γδ T cells even when the CAR is switched off under normoxic conditions. Furthermore, for targets where on-target, off tumour toxicity is unlikely, the ODD may be deleted from the CAR construct. In this scenario, CAR expression will still be upregulated in hypoxia due to the influence of the HRE while maintaining basal CAR expression in normoxic healthy tissues. Eventual translation of the HypoxiCAR to the clinic would offer significant benefits to patients with locally advanced solid cancers where other modalities such as radiotherapy and chemotherapy are ineffective due to the influence of intratumoural hypoxia.

7.2 Conclusion

Gamma delta (γδ) T cells are a unique group of immune effector cells with the ability to rapidly respond to a range of pathogens and cellular stresses while maintaining adaptive immune features of T cell receptor specificity and immunological memory. In health, γδ T cell subsets bearing the Vδ1 TCR are enriched within peripheral tissues where they perform key roles in tumour immune surveillance. Therefore, these highly potent Vδ1 T cells are attractive candidates for adoptive cell therapy against solid cancers.

The tumour specificity conferred by a chimeric antigen receptor (CAR) further enhances the efficacy of immune cells and for the first time, it was shown that Vδ1 T cells expanded with anti-CD3 (OKT3) and Interleukin-15 can be transduced with a B7-H3 specific CAR. The enhanced antitumour efficacy demonstrated *in vitro* raises significant interest for clinical translation as B7-H3 is overexpressed across a wide range of solid tumours.

To overcome the hurdles against CAR T cell efficacy in the solid tumour microenvironment, further strategies were explored including a dual-hypoxia sensing CAR receptor which is switched on within the hypoxic tumour microenvironment and switched off in normoxic conditions thereby minimizing the risks of on-target off tumour toxicity and tonic CAR signalling. Furthermore, a constitutively active STAT5B construct was developed and transduced to γδ T cells to confer enhanced cytokine-independent proliferation and persistence.

Indeed, harnessing the potent anti-cancer properties of γδ T cells will provide a new, powerful therapeutic tool against a wide range of cancers and it is anticipated that clinical translation of the strategies evaluated in this project will result in significantly improved patient outcomes.

APPENDIX

Cell lines

Cell line	Description	Culture medium	Source
Jurkat Wild type	Human Acute T-lymphocytic leukaemia	RPMI + 10% FCS	Anderson Lab
Jurkat B7H3+	Human Acute T-lymphocytic leukaemia transduced to overexpress B7-H3	RPMI + 10% FCS	Anderson Lab
Jurkat B7H3+ GFP+	Human Acute T-lymphocytic leukaemia transduced to overexpress B7-H3 and GFP	RPMI + 10% FCS	Donovan Lab
LAN1	Human neuroblastoma	DMEM +10% FCS	Anderson Lab
U87	Human glioblastoma	DMEM +10% FCS	Anderson Lab
HEK 293T	Human Embryonic Kidney	DMEM +10% FCS (no antibiotics)	Anderson Lab
SiHa	Human cervical cancer	DMEM +10% FCS	Chester Lab
HeLa	Human cervical cancer	DMEM +10% FCS	Chester Lab
Caski	Human cervical cancer	DMEM +10% FCS	Chester Lab
3T3	Mouse fibroblast	DMEM +10% FCS	Chester Lab

Table A1. List of cell lines with the respective culture media and sources

Flow cytometry and MACS antibodies

Antigen	Fluorophore or conjugate	Clone	Manufacturer	Catalogue number
CD3	FITC	UCHT1	Biolegend	300405
CD3	PE/Dazzle 594	UCHT1	Biolegend	300450
Vdelta1 TCR	APC	REA173	Miltenyi	130-118-968
Vdelta 2 TCR	PE	123R3	Miltenyi	130-100-212
Vdelta 2 TCR	PE	B6	Biolegend	331407
Alpha/Beta TCR	VioBlue	REA652	Miltenyi	130-119-618
Alpha/Beta TCR	PE-Vio 770	BW242/412	Miltenyi	130-113-532
B7-H3	PE	DCN.70	Biolegend	331606
CD56	PerCP/Cy 5.5	5.1H11	Biolegend	362525
CD56	Alexa Fluor 488	HCD56	Biolegend	318312
CD107a	FITC	H4A3	Biolegend	328606
B7-H3	PE	DCN.70	Biolegend	331606
CD34	Alexa Fluor 488	Qbend/10	Biotechne	FAB7227G
CD34	Alexa Fluor 700	Qbend/10	Biotechne	FAB722N
pSTAT5 (Tyr694)	PE	A17016B	Biolegend	936904
Interferon-γ	BV605	B27	Biolegend	506542
Granzyme B	Pacific Blue	GB11	Biolegend	515408
IL17A	PerCP/Cy 5.5	BL168	Biolegend	512314
PD-1 (CD279)	APC/Fire 750	EH12.2H7	Biolegend	329954
CD45RA	PE	T6D11	Miltenyi	130-113-918
CCR7	Alexa Fluor 700	G043H7	Biolegend	353244

CCR7 (CD197)	Alexa fluor 700	G043H7	Biolegend	353244
CD69	FITC	FN50	Biolegend	310904
NKG2D	PerCP/Cy 5.5	1D11	Biolegend	320818
His-tag	PE	J095G46	Biolegend	362603
His-tag	FITC	GG11.8F3.5.1	Miltenyi	130-123-547
Alpha/Beta TCR	Biotin	BW242/412	Miltenyi	130-113-529
Alpha/Beta TCR	Biotin	IP26	Biolegend	306704
CD56	Biotin	HCD56	Biolegend	318320
Vdelta 2 TCR	Biotin	REA771	Miltenyi	130-111-008
Alpha/Beta TCR (cliniMACS)	Biotin	n/a	Miltenyi	173-01
Biotin (cliniMACS anti-Biotin reagent)	-	n/a	Miltenyi	701-48
IgG1k Isotype control	BV605	MOPC-21	Biolegend	400162
IgG1k Isotype control	Pacific Blue	MOPC-21	Biolegend	400151
IgG1k Isotype control	FITC	MOPC-21	Biolegend	400110
IgG1k Isotype control	PerCP/Cy 5.5	MOPC-21	Biolegend	400150
IgG1k Isotype control	PE	MOPC-21	Biolegend	400140

Table A2: List of flow cytometry and MACS antibodies

List of plasmids and sources

Plasmid	Antibiotic resistance gene	Source
TE9-CD28z CAR	Ampicillin	Anderson lab
P23 CAR	Ampicillin	Arnold lab
STAT5b wild type gene block	Kanamycin	Thermofisher
STAT5b N642H gene block	Kanamycin	Thermofisher

Table A3: List of plasmids

Antibiotic	Working concentration	Manufacturer	Storage of Stock solution
Ampicillin	100 µg/ml	Sigma-Aldrich	-20ºC
Kanamycin sulphate	50 µg/ml	Life Technologies	4ºC

Table A4: Details of antibiotics for bacterial plasmid selection

REFERENCES

1. Dong D, Zheng L, Lin J, Zhang B, Zhu Y, Li N, et al. Structural basis of assembly of the human T cell receptor–CD3 complex. Nature 2019;573(7775):546–52.

2. Hodges E, Krishna MT, Pickard C. Diagnostic role of tests for T cell receptor (TCR) genes. J Clin Pathol 2003;56:1–11.

3. Hayday AC, Saito H, Gillies SD, Kranz DM, Tanigawa G, Eisen HN, et al. Structure, organization, and somatic rearrangement of T cell gamma genes. Cell 1985;40(2):259–69.

4. Born W, Miles C, White J, O'Brien R, Freed JH, Marrack P, et al. Peptide sequences of T-cell receptor δ and γ chains are identical to predicted X and γ proteins. Nature 1987;330(6148):572–4.

5. Chien Y hsiu, Meyer C, Bonneville M. γδ T Cells: First Line of Defense and Beyond . Annu Rev Immunol 2014;32(1):121–55.

6. Born WK, Kemal Aydintug M, O'brien RL. Diversity of γδ T-cell antigens. Cell Mol Immunol2013;10(1):13–20.

7. Pistoia V, Tumino N, Vacca P, Veneziani I, Moretta A, Locatelli F, et al. Human γδ T-Cells: From surface receptors to the therapy of high-risk leukemias. Front Immunol2018;9(MAY).

8. Deseke M, Prinz I. Ligand recognition by the γδ TCR and discrimination between homeostasis and stress conditions [Internet]. Cell Mol Immunol2020 [cited 2021 Jan 18];17(9):914–24. Available from: https://doi.org/10.1038/s41423-020-0503-y

9. Morita CT, Verma S, Aparicio P, Martinez-A. C, Spits H, Brenner MB. Functionally distinct subsets of human γ/δ T cells. Eur J Immunol 1991;21(12):2999–3007.

10. Bottino C, Tambussi G, Ferrini S, Ciccone E, Varese P, Mingari MC, et al. Two subsets of human T lymphocytes expressing γ/δ antigen receptor are identifiable by monoclonal antibodies directed to two distinct molecular forms of the receptor. Journal of Experimental Medicine 1988;168(2):491–505.

11. Wu D, Wu P, Qiu F, Wei Q, Huang J. Human γδT-cell subsets and their involvement in tumor immunity. Cell Mol Immunol2017;14(3):245–53.

12. Caccamo N. Sex-specific phenotypical and functional differences in peripheral human V 9/V 2 T cells. J Leukoc Biol 2006;79(4):663–6.

13. Schondelmaier S, Wesch D, Pechhold K, Kabelitz D. Vγ gene usage in peripheral blood γδ T cells. Immunol Lett 1993;38(2):121–6.

14. Argentati K, Re F, Donnini A, Tucci MG, Bartozzi B, Bernardini G, et al. Numerical and functional alterations of circulating γδ T lymphocytes in aged people and centenarians. J Leukoc Biol 2002;72(1):65–71.

15. Fonseca S, Pereira V, Lau C, Teixeira M dos A, Bini-Antunes M, Lima M. Human Peripheral Blood Gamma Delta T Cells: Report on a Series of Healthy Caucasian Portuguese Adults and Comprehensive Review of the Literature. Cells 2020;9(3):729.

16. Hviid L, Akanmori BD, Loizon S, Kurtzhals JAL, Ricke CH, Lim A, et al. High frequency of circulating γδ T cells with dominance of the Vδ1 subset in a healthy population. Int Immunol 2000;12(6):797–805.

17. Cairo C, Armstrong CL, Cummings JS, Deetz CO, Tan M, Lu C, et al. Impact of age, gender, and race on circulating γδ T cells. Hum Immunol 2010;71(10):968–75.

18. Wesch D, Hinz T, Kabelitz D. Analysis of the TCR V γ repertoire in healthy donors and HIV-1-infected individuals. 1998.

19. Déchanet J, Merville P, Lim A, Retière C, Pitard V, Lafarge X, et al. Implication of γδ T cells in the human immune response to cytomegalovirus. Journal of Clinical Investigation 1999;103(10):1437–49.

20. Knight A, Madrigal AJ, Grace S, Sivakumaran J, Kottaridis P, Mackinnon S, et al. The role of Vδ2-negative γδ T cells during cytomegalovirus reactivation in recipients of allogeneic stem cell transplantation. Blood 2010;116(12):2164–72.

21. Fujishima N, Hirokawa M, Fujishima M, Yamashita J, Saitoh H, Ichikawa Y, et al. Skewed T cell receptor repertoire of Vδ1+ γδ T lymphocytes after human allogeneic haematopoietic stem cell transplantation and the potential role for Epstein-Barr virus-infected B cells in clonal restriction. Clin Exp Immunol 2007;149(1):70–9.

22. Hviid L, Kurtzhals JAL, Adabayeri V, Loizon S, Kemp K, Goka BQ, et al. Perturbation and proinflammatory type activation of vδ1+ γδ t cells in african children with plasmodium falciparum malaria. Infect Immun 2001;69(5):3190–6.

23. Girardi M, Oppenheim DE, Steele CR, Lewis JM, Glusac E, Filler R, et al. Regulation of cutaneous malignancy by γδ T cells. Journal of Immunology 2018;200(9):3031–5.

24. Okada R, Kondo T, Matsuki F, Takata H, Takiguchi M. Phenotypic classification of human CD4+ T cell subsets and their differentiation. Int Immunol 2008;20(9):1189–99.

25. Hamann D, Roos MTL, Van Lier RAW. Faces and phases of human CD8+ T-cell development. Immunol Today1999;20(4):177–80.

26. Takata H, Takiguchi M. Three Memory Subsets of Human CD8 + T Cells Differently Expressing Three Cytolytic Effector Molecules . The Journal of Immunology 2006;177(7):4330–40.

27. Fritsch RD, Shen X, Sims GP, Hathcock KS, Hodes RJ, Lipsky PE. Stepwise Differentiation of CD4 Memory T Cells Defined by Expression of CCR7 and CD27. The Journal of Immunology 2005;175(10):6489–97.

28. Sallusto F, Lenig D, Förster R, Lipp M, Lanzavecchia A. Two subsets of memory T lymphocytes with distinct homing potentials and effector functions. Nature 1999;401(6754):708–12.

29. Butcher EC, Picker LJ. Lymphocyte homing and homeostasis. Science (1979) 1996;272(5258):60–6.

30. Sallusto F, Kremmer E, Palermo B, Hoy A, Ponath P, Qin S, et al. Switch in chemokine receptor expression upon TCR stimulation reveals novel homing potential for recently activated T cells. Eur J Immunol 1999;29(6):2037–45.

31. Mullen KM, Gocke AR, Allie R, Ntranos A, Grishkan I V., Pardo C, et al. Expression of CCR7 and CD45RA in CD4 + and CD8 + subsets in cerebrospinal fluid of 134 patients with inflammatory and non-inflammatory neurological diseases. J Neuroimmunol 2012;249(1–2):86–92.

32. Dieli F, Poccia F, Lipp M, Sireci G, Caccamo N, Di Sano C, et al. Differentiation of effector/memory Vδ2 T cells and migratory routes in lymph nodes or inflammatory sites. Journal of Experimental Medicine 2003;198(3):391–7.

33. Martin MD, Badovinac VP. Defining memory CD8 T cell. Front Immunol2018;9(NOV):2692.

34. Willcox BE, Willcox CR. γδ TCR ligands: the quest to solve a 500-million-year-old mystery. Nature Immunology 2019 20:2 [Internet] 2019 [cited 2024 Jan 21];20(2):121–8. Available from: https://www.nature.com/articles/s41590-018-0304-y

35. Davey MS, Willcox CR, Joyce SP, Ladell K, Kasatskaya SA, McLaren JE, et al. Clonal selection in the human Vδ1 T cell repertoire indicates γδ TCR-dependent adaptive immune surveillance. Nat Commun [Internet] 2017 [cited 2024 Jan 21];8. Available from: /pmc/articles/PMC5337994/

36. Khairallah C, Netzer S, Villacreces A, Juzan M, Rousseau B, Dulanto S, et al. γδ T Cells Confer Protection against Murine Cytomegalovirus (MCMV). PLoS Pathog [Internet] 2015 [cited 2024 Jan 21];11(3):e1004702. Available from: https://journals.plos.org/plospathogens/article?id=10.1371/journal.ppat.1004702

37. Sell S, Dietz M, Schneider A, Holtappels R, Mach M, Winkler TH. Control of Murine Cytomegalovirus Infection by γδ T Cells. PLoS Pathog [Internet] 2015 [cited 2024 Jan 21];11(2):e1004481. Available from: https://journals.plos.org/plospathogens/article?id=10.1371/journal.ppat.1004481

38. Shen Y, Zhou D, Qiu L, Lai X, Simon M, Shen L, et al. Adaptive immune response of Vγ2Vδ2+ T cells during mycobacterial infections. Science (1979) 2002;295(5563):2255–8.

39. Eberl M, Engel R, Beck E, Jomaa H. Differentiation of human γδ T cells towards distinct memory phenotypes. Cell Immunol 2002;218(1–2):1–6.

40. Pitard V, Roumanes D, Lafarge X, Couzi L, Garrigue I, Lafon ME, et al. Long-term expansion of effector/memory V{delta}2- {gamma}-{delta} T cells is a specific blood signature of CMV infection. Blood 2008;112(4):1317–24.

41. Li H, Lebedeva MI, Llera AS, Fields BA, Brenner MB, Mariuzza RA. Structure of the Vδ domain of a human γδ T-cell antigen receptor. Nature 1998;391(6666):502–6.

42. Correa I, Bix M, Liao NS, Zijlstrat M, Jaenischt R, Raulet D. Most v6 T cells develop normally in f32-microglobulin-deficient mice (major histocompatibility complex class I/positive selection/T-celi development). 1992.

43. Schweighoffer E, Fowlkes BJ. Positive selection is not required for thymic maturation of transgenic γδ T cells. Journal of Experimental Medicine 1996;183(5):2033–41.

44. Adams EJ, Gu S, Luoma AM. Human gamma delta T cells: Evolution and ligand recognition. Cell Immunol2015;296(1):31–40.

45. Davis MM, Bjorkman PJ. T-cell antigen receptor genes and T-cell recognition. Nature1988;334(6181):395–402.

46. Rock EP, Sibbald PG, Davis MM, Chien YH. CDR3 Length in Antigen-specific Immune Receptors. 1994.

47. Thedrez A, Sabourin C, Gertner J, Devilder MC, Allain-Maillet S, Fournié JJ, et al. Self/non-self discrimination by human γδ T cells: Simple solutions for a complex issue? Immunol Rev2007;215(1):123–35.

48. Constant P, Davodeau F, Peyrat MA, Poquet Y, Puzo G, Bonneville M, et al. Stimulation of human γδ T cells by nonpeptidic mycobacterial ligands. Science (1979) 1994;264(5156):267–70.

49. Chen ZW. Multifunctional immune responses of HMBPP-specific Vγ2Vδ2 T cells in M. tuberculosis and other infections. Cell Mol Immunol2013;10(1):58–64.

50. Tanaka Y, Tanaka Y, Bloom BR, Morita CT, Brenner MB, Nieves E. Natural and synthetic non-peptide antigens recognized by human γδ T cells. Nature1995;375(6527):155–8.

51. Bukowski JF, Morita CT, Brenner MB. Human γδ T cells recognize alkylamines derived from microbes, edible plants, and tea: Implications for innate immunity. Immunity 1999;11(1):57–65.

52. Gober HJ, Kistowska M, Angman L, Jenö P, Mori L, De Libero G. Human T cell receptor γδ cells recognize endogenous mevalonate metabolites in tumor cells. Journal of Experimental Medicine 2003;197(2):163–8.

53. Gu S, Sachleben JR, Boughter CT, Nawrocka WI, Borowska MT, Tarrasch JT, et al. Phosphoantigen-induced conformational change of butyrophilin 3A1 (BTN3A1) and its implication on Vγ9Vδ2 T cell activation. Proc Natl Acad Sci U S A 2017;114(35):E7311–20.

54. Abeler-Dörner L, Swamy M, Williams G, Hayday AC, Bas A. Butyrophilins: An emerging family of immune regulators. Trends Immunol2012;33(1):34–41.

55. Harly C, Guillaume Y, Nedellec S, Peigné CM, Mönkkönen H, Mönkkönen J, et al. Key implication of CD277/butyrophilin-3 (BTN3A) in cellular stress sensing by a major human γδ T-cell subset. Blood [Internet] 2012 [cited 2023 Jun 29];120(11):2269–79. Available from: https://dx.doi.org/10.1182/blood-2012-05-430470

56. Salim M, Knowles TJ, Baker AT, Davey MS, Jeeves M, Sridhar P, et al. BTN3A1 Discriminates γδ T Cell Phosphoantigens from Nonantigenic Small Molecules via a Conformational Sensor in Its B30.2 Domain. ACS Chem Biol 2017;12(10):2631–43.

57. Rigau M, Ostrouska S, Fulford TS, Johnson DN, Woods K, Ruan Z, et al. Butyrophilin 2A1 is essential for phosphoantigen reactivity by gd T cells. Science (1979) [Internet]

2020 [cited 2023 Jun 29];367(6478). Available from: https://www.science.org/doi/10.1126/science.aay5516

58. Karunakaran MM, Willcox CR, Salim M, Paletta D, Fichtner AS, Noll A, et al. Butyrophilin-2A1 Directly Binds Germline-Encoded Regions of the Vγ9Vδ2 TCR and Is Essential for Phosphoantigen Sensing. Immunity 2020;52(3):487-498.e6.

59. Cano CE, Pasero C, De Gassart A, Briantais A, Charlotte Le Floch A, Olive D, et al. BTN2A1, an immune checkpoint targeting Vγ9Vδ2 T cell cytotoxicity against malignant cells. Cell Rep [Internet] 2021 [cited 2023 Jun 29];36. Available from: https://doi.org/10.1016/j.celrep.2021.109359

60. Kalyan S, Kabelitz D. Defining the nature of human γδ T cells: A biographical sketch of the highly empathetic. Cell Mol Immunol2013;10(1):21–9.

61. Bonneville M, O'Brien RL, Born WK. γ δ T cell effector functions: A blend of innate programming and acquired plasticity. Nat Rev Immunol2010;10(7):467–78.

62. Pietschmann K, Beetz S, Welte S, Martens I, Gruen J, Oberg HH, et al. Toll-Like Receptor Expression and Function in Subsets of Human γδ T Lymphocytes. Scand J Immunol 2009;70(3):245–55.

63. LAMB LS, HENSLEE-DOWNEY PJ, PARRISH RS, GODDER K, THOMPSON J, LEE C, et al. Rapid Communication: Increased Frequency of TCRγδ+ T Cells in Disease-Free Survivors Following T Cell-Depleted, Partially Mismatched, Related Donor Bone Marrow Transplantation for Leukemia. J Hematother 1996;5(5):503–9.

64. Godder KT, Henslee-Downey PJ, Mehta J, Park BS, Chiang KY, Abhyankar S, et al. Long term disease-free survival in acute leukemia patients recovering with increased γδ T cells after partially mismatched related donor bone marrow transplantation. Bone Marrow Transplant 2007;39(12):751–7.

65. Gentles AJ, Newman AM, Liu CL, Bratman S V., Feng W, Kim D, et al. The prognostic landscape of genes and infiltrating immune cells across human cancers. Nat Med 2015;21(8):938–45.

66. Groh V, Steinle A, Bauer S, Spies T. Recognition of stress-induced MHC molecules by intestinal epithelial γδ T cells. Science (1979) 1998;279(5357):1737–40.

67. Gasser S, Orsulic S, Brown EJ, Raulet DH. The DNA damage pathway regulates innate immune system ligands of the NKG2D receptor. Nature 2005;436(7054):1186–90.

68. Ghadially H, Brown L, Lloyd C, Lewis L, Lewis A, Dillon J, et al. MHC class i chain-related protein A and B (MICA and MICB) are predominantly expressed intracellularly in tumour and normal tissue. Br J Cancer 2017;116(9):1208–17.

69. Simões C, Silva I, Carvalho A, Silva S, Santos S, Marques G, et al. Quantification and phenotypic characterization of peripheral blood Vδ1 + T cells in chronic lymphocytic leukemia and monoclonal B cell lymphocytosis. Cytometry B Clin Cytom 2019;96(2):164–8.

70. Poggi A, Venturino C, Catellani S, Clavio M, Miglino M, Gobbi M, et al. Vδ1 T lymphocytes from B-CLL patients recognize ULBP3 expressed on leukemic B cells and up-regulated by trans-retinoic acid. Cancer Res 2004;64(24):9172–9.

71. Wu Y, Kyle-Cezar F, Woolf RT, Naceur-Lombardelli C, Owen J, Biswas D, et al. An innate-like Vδ1+ γδ T cell compartment in the human breast is associated with remission in triple-negative breast cancer. Sci Transl Med 2019;11(513).

72. Meraviglia S, Lo Presti E, Tosolini M, Mendola C La, Orlando V, Todaro M, et al. Distinctive features of tumor-infiltrating γδ T lymphocytes in human colorectal cancer Distinctive features of tumor-infiltrating gd T lymphocytes in human colorectal cancer. 2017;

73. de Vries NL, van de Haar J, Veninga V, Chalabi M, Ijsselsteijn ME, van der Ploeg M, et al. γδ T cells are effectors of immunotherapy in cancers with HLA class I defects. Nature 2023 613:7945 [Internet] 2023 [cited 2023 Jun 29];613(7945):743–50. Available from: https://www.nature.com/articles/s41586-022-05593-1

74. Wu P, Wu D, Ni C, Ye J, Chen W, Hu G, et al. γδT17 cells promote the accumulation and expansion of myeloid-derived suppressor cells in human colorectal cancer. Immunity 2014;40(5):785–800.

75. Knight A, MacKinnon S, Lowdell MW. Human Vdelta1 gamma-delta T cells exert potent specific cytotoxicity against primary multiple myeloma cells. Cytotherapy 2012;14(9):1110–8.

76. Siegers GM, Dhamko H, Wang XH, Mathieson AM, Kosaka Y, Felizardo TC, et al. Human Vδ1 γδ T cells expanded from peripheral blood exhibit specific cytotoxicity against B-cell chronic lymphocytic leukemia-derived cells. Cytotherapy 2011;13(6):753–64.

77. Maeurer MJ, Martin D, Walter W, Liu K, Zitvogel L, Halusczcak K, et al. Human intestinal Vδ1+ T lymphocytes recognize tumor cells of epithelial origin. Journal of Experimental Medicine 1996;183(4):1681–96.

78. Simões AE, di Lorenzo B, Silva-Santos B. Molecular Determinants of Target Cell Recognition by Human γδ T Cells. Front Immunol [Internet] 2018 [cited 2023 Feb 25];9(APR):27. Available from: /pmc/articles/PMC5934422/

79. Bauer S. Activation of NK cells and T cells by NKG2D, a receptor for stress-inducible MICA. 1999 [cited 2023 Feb 25];Available from: https://www.researchgate.net/publication/235235798

80. Gong T, Liu L, Jiang W, Zhou R. DAMP-sensing receptors in sterile inflammation and inflammatory diseases. Nature Reviews Immunology 2019 20:2 [Internet] 2019 [cited 2023 Feb 25];20(2):95–112. Available from: https://www.nature.com/articles/s41577-019-0215-7

81. Correia D v., Lopes A, Silva-Santos B. Tumor cell recognition by γδ T lymphocytes: T-cell receptor vs. NK-cell receptors. Oncoimmunology [Internet] 2013 [cited 2023 Feb 25];2(1). Available from: /pmc/articles/PMC3583939/

82. Willcox BE, Willcox CR. γδ TCR ligands: the quest to solve a 500-million-year-old mystery. Nature Immunology 2019 20:2 [Internet] 2019 [cited 2023 Feb 25];20(2):121–8. Available from: https://www.nature.com/articles/s41590-018-0304-y

83. Wakita D, Sumida K, Iwakura Y, Nishikawa H, Ohkuri T, Chamoto K, et al. Tumor-infiltrating IL-17-producing γδ T cells support the progression of tumor by promoting

angiogenesis. Eur J Immunol [Internet] 2010 [cited 2023 Jun 23];40(7):1927–37. Available from: https://onlinelibrary.wiley.com/doi/full/10.1002/eji.200940157

84. Caccamo N, La Mendola C, Orlando V, Meraviglia S, Todaro M, Stassi G, et al. Differentiation, phenotype, and function of interleukin-17–producing human Vγ9Vδ2 T cells. Blood [Internet] 2011 [cited 2023 Jun 23];118(1):129–38. Available from: https://dx.doi.org/10.1182/blood-2011-01-331298

85. Rei M, Goncąlves-Sousa N, Lancą T, Thompson RG, Mensurado S, Balkwill FR, et al. Murine CD27(-) Vγ6(+) γδ T cells producing IL-17A promote ovarian cancer growth via mobilization of protumor small peritoneal macrophages. Proc Natl Acad Sci U S A [Internet] 2014 [cited 2023 Jun 23];111(34):E3562–70. Available from: https://www.pnas.org/doi/abs/10.1073/pnas.1403424111

86. Hu G, Wu P, Cheng P, Zhang Z, Wang Z, Yu X, et al. Tumor-infiltrating CD39+ γδTregs are novel immunosuppressive T cells in human colorectal cancer. Oncoimmunology [Internet] 2017 [cited 2023 Jun 23];6(2). Available from: https://www.tandfonline.com/doi/abs/10.1080/2162402X.2016.1277305

87. Park JH, Lee HK. Function of γδ T cells in tumor immunology and their application to cancer therapy. Experimental & Molecular Medicine 2021 53:3 [Internet] 2021 [cited 2023 Jun 23];53(3):318–27. Available from: https://www.nature.com/articles/s12276-021-00576-0

88. Gentles AJ, Newman AM, Liu CL, Bratman S V., Feng W, Kim D, et al. The prognostic landscape of genes and infiltrating immune cells across human cancers. Nat Med [Internet] 2015 [cited 2023 Mar 8];21(8):938–45. Available from: https://pubmed.ncbi.nlm.nih.gov/26193342/

89. Wu Y, Kyle-Cezar F, Woolf RT, Naceur-Lombardelli C, Owen J, Biswas D, et al. An innate-like Vδ1+ γδ T cell compartment in the human breast is associated with remission in Triple Negative Breast Cancer. Sci Transl Med [Internet] 2019 [cited 2023 Mar 8];11(513). Available from: /pmc/articles/PMC6877350/

90. DeRenzo C, Krenciute G, Gottschalk S. The Landscape of CAR T Cells Beyond Acute Lymphoblastic Leukemia for Pediatric Solid Tumors. American Society of Clinical Oncology Educational Book 2018;(38):830–7.

91. Kuwana Y, Asakura Y, Utsunomiya N, Nakanishi M, Arata Y, Itoh S, et al. Expression of chimeric receptor composed of immunoglobulin-derived V resions and T-cell receptor-derived C regions. Biochem Biophys Res Commun 1987;149(3):960–8.

92. Gross G, Waks T, Eshhar Z. Expression of immunoglobulin-T-cell receptor chimeric molecules as functional receptors with antibody-type specificity. Proc Natl Acad Sci U S A [Internet] 1989 [cited 2023 Jun 19];86(24):10024. Available from: /pmc/articles/PMC298636/?report=abstract

93. Eshhar Z, Waks T, Gross G, Schindler DG. Specific activation and targeting of cytotoxic lymphocytes through chimeric single chains consisting of antibody-binding domains and the gamma or zeta subunits of the immunoglobulin and T-cell receptors. Proc Natl Acad Sci U S A [Internet] 1993 [cited 2023 Jun 19];90(2):720. Available from: /pmc/articles/PMC45737/?report=abstract

94. Eshhar Z, Bach N, Fitzer-Attas CJ, Gross G, Lustgarten J, Waks T, et al. The T-body approach: potential for cancer immunotherapy. Springer Semin Immunopathol [Internet] 1996 [cited 2021 Dec 8];18(2):199–209. Available from: https://pubmed.ncbi.nlm.nih.gov/8908700/

95. Brocker T. Chimeric Fv-ζ or Fv-ε receptors are not sufficient to induce activation or cytokine production in peripheral T cells. Blood 2000;96(5):1999–2001.

96. Kershaw MH, Westwood JA, Parker LL, Wang G, Eshhar Z, Mavroukakis SA, et al. A Phase I Study on Adoptive Immunotherapy Using Gene-Modified T Cells for Ovarian Cancer. Clinical Cancer Research [Internet] 2006 [cited 2023 Jun 19];12(20):6106–15. Available from: https://dx.doi.org/10.1158/1078-0432.CCR-06-1183

97. Thistlethwaite FC, Gilham DE, Guest RD, Rothwell DG, Pillai M, Burt DJ, et al. The clinical efficacy of first-generation carcinoembryonic antigen (CEACAM5)-specific CAR T cells is limited by poor persistence and transient pre-conditioning-dependent respiratory toxicity. Cancer Immunology, Immunotherapy [Internet] 2017 [cited 2023 Jun 19];66(11):1425. Available from: /pmc/articles/PMC5645435/

98. Finney HM, Akbar AN, Lawson ADG. Activation of Resting Human Primary T Cells with Chimeric Receptors: Costimulation from CD28, Inducible Costimulator, CD134, and CD137 in Series with Signals from the TCR Chain. The Journal of Immunology [Internet] 2004 [cited 2023 Jun 19];172:104–13. Available from: http://journals.aai.org/jimmunol/article-pdf/172/1/104/1178355/104.pdf

99. Hombach AA, Rappl G, Abken H. Arming Cytokine-induced Killer Cells With Chimeric Antigen Receptors: CD28 Outperforms Combined CD28–OX40 “Super-stimulation.” Molecular Therapy [Internet] 2013 [cited 2023 Jun 19];21(12):2268. Available from: /pmc/articles/PMC3863798/

100. Maude SL, Laetsch TW, Buechner J, Rives S, Boyer M, Bittencourt H, et al. Tisagenlecleucel in Children and Young Adults with B-Cell Lymphoblastic Leukemia. New England Journal of Medicine [Internet] 2018 [cited 2023 Jun 19];378(5):439–48. Available from: https://www.nejm.org/doi/full/10.1056/NEJMoa1709866

101. FDA approval brings first gene therapy to the United States | FDA [Internet]. [cited 2023 Jun 20];Available from: https://www.fda.gov/news-events/press-announcements/fda-approval-brings-first-gene-therapy-united-states

102. Finlay WJJ, Bloom L, Cunningham O. Phage display: a powerful technology for the generation of high specificity affinity reagents from alternative immune sources. Methods Mol Biol [Internet] 2011 [cited 2023 Jun 20];681:87–101. Available from: https://link.springer.com/protocol/10.1007/978-1-60761-913-0_6

103. Wesolowski J, Alzogaray V, Reyelt J, Unger M, Juarez K, Urrutia M, et al. Single domain antibodies: promising experimental and therapeutic tools in infection and immunity. Med Microbiol Immunol [Internet] 2009 [cited 2023 Jun 11];198(3):157. Available from: /pmc/articles/PMC2714450/

104. Cilta-cel OK’d for Multiple Myeloma. Cancer Discov [Internet] 2022 [cited 2023 Jun 20];12(5):1176. Available from: https://dx.doi.org/10.1158/2159-8290.CD-NB2022-0019

105. Berdeja JG, Madduri D, Usmani SZ, Jakubowiak A, Agha M, Cohen AD, et al. Ciltacabtagene autoleucel, a B-cell maturation antigen-directed chimeric antigen receptor T-cell therapy in patients with relapsed or refractory multiple myeloma (CARTITUDE-1): a phase 1b/2 open-label study. The Lancet [Internet] 2021 [cited 2023 Jun 11];398(10297):314–24. Available from: http://www.thelancet.com/article/S0140673621009338/fulltext

106. Munshi NC, Anderson LD, Shah N, Madduri D, Berdeja J, Lonial S, et al. Idecabtagene Vicleucel in Relapsed and Refractory Multiple Myeloma. New England Journal of Medicine [Internet] 2021 [cited 2023 Jun 11];384(8):705–16. Available from: https://www.nejm.org/doi/full/10.1056/nejmoa2024850

107. Branella GM, Spencer HT. Natural Receptor- and Ligand-Based Chimeric Antigen Receptors: Strategies Using Natural Ligands and Receptors for Targeted Cell Killing. Cells [Internet] 2022 [cited 2023 Feb 25];11(1). Available from: /pmc/articles/PMC8750724/

108. Wong DP, Roy NK, Zhang K, Anukanth A, Asthana A, Shirkey-Son NJ, et al. A BAFF ligand-based CAR-T cell targeting three receptors and multiple B cell cancers. Nature Communications 2022 13:1 [Internet] 2022 [cited 2023 Feb 25];13(1):1–17. Available from: https://www.nature.com/articles/s41467-021-27853-w

109. Ramírez-Chacón A, Betriu-Méndez S, Bartoló-Ibars A, González A, Martí M, Juan M. Ligand-based CAR-T cell: Different strategies to drive T cells in future new treatments. Front Immunol 2022;13:5241.

110. Weinkove R, George P, Dasyam N, McLellan AD. Selecting costimulatory domains for chimeric antigen receptors: functional and clinical considerations. Clin Transl Immunology [Internet] 2019 [cited 2021 Dec 8];8(5). Available from: /pmc/articles/PMC6511336/

111. Sadelain M, Brentjens R, Rivière I. The basic principles of chimeric antigen receptor design. Cancer Discov 2013;3(4):388–98.

112. Zhang H, Snyder KM, Suhoski MM, Maus M v., Kapoor V, June CH, et al. 4-1BB Is Superior to CD28 Costimulation for Generating CD8+ Cytotoxic Lymphocytes for Adoptive Immunotherapy. J Immunol [Internet] 2007 [cited 2021 Dec 8];179(7):4910. Available from: /pmc/articles/PMC3809056/

113. Porter DL, Hwang WT, Frey N v., Lacey SF, Shaw PA, Loren AW, et al. Chimeric antigen receptor T cells persist and induce sustained remissions in relapsed refractory chronic lymphocytic leukemia. Sci Transl Med [Internet] 2015 [cited 2021 Dec 8];7(303). Available from: https://www.science.org/doi/abs/10.1126/scitranslmed.aac5415

114. Kawalekar OU, O'connor RS, Fraietta JA, Blair IA, Milone MC, Correspondence CHJ. Distinct Signaling of Coreceptors Regulates Specific Metabolism Pathways and Impacts Memory Development in CAR T Cells. Immunity [Internet] 2016 [cited 2021 Dec 8];44:380–90. Available from: http://dx.doi.org/10.1016/j.immuni.2016.01.021

115. Ying Z, He T, Wang X, Zheng W, Lin N, Tu M, et al. Parallel Comparison of 4-1BB or CD28 Co-stimulated CD19-Targeted CAR-T Cells for B Cell Non-Hodgkin's Lymphoma.

Mol Ther Oncolytics [Internet] 2019 [cited 2021 Dec 8];15:60–8. Available from: http://www.cell.com/article/S2372770519300737/fulltext

116. Selli ME, Landmann J, Terekhova M, Lattin J, Heard A, Hsu YS, et al. Costimulatory domains direct distinct fates of CAR-driven T-cell dysfunction. Blood [Internet] 2023 [cited 2023 Jun 30];141(26):3153–65. Available from: https://ashpublications.org/blood/article/doi/10.1182/blood.2023020100/495574/Costimulatory-domains-direct-distinct-fates-of-CAR

117. Dai Q, Han P, Qi X, Li F, Li M, Fan L, et al. 4-1BB Signaling Boosts the Anti-Tumor Activity of CD28-Incorporated 2nd Generation Chimeric Antigen Receptor-Modified T Cells. Front Immunol 2020;11:2931.

118. Drent E, Poels R, Ruiter R, van de Donk NWCJ, Zweegman S, Yuan H, et al. Combined CD28 and 4-1BB Costimulation Potentiates Affinity-tuned Chimeric Antigen Receptor–engineered T Cells. Clinical Cancer Research [Internet] 2019 [cited 2021 Dec 8];25(13):4014–25. Available from: https://clincancerres.aacrjournals.org/content/25/13/4014

119. Straathof K, Flutter B, Wallace R, Jain N, Loka T, Depani S, et al. Antitumor activity without on-target off-tumor toxicity of GD2-chimeric antigen receptor T cells in patients with neuroblastoma. Sci Transl Med [Internet] 2020 [cited 2021 Dec 8];12:6169. Available from: https://www.science.org

120. Heczey A, Louis CU, Savoldo B, Dakhova O, Durett A, Grilley B, et al. CAR T Cells Administered in Combination with Lymphodepletion and PD-1 Inhibition to Patients with Neuroblastoma. Molecular Therapy [Internet] 2017 [cited 2021 Dec 8];25(9):2214. Available from: /pmc/articles/PMC5589058/

121. Schaft N. The Landscape of CAR-T Cell Clinical Trials against Solid Tumors—A Comprehensive Overview. Cancers (Basel) [Internet] 2020 [cited 2023 Jun 22];12(9):1–36. Available from: /pmc/articles/PMC7563774/

122. Hou AJ, Chen LC, Chen YY. Navigating CAR-T cells through the solid-tumour microenvironment. Nature Reviews Drug Discovery 2021 20:7 [Internet] 2021 [cited 2021 Dec 8];20(7):531–50. Available from: https://www.nature.com/articles/s41573-021-00189-2

123. Edeline J, Houot R, Marabelle A, Alcantara M. CAR-T cells and BiTEs in solid tumors: challenges and perspectives. J Hematol Oncol [Internet] 2021 [cited 2021 Dec 8];14(1):1–12. Available from: https://jhoonline.biomedcentral.com/articles/10.1186/s13045-021-01067-5

124. Capsomidis A, Benthall G, van Acker HH, Fisher J, Kramer AM, Abeln Z, et al. Chimeric Antigen Receptor-Engineered Human Gamma Delta T Cells: Enhanced Cytotoxicity with Retention of Cross Presentation. Mol Ther [Internet] 2018 [cited 2021 Dec 8];26(2):354–65. Available from: https://pubmed.ncbi.nlm.nih.gov/29310916/

125. Kosti P, Opzoomer JW, Larios-Martinez KI, Henley-Smith R, Scudamore CL, Okesola M, et al. Hypoxia-sensing CAR T cells provide safety and efficacy in treating solid tumors. Cell Rep Med [Internet] 2021 [cited 2021 Dec 8];2(4). Available from: https://pubmed.ncbi.nlm.nih.gov/33948568/

126. Liu E, Marin D, Banerjee P, Macapinlac HA, Thompson P, Basar R, et al. Use of CAR-Transduced Natural Killer Cells in CD19-Positive Lymphoid Tumors. New England Journal of Medicine [Internet] 2020 [cited 2023 Jul 1];382(6):545–53. Available from: https://www.nejm.org/doi/full/10.1056/NEJMoa1910607

127. Del Bufalo F, De Angelis B, Caruana I, Del Baldo G, De Ioris MA, Serra A, et al. GD2-CART01 for Relapsed or Refractory High-Risk Neuroblastoma. N Engl J Med [Internet] 2023 [cited 2023 Jun 22];388(14):1284–95. Available from: http://www.ncbi.nlm.nih.gov/pubmed/37018492

128. Majzner RG, Ramakrishna S, Yeom KW, Patel S, Chinnasamy H, Schultz LM, et al. GD2-CAR T cell therapy for H3K27M-mutated diffuse midline gliomas. Nature [Internet] 2022 [cited 2023 Jun 22];603(7903):934. Available from: /pmc/articles/PMC8967714/

129. Vitanza NA, Wilson AL, Huang W, Seidel K, Brown C, Gustafson JA, et al. Intraventricular B7-H3 CAR T Cells for Diffuse Intrinsic Pontine Glioma: Preliminary First-in-Human Bioactivity and Safety. Cancer Discov [Internet] 2023 [cited 2023 Jun 23];13(1):114–31. Available from: https://pubmed.ncbi.nlm.nih.gov/36259971/

130. O'Rourke DM, Nasrallah MP, Desai A, Melenhorst JJ, Mansfield K, Morrissette JJD, et al. A single dose of peripherally infused EGFRvIII-directed CAR T cells mediates antigen loss and induces adaptive resistance in patients with recurrent glioblastoma. Sci Transl Med [Internet] 2017 [cited 2023 Jun 22];9(399). Available from: /pmc/articles/PMC5762203/

131. Morgan RA, Yang JC, Kitano M, Dudley ME, Laurencot CM, Rosenberg SA. Case Report of a Serious Adverse Event Following the Administration of T Cells Transduced With a Chimeric Antigen Receptor Recognizing ERBB2. Molecular Therapy [Internet] 2010 [cited 2023 Jun 22];18(4):843. Available from: /pmc/articles/PMC2862534/

132. Phase I Study of Autologous CAR T-Cells Targeting the B7-H3 Antigen in Recurrent Epithelial Ovarian - Full Text View - ClinicalTrials.gov [Internet]. [cited 2023 Jun 23];Available from: https://classic.clinicaltrials.gov/ct2/show/NCT04670068

133. Pilot Study of B7-H3 CAR-T in Treating Patients With Recurrent and Refractory Glioblastoma - Full Text View - ClinicalTrials.gov [Internet]. [cited 2023 Jun 23];Available from: https://classic.clinicaltrials.gov/ct2/show/NCT04385173?term=CAR+T+B7-H3&draw=2&rank=2

134. EGFR/B7H3 CAR-T on Lung Cancer and Triple Negative Breast Cancer - Full Text View - ClinicalTrials.gov [Internet]. [cited 2023 Jun 23];Available from: https://classic.clinicaltrials.gov/ct2/show/NCT05341492?term=CAR+T+B7-H3&draw=2&rank=8

135. Study Of B7H3 CAR-T Cells in Treating Advanced Liver Cancer - Full Text View - ClinicalTrials.gov [Internet]. [cited 2023 Jun 23];Available from: https://classic.clinicaltrials.gov/ct2/show/NCT05323201?term=CAR+T+B7-H3&draw=2&rank=9

136. CD276-targeted Chimeric Antigen Receptor T Cells in Treatment With Advanced Pancreatic Cancer - Full Text View - ClinicalTrials.gov [Internet]. [cited 2023 Jun

23];Available from: https://classic.clinicaltrials.gov/ct2/show/NCT05143151?term=CAR+T+B7-H3&draw=3&rank=19

137. Study of Anti-5T4 CAR-raNK Cell Therapy in Locally Advanced or Metastatic Solid Tumors - Full Text View - ClinicalTrials.gov [Internet]. [cited 2023 Jun 23];Available from: https://classic.clinicaltrials.gov/ct2/show/NCT05137275?term=allogeneic+CAR+solid&draw=2&rank=4

138. Allogeneic NKG2DL-targeting CAR γδ T Cells (CTM-N2D) in Advanced Cancers - Full Text View - ClinicalTrials.gov [Internet]. [cited 2023 Jun 23];Available from: https://classic.clinicaltrials.gov/ct2/show/NCT05302037?term=allogeneic+gamma+delta+CAR+TUMOUR&draw=2&rank=4

139. Approved Cellular and Gene Therapy Products | FDA [Internet]. [cited 2023 Feb 24];Available from: https://www.fda.gov/vaccines-blood-biologics/cellular-gene-therapy-products/approved-cellular-and-gene-therapy-products

140. Chapoval AI, Ni J, Lau JS, Wilcox RA, Flies DB, Liu D, et al. B7-H3: A costimulatory molecule for T cell activation and IFN-γ production. Nat Immunol [Internet] 2001 [cited 2021 Jan 26];2(3):269–74. Available from: http://immunol.nature.com

141. Zhou YH, Chen YJ, Ma ZY, Xu L, Wang Q, Zhang GB, et al. 4IgB7-H3 is the major isoform expressed on immunocytes as well as malignant cells. Tissue Antigens [Internet] 2007 [cited 2023 Jun 18];70(2):96–104. Available from: https://onlinelibrary.wiley.com/doi/full/10.1111/j.1399-0039.2007.00853.x

142. Chapoval AI, Ni J, Lau JS, Wilcox RA, Flies DB, Liu D, et al. B7-H3: A costimulatory molecule for T cell activation and IFN-γ production. Nature Immunology 2001 2:3 [Internet] 2001 [cited 2023 Jun 18];2(3):269–74. Available from: https://www.nature.com/articles/ni0301_269

143. Suh WK, Gajewska BU, Okada H, Gronski MA, Bertram EM, Dawicki W, et al. The B7 family member B7-H3 preferentially down-regulates T helper type 1–mediated immune responses. Nature Immunology 2003 4:9 [Internet] 2003 [cited 2023 Jun 18];4(9):899–906. Available from: https://www.nature.com/articles/ni967

144. Luo L, Zhu G, Xu H, Yao S, Zhou G, Zhu Y, et al. B7-H3 Promotes Pathogenesis of Autoimmune Disease and Inflammation by Regulating the Activity of Different T Cell Subsets. PLoS One [Internet] 2015 [cited 2023 Jun 18];10(6). Available from: /pmc/articles/PMC4465912/

145. Lee YH, Martin-Orozco N, Zheng P, Li J, Zhang P, Tan H, et al. Inhibition of the B7-H3 immune checkpoint limits tumor growth by enhancing cytotoxic lymphocyte function. Cell Res [Internet] 2017 [cited 2023 Jun 18];27(8):1034. Available from: /pmc/articles/PMC5539354/

146. Lee YH, Martin-Orozco N, Zheng P, Li J, Zhang P, Tan H, et al. Inhibition of the B7-H3 immune checkpoint limits tumor growth by enhancing cytotoxic lymphocyte function. Cell Res 2017;27(8):1034–45.

147. Zhang J, Wang J, Marzese DM, Wang X, Yang Z, Li C, et al. B7H3 regulates differentiation and serves as a potential biomarker and theranostic target for human glioblastoma. Laboratory Investigation 2019;99(8):1117–29.

148. Dong P, Xiong Y, Yue J, Hanley SJB, Watari H. B7H3 As a promoter of metastasis and promising therapeutic target. Front Oncol2018;8(JUL).

149. Yamato I, Sho M, Nomi T, Akahori T, Shimada K, Hotta K, et al. Clinical importance of B7-H3 expression in human pancreatic cancer. Br J Cancer 2009;101(10):1709–16.

150. Data from MacroGenics' Ongoing Phase 1 Study of Enoblituzumab (MGA271) Presented at 30th Annual SITC Meeting 2015.

151. Shenderov E, De Marzo AM, Lotan TL, Wang H, Chan S, Lim SJ, et al. Neoadjuvant enoblituzumab in localized prostate cancer: a single-arm, phase 2 trial. Nature Medicine 2023 29:4 [Internet] 2023 [cited 2023 Jun 19];29(4):888–97. Available from: https://www.nature.com/articles/s41591-023-02284-w

152. Kramer K, Pandit-Taskar N, Kushner BH, Zanzonico P, Humm JL, Tomlinson U, et al. Phase 1 study of intraventricular 131I-omburtamab targeting B7H3 (CD276)-expressing CNS malignancies. J Hematol Oncol [Internet] 2022 [cited 2023 Jun 19];15(1):1–12. Available from: https://jhoonline.biomedcentral.com/articles/10.1186/s13045-022-01383-4

153. Tang X, Wang Y, Huang J, Zhang Z, Liu F, Xu J, et al. Administration of B7-H3 targeted chimeric antigen receptor-T cells induce regression of glioblastoma. Signal Transduction and Targeted Therapy 2021 6:1 [Internet] 2021 [cited 2023 Jun 22];6(1):1–3. Available from: https://www.nature.com/articles/s41392-021-00505-7

154. Brown CE, Alizadeh D, Starr R, Weng L, Wagner JR, Naranjo A, et al. Regression of Glioblastoma after Chimeric Antigen Receptor T-Cell Therapy. New England Journal of Medicine [Internet] 2016 [cited 2023 Jun 22];375(26):2561–9. Available from: https://www.nejm.org/doi/full/10.1056/nejmoa1610497

155. Nucleotide BLAST: Search nucleotide databases using a nucleotide query [Internet]. [cited 2023 Jan 20];Available from: https://blast.ncbi.nlm.nih.gov/Blast.cgi?PROGRAM=blastn&PAGE_TYPE=BlastSearch&LINK_LOC=blasthome

156. Capsomidis A, Benthall G, Van Acker HH, Fisher J, Kramer AM, Abeln Z, et al. Chimeric Antigen Receptor-Engineered Human Gamma Delta T Cells: Enhanced Cytotoxicity with Retention of Cross Presentation. Mol Ther 2018;26(2):354–65.

157. Kavanagh KL, Guo K, Dunford JE, Wu X, Knapp S, Ebetino FH, et al. The molecular mechanism of nitrogen-containing bisphosphonates as antiosteoporosis drugs. Proc Natl Acad Sci U S A 2006;103(20):7829.

158. Roelofs AJ, Jauhiainen M, Mönkkönen H, Rogers MJ, Mönkkönen J, Thompson K. Peripheral blood monocytes are responsible for γδ T cell activation induced by zoledronic acid through accumulation of IPP/DMAPP. Br J Haematol 2009;144(2):245–50.

159. Vavassori S, Kumar A, Wan GS, Ramanjaneyulu GS, Cavallari M, El Daker S, et al. Butyrophilin 3A1 binds phosphorylated antigens and stimulates human γδ T cells. Nature Immunology 2013 14:9 [Internet] 2013 [cited 2023 Jun 17];14(9):908–16. Available from: https://www.nature.com/articles/ni.2665

160. Meraviglia S, Eberl M, Vermijlen D, Todaro M, Buccheri S, Cicero G, et al. In vivo manipulation of V9V2 T cells with zoledronate and low-dose interleukin-2 for immunotherapy of advanced breast cancer patients. Clin Exp Immunol 2010;161(2):290–7.

161. Kakimi K, Matsushita H, Masuzawa K, Karasaki T, Kobayashi Y, Nagaoka K, et al. Adoptive transfer of zoledronate-expanded autologous Vγ9Vδ2 T-cells in patients with treatment-refractory non-small-cell lung cancer: a multicenter, open-label, single-arm, phase 2 study. J Immunother Cancer 2020;8:1185.

162. Fisher JPH, Heuijerjans J, Yan M, Gustafsson K, Anderson J. γδ T cells for cancer immunotherapy: A systematic review of clinical trials. Oncoimmunology [Internet] 2014 [cited 2023 Jun 30];3(1). Available from: /pmc/articles/PMC3984269/

163. Mensurado S, Blanco-Domínguez R, Silva-Santos B. The emerging roles of γδ T cells in cancer immunotherapy. Nature Reviews Clinical Oncology 2023 20:3 [Internet] 2023 [cited 2023 Jun 30];20(3):178–91. Available from: https://www.nature.com/articles/s41571-022-00722-1

164. Xu Y, Xiang Z, Alnaggar M, Kouakanou L, Li J, He J, et al. Allogeneic Vγ9Vδ2 T-cell immunotherapy exhibits promising clinical safety and prolongs the survival of patients with late-stage lung or liver cancer. Cell Mol Immunol 2020;1–13.

165. Correia D V., Fogli M, Hudspeth K, Gomes Da Silva M, Mavilio D, Silva-Santos B. Differentiation of human peripheral blood Vδ1+ T cells expressing the natural cytotoxicity receptor NKp30 for recognition of lymphoid leukemia cells. Blood 2011;118(4):992–1001.

166. Wu D, Wu P, Wu X, Ye J, Wang Z, Zhao S, et al. Ex vivo expanded human circulating vδ1 γδT cells exhibit favorable therapeutic potential for colon cancer. Oncoimmunology [Internet] 2015 [cited 2021 Jan 25];4(3):1–13. Available from: /pmc/articles/PMC4404819/?report=abstract

167. Almeida AR, Correia D V., Fernandes-Platzgummer A, Da Silva CL, Da Silva MG, Anjos DR, et al. Delta one T cells for immunotherapy of chronic lymphocytic leukemia: Clinical-grade expansion/differentiation and preclinical proof of concept. Clinical Cancer Research 2016;22(23):5795–804.

168. Makkouk A, Yang X, Barca T, Lucas A, Turkoz M, S Wong JT, et al. Off-the-shelf Vδ1 gamma delta T cells engineered with glypican-3 (GPC-3)-specific chimeric antigen receptor (CAR) and soluble IL-15 display robust antitumor efficacy against hepatocellular carcinoma. J Immunother Cancer [Internet] 2021 [cited 2023 Feb 23];9:3441. Available from: http://jitc.bmj.com/

169. Ferry GM, Agbuduwe C, Forrester M, Dunlop S, Chester K, Fisher J, et al. A Simple and Robust Single-Step Method for CAR-Vδ1 γδT Cell Expansion and Transduction for Cancer Immunotherapy. Front Immunol 2022;13:2419.

170. Waldmann TA. The shared and contrasting roles of interleukin-2 (IL-2) and IL-15 in the life and death of normal and neoplastic lymphocytes: implications for cancer therapy. Cancer Immunol Res [Internet] 2015 [cited 2023 Feb 23];3(3):219. Available from: /pmc/articles/PMC4351780/

171. Nagae M, Soga K, Morita-Matsumoto K, Hanashima S, Ikeda A, Yamamoto K, et al. Phytohemagglutinin from Phaseolus vulgaris (PHA-E) displays a novel glycan recognition mode using a common legume lectin fold. Glycobiology 2014;24(4):368–78.

172. Hamelryck TW, Dao-Thi MH, Poortmans F, Chrispeels MJ, Wyns L, Loris R. The crystallographic structure of phytohemagglutinin-L. Journal of Biological Chemistry 1996;271(34):20479–85.

173. Valentine MA, Tsoukas CD, Rhodes G, Vaughan JH, Carson DA. Phytohemagglutinin binds to the 20-kDa molecule of the T3 complex. Eur J Immunol 1985;15(8):851–4.

174. Morath A, Schamel WW. αβ and γδ T cell receptors: Similar but different. J Leukoc Biol 2020;107(6):1045–55.

175. Nicolas L, Monneret G, Debard AL, Blesius A, Gutowski MC, Salles G, et al. Human γδ T cells express a higher TCR/CD3 complex density than αβ T cells. Clinical Immunology 2001;98(3):358–63.

176. Hong JJ, Amancha PK, Rogers K, Ansari AA, Villinger F. Re-Evaluation of PD-1 Expression by T Cells as a Marker for Immune Exhaustion during SIV Infection. PLoS One [Internet] 2013 [cited 2023 Feb 23];8(3):e60186. Available from: https://journals.plos.org/plosone/article?id=10.1371/journal.pone.0060186

177. Kinter AL, Godbout EJ, McNally JP, Sereti I, Roby GA, O'Shea MA, et al. The Common γ-Chain Cytokines IL-2, IL-7, IL-15, and IL-21 Induce the Expression of Programmed Death-1 and Its Ligands. The Journal of Immunology [Internet] 2008 [cited 2023 Feb 23];181(10):6738–46. Available from: https://journals.aai.org/jimmunol/article/181/10/6738/38631/The-Common-Chain-Cytokines-IL-2-IL-7-IL-15-and-IL

178. Naldini L, Blömer U, Gallay P, Ory D, Mulligan R, Gage FH, et al. In vivo gene delivery and stable transduction of nondividing cells by a lentiviral vector. Science (1979) [Internet] 1996 [cited 2023 Jun 23];272(5259):263–7. Available from: https://www.science.org

179. Jarrosson-Wuilleme L, Goujon C, Bernaud J, Rigal D, Darlix JL, Cimarelli A. Transduction of Nondividing Human Macrophages with Gammaretrovirus-Derived Vectors. J Virol [Internet] 2006 [cited 2023 Jun 23];80(3):1152. Available from: /pmc/articles/PMC1346929/

180. Lukjanov V, Koutná I, Šimara P. CAR T-Cell Production Using Nonviral Approaches. J Immunol Res [Internet] 2021 [cited 2023 Jun 23];2021. Available from: /pmc/articles/PMC8019376/

181. Yant SR, Meuse L, Chiu W, Ivics Z, Izsvak Z, Kay MA. Somatic integration and long-term transgene expression in normal and haemophilic mice using a DNA transposon

system. Nat Genet [Internet] 2000 [cited 2023 Jun 23];25(1):35–41. Available from: https://pubmed.ncbi.nlm.nih.gov/10802653/

182. Harris E, Elmer JJ. Optimization of electroporation and other non-viral gene delivery strategies for T cells. Biotechnol Prog [Internet] 2021 [cited 2023 Jun 23];37(1):e3066. Available from: https://onlinelibrary.wiley.com/doi/full/10.1002/btpr.3066

183. Billingsley MM, Singh N, Ravikumar P, Zhang R, June CH, Mitchell MJ. Ionizable Lipid Nanoparticle-Mediated mRNA Delivery for Human CAR T Cell Engineering. Nano Lett [Internet] 2020 [cited 2023 Jun 23];20(3):1578. Available from: /pmc/articles/PMC7313236/

184. Birley K. Development of novel B7-H3 targeted CAR therapy for neuroblastoma. Doctoral thesis, UCL (University College London) 2021;

185. Philip B, Kokalaki E, Mekkaoui L, Thomas S, Straathof K, Flutter B, et al. A highly compact epitope-based marker/suicide gene for easier and safer T-cell therapy. Blood [Internet] 2014 [cited 2023 Mar 8];124(8):1277–87. Available from: https://pubmed.ncbi.nlm.nih.gov/24970931/

186. Tang OY, Tian L, Yoder T, Xu R, Kulikovskaya I, Gupta M, et al. PD1 Expression in EGFRvIII-Directed CAR T Cell Infusion Product for Glioblastoma Is Associated with Clinical Response. Front Immunol 2022;13:2127.

187. Coffelt SB, Kersten K, Doornebal CW, Weiden J, Vrijland K, Hau CS, et al. IL-17-producing γδ T cells and neutrophils conspire to promote breast cancer metastasis. Nature 2015 522:7556 [Internet] 2015 [cited 2023 Mar 8];522(7556):345–8. Available from: https://www.nature.com/articles/nature14282

188. Silva-Santos B, Serre K, Norell H. γδ T cells in cancer. Nature Reviews Immunology 2015 15:11 [Internet] 2015 [cited 2023 Mar 8];15(11):683–91. Available from: https://www.nature.com/articles/nri3904

189. Van Acker HH, Anguille S, Willemen Y, Van Den Bergh JM, Berneman ZN, Lion E, et al. Interleukin-15 enhances the proliferation, stimulatory phenotype, and antitumor effector functions of human gamma delta T cells. J Hematol Oncol [Internet] 2016 [cited 2023 Mar 8];9(1):1–13. Available from: /pmc/articles/PMC5041439/

190. Gattinoni L, Schaft N, Van Acker HH, Anderson J, Aehnlich P, Micaela A, et al. Expansion With IL-15 Increases Cytotoxicity of Vγ9Vδ2 T Cells and Is Associated With Higher Levels of Cytotoxic Molecules and T-bet. Frontiers in Immunology | www.frontiersin.org [Internet] 2020 [cited 2023 Mar 8];1:1868. Available from: www.frontiersin.org

191. Van Acker HH, Anguille S, Willemen Y, Van Den Bergh JM, Berneman ZN, Lion E, et al. Interleukin-15 enhances the proliferation, stimulatory phenotype, and antitumor effector functions of human gamma delta T cells. J Hematol Oncol [Internet] 2016 [cited 2023 Mar 8];9(1):1–13. Available from: https://pubmed.ncbi.nlm.nih.gov/27686372/

192. Burton JD, Bamford RN, Peters C, Grant AJ, Kurys G, Goldman CK, et al. A lymphokine, provisionally designated interleukin T and produced by a human adult T-cell leukemia line, stimulates T-cell proliferation and the induction of lymphokine-activated killer

cells. Proc Natl Acad Sci U S A [Internet] 1994 [cited 2023 Apr 5];91(11):4935. Available from: /pmc/articles/PMC43904/?report=abstract

193. Grabstein KH, Eisenman J, Shanebeck K, Rauch C, Srinivasan S, Fung V, et al. Cloning of a T cell growth factor that interacts with the β chain of the interleukin-2 receptor. Science (1979) [Internet] 1994 [cited 2023 Apr 5];264(5161):965–8. Available from: https://www.science.org

194. Sugamura K, Asao H, Kondo M, Tanaka N, Ishii N, Ohbo K, et al. The Interleukin-2 Receptor γ Chain: Its Role in the Multiple Cytokine Receptor Complexes and T Cell Development in XSCID. https://doi.org/101146/annurev.immunol141179 [Internet] 2003 [cited 2023 Apr 5];14:179–205. Available from: https://www.annualreviews.org/doi/abs/10.1146/annurev.immunol.14.1.179

195. Waldmann TA. The biology of interleukin-2 and interleukin-15: implications for cancer therapy and vaccine design. Nature Reviews Immunology 2006 6:8 [Internet] 2006 [cited 2023 Mar 27];6(8):595–601. Available from: https://www.nature.com/articles/nri1901

196. Johnston JA, Bacon CM, Finbloomi DS, Rees RC, Kaplanii D, Shibuyaii K, et al. Tyrosine phosphorylation and activation of STAT5, STAT3, and Janus kinases by interleukins 2 and 15. 1995 [cited 2023 Apr 6];92:8705–9. Available from: https://www.pnas.org

197. Ring AM, Lin JX, Feng D, Mitra S, Rickert M, Bowman GR, et al. Mechanistic and structural insight into the functional dichotomy between interleukin-2 and interleukin-15. Nat Immunol [Internet] 2012 [cited 2023 Apr 7];13(12):1187. Available from: /pmc/articles/PMC3501574/

198. Lehours P, Raher S, Dubois S, Guo J, Godard A, Jacques Y. Subunit structure of the high and low affinity human interleukin-15 receptors. Eur Cytokine Netw [Internet] 2000 [cited 2023 Apr 6];11(2):207–15. Available from: https://www.jle.com/fr/revues/ecn/e-docs/subunit_structure_of_the_high_and_low_affinity_human_interleukin_15_receptors._90364/article.phtml?tab=texte

199. Ring AM, Lin JX, Feng D, Mitra S, Rickert M, Bowman GR, et al. Mechanistic and structural insight into the functional dichotomy between interleukin-2 and interleukin-15. Nat Immunol [Internet] 2012 [cited 2023 Apr 6];13(12):1187. Available from: /pmc/articles/PMC3501574/

200. Fontenot JD, Rasmussen JP, Gavin MA, Rudensky AY. A function for interleukin 2 in Foxp3-expressing regulatory T cells. Nature Immunology 2005 6:11 [Internet] 2005 [cited 2023 Apr 6];6(11):1142–51. Available from: https://www.nature.com/articles/ni1263

201. Refaeli Y, Van Parijs L, London CA, Tschopp J, Abbas AK. Biochemical mechanisms of IL-2-regulated Fas-mediated T cell apoptosis. Immunity [Internet] 1998 [cited 2023 Apr 6];8(5):615–23. Available from: https://pubmed.ncbi.nlm.nih.gov/9620682/

202. Dubois S, Mariner J, Waldmann TA, Tagaya Y. IL-15Rα Recycles and Presents IL-15 In trans to Neighboring Cells. Immunity 2002;17(5):537–47.

203. Chirifu M, Hayashi C, Nakamura T, Toma S, Shuto T, Yamagata Y, et al. Crystal structure of the IL-15–IL-15Rα complex, a cytokine-receptor unit presented in trans. Nature Immunology 2007 8:9 [Internet] 2007 [cited 2023 Apr 6];8(9):1001–7. Available from: https://www.nature.com/articles/ni1492

204. Mak TW, Saunders ME. Cytokines and Cytokine Receptors. The Immune Response 2006;463–516.

205. IL15 interleukin 15 [Homo sapiens (human)] - Gene - NCBI [Internet]. [cited 2023 Apr 6];Available from: https://www.ncbi.nlm.nih.gov/gene/3600

206. Osinalde N, Sanchez-Quiles V, Akimov V, Guerra B, Blagoev B, Kratchmarova I. Simultaneous dissection and comparison of IL-2 and IL-15 signaling pathways by global quantitative phosphoproteomics. Proteomics [Internet] 2015 [cited 2023 Apr 6];15(2–3):520–31. Available from: https://onlinelibrary.wiley.com/doi/full/10.1002/pmic.201400194

207. Morris R, Kershaw NJ, Babon JJ. The molecular details of cytokine signaling via the JAK/STAT pathway. Protein Sci [Internet] 2018 [cited 2023 Apr 12];27(12):1984. Available from: /pmc/articles/PMC6237706/

208. Feng J, Witthuhn BA, Matsuda T, Kohlhuber F, Kerr IM, Ihle JN. Activation of Jak2 Catalytic Activity Requires Phosphorylation of Y 1007 in the Kinase Activation Loop. Mol Cell Biol 1997;17(5):2497–501.

209. Morris R, Kershaw NJ, Babon JJ. The molecular details of cytokine signaling via the JAK/STAT pathway. Protein Sci [Internet] 2018 [cited 2023 Apr 12];27(12):1984. Available from: /pmc/articles/PMC6237706/

210. Miyazaki T, Kawahara A, Fujii H, Nakagawa Y, Minami Y, Liu ZJ, et al. Functional Activation of Jak1 and Jak3 by Selective Association with IL-2 Receptor Subunits. Science (1979) [Internet] 1994 [cited 2023 Apr 12];266(5187):1045–7. Available from: https://www.science.org/doi/10.1126/science.7973659

211. Hu X, li J, Fu M, Zhao X, Wang W. The JAK/STAT signaling pathway: from bench to clinic. Signal Transduction and Targeted Therapy 2021 6:1 [Internet] 2021 [cited 2023 Apr 12];6(1):1–33. Available from: https://www.nature.com/articles/s41392-021-00791-1

212. Levy DE, Darnell JE. STATs: transcriptional control and biological impact. Nature Reviews Molecular Cell Biology 2002 3:9 [Internet] 2002 [cited 2023 Apr 12];3(9):651–62. Available from: https://www.nature.com/articles/nrm909

213. Quelle FW, Shimoda K, Thierfelder W, Fischer C, Kim A, Ruben SM, et al. Cloning of murine Stat6 and human Stat6, Stat proteins that are tyrosine phosphorylated in responses to IL-4 and IL-3 but are not required for mitogenesis. Mol Cell Biol [Internet] 1995 [cited 2023 Apr 12];15(6):3336. Available from: /pmc/articles/PMC230567/?report=abstract

214. Hou J, Schindler U, Henzel WJ, Wong SC, McKnight SL. Identification and purification of human stat proteins activated in response to interleukin-2. Immunity 1995;2(4):321–9.

215. Araujo ED de, Orlova A, Neubauer HA, Bajusz D, Seo HS, Dhe-Paganon S, et al. Structural Implications of STAT3 and STAT5 SH2 Domain Mutations. Cancers (Basel) [Internet] 2019 [cited 2023 Apr 13];11(11). Available from: /pmc/articles/PMC6895964/

216. Jenks JA, Seki S, Kanai T, Huang J, Morgan AA, Scalco RC, et al. Differentiating the roles of STAT5B and STAT5A in human CD4+ T cells. Clin Immunol [Internet] 2013 [cited 2023 Apr 13];148(2):227. Available from: /pmc/articles/PMC4169138/

217. Teglund S, McKay C, Schuetz E, Van Deursen JM, Stravopodis D, Wang D, et al. Stat5a and Stat5b Proteins Have Essential and Nonessential, or Redundant, Roles in Cytokine Responses. Cell 1998;93(5):841–50.

218. Kanai T, Seki S, Jenks JA, Kohli A, Kawli T, Martin DP, et al. Identification of STAT5A and STAT5B Target Genes in Human T Cells. PLoS One [Internet] 2014 [cited 2023 Apr 13];9(1):86790. Available from: /pmc/articles/PMC3907443/

219. Mishra A, Sullivan L, Caligiuri MA. Molecular Pathways: Interleukin-15 Signaling in Health and in Cancer. Clin Cancer Res [Internet] 2014 [cited 2023 Apr 13];20(8):2044. Available from: /pmc/articles/PMC3989546/

220. Rawlings JS, Rosler KM, Harrison DA. The JAK/STAT signaling pathway. J Cell Sci [Internet] 2004 [cited 2023 Apr 13];117(8):1281–3. Available from: https://journals.biologists.com/jcs/article/117/8/1281/28255/The-JAK-STAT-signaling-pathway

221. Kanai T, Seki S, Jenks JA, Kohli A, Kawli T, Martin DP, et al. Identification of STAT5A and STAT5B Target Genes in Human T Cells. PLoS One [Internet] 2014 [cited 2023 Apr 13];9(1):86790. Available from: /pmc/articles/PMC3907443/

222. Starr R, Willson TA, Viney EM, Murray LJL, Rayner JR, Jenkins BJ, et al. A family of cytokine-inducible inhibitors of signalling. Nature 1997 387:6636 [Internet] 1997 [cited 2023 Apr 13];387(6636):917–21. Available from: https://www.nature.com/articles/43206

223. Seif F, Khoshmirsafa M, Aazami H, Mohsenzadegan M, Sedighi G, Bahar M. The role of JAK-STAT signaling pathway and its regulators in the fate of T helper cells. Cell Communication and Signaling 2017 15:1 [Internet] 2017 [cited 2023 Apr 13];15(1):1–13. Available from: https://biosignaling.biomedcentral.com/articles/10.1186/s12964-017-0177-y

224. Endo TA, Masuhara M, Yokouchi M, Suzuki R, Sakamoto H, Mitsui K, et al. A new protein containing an SH2 domain that inhibits JAK kinases. Nature 1997 387:6636 [Internet] 1997 [cited 2023 Apr 13];387(6636):921–4. Available from: https://www.nature.com/articles/43213

225. Andersen JN, Mortensen OH, Peters GH, Drake PG, Iversen LF, Olsen OH, et al. Structural and Evolutionary Relationships among Protein Tyrosine Phosphatase Domains. https://doi.org/101128/MCB21217117-71362001 [Internet] 2023 [cited 2023 Apr 13];21(21):7117–36. Available from: https://www.tandfonline.com/doi/abs/10.1128/MCB.21.21.7117-7136.2001

226. Hu X, li J, Fu M, Zhao X, Wang W. The JAK/STAT signaling pathway: from bench to clinic. Signal Transduction and Targeted Therapy 2021 6:1 [Internet] 2021 [cited 2023 Apr 13];6(1):1–33. Available from: https://www.nature.com/articles/s41392-021-00791-1

227. Gai L, Zhu Y, Zhang C, Meng X. Targeting Canonical and Non-Canonical STAT Signaling Pathways in Renal Diseases. Cells [Internet] 2021 [cited 2023 Apr 13];10(7). Available from: /pmc/articles/PMC8305338/

228. Mohr A, Chatain N, Domoszlai T, Rinis N, Sommerauer M, Vogt M, et al. Dynamics and non-canonical aspects of JAK/STAT signalling. Eur J Cell Biol 2012;91(6–7):524–32.

229. Ruff-Jamison S, Zhong Z, Wen Z, Chen K, Darnell JE, Cohen S. Epidermal growth factor and lipopolysaccharide activate Stat3 transcription factor in mouse liver. Journal of Biological Chemistry 1994;269(35):21933–5.

230. Dur Valgeirsdoâ Ttir S, Paukku K, Silvennoinen O, Heldin CH, Claesson-Welsh L. Activation of Stat5 by platelet-derived growth factor (PDGF) is dependent on phosphorylation sites in PDGF b-receptor juxtamembrane and kinase insert domains. 1998;

231. Vainchenker W, Kralovics R. Genetic basis and molecular pathophysiology of classical myeloproliferative neoplasms. Blood [Internet] 2017 [cited 2023 Apr 13];129(6):667–79. Available from: https://ashpublications.org/blood/article/129/6/667/36324/Genetic-basis-and-molecular-pathophysiology-of

232. Flex E, Petrangeli V, Stella L, Chiaretti S, Hornakova T, Knoops L, et al. Somatically acquired JAK1 mutations in adult acute lymphoblastic leukemia. J Exp Med [Internet] 2008 [cited 2023 Apr 14];205(4):751. Available from: /pmc/articles/PMC2292215/

233. Kofoed EM, Hwa V, Little B, Woods KA, Buckway CK, Tsubaki J, et al. Growth Hormone Insensitivity Associated with a STAT5b Mutation . New England Journal of Medicine [Internet] 2003 [cited 2023 Apr 14];349(12):1139–47. Available from: https://www.nejm.org/doi/10.1056/NEJMoa022926

234. de Araujo ED, Erdogan F, Neubauer HA, Meneksedag-Erol D, Manaswiyoungkul P, Eram MS, et al. Structural and functional consequences of the STAT5BN642H driver mutation. Nature Communications 2019 10:1 [Internet] 2019 [cited 2023 Apr 14];10(1):1–15. Available from: https://www.nature.com/articles/s41467-019-10422-7

235. Küçük C, Jiang B, Hu X, Zhang W, Chan JKC, Xiao W, et al. Activating mutations of STAT5B and STAT3 in lymphomas derived from γδ-T or NK cells. Nat Commun [Internet] 2015 [cited 2023 Apr 14];6:6025. Available from: /pmc/articles/PMC7743911/

236. Farrar MA. Design and Use of Constitutively Active STAT5 Constructs. Methods Enzymol 2010;485(C):583–96.

237. Transcript: ENST00000293328.8 (STAT5B-201) - cDNA sequence - Homo_sapiens - Ensembl genome browser 109 [Internet]. [cited 2023 Mar 24];Available from:

https://www.ensembl.org/Homo_sapiens/Transcript/Sequence_cDNA?db=core;g=ENSG00000173757;r=17:42199176-42288633;t=ENST00000293328

238. Conlon KC, Lake Potter E, Pittaluga S, Lee CCR, Miljkovic MD, Fleisher TA, et al. IL-15 by continuous i.v. infusion to adult patients with solid tumors in a Phase I trial induced dramatic NK cell subset expansion. Clin Cancer Res [Internet] 2019 [cited 2023 Mar 27];25(16):4945. Available from: /pmc/articles/PMC6697593/

239. Bandapalli OR, Schuessele S, Kunz JB, Rausch T, Stütz AM, Tal N, et al. The activating STAT5B N642H mutation is a common abnormality in pediatric T-cell acute lymphoblastic leukemia and confers a higher risk of relapse. Haematologica [Internet] 2014 [cited 2023 Apr 3];99(10):e188. Available from: /pmc/articles/PMC4181267/

240. Pham HTT, Maurer B, Prchal-Murphy M, Grausenburger R, Grundschober E, Javaheri T, et al. STAT5BN642H is a driver mutation for T cell neoplasia. J Clin Invest [Internet] 2018 [cited 2023 Apr 3];128(1):387. Available from: /pmc/articles/PMC5749501/

241. Rajala HLM, Eldfors S, Kuusanmäki H, Van Adrichem AJ, Olson T, Lagström S, et al. Discovery of somatic STAT5b mutations in large granular lymphocytic leukemia. Blood [Internet] 2013 [cited 2023 Apr 3];121(22):4541–50. Available from: https://ashpublications.org/blood/article/121/22/4541/31378/Discovery-of-somatic-STAT5b-mutations-in-large

242. de Araujo ED, Erdogan F, Neubauer HA, Meneksedag-Erol D, Manaswiyoungkul P, Eram MS, et al. Structural and functional consequences of the STAT5BN642H driver mutation. Nature Communications 2019 10:1 [Internet] 2019 [cited 2023 Apr 2];10(1):1–15. Available from: https://www.nature.com/articles/s41467-019-10422-7

243. Philip B, Kokalaki E, Mekkaoui L, Thomas S, Straathof K, Flutter B, et al. A highly compact epitope-based marker/suicide gene for easier and safer T-cell therapy. Blood [Internet] 2014 [cited 2023 Apr 3];124(8):1277–87. Available from: https://ashpublications.org/blood/article/124/8/1277/33527/A-highly-compact-epitope-based-marker-suicide-gene

244. Pham HTT, Maurer B, Prchal-Murphy M, Grausenburger R, Grundschober E, Javaheri T, et al. STAT5BN642H is a driver mutation for T cell neoplasia. J Clin Invest [Internet] 2018 [cited 2023 Apr 3];128(1):387. Available from: /pmc/articles/PMC5749501/

245. Melenhorst JJ, Chen GM, Wang M, Porter DL, Chen C, Collins MKA, et al. Decade-long leukaemia remissions with persistence of CD4+ CAR T cells. Nature 2022 602:7897 [Internet] 2022 [cited 2023 Apr 5];602(7897):503–9. Available from: https://www.nature.com/articles/s41586-021-04390-6

246. Wittibschlager V, Bacher U, Seipel K, Porret N, Wiedemann G, Haslebacher C, et al. CAR T-Cell Persistence Correlates with Improved Outcome in Patients with B-Cell Lymphoma. Int J Mol Sci [Internet] 2023 [cited 2023 Apr 5];24(6):5688. Available from: https://www.mdpi.com/1422-0067/24/6/5688/htm

247. McKeown SR. Defining normoxia, physoxia and hypoxia in tumours—implications for treatment response. Br J Radiol [Internet] 2014 [cited 2023 Jan 7];87(1035). Available from: /pmc/articles/PMC4064601/

248. Thiruthaneeswaran N, Bibby BAS, Yang L, Hoskin PJ, Bristow RG, Choudhury A, et al. Lost in application: Measuring hypoxia for radiotherapy optimisation. Eur J Cancer 2021;148:260–76.

249. Noman MZ, Hasmim M, Lequeux A, Xiao M, Duhem C, Chouaib S, et al. Improving Cancer Immunotherapy by Targeting the Hypoxic Tumor Microenvironment: New Opportunities and Challenges. Cells 2019, Vol 8, Page 1083 [Internet] 2019 [cited 2023 Jan 7];8(9):1083. Available from: https://www.mdpi.com/2073-4409/8/9/1083/htm

250. Carreau A, Hafny-Rahbi B el, Matejuk A, Grillon C, Kieda C. Why is the partial oxygen pressure of human tissues a crucial parameter? Small molecules and hypoxia. J Cell Mol Med 2011;15(6):1239–53.

251. Fyles AW, Milosevic M, Wong R, Kavanagh MC, Pintilie M, Sun A, et al. Oxygenation predicts radiation response and survival in patients with cervix cancer. Radiother Oncol [Internet] 1998 [cited 2023 Jan 7];48(2):149–56. Available from: https://pubmed.ncbi.nlm.nih.gov/9783886/

252. Sundfør K, Lyng H, Tropé CG, Rofstad EK. Treatment outcome in advanced squamous cell carcinoma of the uterine cervix: relationships to pretreatment tumor oxygenation and vascularization. Radiother Oncol [Internet] 2000 [cited 2023 Jan 7];54(2):101–7. Available from: https://pubmed.ncbi.nlm.nih.gov/10699471/

253. Nordsmark M, Bentzen SM, Rudat V, Brizel D, Lartigau E, Stadler P, et al. Prognostic value of tumor oxygenation in 397 head and neck tumors after primary radiation therapy. An international multi-center study. Radiotherapy and Oncology 2005;77(1):18–24.

254. Rajaganeshan R, Prasad R, Guillou PJ, Poston G, Scott N, Jayne DG. The role of hypoxia in recurrence following resection of Dukes' B colorectal cancer. Int J Colorectal Dis [Internet] 2008 [cited 2023 Jan 7];23(11):1049–55. Available from: https://pubmed.ncbi.nlm.nih.gov/18594846/

255. Milosevic M, Warde P, Meńard C, Chung P, Toi A, Ishkanian A, et al. Tumor hypoxia predicts biochemical failure following radiotherapy for clinically localized prostate cancer. Clin Cancer Res [Internet] 2012 [cited 2023 Jan 7];18(7):2108–14. Available from: https://pubmed.ncbi.nlm.nih.gov/22465832/

256. GRAY LH, CONGER AD, EBERT M, HORNSEY S, SCOTT OC. The concentration of oxygen dissolved in tissues at the time of irradiation as a factor in radiotherapy. Br J Radiol [Internet] 1953 [cited 2023 Jan 8];26(312):638–48. Available from: https://pubmed.ncbi.nlm.nih.gov/13106296/

257. Vaupel P, Schlenger K, Knoop C, Höckel M. Oxygenation of human tumors: evaluation of tissue oxygen distribution in breast cancers by computerized O2 tension measurements. Cancer Res 1991;51(12):3316–22.

258. The Nobel Prize in Physiology or Medicine 2019 [Internet]. [cited 2023 Jan 8];Available from: https://www.nobelprize.org/prizes/medicine/2019/summary/

259. Semenza GL, Wang GL. A nuclear factor induced by hypoxia via de novo protein synthesis binds to the human erythropoietin gene enhancer at a site required for

transcriptional activation. Mol Cell Biol [Internet] 1992 [cited 2023 Jan 8];12(12):5447. Available from: /pmc/articles/PMC360482/?report=abstract

260. Wang GL, Jiang BH, Rue EA, Semenza GL. Hypoxia-inducible factor 1 is a basic-helix-loop-helix-PAS heterodimer regulated by cellular O2 tension. Proc Natl Acad Sci U S A [Internet] 1995 [cited 2023 Jan 8];92(12):5510. Available from: /pmc/articles/PMC41725/?report=abstract

261. Luo Z, Tian M, Yang G, Tan Q, Chen Y, Li G, et al. Hypoxia signaling in human health and diseases: implications and prospects for therapeutics. Signal Transduction and Targeted Therapy 2022 7:1 [Internet] 2022 [cited 2023 Jan 3];7(1):1–30. Available from: https://www.nature.com/articles/s41392-022-01080-1

262. Ratcliffe PJ. HIF-1 and HIF-2: Working alone or together in hypoxia? Journal of Clinical Investigation 2007;117(4):862–5.

263. Makino Y, Kanopka A, Wilson WJ, Tanaka H, Poellinger L. Inhibitory PAS Domain Protein (IPAS) Is a Hypoxia-inducible Splicing Variant of the Hypoxia-inducible Factor-3α Locus. Journal of Biological Chemistry 2002;277(36):32405–8.

264. Fukuda R, Hirota K, Fan F, Jung Y do, Ellis LM, Semenza GL. Insulin-like Growth Factor 1 Induces Hypoxia-inducible Factor 1-mediated Vascular Endothelial Growth Factor Expression, Which is Dependent on MAP Kinase and Phosphatidylinositol 3-Kinase Signaling in Colon Cancer Cells. Journal of Biological Chemistry 2002;277(41):38205–11.

265. Jaakkola P, Mole DR, Tian YM, Wilson MI, Gielbert J, Gaskell SJ, et al. Targeting of HIF-α to the von Hippel-Lindau ubiquitylation complex by O2-regulated prolyl hydroxylation. Science (1979) [Internet] 2001 [cited 2023 Jan 9];292(5516):468–72. Available from: https://www.science.org/doi/10.1126/science.1059796

266. Pugh CW, Ratcliffe PJ. Regulation of angiogenesis by hypoxia: role of the HIF system. Nature Medicine 2003 9:6 [Internet] 2003 [cited 2023 Jan 8];9(6):677–84. Available from: https://www.nature.com/articles/nm0603-677

267. Lando D, Peet DJ, Gorman JJ, Whelan DA, Whitelaw ML, Bruick RK. FIH-1 is an asparaginyl hydroxylase enzyme that regulates the transcriptional activity of hypoxia-inducible factor. Genes Dev [Internet] 2002 [cited 2023 Jan 8];16(12):1466. Available from: /pmc/articles/PMC186346/

268. Semenza GL, Jiang BH, Leung SW, Passantino R, Concordat JP, Maire P, et al. Hypoxia Response Elements in the Aldolase A, Enolase 1, and Lactate Dehydrogenase A Gene Promoters Contain Essential Binding Sites for Hypoxia-inducible Factor 1. Journal of Biological Chemistry 1996;271(51):32529–37.

269. Wu D, Potluri N, Lu J, Kim Y, Rastinejad F. Structural integration in hypoxia-inducible factors. Nature [Internet] 2015;524(7565):303–8. Available from: https://doi.org/10.1038/nature14883

270. Ortiz-Barahona A, Villar D, Pescador N, Amigo J, del Peso L. Genome-wide identification of hypoxia-inducible factor binding sites and target genes by a probabilistic model integrating transcription-profiling data and in silico binding site

prediction. Nucleic Acids Res [Internet] 2010 [cited 2023 Jan 8];38(7):2332–45. Available from: https://academic.oup.com/nar/article/38/7/2332/3100568

271. Semenza GL. Targeting HIF-1 for cancer therapy. Nature Reviews Cancer 2003 3:10 [Internet] 2003 [cited 2023 Jan 8];3(10):721–32. Available from: https://www.nature.com/articles/nrc1187

272. al Tameemi W, Dale TP, Al-Jumaily RMK, Forsyth NR. Hypoxia-Modified Cancer Cell Metabolism. Front Cell Dev Biol 2019;7:4.

273. Harris AL. Hypoxia — a key regulatory factor in tumour growth. Nature Reviews Cancer 2002 2:1 [Internet] 2002 [cited 2023 Jan 9];2(1):38–47. Available from: https://www.nature.com/articles/nrc704

274. Zhong H, de Marzo AM, Laughner E, Lim M, Hilton DA, Zagzag D, et al. Overexpression of hypoxia-inducible factor 1alpha in common human cancers and their metastases. Cancer Res 1999;59(22):5830–5.

275. Elhoseiny MS, Abdelfattah MR, el Gendy OS. Hypoxia-inducible factor 1 alpha (HIF-1α) and its prognostic value in acute myeloid leukemia. Hematology & Transfusion International Journal [Internet] 2017 [cited 2023 Jan 9];Volume 4(Issue 1). Available from: https://medcraveonline.com/HTIJ/HTIJ-04-00073.php

276. Griggio V, Vitale C, Todaro M, Riganti C, Kopecka J, Salvetti C, et al. HIF-1α is over-expressed in leukemic cells from TP53-disrupted patients and is a promising therapeutic target in chronic lymphocytic leukemia. Haematologica [Internet] 2020 [cited 2023 Jan 9];105(4):1042–54. Available from: https://haematologica.org/article/view/9339

277. Ghosh AK, Shanafelt TD, Cimmino A, Taccioli C, Volinia S, Liu CG, et al. Aberrant regulation of pVHL levels by microRNA promotes the HIF/VEGF axis in CLL B cells. Blood [Internet] 2009 [cited 2023 Jan 9];113(22):5568–74. Available from: https://ashpublications.org/blood/article/113/22/5568/107745/Aberrant-regulation-of-pVHL-levels-by-microRNA

278. Ringshausen I, Schneller F, Bogner C, Hipp S, Duyster J, Peschel C, et al. Constitutively activated phosphatidylinositol-3 kinase (PI-3K) is involved in the defect of apoptosis in B-CLL: association with protein kinase Cδ. Blood [Internet] 2002 [cited 2023 Jan 9];100(10):3741–8. Available from: https://ashpublications.org/blood/article/100/10/3741/106361/Constitutively-activated-phosphatidylinositol-3

279. Ding X chen, Wang L liang, Zhang X dong, Xu J long, Li P feng, Liang H, et al. The relationship between expression of PD-L1 and HIF-1α in glioma cells under hypoxia. J Hematol Oncol [Internet] 2021 [cited 2023 Jan 9];14(1):1–5. Available from: https://jhoonline.biomedcentral.com/articles/10.1186/s13045-021-01102-5

280. Bailey CM, Liu Y, Liu M, Du X, Devenport M, Zheng P, et al. Targeting HIF-1α abrogates PD-L1–mediated immune evasion in tumor microenvironment but promotes tolerance in normal tissues. J Clin Invest [Internet] 2022 [cited 2023 Jan 9];132(9). Available from: https://doi.org/10.1172/JCI159473

281. Lau EYT, Ho NPY, Lee TKW. Cancer stem cells and their microenvironment: Biology and therapeutic implications. Stem Cells Int 2017;2017.

282. Liberti M v., Locasale JW. The Warburg Effect: How Does it Benefit Cancer Cells? Trends Biochem Sci 2016;41(3):211–8.

283. Warburg Berlin-Dahlem O. THE METABOLISM OF CARCINOMA CELLS. [cited 2023 Jan 10];Available from: http://aacrjournals.org/jcancerres/article-pdf/9/1/148/2171202/148.pdf

284. Akakura N, Kobayashi M, Horiuchi I, Suzuki A, Wang J, Chen J, et al. Constitutive expression of hypoxia-inducible factor-1alpha renders pancreatic cancer cells resistant to apoptosis induced by hypoxia and nutrient deprivation. Cancer Res 2001;61(17):6548–54.

285. Semenza GL. The hypoxic tumor microenvironment: A driving force for breast cancer progression. Biochimica et Biophysica Acta (BBA) - Molecular Cell Research 2016;1863(3):382–91.

286. Gilkes DM, Semenza GL, Wirtz D. Hypoxia and the extracellular matrix: drivers of tumour metastasis. Nature Reviews Cancer 2014 14:6 [Internet] 2014 [cited 2023 Jan 10];14(6):430–9. Available from: https://www.nature.com/articles/nrc3726

287. Cramer T, Yamanishi Y, Clausen BE, Förster I, Pawlinski R, Mackman N, et al. HIF-1α Is Essential for Myeloid Cell-Mediated Inflammation. Cell 2003;112(5):645–57.

288. Yoshida N, Granger DN, Anderson DC, Rothlein R, Lane C, Kvietys PR. Anoxia/reoxygenation-induced neutrophil adherence to cultured endothelial cells. Am J Physiol [Internet] 1992 [cited 2023 Jan 11];262(6 Pt 2). Available from: https://pubmed.ncbi.nlm.nih.gov/1352432/

289. Laoui D, van Overmeire E, Conza G di, Aldeni C, Keirsse J, Morias Y, et al. Tumor hypoxia does not drive differentiation of tumor-associated macrophages but rather fine-tunes the M2-like macrophage population. Cancer Res [Internet] 2014 [cited 2023 Jan 11];74(1):24–30. Available from: https://aacrjournals.org/cancerres/article/74/1/24/592709/Tumor-Hypoxia-Does-Not-Drive-Differentiation-of

290. Yamada N, Yamanegi K, Ohyama H, Hata M, Nakasho K, Futani H, et al. Hypoxia downregulates the expression of cell surface MICA without increasing soluble MICA in osteosarcoma cellsin a HIF-1α-dependent manner. Int J Oncol [Internet] 2012 [cited 2023 Jan 11];41(6):2005–12. Available from: http://www.spandidos-publications.com/10.3892/ijo.2012.1630/abstract

291. Sceneay J, Chow MT, Chen A, Halse HM, Wong CSF, Andrews DM, et al. Primary tumor hypoxia recruits CD11b+/Ly6Cmed/ Ly6G+ immune suppressor cells and compromises NK cell cytotoxicity in the premetastatic niche. Cancer Res [Internet] 2012 [cited 2023 Jan 11];72(16):3906–11. Available from: https://aacrjournals.org/cancerres/article/72/16/3906/576031/Primary-Tumor-Hypoxia-Recruits-CD11b-Ly6Cmed-Ly6G

292. Caldwell CC, Kojima H, Lukashev D, Armstrong J, Farber M, Apasov SG, et al. Differential Effects of Physiologically Relevant Hypoxic Conditions on T Lymphocyte

Development and Effector Functions. The Journal of Immunology [Internet] 2001 [cited 2023 Jan 11];167(11):6140–9. Available from: https://journals.aai.org/jimmunol/article/167/11/6140/70529/Differential-Effects-of-Physiologically-Relevant

293. Finlay DK, Rosenzweig E, Sinclair L v., Carmen FC, Hukelmann JL, Rolf J, et al. PDK1 regulation of mTOR and hypoxia-inducible factor 1 integrate metabolism and migration of CD8+ T cells. J Exp Med [Internet] 2012 [cited 2023 Jan 11];209(13):2441. Available from: /pmc/articles/PMC3526360/

294. Chang CH, Qiu J, O'Sullivan D, Buck MD, Noguchi T, Curtis JD, et al. Metabolic Competition in the Tumor Microenvironment Is a Driver of Cancer Progression. Cell [Internet] 2015 [cited 2023 Jan 11];162(6):1229–41. Available from: http://www.cell.com/article/S0092867415010296/fulltext

295. Chouaib S, Noman MZ, Kosmatopoulos K, Curran MA. Hypoxic stress: obstacles and opportunities for innovative immunotherapy of cancer. Oncogene 2017 36:4 [Internet] 2016 [cited 2023 Jan 11];36(4):439–45. Available from: https://www.nature.com/articles/onc2016225

296. Deng B, Zhu JM, Wang Y, Liu TT, Ding YB, Xiao WM, et al. Intratumor Hypoxia Promotes Immune Tolerance by Inducing Regulatory T Cells via TGF-β1 in Gastric Cancer. PLoS One [Internet] 2013 [cited 2023 Jan 11];8(5):e63777. Available from: https://journals.plos.org/plosone/article?id=10.1371/journal.pone.0063777

297. Wang B, Zhao Q, Zhang Y, Liu Z, Zheng Z, Liu S, et al. Targeting hypoxia in the tumor microenvironment: a potential strategy to improve cancer immunotherapy. Journal of Experimental & Clinical Cancer Research 2021 40:1 [Internet] 2021 [cited 2023 Jan 11];40(1):1–16. Available from: https://jeccr.biomedcentral.com/articles/10.1186/s13046-020-01820-7

298. Noman MZ, Desantis G, Janji B, Hasmim M, Karray S, Dessen P, et al. PD-L1 is a novel direct target of HIF-1α, and its blockade under hypoxia enhanced MDSC-mediated T cell activation. J Exp Med [Internet] 2014 [cited 2023 Jan 11];211(5):781. Available from: /pmc/articles/PMC4010891/

299. Alsaab HO, Sau S, Alzhrani R, Tatiparti K, Bhise K, Kashaw SK, et al. PD-1 and PD-L1 checkpoint signaling inhibition for cancer immunotherapy: mechanism, combinations, and clinical outcome. Front Pharmacol 2017;8(AUG):561.

300. A Pilot Study of EZN-2968, an Antisense Oligonucleotide Inhibitor of HIF-1alpha, in Adults With Advanced Solid Tumors With Liver Metastases - Full Text View - ClinicalTrials.gov [Internet]. [cited 2023 Jan 12];Available from: https://www.clinicaltrials.gov/ct2/show/NCT01120288

301. Jonasch E, Donskov F, Iliopoulos O, Rathmell WK, Narayan VK, Maughan BL, et al. Belzutifan for Renal Cell Carcinoma in von Hippel–Lindau Disease. New England Journal of Medicine [Internet] 2021 [cited 2023 Jan 12];385(22):2036–46. Available from: https://www.nejm.org/doi/full/10.1056/NEJMoa2103425

302. Phillips RM. Targeting the hypoxic fraction of tumours using hypoxia-activated prodrugs. Cancer Chemother Pharmacol [Internet] 2016 [cited 2023 Jan 12];77(3):441. Available from: /pmc/articles/PMC4767869/

303. Juillerat A, Marechal A, Filhol JM, Valogne Y, Valton J, Duclert A, et al. An oxygen sensitive self-decision making engineered CAR T-cell. Scientific Reports 2017 7:1 [Internet] 2017 [cited 2023 Jan 12];7(1):1–8. Available from: https://www.nature.com/articles/srep39833

304. Kosti P, Opzoomer JW, Larios-Martinez KI, Henley-Smith R, Scudamore CL, Okesola M, et al. Hypoxia-sensing CAR T cells provide safety and efficacy in treating solid tumors. Cell Rep Med 2021;2(4):100227.

305. Neelapu SS, Hamadani M, Miklos DB, Holmes H, Hinkle J, Kennedy-Wilde J, et al. A phase 1 study of ADI-001: Anti-CD20 CAR-engineered allogeneic gamma delta (γδ) T cells in adults with B-cell malignancies. https://doi.org/101200/JCO20224016_suppl7509 2022;40(16_suppl):7509–7509.

306. Sanz M, Mann BT, Ryan PL, Bosque A, Pennington DJ, Hackstein H, et al. Deep characterization of human γδ T cell subsets defines shared and lineage-specific traits. Front Immunol 2023;14:1148988.

307. Tokarew N, Ogonek J, Endres S, von Bergwelt-Baildon M, Kobold S. Teaching an old dog new tricks: next-generation CAR T cells. British Journal of Cancer 2018 120:1 [Internet] 2018 [cited 2023 Feb 25];120(1):26–37. Available from: https://www.nature.com/articles/s41416-018-0325-1